Investigation into infectious bronchitis virus (IBV) spike glycoprotein glycosylation, pathogenicity and tropism

A thesis submitted in accordance with the requirements of the University of Liverpool for the degree of Doctor in Philosophy

by Phoebe Stevenson-Leggett

September 2018

UNIVERSITY OF LIVERPOOL

THE Pirbright INSTITUTE

Abstract

Infectious bronchitis virus (IBV) is the most economically damaging virus to the poultry industry, presenting a major threat to the health and productivity of both commercial and backyard flocks. Better understanding of the molecular mechanisms involved in virus infection and the properties that allow it to be such a successful pathogen is required to improve vaccination strategies and control of the disease. The spike (S) protein of IBV is responsible for attachment and entry into host cells. Like other viral attachment proteins, IBV S is highly glycosylated. Using mass spectrometry techniques as well as cellular inhibitors and deglycosylating enzymes, the glycan profile of IBV was further elucidated and a possible role for glycosylation in reducing antibody binding was suggested. The role of the S protein in pathogenicity is somewhat unclear. Previous studies have investigated IBV pathogenicity using recombinant viruses with a non-pathogenic backbone expressing heterologous spikes. In the present study, the S gene has been modified within a pathogenic backbone to assess the potential to alter pathogenicity. Firstly, a pathogenic virus expressing a non-pathogenic S protein was generated and characterised *in vitro* and *in vivo*. These studies revealed that the S gene was a factor in IBV pathogenicity. This was confirmed as a gene-specific effect through the generation and characterisation of a second virus, expressing the S protein from a heterologous pathogenic strain of IBV. This virus retained the ability to cause disease despite replacement of the S gene. Defining the cellular factors required by the virus to enter and successfully replicate in a given cell enables propagation of viruses not usually able to replicate in cell culture. Lastly, the cellular conditions necessary for IBV infection were investigated in the context of protease cleavage of the spike glycoprotein and in terms of temperature sensitivity, offering a possible mechanism of attenuation in some strains and a platform for more efficient vaccine production.

Table of contents

Acknowledgements

Firstly I must thank The Pirbright Institute and the University of Liverpool for the funding and opportunity to complete this project.

To Erica, the Tiny Tyrant, thank you for your constant support and patience, I couldn't have asked for a better supervisor. Thanks also to Paul Britton, Munir Iqbal and Julian Hiscox for their advice and supervision over the years. Thank you to Sarah for helping with anything and everything, and thank you for not killing me… yet. Thank you to Michael, Giulia and Isobel for your invaluable assistance and entertainment, science would be very boring without you.

To Helena, Ross, Nicole, Matt, Ben and all the other members of the NCI group, past and present, for the help, guidance and dancing. To Andrew, Kate and the Birnaviruses group, thanks for your help with animal experiments and entertainment at tea times. Special thanks to Tom Peacock and Simon Spiro for their help with glycan analysis and to Stuart Armstrong for completing the mass spectrometry analyses.

Tom Whitehead and Bella thanks for sharing in the struggle and the gin, didn't we have a nice time! Katy and Ross, my beautiful drinking swans, thank you (I think). Jess and Laura, thanks for being the most iconic duo in town.

Enormous thanks to The Mates and all other friends far and wide, I don't know what I'd do without you. An even more enormous thank you to all my parents, Mum and Chris, Dad and Sue, for supporting me in all my choices, I am eternally grateful. Finally thank you to Cobweb, my favourite idiot.

Declaration

I declare that, unless otherwise stated, the main body of work described in this thesis is my own and the use of materials and services from other sources are fully acknowledged. Any data generated by others has been properly acknowledged and referenced.

Publications

Paper publications:

Bickerton EJ, Maier HJ, Stevenson-Leggett P, *et al.* "The S2 subunit of infectious bronchitis virus Beaudette is a determinant of cellular tropism" Journal of Virology Jul 2018

Maier HJ, Cottam EM, Stevenson-Leggett P, *et al*. "Visualizing the autophagy pathway in avian cells and its application to studying infectious bronchitis virus." *Autophagy*. 2013;9(4):496-509

Stevenson-Leggett P, Britton P, Bickerton E. "Generation of a recombinant infectious bronchitis virus suggests that the S protein is a determinant of pathogenicity", 9th International Symposium on Avian Corona- and Pneumoviruses, 2016 *Conference Proceedings*

Stevenson-Leggett P, Armstrong S, Hiscox JA, Bickerton E., "Identification and characterisation of N-linked glycosylation sites in IBV S glycoproteins" ***(In progress)***

Stevenson-Leggett P, Keep S, Britton P, Bickerton E., "Investigating the role of the IBV S glycoprotein in pathogenicity" ***(In progress)***

Stevenson-Leggett P, Keep S, Britton P, Bickerton E., "Characterising temperature sensitivity in IBV: a potential mechanism of attenuation" ***(In progress)***

Posters

Global Alliance for Research on Avian Diseases (GARAD) Conference, Hanoi, Vietnam, 2018, "Elucidating infectious bronchitis pathogenicity mechanisms: the role of the spike protein" Phoebe Stevenson-Leggett, Sarah Keep, Michael Oade, Paul Britton, Erica Bickerton

XIVth Nidovirus International Symposium, Kansas City, MO, USA 2017: "The IBV S protein as a determinant of pathogenicity" Phoebe Stevenson-Leggett, Sarah Keep, Paul Britton, Julian Hiscox, Erica Bickerton

Microbiology Society Annual Conferences:

2017: Edinburgh UK: "Investigating spike glycoprotein glycosylation in infectious bronchitis virus (IBV)" Phoebe Stevenson-Leggett, Paul Britton, Julian Hiscox, Munir Iqbal, Erica Bickerton ***(Poster presentation and flash presentation)***

2016: Liverpool, UK: "Investigating glycosylation in the spike glycoprotein of IBV" Phoebe Stevenson-Leggett, Paul Britton, Julian Hiscox, Munir Iqbal, Erica Bickerton

2015: Birmingham, UK: "Generation of a recombinant infectious bronchitis virus (IBV) towards rational vaccine development" Phoebe Stevenson-Leggett, Sarah Keep, Paul Britton, Erica Bickerton

Positive Strand RNA Viruses (Keystone Symposium), Austin TX USA, 2016: "Generation of a recombinant avian coronavirus suggests the S protein is a determinant of pathogenicity" Phoebe Stevenson-Leggett, Sarah Keep, Paul Britton, Erica Bickerton

Oral presentations:

2018: Microbiology Society Annual Spring Conference, Birmingham UK, Offered paper: "Understanding infectious bronchitis virus pathogenicity: the role of the spike protein" Phoebe Stevenson-Leggett, Sarah Keep, Paul Britton, Erica Bickerton

2016: 9th International Symposium on Avian Corona- and Pneumoviruses, Utrecht Netherlands and Microbiology Society Avian Focus Meeting, London UK

Offered paper: “Generation of a recombinant IBV suggests the S protein is a determinant of pathogenicity” Phoebe Stevenson-Leggett, Sarah Keep, Paul Britton, Erica Bickerton

2015: IBV COST Action FA1207 PhD Network Meeting, Uppsala Sweden “Investigating glycosylation in the spike protein of infectious bronchitis virus” Phoebe Stevenson-Leggett, Julian Hiscox, Paul Britton, Erica Bickerton

List of Tables and Figures

Abbreviations

ACE2 – Angiotensin I converting enzyme 2

AmpR – Ampicillin resistance

Arg/R – Arginine

Asn/N – Asparagine

BCoV – Bovine coronavirus

BES – *N,N*-bis(2-hydroxyethyl)-2-aminoethanesulphonic acid

BHK – Baby hamster kidney

BSA – Bovine serum albumin

CD – Circular dichroism

CEACAM1 – Carcinoembryonic antigen-cell adhesion molecule

CK – Chick kidney

CoV – Coronavirus

cpe – cytopathic effect

Cryo-EM – Cryogenic electron microscopy

CSFV – Classical swine fever virus

CT – Cytoplasmic tail

CTG – CellTiter-Glo

Da – Dalton

DMEM – Dulbecco's minimum essential medium

DMV – Double membrane vesicle

dNTP – Deoxyribonucleotide triphosphate

Dol-P – dolichol phosphate

DPP4 – Dipeptidyl peptidase 4

dsRNA – Double-stranded RNA

DTT – Dithiothreitol

E – Envelope

EM – Electron microscopy

EMEM – Eagle's minimum essential medium

EP – Egg passage

ER – Endoplasmic reticulum

ERGIC – Endoplasmic reticulum Golgi intermediate compartment

ESI – Electrospray ionisation

EThcD – Electron transfer/high energy collision dissociation –

FBS – Foetal bovine serum

FcoV – Feline coronavirus

FIPV – Feline infectious peritonitis virus

Glc – Glucose

Man – Mannose

$Glc_3Man_9GlcNAc_2$ – tetradecaoligosaccharide

GMEM – Glasgow's minimum essential medium

gp – Glycoprotein

gpt – guanine phosphoribosyltransferase

H – Hypoxanthine

HA – Hemagglutinin

HCD – High-energy collisional dissociation

HCoV – Human coronavirus

HIV-1 – Human immunodeficiency virus 1

HR – Heptad repeat

HS – Heparan sulphate

IB – Infectious bronchitis

IBV – Infectious bronchitis virus

IF – Immunofluorescence

IFN – Interferon

kb – Kilobases

Kif – Kifunensine

LC – Liquid chromatography

LCMV – Lymphocytic choriomeningitis virus

M – Membrane

MeOH – Methanol

MERS-CoV – Middle East respiratory syndrome coronavirus

$MgCl_2$ – Magnesium chloride

MHV – Mouse hepatitis virus

MOI – Multiplicity of infection

MPA – Mycophenolic acid

MS – Mass spectrometry

MXH – Mycophenolic acid/Xanthine/Hypoxanthine

N – Nucleocapsid

NAc – *N*-Acetylglucosamine

$NaHCO_3$ – Sodium bicarbonate

NaN_3 – Sodium azide

NARF – National Avian Research Facility

NBBS – New-born bovine serum

nsp – Non-structural protein

ORF – Open reading frame

ori – origin of replication

PAGE – Polyacrylamide gel electrophoresis

PBS – Phosphate buffered saline

PBS-T – Phosphate buffered saline with Tween-20

PCR – Polymerase chain reaction

PEDV – Porcine epidemic diarrhoea virus

Pen/Strep – Penicillin/Streptomycin

PFA – Paraformaldehyde

PFGE – Pulsed field gel electrophoresis

pfu – Plaque forming unit

Phe/F – Phenylalanine

PIC – Protein inhibitor cocktail

PLPro – Papain-like protease

PNGS – Predicted N-linked glycosylation site

pi – Post-infection

pp – Polyprotein

Pro/P – Proline

RBD – Receptor binding domain

RdRp – RNA-dependent RNA polymerase

rFPV – Recombinant fowlpox virus

rIBV – Recombinant infectious bronchitis virus

RIPA – Radioimmunoprecipitation assay

RIR – Rhode Island Red

RNP – Ribonucleoprotein

rph – Revolutions per hour

RSV – Respiratory syncytial virus

RT – Reverse transcription

RTC – Replication-transcription complex

rVV – Recombinant vaccinia virus

S – Spike

SARS-CoV – Severe acute respiratory syndrome coronavirus

SDS – Sodium dodecyl sulphate

SDS-PAGE – SDS-polyacrylamide gel electrophoresis

Ser/S – Serine

sg – Sub-genomic

SPF – Specific pathogen free

ss – Single stranded

SW – Swainsonine

TBE – Tris/Borate/EDTA

TCoV – Turkey coronavirus

TDS – Transient dominant selection

TE – Tris-EDTA

TGEV – Transmissible gastroenteritis virus

Thr/T – Threonine

TM – Transmembrane

TOC – Tracheal organ culture

TPB – Tryptose phosphate broth

TPCK – Tosyl phenylalanyl chloromethyl ketone

TRS – Transcription regulatory sequence

TRS-B – Body transcription regulatory sequence

TRS-L – Leader transcription regulatory sequence

UDP – Uridine diphosphate

UGGT1 – UDP-Glc:glycoprotein glucosyltransferase I

UTR – Untranslated region

VV – Vaccinia virus

WB – Western blot

X – Xanthine

Chapter 1: Introduction

1.1 The *Nidovirales*

The *Nidovirales* are an order of viruses encoded by positive sense, single stranded RNA genomes. The order comprises three distinct families known as the *Arteriviridae*, the *Roniviridae* and the *Coronaviridae*. The *Coronavirinae* and *Torovirinae* are distinct genera within the *Coronaviridae* family (King et al., 2012, Gonzalez et al., 2003). While the members of the *Nidovirales* are genetically diverged, they all use very similar mechanisms to replicate their RNA genomes, involving the production of sub-genomic RNA molecules. All nidoviruses encode a complex set of proteins within their genomes which facilitate efficient transcription and translation. In all nidoviruses, the genes encoding these proteins make up at least two thirds of the whole genome (reviewed by Posthuma et al. 2017). The process of replication as well as the functions of these proteins are described in more detail in future sections.

While the nidoviruses are united in their mechanisms of replication, they can exhibit very different virion morphologies. Coronaviruses are classically spherical in shape with spike-like projections on the virion surface whereas toroviruses and bafiniviruses are often rod-shaped (International Committee for the Taxonomy of Viruses (ICTV) 9th Report 2011). These viruses can also be distinguished by the size of their genome. Coronaviruses boast extremely large genomes of approximately 26-32 kilobases (kb), the largest of any RNA virus (Gorbalenya et al., 2006, Sawicki, 2009). In contrast, arterivirus genomes are much shorter, comprising approximately 13kb. Arterivirus virions are also considerably smaller in diameter than those of related nidoviruses (Snijder and Meulenberg, 1998). Nidoviruses infect a wide range of hosts including vertebrate and invertebrate species. They include many pathogens of great importance in both human and animal health, some of which are considered significant

emerging pathogens (Weiss and Navas-Martin, 2005). The phylogenetic relationships between the families of viruses within the *Nidovirales* is demonstrated in Figure 1.1.

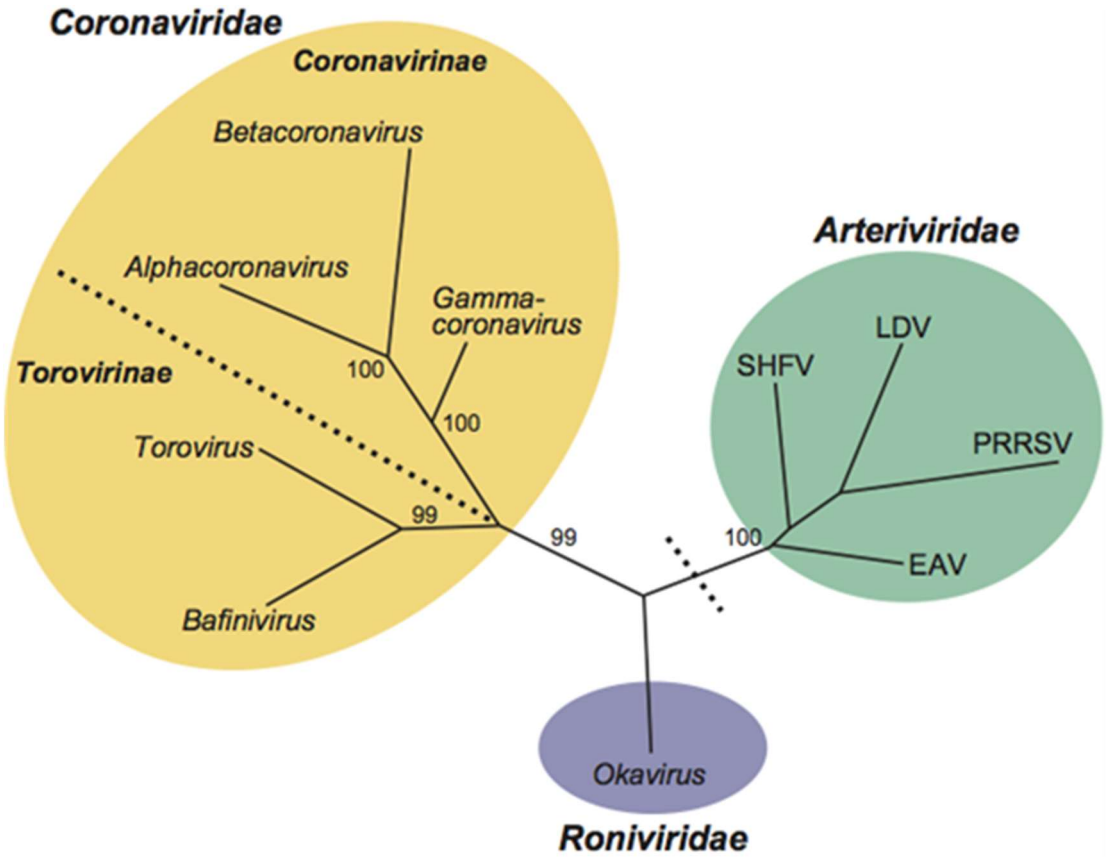

Figure 1.1: Phylogenetic relationships between members of the *Nidovirales*. The three groups within the order are *Arteriviridae*, *Roniviridae* and the *Coronaviridae*, containing the *Coronavirinae* and the *Torovirinae*. Examples are given for each group and their divergence is stated. Taken from the International Committee for the Taxonomy of Viruses (ICTV) 9th Report, 2011.

1.2 The *Coronavirinae*

The *Coronavirinae* are a subfamily of viruses within the order Nidovirales, alongside the *Torovirinae* and *Arterivirinae*. The *Coronavirinae* are divided into four genera, alpha, beta, gamma and the more recently established genus, *Deltacoronavirus*. Examples of coronaviruses belonging to each genus are detailed in Table 1.1. Viruses included in these genera pose significant threats to both human and animal health as well as global food security. Coronaviruses include the emerging pathogens such as severe acute respiratory syndrome coronavirus (SARS-CoV) and Middle East respiratory syndrome virus (MERS-CoV), both of which caused significant outbreaks in 2003 and 2012, respectively (Zaki et al., 2012, Peiris et al., 2003).

Coronaviruses of veterinary importance affect a wide range of species causing both respiratory and enteric disease. They include feline coronavirus or feline infectious peritonitis virus (FCoV/FIPV) and infectious bronchitis virus (IBV), an endemic pathogen of chickens. Those affecting pigs include porcine epidemic diarrhoea virus (PEDV) and transmissible gastroenteritis virus (TGEV). Bovine coronavirus (BCoV) is an important pathogen causing disease in calves. In domestic animals, infection with coronaviruses is often associated with concurrent or secondary bacterial infections, resulting in increased mortality and severe economic losses in the meat and dairy industries (Weiss and Navas-Martin, 2005).

Table 1.1: Coronavirinae genera and species

Genus	***Species***
ALPHACORONAVIRUS	Minopterus bat coronavirus 1
	Transmissible gastroenteritis virus (TGEV)
	Scotophilus bat coronavirus 512
	Porcine epidemic diarrhoea virus (PEDV)
	Human coronavirus 229E
	Human coronavirus NL63
	Rhinolophus bat coronavirus HKU2
	Feline coronavirus (FCoV)
BETACORONAVIRUS	Murine Coronavirus (MHV)
	Human coronavirus HKU1
	Betacoronavirus 1
	SARS coronavirus
	Bovine coronavirus (BCoV)
	Tylonycteris bat coronavirus HKU4
	Pipistrellus bat coronavirus HKU5
GAMMACORONAVIRUS	Beluga whale coronavirus SW1
	Avian coronavirus (IBV)
DELTACORONAVIRUS	Munia coronavirus
	Bulbul coronavirus
	Thrush coronavirus

The coronaviruses are classified into four genera: the alpha, beta, gamma and Deltacoronaviruses*. Here, IBV is referred to as avian coronavirus. Adapted from the International Committee for the Taxonomy of Viruses (ICTV), Coronavirinae Figures, 2009.*

1.3 Infectious bronchitis virus (IBV)

IBV is the prototype *Gammacoronavirus*, infecting domestic chickens (*Gallus gallus*) in both commercial flocks for food production and so-called "backyard" settings. It is a highly contagious pathogen spread by droplet transmission. Virus infection causes severe disease in poultry and can lead to fatal secondary bacterial infections, resulting in massive economic losses in the poultry industry worldwide. Frequent mutations in its large genome mean the virus exists as many different serotypes, with new variants continuously emerging (de Wit et al., 2011).

There is no universally agreed method for classifying IBV types, creating difficulty in arranging the viruses into groups and analysing their phylogenetic relationships. Historically, viruses were classified according to their pathologies and *in vitro* immunology, into pathotypes and serotypes respectively. More recently, genotyping has become a more widely used method of classification, achieved through RT-PCR analysis of the nucleotide sequences of gene encoding the attachment protein, the spike (S) gene (Lee et al., 2003, Handberg et al., 1999).

Serotyping has become less practical as a method of differentiation due to the constant emergence of new variants. Additionally, minor sequence variation in the S gene can lead to major changes in the serotype of the virus (Cavanagh et al., 1992). With the high rate of mutation observed in IBV and the fact that each serotype requires a validated neutralisation test, this method is unable to accurately classify all new variants. IBV strains can also be classified into protectotypes, based on the complete immune response to infection. While this method provides the most information about the efficacy of vaccine candidates, expensive resources and a lot of time are required to achieve accurate classification, making it impractical on a large scale (reviewed by de Wit et al., 2011).

Recently, a method was proposed for centralising and streamlining the classification process of IBV strains, based on grouping viruses by their S phylogeny. Within this system, 32 distinct

viral lineages have been identified, making up 6 different genotypes of IBV (Valastro et al., 2016).

Two of the most well studied strains of IBV both belong to the Massachusetts (Mass) serotype: M41 and Beaudette. These strains are both adapted to replication in cell culture and so are easier to propagate and characterise *in vitro* compared to many of the circulating field strains. Other widely studied serotypes include Connecticut and Arkansas (Ark) types. Vaccines against IBV are often based on strains within these genotypes, all of which originate from the USA. Viruses in the originally European 4/91 genotype have been identified in affected regions across the world, including Latin America, the Middle East and more recently, Japan (reviewed by Bande, 2017). Viruses belonging to the QX and Q1 genotypes are also prominent throughout the world and have caused major problems in infected flocks since their original isolation in China in the 1990s, with disease characterised by proventriculitis and oviduct swelling (YuDong et al., 1998). The disease symptoms associated with infection with these serotypes differ greatly from the cold-like respiratory symptoms associated with Mass infections, highlighting the variety of ways in which IBV can cause economic losses and reiterating the importance for effective detection and control.

1.4 Genome organisation:

Coronaviruses are large, enveloped viruses with single stranded (ss) positive sense RNA genomes ranging from 26-31kb in length, the largest of any RNA virus. The IBV genome is 27.6kb (Boursnell et al., 1987). Organisation of the genome is detailed in Figure 1.2. Coronavirus genomes are polyadenylated at the 3’ end and include a 5’ methylated cap. Untranslated regions (UTRs) are found at both the 5' and 3' ends of the genome and have been implicated in regulating replication and translation through the presence of *cis*-acting sequences (Senanayake and Brian, 1999, Yang and Leibowitz, 2015).

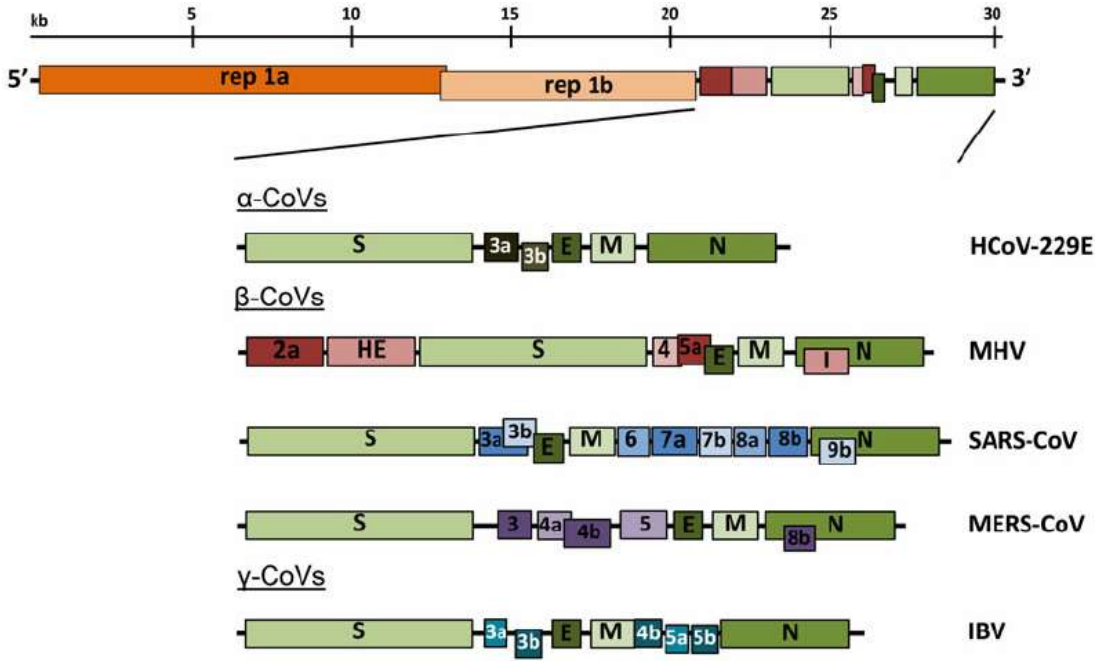

Figure 1.2: Coronavirus genome organisation. The 5' two thirds of the genome encode the two replicase polyproteins (pp1a and pp1b). The 3' third encodes the structural and accessory genes. The genome depicted at the top is MHV and examples of each genus of coronavirus are detailed below. IBV is the representative for the gammacoronaviruses. Figure taken from Fehr and Perlman, 2015.

The 5' two thirds of the coronavirus genome are comprised of the replicase gene which is translated into two large polyproteins (pp) and subsequently cleaved by virus-encoded proteases into 16 non-structural proteins (nsps), performing a variety of functions in the replication cycle. The nsps and their related functions are detailed in Table 1.2. The replicase genes of IBV and other gammacoronaviruses encode only 15 nsps as they do not encode nsp1; however nsp2-16 correspond to the proteins expressed in other coronaviruses. Notable functions of the nsps include the exonuclease activity of nsp14, the RNA-dependent RNA polymerase (RdRp) encoded in nsp12 and the methyltransferase activity exhibited by

nsp16, involved in the capping mechanisms required for translation of viral RNA (Ziebuhr et al., 2000). The exact function of nsp11 is unclear but there have been studies showing that the cleavage events that result in the formation of nsp11 and 12 are not required for viral replication *in vitro* (Fang et al., 2008). The 3' third of the genome includes the genes encoding the structural and accessory proteins.

Table 1.2: List of non-structural proteins (nsp) expressed from the coronavirus replicase gene.

Protein	Function
nsp1	Promotes cellular mRNA degradation and blocks host cell translation, results in blocking innate immune response
nsp2	No known function, binds to prohibitin proteins
nsp3	Large, multi-domain transmembrane protein, activities include: • Ubl1 and Ac domains, interact with N protein • ADRP activity, promotes cytokine expression • PLPro/Deubiquitinase domain, cleaves viral polyprotein and blocks host innate immune response • Ubl2, NAB, G2M, SUD, Y domains, unknown functions
nsp4	Potential transmembrane scaffold protein, important for proper structure of DMVs
nsp5	Mpro, cleaves viral polyprotein
nsp6	Potential transmembrane scaffold protein
nsp7	Forms hexadecameric complex with nsp8, may act as processivity clamp for RNA polymerase
nsp8	Forms hexadecameric complex with nsp7, may act as processivity clamp for RNA polymerase; may act as primase
nsp9	RNA binding protein
nsp10	Cofactor for nsp16 and nsp14, forms heterodimer with both and stimulates ExoN and 2-O-MT activity
nsp11	Unknown function
nsp12	RdRp
nsp13	RNA helicase, 5' triphosphatase
nsp14	N7 MTase) and 3'-5' exoribonuclease, ExoN; N7 MTase adds 5' cap to viral RNAs, ExoN activity is important for proofreading of viral genome
nsp15	Viral endoribonuclease, NendoU
nsp16	2'-O-MT; shields viral RNA from MDA5 recognition

The function or putative function of each protein is listed. IBV does not express nsp1. Adapted from Fehr and Perlman, 2015 (Fehr and Perlman 2015).

1.5 Coronavirus structural proteins

Four structural proteins are encoded in the 3' end of the coronavirus genome. They include the spike (S), envelope (E), membrane (M) and nucleocapsid (N) proteins and are arranged in the order S-E-M-N. They perform a variety of functions during infection from attachment and fusion to genome packaging and virus release.

1.5.1 Envelope (E) protein

The E protein is a small membrane protein between 76 and 109 amino acids in size. It has a single hydrophobic domain and is present in small quantities in the viral membrane (Ruch and Machamer, 2012). It is thought to be a transmembrane protein involved in a number of viral processes during infection. Similar to that of the influenza M2 protein and the SH protein of respiratory syncytial virus (RSV) (Alvarado-Facundo et al., 2015, Gan et al., 2012), ion channel activity has been observed in the coronavirus E protein (Verdia-Baguena et al., 2012, Nieto-Torres et al., 2015b). This activity is a common target for antivirals, as inhibition of the ion channel activity has been shown to restrict coronavirus replication (Wilson et al., 2006, Nieto-Torres et al., 2015a). Roles for the E protein have been suggested in MHV assembly and exit (Ye and Hogue, 2007). The protein has also been implicated in pathogenesis in SARS-CoV (DeDiego et al., 2007).

1.5.2 Membrane (M) protein

The M protein has three transmembrane domains. It is a small protein of around 220 amino acids and is the most abundant protein in the virus membrane (Klumperman et al., 1994). The M protein is thought to be involved in virus assembly and also interacts with the other viral proteins (Corse and Machamer, 2003). It has been suggested that the protein exhibits two different conformations in order to function in creating the shape of the virus particle and interacting with the N protein (Neuman et al., 2011). During virus assembly, M self-

associates, incorporates S into the virion and also selectively packages the section of N that interacts with the RNA genome.

1.5.3 Nucleocapsid (N) protein

The coronavirus N protein is a basic protein produced in large quantities during infection (Lomniczi and Morser, 1981). The IBV N protein consists of 409 amino acids. It performs multiple functions in the virus lifecycle including encapsulating the genomic RNA through interactions with its N-terminus, regulating host translation and facilitating efficient viral transcription (Hurst et al., 2005, McBride et al., 2014). N-mediated interference with the host immune response to IBV infection has also been suggested (Hu et al., 2017, Chen and Ly, 2017).

1.5.4 Spike (S) protein

The coronavirus S protein is a type I membrane glycoprotein that protrudes from the surface of the virion, providing the characteristic corona morphology (Bosch et al., 2003). It is the largest protein encoded in the genome and is responsible for both attachment to host cells and fusion of viral and cellular membranes. The size of the protein varies between coronaviruses; the IBV S protein is 1162 amino acids in length and has a molecular weight of approximately 180 kilodaltons (kDa).

In some coronaviruses, including IBV and MHV, the S protein is cleaved by furin during protein synthesis into two non-covalently linked subunits termed S1 and S2. In the Beaudette strain of IBV, this cleavage event occurs at the amino acid sequence RRFRR (Cavanagh et al., 1986), although the exact sequence varies among strains (Jackwood et al., 2001). IBV S1 is approximately 519 amino acids long and makes up the globular head of the glycoprotein, containing the receptor binding domain (RBD). The S1 subunit consists of two distinct domains, the N-terminal domain (S1-NTD) and the C-terminal domain (S1-CTD). The RBD for

IBV has previously been mapped to amino acids in the NTD. More recent evidence has shown that IBV S1-CTD also contains receptor binding motifs, similar to coronaviruses belonging to the other genera (Shang et al., 2018). IBV S2 (625 amino acids) makes up the stalk portion of the protein and has been implicated in cellular tropism (Bickerton et al., 2018). Morphology of coronavirus virions and the structure of their S genes are shown in Figure 1.3.

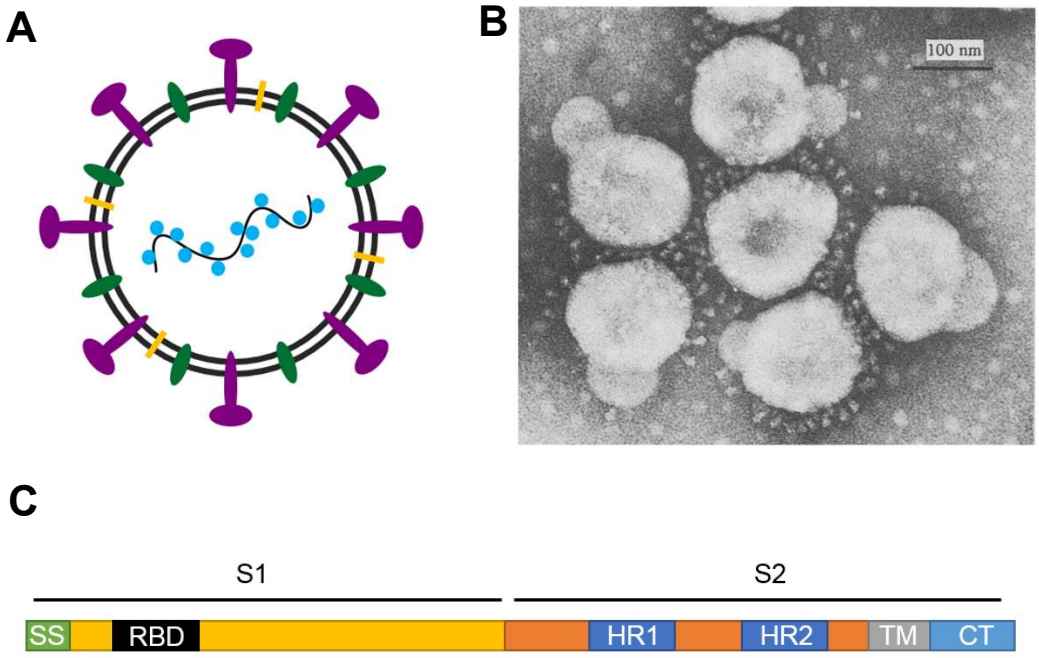

Figure 1.3: Coronavirus virion morphology and S gene structure. (A) Schematic representation of a coronavirus virion with S protein projections shown in purple, M protein shown in green, E protein shown in yellow and N protein shown in blue surrounding the RNA genome. **(B)** Electron micrograph image of IBV virions, approximately 120nm in diameter, with clear spike-like projections in a characteristic corona formation. EM image taken from Lanser and Howard, 1980 (Lanser and Howard, 1980). **(C)** Schematic representation of a coronavirus S gene. The S1 subunit encodes the signal sequence and the receptor binding domain (RBD). The S2 subunit encodes two heptad repeat (HR) regions, the transmembrane domain and the cytoplasmic tail. Gene sections are not to scale.

The S protein consists of a signal sequence, stated as amino acids 1-18 in the M41 strain (Promkuntod et al., 2014) at the N-terminal end followed by the ectodomain, transmembrane (TM) domain and cytoplasmic tail (CT). The latter regions are responsible for anchoring the protein to the virion membrane. The ectodomain contains a furin cleavage site (S1/S2) and two heptad repeat (HR) regions. The HR regions are involved in protein monomer oligomerisation (Groot et al., 1987). During infection, the protein localises to the endoplasmic reticulum (ER) (Delmas and Laude, 1990) and is then translocated to the ER-Golgi intermediate compartment (ERGIC) and Golgi for further processing including glycosylation (Cavanagh, 1983). Oligosaccharides are added to the protein surface via specific asparagine residues as part of the N-linked glycosylation process of protein modification (described in Sections 1.8 and 9).

Attachment to the host cell and processing by cellular proteases results in major conformational changes in the structure of the S glycoprotein leading to fusion of the viral and cellular membranes (Walls et al., 2017, Belouzard et al., 2012). The post-fusion conformation of the protein must be achieved in order for fusion and entry to occur. The virus is thought to enter the cell by endocytosis which, in the case of IBV, is pH dependent (Chu et al., 2006). The viral fusion peptide (located in the S2 subunit) is then exposed and inserted into the membranes of vesicles, mediating fusion with the viral envelope (Bosch et al., 2003). The result of these fusion events is the release of the ribonucleoprotein (RNP) containing the viral genome into the cytoplasm, beginning the process of genome replication.

Further understanding of the molecular mechanisms employed by the S protein to mediate attachment and fusion have been revealed recently. The structures of certain coronavirus S proteins have recently been elucidated using electron microscopy (EM) techniques. Walls *et al* have studied the S protein of the human coronavirus NL63 (HCoV NL63) and MHV using

cryo-EM, revealing the pre-fusion structure of the protein (Walls et al., 2016a, Walls et al., 2017). Others have also identified key conformational changes required to allow proper receptor binding and fusion in the SARS-CoV S glycoprotein (Gui et al., 2017).

More recently still, the structure of the IBV S protein ectodomain was solved using similar techniques. The protein structure of the S protein of a pathogenic IBV strain (M41) was revealed by Shang *et al* in order to investigate functional evolution. This study investigated the structure of the S proteins of the different coronavirus genera, providing crucial insight into how these proteins have diverged, allowing such a wide host range between viruses (Shang et al., 2018). Their results revealed a so called evolutionary spectrum of coronavirus S proteins, in which gamma- and betacoronavirus S1-NTDs appeared to be the most evolved compared to the other genera. This study postulates that coronavirus S1-NTDs are evolved from host galectin molecules, in order to imitate host proteins and avoid recognition by the immune system. They identified similarities in the structures of all coronavirus S1-NTDs in the structural folds within the protein. Differences were identified between the proteins of different genera, in that gamma and *Betacoronavirus* S1-NTDs have evolved to include partial ceilings covering the sugar binding site within this domain. This is thought to function as protection from the immune response, however the ceiling in the *Betacoronavirus* MHV has further evolved to become a binding partner for a novel protein receptor. Through the investigations of the S protein structure, this study also identified 20 sites at which the protein is glycosylated. This study was the first of its kind to describe in detail the ectodomain of a *Gammacoronavirus* S protein, with two distinct domains in S1, and two HR regions and the fusion peptide (FP) located in the S2 subunit.

1.5.5 S1 subunit

The S1 subunit is responsible for attachment to host cells through interactions with cellular receptors. As described previously, the receptor with which the IBV S protein interacts remains unknown however the RBD has been mapped to amino acids 19-272 in M41 (Promkuntod et al., 2014). Other coronaviruses are known to interact with a variety of molecules on the surface of host cells. The S protein of SARS-CoV binds to human angiotensin I converting enzyme 2 (ACE2) (Li et al., 2003). MERS-CoV S1 interacts with specific residues of dipeptidyl peptidase 4 (DPP4) to enter the cells of susceptible hosts including humans and camels (Raj et al., 2013). MHV enters cells through interactions with the adhesion molecule carcinoembryonic antigen-cell adhesion molecule (CEACAM1), the first coronavirus receptor to be identified (Belouzard et al., 2012, Dveksler et al., 1991). The receptor for IBV and other gammacoronaviruses is yet to be identified. Interactions with sialic acids have been suggested as a possible mechanism for virus entry (Li, 2015, Schwegmann-Wessels and Herrler, 2006, Winter et al., 2006). For other avian gammacoronaviruses such as the closely related turkey coronavirus (TCoV), recent studies have also identified glycan receptors as possible interacting partners during virus entry (Wickramasinghe et al., 2015).

The S1 subunit is the main antigenic target of IBV, against which the host immune response is directed (Kant et al., 1992). There is huge diversity among the S1 sequences of IBV strains, rendering broad cross-protection through vaccination near-impossible. IBV detection, genotyping and strain differentiation are achieved through sequencing of the S1 subunit (Ariyoshi et al., 2010, De Wit, 2000). Figure 1.4 shows an example of the phylogenetic relationships between a variety of IBV strains based on their S1 nucleotide sequences, highlighting the vast variability between genotypes (Manswr et al., 2018).

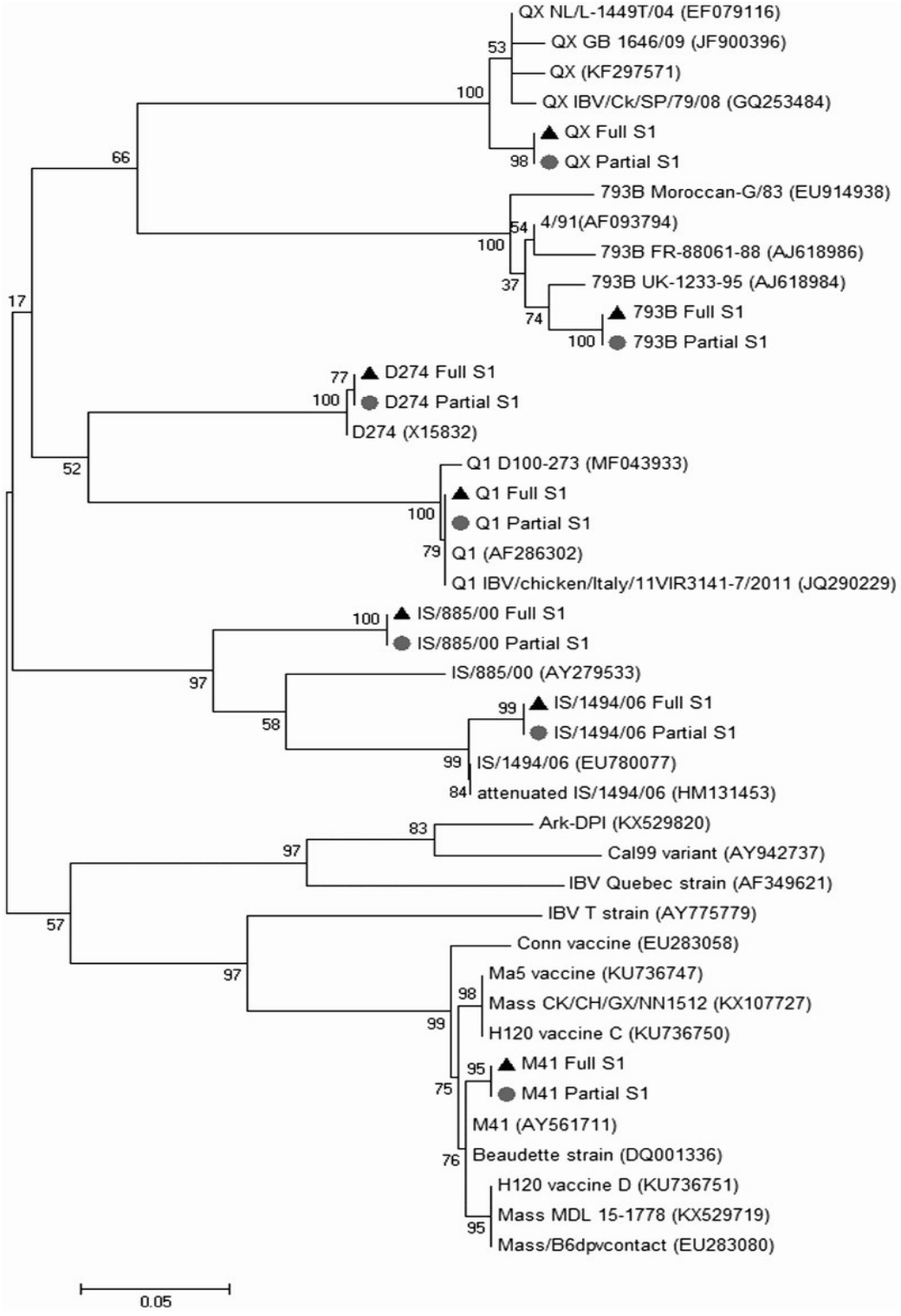

Figure 1.4: Example of phylogenetic relationships of a variety of IBV strains based on full (black triangles) and partial (grey circles) amino acid sequences of the S1 gene. Field strains collected in the Middle East and reference strains were analysed based on the sequences of the S1 gene. Figure taken from Manswr et al (2018).

1.5.6 S2 subunit

The primary function of the S2 subunit is fusion of the viral and cellular membranes following attachment to host cells. This segment of the protein contains two HR regions. Mutations within these regions have been shown to affect fusion activity. Disruption of the leucine-rich motifs within the HR regions can affect protein oligomerisation and abolish cell to cell fusion (Luo et al., 1999). In other studies, mutations in HR1 increased fusion activity and influenced coronavirus infectivity in cell culture (Yamada et al., 2009). S2 fusion mechanisms have been investigated as a possible option for treatment of MERS-CoV infections, through action of synthetic HR peptides (Lu et al., 2014).

As well as attachment and fusion, the IBV S protein as a whole is known to be a determinant of *in vitro* cellular tropism, as shown by the generation of recombinant viruses with modified S proteins altering the tropism of the resultant virus. This was demonstrated through the insertion of the M41 S gene into the Beaudette genome, resulting in the loss of the extended host tropism usually observed with Beaudette strains (Casais et al., 2003). More recently, tropism was found to be directly influenced by the S2 subunit. Beaudette strains are known to infect and replicate in Vero cells as well as primary avian cells, a feature that has been attributed to the presence of a secondary cleavage site in the S2 sequence, located within the amino acid motif RRR at position 690 (Yamada and Liu, 2009). This motif is known as the S2' cleavage site and has been studied by several groups in the context of host tropism, where the insertion of this specific sequence into the S protein allowed virus replication in classically non-permissive cells (Bickerton et al., 2018, Madu et al., 2007). S2' cleavage has been observed in other coronaviruses from different genera, including MERS-CoV (Millet et al., 2016).

Compared to the S1 subunit, the sequences of IBV S2 genes are much more conserved between strains. Epitopes recognised by neutralising antibodies have been located in the S2

subunits of the SARS-CoV and MERS-CoV S proteins (Keng et al., 2005, Yang et al., 2014). The presence and conservation of these epitopes has implications for cross-protection by vaccination.

1.6 IBV accessory proteins and functions

IBV expresses four well known and one more recently identified accessory proteins, encoded by three genes termed 3, 4b and 5. 3a and 3b and 5a and 5b are expressed from gene 3 and gene 5, respectively. Although they are non-essential for *in vitro* replication, recent studies have shown reductions in pathogenicity following deletions in the accessory genes 3 and 5 (Laconi et al., 2018, van Beurden et al., 2018). IBV 3a has been implicated in modulation of the interferon (IFN) response to IBV infection (Kint et al., 2015). IBV 5b has been implicated in host cell shutoff (Kint et al., 2016). Gene 5 as a whole has been shown to be dispensable for *in vitro* replication (Casais et al., 2005) and has more recently been studied in the context of pathogenicity and vaccination (van Beurden et al., 2018). The transcript for a fifth, IBV-specific accessory gene was identified more recently. The function of this putative protein, termed 4b, is still unknown (Bentley et al., 2013).

1.7 Coronavirus genome replication and lifecycle

Coronavirus replication takes place in the cytoplasm following virus entry into the host cell by endocytosis. Each stage of the coronavirus lifecycle is outlined in Figure 1.5.

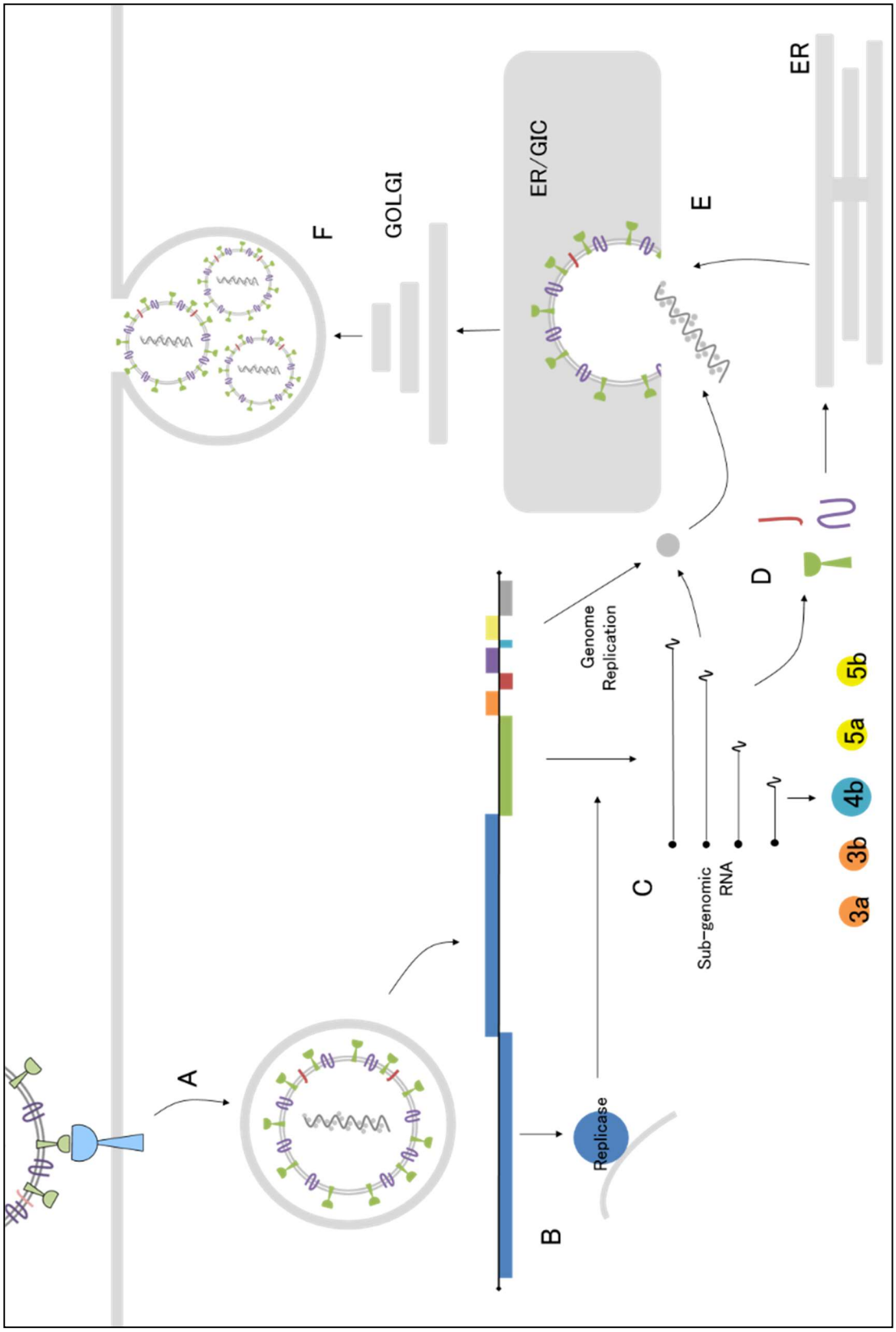
A
B
C
D
E
F
Replicase
Genome Replication
Sub-genomic RNA
3a
3b
4b
5a
5b
GOLGI
ER/GIC
ER

Figure 1.5: Schematic representation of a coronavirus replication cycle. The virus enters the cell by endocytosis following attachment and fusion via the S protein **(A)**. The genome is then released into the cytoplasm **(B)** initiating translation of ORF1a and b and generation of the nested set of sub-genomic mRNAs **(C)** encoding the accessory and structural proteins **(D)**. The structural proteins are transported to the ER via the secretory pathway and then to the ERGIC where the genome is packaged by the nucleocapsid (N) protein and structural proteins are incorporated into the virions **(E)**. Mature virions are transported to the Golgi and are released from the cell by budding **(F)**. Schematic courtesy of Dr Ross Hall.

1.7.1 Virus entry and cellular tropism

As previously discussed, coronaviruses enter the cell through interactions with a range of host cell receptors. Since the receptor for IBV is still unidentified, the exact mechanisms of virus entry are not well defined. It has been shown that major conformational changes occur within coronavirus S proteins following attachment to the appropriate receptor, which are essential for the induction of fusion and thus completion of the entry process (Walls et al., 2017, Matsuyama and Taguchi, 2009).

The post-fusion structure of the S protein is induced by cellular factors such as exposure to proteases (Li et al., 2006, Xu et al., 2004). Cleavage of the gammacoronavirus S protein into its two functional subunits S1 and S2 is mediated by furin. However this cleavage event is not required in all coronaviruses and is rarely seen in alpha- and betacoronaviruses. Susceptibility to secondary cleavage events by cellular proteases such as trypsin, have been implicated in cellular tropisms of various coronaviruses including IBV, where the presence of the S2' site is suggested to be responsible for the extended host tropism of the Beaudette strain (Belouzard et al., 2012, Millet and Whittaker, 2015). The S2' site has also been associated with heparan sulphate (HS) binding (Madu et al., 2007). The combination of the

S2' site and the protease environment of the host cell are thought to heavily influence coronavirus tropism. Extended tropism as a result of S protein processing by exogenous cellular proteases has also been observed in MERS-CoV (Park et al., 2016). Increases in pathogenesis and virulence in SARS-CoV have also been associated with proteolytic processing of the S protein, with reductions in virus neutralisation observed following cleavage by serine proteases (Glowacka et al., 2011).

The range of *in vitro* tropisms exhibited by IBV strains varies quite significantly. Field strains are often only capable of replicating in *ex vivo* organ cultures or even in embryonated eggs, creating difficulty during attempts to characterise the strains in laboratory settings. Strains within the same serotype can exhibit very different tropisms. This can be demonstrated by two cell culture-adapted strains of the Massachusetts serotype where, in contrast to the extended tropism of Beaudette, M41 is only able to grow in primary avian cells such as chick kidney (CK) cells. Alterations in the cellular tropism of IBV strains have been demonstrated using recombinant viruses expressing heterologous S proteins (Hodgson et al., 2004, Armesto et al., 2011). Other factors such as temperature are also thought to influence coronavirus tropism (Dubois-Dalcq et al., 1982).

1.7.2 Transcription and translation

Following virus entry and genome release, viral replication begins. The first stage in coronavirus genome replication is the translation of the proteins encoded by the replicase gene, the largest gene in the genome comprising two open reading frames (ORF) known as ORF 1a and ORF1b. These two ORFs encode polyproteins pp1a and pp1ab. Expression of both of these proteins is achieved through use of a slippery sequence and an RNA pseudoknot, causing a ribosomal frameshift from ORF1a to ORF1b. The pseudoknot is unwound by the ribosome and translation continues until a pp1a stop codon is reached. If the pseudoknot interrupts elongation and the ribosome pauses on the slippery sequence, a -1 frameshift

occurs in which the reading frame moves back by one nucleotide. Following this frameshift the ribosome is able to disrupt the pseudoknot and move on to translate the pp1b ORF (Fehr and Perlman, 2015; Sawicki et al., 2007).

Coronavirus pp1a and pp1ab encode 16 non-structural proteins (nsps) or 15 in the case of IBV and other gammacoronaviruses. Following translation, the polyproteins are cleaved by the viral papain-like proteases (PLpro) encoded in nsp3 into the remaining nsps, the functions of which are summarised in Table 1.2. Additionally, nsp5 acts as a 3C-like protease ($3CL^{pro}$), which has been shown to be essential for *Betacoronavirus* translation (Lu et al., 1995).

Some of the nsps assemble to form the replication transcription complexes (RTC), where nascent RNA is synthesised. During replication, negative sense sub-genomic (sg) RNAs are generated through discontinuous transcription. Negative sense full length genome templates are simultaneously produced by continuous transcription (Sawicki et al., 2007). The mechanisms involved in these processes are not yet fully elucidated. However it is known that coronavirus transcription involves transcription regulatory sequences (TRSs), which are short sequences of 6-8 nucleotides (Hiscox et al., 1995, Sola et al., 2005). In IBV the sequence is usually CUUAACAA. There is a TRS at the 5' end of the genome known as the TRS leader sequence (TRS-L) and at the beginning of each ORF downstream of ORF1ab, known as the TRS body sequence (TRS-B). In most cases, the TRS-B preceding each individual gene is complementary to the 5' TRS-L, however there are exceptions depending on the nature of the TRS in that some are canonical and some are non-canonical. Secondary structures of the TRS-B are also thought to be involved (Sawicki and Sawicki, 2005, Bentley et al., 2013).

Like all positive-sense RNA viruses, coronaviruses are known to induce extensive membrane rearrangements upon infection of the host cells (Mackenzie, 2005). Double membrane vesicles (DMVs) serve as the location for the RTCs in infected cells. These RTCs are the structures in which genome replication takes place (Miller and Krijnse-Locker, 2008). DMVs,

spherules and zippered ER can all be observed during IBV infection (Maier et al., 2016, Maier et al., 2013). The RTC initiates transcription at the 3’ end of the viral genome and proceeds upstream until a TRS-B is encountered and transcription pauses. At this point the process can either continue until another TRS-B is detected or undergo a translocation to the 5’ end, resulting in the presence of a so-called anti-leader sequence at the 3’ end of the newly synthesised sgRNA. The process culminates in a selection of sgRNAs of different lengths. Negative sgRNAs and full length genome transcripts then serve as templates for the generation of positive sense sgRNAs and entire viral genome copies. The process of genome transcription is summarised in Figure 1.6.

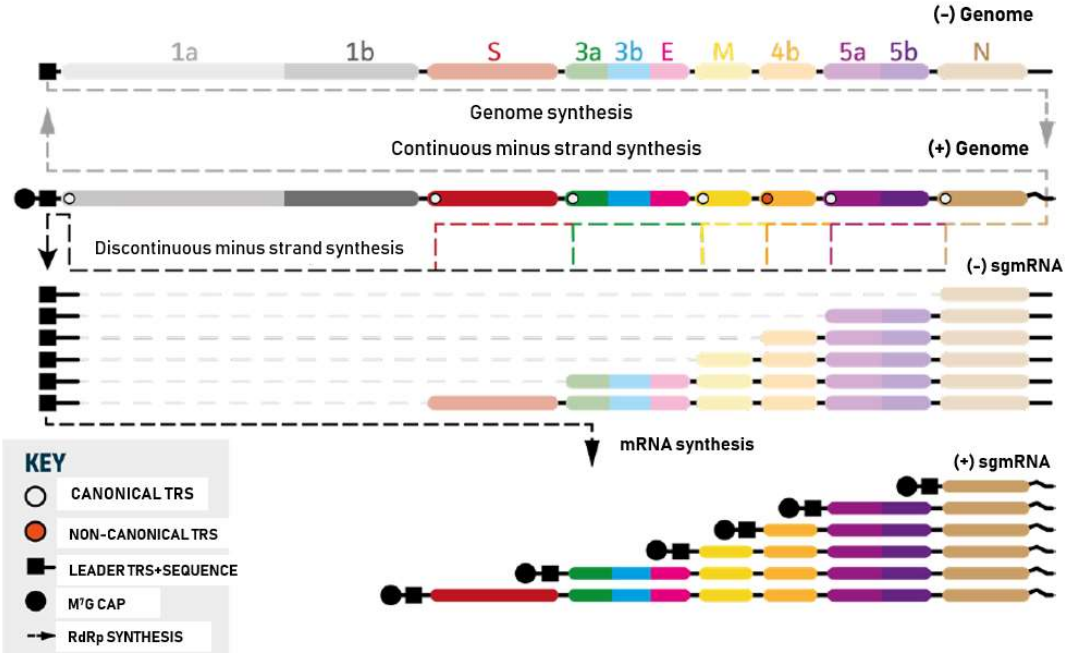

Figure 1.6: Coronavirus genome transcription. Coronavirus genomic RNA is transcribed by both continuous and discontinuous transcription, initiated at the 3' end of the genome by the viral replication-transcription complex (RTC). It continues upstream until a transcription regulatory sequence-body (TRS-B) is detected and transcription either continues (continuous transcription) or undergoes a translocation to the TRS-Leader sequence (TRS-L) at the 5' end of the genome (discontinuous transcription). The process of discontinuous transcription generates a nested set of negative sense sub-genomic RNAs (sgRNAs) which act as templates for positive sense sgRNAs. These are translated into viral proteins. Continuous transcription generates negative sense copies of the viral genome which are used as templates for the synthesis of full-length, positive sense single stranded RNA genomes (Sawicki et al. 2007; Yang and Leibowitz 2015).

1.7.3 Virus assembly and exit

The structural proteins (S, E, M and N) are translated from the sgRNAs, as are the accessory proteins. Following translation, the structural proteins are transported to the ER and then via the secretory pathway to the ERGIC where mature virions are formed (Fehr and Perlman, 2015, Krijnse-Locker, 1994). The E and M proteins are known to be involved in coronavirus assembly and exit (Vennema et al., 1996, Neuman et al., 2011, Ruch and Machamer, 2011). Once mature virions are completely assembled they are transported to the cell surface and released by exocytosis.

1.8 *N*-linked protein glycosylation

N-linked glycosylation is a form of co- and post-translational modification where oligosaccharides are attached to proteins at the asparagine (Asn/N) residue in the sequence Asn-X-Serine (Ser/S)/Threonine (Thr/T), where X represents any amino acid except Proline (Pro/P). The oligosaccharide core is synthesised and attached to the appropriate Asn residue on a nascent protein in the ER before the protein moves through the secretory pathway to the Golgi for further processing and enzymatic trimming.

The process of N-linked glycosylation of proteins in the ER can be broadly divided into two stages. Firstly, the core glycan is assembled on the membrane-anchored ER lipid dolichol phosphate (Dol-P) in the cytosol (Schwarz and Aebi, 2011). This begins with the attachment of the initial *N*-Acetylglycosamine (NAc) to the Dol-P followed by the sequential addition of mannose molecules. At this point the oligosaccharide is flipped into the luminal side of the ER by an enzyme known as flippase (Rush, 2015, Sanyal and Menon, 2009). This is followed by a series of assembly steps involving various glycosyltransferases which catalyse the transfer of more mannose and glucose molecules to the growing glycan, resulting in the

preparation of a tetradecaoligosachharide ($Glc_3Man_9GlcNAc_2$) that is ready for transfer onto the appropriate Asn residue in the nascent peptide. The second stage of N-linked glycosylation in the ER occurs when the enzyme oligosaccharyltransferase (OST) catalyses the covalent linkage of the core $Glc_3Man_9GlcNAc_2$ structure to the amide group of the Asn in suitable N-glycosylation seqons (Asn-X-Ser/Thr) (Ferris et al., 2014, Hubbard, 1988). Following this reaction, ER mannosidases act on the glycan structures to remove and add specific sugars in a step-wise fashion until the protein is correctly folded and ready to be transferred to the Golgi for further processing. The processes involved in N-glycan core assembly in the ER are summarised in Figure 1.7.

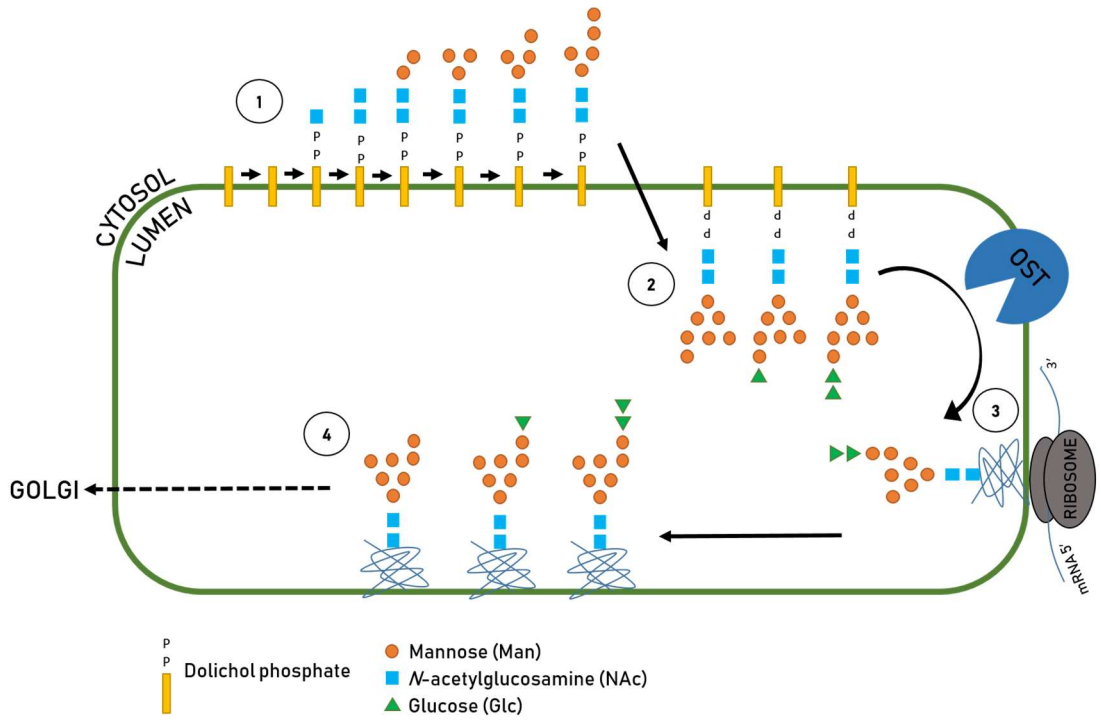

Figure 1.7: A simplified schematic detailing synthesis of the N-glycan core oligosaccharide in the ER. 1. Generation of the oligosaccharide core begins in the cytosol where the initial oligosaccharide composed of N-Acetylglucosamine and glucose (GlcNAc) is assembled onto dolichol phosphate (Dol-P), which resides in the membrane of the ER. These reactions are catalysed by glycosyltransferases, using uridine diphosphate (UDP)-GlcNac and UDP-Man as substrates from which the GlcNAc and mannose molecules are donated. **2.** Following several reactions in which sugar molecules are added sequentially to the Dol-P GlcNAc molecule, the core is "flipped" into the ER lumen where more molecules are added to the core structure. This is catalysed by an enzyme known as flippase. **3.** The oligosaccharide is transferred to nascent protein (blue squiggle) at an appropriate Asn residue through interaction with the oligosaccharyltransferase (OST) complex. **4.** Once attached, the glycan core undergoes a series of trimming reactions, catalysed by enzymes such as ER α-mannosidase I before transportation to the Golgi for further trimming and processing. Figure adapted from Aebi, 2013 (review).

As the glycans are attached and processed in the ER, the folding protein must also pass certain check-points in order to continue and avoid being directed to the ER-associated degradation (ERAD) pathway (protein folding and quality control mechanisms reviewed by Xu and Ng, 2015). After the first glucose residue is removed from the glycan chain on the luminal side of the ER, the protein enters the calnexin cycle, in which the protein is bound by other enzymes and factors in order to ensure it achieves a native conformation and the correct disulphide bonds. This results in the engagement of the enzyme UDP-Glc:glycoprotein glucosyltransferase I (UGGT1) which selectively binds to N-glycans which have been subjected to the action of different glucosidases and are now fully deglucosylated (Braakman and Bulleid, 2011). Once bound, UGGT1 determines whether the protein has achieved the correct conformation. If the protein is correctly folded, it is released and allowed to proceed to the Golgi for further trimming and processing. Those that are not in the correct native conformation are reglucosylated (with the addition of a glucose molecule), and re-entered into the calnexin cycle until the correct conformation is achieved, or until quality control mechanisms interrupt the cycle and the protein is targeted for degradation (Maattanen et al., 2010). The involvement of N-glycans in these processes is vital to ensure that the nascent protein folds correctly and can thus exit the calnexin cycle in order to progress through to the Golgi along the secretory pathway (Hebert and Molinari, 2012). Further processing of glycans occurs here, where glycan structures are shaped and trimmed by mannosidase II (reviewed by Rose (2012)) . This results in the formation of a range of glycan structures on the surface of proteins. The stacking formation of the Golgi compartments is thought to be crucial in protein glycosylation pathways. It has been shown that disruption of the factors that affect stacking can have dramatic effects on the numbers of glycans present on the proteins (Zhang and Wang, 2016, Veenendaal et al., 2014).

After emerging from the Golgi, the newly glycosylated proteins move through the Golgi network where their glycans are subjected to extensive trimming and processing by cellular

enzymes including mannosidases and glucosidases. The extent to which the glycans are trimmed results in the formation of different classes of glycan, divided into simple, complex and hybrid type depending on their composition. Simple, or high mannose, glycans are composed primarily of mannose molecules and are not subject to such extensive processing as the other classes of glycan (Schwarz and Aebi, 2011). The different classes of glycan arise in different compartments within the Golgi apparatus, owing to the fact that the enzymes which produce each type are only resident in specific places (for a comprehensive review of the location of enzymes within the Golgi apparatus, see Nilsson *et al.*, 2009). High mannose glycans are usually generated as a result of the actions of mannosidases in the *cis*- and *medial*-Golgi, whereas complex glycans, which comprise a more diverse range of sugar residues including sialic acids, are produced as a result of enzyme reactions leading to terminal glycosylation in the *trans*-Golgi (Stanley, 2011). Examples of each glycan type and the location in which they are produced is detailed in Figure 1.8.

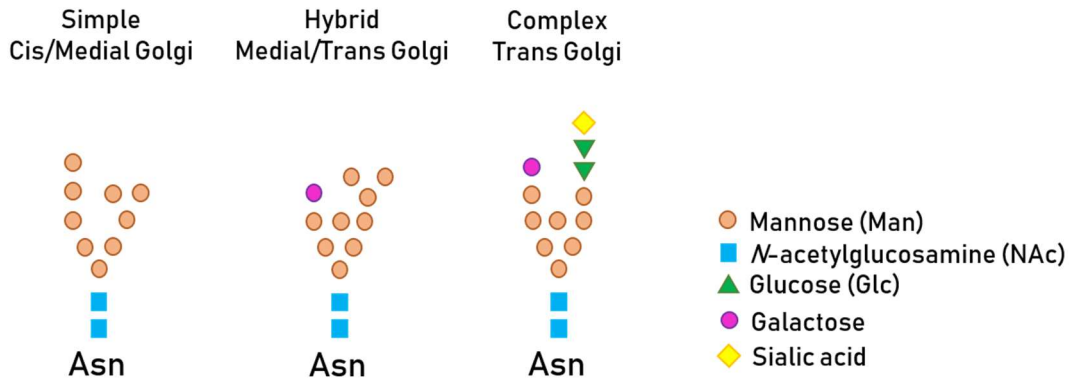

Figure 1.8: Schematic representation of glycan structures generated as a result of processing in the Golgi. Simple or high mannose glycans consist mainly of mannose (orange) residues and are generated from enzymatic processing in the *cis*- and *medial*-Golgi. Hybrid glycans comprise a mannose branch and a branch with a more diverse range of sugar residues including galactose (pink), for example. These are produced due to processing by enzymes in the *medial*- and *trans*-Golgi. Complex glycans are produced in the *trans*-Golgi and are made up of a range of sugar molecules including glucose, galactose and sialic acids.

1.9 *N*-linked glycosylation in viral proteins

The complexities of the processes described above highlight the key role that N-glycans play within the cycles of protein folding and quality control in mammalian cells. As viruses utilise and hijack the host cellular pathways to decorate their own proteins, naturally any deviation or interference with the mechanisms involved in these events can majorly disrupt the production of viral as well as host-derived proteins in infected cells. Alterations to this process by modifying the glycan processing pathways have been investigated in viral proteins such as influenza HA, where the addition of glycans to the protein resulted in vastly altered folding and intracellular transport (Gallagher, 1988). In addition to contributing to the correct folding patterns of the proteins, modified glycosylation can have major downstream effects on function and its interactions with other viral components.

N-linked glycosylation has been extensively characterised in viruses such as influenza and human immunodeficiency virus (HIV-1). The gp120 envelope protein of HIV-1 is heavily glycosylated, with the weight of the attached oligosaccharides contributing to over half of the protein's molecular weight. It is suggested that the glycans present on gp120 are involved in modulating immunogenicity. Research has been undertaken to investigate the involvement of the glycosylation profile of gp120 in virus infectivity and antibody mediated virus neutralisation. Removal of glycosylation at specific sites can increase sensitivity to neutralising antibodies in some cases without affecting viral infectivity (Wang et al., 2013).

There is also a large body of work surrounding the glycosylation observed in the hemagglutinin (HA) protein of influenza. N-linked glycosylation has been shown to influence both virulence and antigenicity of influenza strains, as well as affecting viral replication *in vitro* (Baigent and McCauley, 2001, Sun et al., 2013). Removal of specific glycosylation sites in HA has been shown to increase the virulence of influenza in infected mice as well as increasing resistance to virus neutralisation (Reading et al., 2009), highlighting the

importance of individual sites as well as the overall levels of glycosylation in the protein. HA glycosylation is also implicated in the mechanisms of virus escape, exhibited by influenza viruses under immune pressures. In this case it is the addition of glycosylation sites that contributes to the distortion or masking of epitopes required for antibody recognition and neutralisation (Zhu et al., 2015, Ping et al., 2008).

The involvement of N-linked glycosylation on the surface of viral proteins is known to contribute to the interactions between the viral protein and the components of the immune system. In HIV-1 gp120, neutralising epitopes are masked by the presence of N-linked glycans, thus providing a mechanism for immune escape (Wolk and Schreiber, 2006). In other viruses, such as classical swine fever virus (CSFV), removal of glycans from the envelope glycoproteins can reduce antibody interactions with specific epitopes resulting in reduced neutralisation, perhaps due to improper protein folding (Gavrilov et al., 2011). Changes in the glycosylation patterns of viral proteins can also interfere with receptor interactions and render the proteins more susceptible to targeting and recognition by various components of the host immune pathways. This is thought to be as a result of changes in the way epitopes are displayed or shielded from recognition by antibodies.

The removal of glycans on the surface of the glycoprotein of lymphocytic choriomeningitis virus (LCMV), an arenavirus, was shown to result in an altered cellular tropism and overall viral fitness in neurons and macrophages, where the deletions led to increased viral replication in one and decreased replication in the other. Addition of glycans onto the already glycosylated protein resulted in reduced viral fusion, highlighting the balance required to achieve optimal protein function (Bonhomme et al., 2013).

1.10 Coronavirus S glycoprotein glycosylation

The coronavirus S glycoprotein exhibits an extremely high level of N-linked glycosylation, similar to what is observed in the HIV gp120 envelope glycoprotein (Binns et al., 1985). Other

viral proteins including the M protein in coronaviruses exhibit some level of glycosylation which may either be N- or O-linked (where the oligosaccharide is attached to a specific oxygen molecule as opposed to an asparagine). The SARS-CoV 3a protein is also known to be O-glycosylated (Oostra et al., 2006). While the most common form of glycosylation among the S glycoproteins of coronaviruses is N-linked, MHV S primarily exhibits O-linked glycosylation, with a very low level of N-linked sites present in some of the strains. (Yamada et al 2000).

Glycosylation in the IBV S glycoprotein is exclusively N-linked. High numbers of potential glycosylation sites have been identified in a variety of coronaviruses (reviewed by Belouzard et al. 2012). The glycosylation observed in these proteins is thought to contribute to a number of processes during virus infection. Interactions between the SARS-CoV S protein and surface lectin molecules have been identified as an alternative entry mechanism (Jeffers et al., 2004, Han et al., 2007). These interactions suggest an important role for spike glycosylation in the mechanisms of vial entry. In the *Alphacoronavirus* TGEV, the glycan composition on the surface of the S and M proteins contributes to conformational changes that influence the antigenicity of these two viral proteins (Delmas and Laude, 1991).

Glycosylation contributes to the overall structure and folding of viral proteins and as such can be utilised by the virus to mask specific epitopes recognised by neutralising antibodies during infection, as observed in HIV-1 infections. The dense glycan shield of the coronavirus S glycoprotein has been investigated in this context using cryo-EM techniques to model the structure of the protein and to elucidate epitopes obscured by the presence of oligosaccharides on the surface of the protein (Walls et al., 2016b).

As with related coronaviruses, the structure and function of the glycan shield in IBV is beginning to be elucidated. Recent studies have identified a high density of glycans on the surface of the IBV S protein (Shang et al., 2018). The role of individual glycans has also been

assessed in certain strains, indicating possible functions in cell-cell fusion during *in vitro* replication (Zheng et al., 2018). Although the role of glycosylation in the context of *in vivo* infection is yet to be defined for IBV, differences between the predicted glycosylation profiles of certain strains have been identified, suggesting a possible correlation between these differences and variations in pathogenicity (Abro et al., 2012).

1.11 IBV pathogenicity factors and determinants

The molecular basis of IBV pathogenesis is not well characterised. Reverse genetics systems have been developed to study the role of specific genes in pathogenicity. A variety of methods are employed to modify the IBV genome, including the use of vaccinia virus (VV) as a vector for the IBV genome (Casais et al., 2001). Others use targeted RNA recombination to produce recombinant viruses (van Beurden et al., 2017).

Pathogenicity in IBV and other coronaviruses is a multifactorial process, with many viral genes implicated in the development of disease. Using a variety of reverse genetics systems, the involvement of various individual genes in viral pathogenicity has been investigated. The replicase gene has been implicated in determining IBV pathogenicity through generation of a chimeric virus containing the replicase gene of the Beaudette strain and the structural and accessory genes of M41. The resultant recombinant virus was non-pathogenic in chickens, implying that the replicase gene was responsible for the attenuation (Armesto et al., 2009). The S gene has been identified as a virulence factor in MHV and has also been implicated in hepatotropism (Phillips et al., 1999). Modifications at specific sites in the S gene of TGEV have been shown to reduce pathogenicity, again indicating an important role for this gene in pathogenesis (Bernard and Laude, 1995). However there has been some contention surrounding the involvement of the IBV S gene in pathogenicity, with previous studies showing that the ectodomain of a heterogeneous strain of IBV was not sufficient to alter the

pathogenicity of the attenuated Beaudette strain (Armesto et al., 2011, Hodgson et al., 2004).

1.12 Infectious bronchitis (IB)

The disease caused by IBV is known as infectious bronchitis (IB), affecting both commercial and back-yard flocks worldwide. The disease was first observed in chicks in the 1930s as a respiratory disease of unknown origin (Schalk and Hawn, 1931). IBV was later identified as the aetiological agent and since then the virus has been detected in countries across the world, with new variants constantly emerging (de Wit et al., 2011).

IB manifests primarily as respiratory disease, characterised by clinical symptoms including snicking (sneezing), rales, watery eyes and lethargy. The primary site of IBV replication in infected birds is the epithelial cells of the trachea. This leads to damage to the cilia that line the organ, resulting in cessation of ciliary activity or ciliostasis. Consequently, secondary bacterial infection is a major problem following IB and is the reason for most of the mortality associated with the disease (Cavanagh and Naqi, 2003).

In addition to respiratory disease, some strains are known to cause extensive pathology in the kidneys and oviducts of infected birds. Examples of this pathology are noted during infection with the QX strain of IBV, where infection causes fluid retention in the oviduct, leading to extreme swelling and a characteristic “penguin-like” stance in affected birds. IBV QX was first identified in the Qingdao region of China in 1996 after an outbreak of disease characterised by swelling of the stomach and oviducts (YuDong et al., 1998).

As a result of the clinical symptoms of infection, IBV-infected broiler birds are prone to reduced weight gain and poorer meat quality. Affected laying birds produce fewer eggs and those that are produced are of lower quality, with soft shells and watery albumen. These clinical manifestations cause significant economic losses in the poultry industry worldwide.

IB is now the number one cause of infectious disease related loss in the poultry industry, with an economic burden of approximately £23million in the UK alone (DEFRA Report 2005).

1.13 IBV vaccination strategies

The vaccine industry for poultry production is worth upwards of $1billion, with the market for IBV vaccines comprising $350million alone. It is estimated that a 10% reduction in productivity as a result of IBV infection costs the global poultry industry £654million (Animal and Veterinary Vaccines Report, Markets and Markets 2017). Control of IBV is therefore essential in protecting both animal welfare and global food security.

Live-attenuated vaccines are the most common method currently used to control IBV in commercial flocks. Inactivated or killed vaccines are used to a lesser extent and do not show the same levels of protection induced by live-attenuated vaccines. The most frequently used vaccine strains are derived from the Massachusetts serotype and include the H120 and H52 strains, both originating from the Netherlands (Bijlenga et al., 2004). Protection offered by these vaccines is often short-lived and due to the ever-emerging new IBV serotypes, cross-protection between strains is inadequate (Cook et al., 2012). As result, individual birds are likely to require multiple vaccines on multiple occasions during their short life-span.

Generation of the vaccine strains is currently achieved through extensive serial passage in embryonated hens' eggs. The process is lengthy and the mechanism of attenuation is largely undefined, highlighting the need for efficient, more targeted vaccine design. In addition, the process itself is quite inefficient, producing different vaccines in each batch. Achieving sufficient attenuation while retaining immunogenicity is also based entirely on trial and error, adding to overall inefficiencies (reviewed by Jordan, 2017).

Numerous recombinant viruses have been investigated as an alternative method for vaccine generation, with the recombinant vaccines inducing protective immunity against IBV

challenge, including some expressing antigens from other pathogens (Yang et al., 2016, Wei et al., 2014). While the S gene has been the primary focus of vaccine development due to its immunogenic nature, some novel recombinant viruses with mutations elsewhere in the genome have been shown to induce protection. Deletions in the accessory genes in recombinant vaccine candidates are attenuated *in vivo* while still conferring protection against challenge (van Beurden et al., 2018). Further research is required to fine tune the process of generating sufficiently attenuated viruses which are still capable of inducing a protective immune response.

1.14 Thesis Aims and Objectives

1. **Characterise the glycosylation profile of the S protein of IBV.**

   Objective 1: Use bioinformatics to identify potential glycosylation sites in the sequences of IBV S genes. Confirm glycosylation at these sites using mass spectrometry.

   Objective 2: Use deglycosylating enzymes and cellular inhibitors to identify glycan classes on the protein surface and assess their molecular weights through western blot. Assess the effects of glycosylation inhibition on viral replication *in vitro*.

   Objective 3: Use reverse genetics to generate a recombinant virus with mutated glycosylation sites in the S glycoprotein. Characterise the virus *in vitro* to assess effects on replication and virus neutralisation.

2. **Use reverse genetics to investigate the role of the S protein in pathogenicity.**

   Objective 1: Use reverse genetics to insert the S gene from a non-pathogenic strain of IBV into the genome of a pathogenic strain. Characterise the virus *in vitro* to assess changes in replication and tropism.

   Objective 2: Characterise the pathogenesis of the recombinant virus *in vivo*. Assess induction of clinical signs and ciliostasis. Use PCR to assess viral dissemination.

3. **Assess the effects of gene replacement on IBV pathogenicity.**

   Objective 1: Use reverse genetics to insert the S gene from a pathogenic strain of IBV into the genome of a heterologous pathogenic strain. Rescue the virus in cells and characterise its replication patterns *ex vivo*.

   Objective 2: Assess the pathogenicity of the recombinant virus *in vivo*. Examine induction of clinical signs and ciliostasis and virus dissemination using PCR.

4. **Explore the cellular factors required for IBV infection.**

Objective 1: Use exogenous trypsin to explore the potential for IBV infection in non-permissive cells.

Objective 2: Use recombinant viruses to assess the role of the S protein in temperature sensitivity.

Chapter 2: Materials and Methods

2.1 Cell culture medium

Table 2.1 CK cell culture medium

Ingredient	*Volume*	*Final concentration*	*Supplier and catalogue number*
1XEagle's minimum essential medium (EMEM)	500ml	1X	Sigma-Aldrich, M2279
New-born bovine serum (NBBS)	50ml	10% v/v	Sigma-Aldrich, N4762
4-(2-hydroxyethyl)-1-piperazineethanesulphonic acid (HEPES) 1M, pH 7.0-7.6	5ml	1% v/v	Sigma-Aldrich, H0887
Penicillin/Streptomycin Solution (Pen/Strep)	1ml	Penicillin 10,000U Streptomycin 10mg	Sigma-Aldrich, P4333
Nystatin	2.5ml	25,000U	Sigma-Aldrich, N1638

Table 2.2: 1X N,N-bis[2-hydroxethyl]-2-Aminoethanesulfonic acid (BES) medium for culture of IBV in CK, DF-1 and Vero cells:

Ingredient	*Volume*	*Final concentration*	*Supplier and catalogue number*
10X EMEM	50ml	1X	Sigma-Aldrich, M0275
Tryptose phosphate broth (TPB)	50ml	10% v/v	Sigma-Aldrich, T8159
Bovine serum albumin (BSA)	10ml	2% v/v	Sigma-Aldrich, A7906
BES (1M)	10ml	20 mM	Sigma-Aldrich, B9879
Sodium bicarbonate ($NaHCO_3$) – 7.5%	14ml	0.2% v/v	Sigma-Aldrich, S8761
L-Glutamine	5ml	2 mM	Sigma-Aldrich, G7513
Nystatin	2.5ml	25,000U	Sigma-Aldrich, N1638
Pen/Strep	0.5ml	Penicillin 10,000U Streptomycin 10mg	Sigma-Aldrich, P4333
H_2O	358ml	------	The Pirbright Institute Type II Endotoxin Free

Table 2.3: 2XBES for use in IBV plaque assays

Ingredient	*Volume*	*Final concentration*	*Supplier and catalogue number*
10X EMEM	100ml	1X	Sigma-Aldrich, M0275
TPB	100ml	20% v/v	Sigma-Aldrich, T8159
BSA	20ml	4% v/v	Sigma-Aldrich, A7906
BES	20ml	40 mM	Sigma-Aldrich, B9879
$NaHCO_3$ (7.5%)	28ml	0.4% v/v	Sigma-Aldrich, S8761
L-Glutamine	5ml	2 mM	Sigma-Aldrich, G7513
Nystatin	2.5ml	25,000U	Sigma-Aldrich, N1638
Pen/Strep	1ml	Penicillin 10,000U Streptomycin 10mg	Sigma-Aldrich, P4333
H_2O	218.5ml	----	The Pirbright Institute Type II Endotoxin Free

Table 2.4: Tracheal organ culture (TOC) growth medium

Ingredient	*Volume*	*Final concentration*	*Supplier and catalogue number*
1XEMEM	500ml	1X	Sigma-Aldrich, M2279
HEPES	20ml	1% v/v	Sigma-Aldrich, H0887
Pen/Strep	1ml	Penicillin 10,000U Streptomycin 10mg	Sigma-Aldrich, P4333
Nystatin	2.5ml	25,000U	Sigma-Aldrich, N1638
L-Glutamine	5ml	2mM	Sigma-Aldrich, G7513

Table 2.5: BHK-21 cell maintenance medium

Ingredient	*Volume*	*Final concentration*	*Supplier and catalogue number*
1XGlasgow MEM (GMEM)	500ml	1X	Sigma-Aldrich, G5154
Foetal bovine serum (FBS)	5.5ml	1% w/v	Sigma-Aldrich, F0926
TPB	55ml	10%	Sigma-Aldrich, T8159

Table 2.6: 1XGMEM for vaccinia virus (VV) infection of BHK-21 cells

Ingredient	*Volume*	*Final concentration*	*Supplier and catalogue number*
1XGMEM	500ml	1X	Sigma-Aldrich, G5154
FBS	5.5ml	1% w/v	Sigma-Aldrich, F0926
TPB	55ml	10% v/v	Sigma-Aldrich, T8159
Pen/Strep	0.5ml	Penicillin 5000U Streptomycin 5mg	Sigma-Aldrich, P4333
Nystatin	2.5ml	25,000U	Sigma-Aldrich, N1638
L-Glutamine	5ml	2mM	Sigma-Aldrich, G7513

Table 2.7: 1XEMEM for VV plaque purification in Vero cells

Ingredient	*Volume*	*Final concentration*	*Supplier and catalogue number*
10XEMEM	50ml	2X	Sigma-Aldrich, M0275
FBS	25ml	10% v/v	Sigma-Aldrich, F0926
$NaHCO_3$ (7.5%)	12.5ml	0.4% v/v	Sigma-Aldrich, S8761
Pen/Strep	1ml	Penicillin 10,000U Streptomycin 10mg	Sigma-Aldrich, P4333
Nystatin	2.5ml	25,000U	Sigma-Aldrich, N1638
H_2O	409ml	-----	The Pirbright Institute Type II Endotoxin Free

Table 2.8: 2XEMEM for VV plaque purification in Vero cells

Ingredient	*Volume*	*Final concentration*	*Supplier and catalogue number*
10XEMEM	100ml	2X	Sigma-Aldrich, M0275
FBS	50ml	10%	Sigma-Aldrich, F0926
$NaHCO_3$ (7.5%)	23ml	0.4%	Sigma-Aldrich, S8761
Pen/Strep	1ml	Penicillin 10,000U Streptomycin 10mg	Sigma-Aldrich, P4333
Nystatin	2.5ml	25,000U	Sigma-Aldrich, N1638
H_2O	311ml	-----	The Pirbright Institute Type II Endotoxin Free

2.2 Cells and eggs

All cells were provided by the Microbiological Services Unit at The Pirbright Institute (Compton Laboratory) or the Central Services Unit at The Pirbright Institute (Pirbright Laboratory).

2.2.1 Primary chick kidney (CK) cells

Chick kidney (CK) cells were prepared from 2-3 week old specific pathogen-free (SPF) Rhode Island Red (RIR) chickens using manual and trypsin disaggregation. CK cells were prepared and grown in CK growth medium (Table 2.1) and 1xBES medium (Table 2.2) during infections.

2.2.2 Continuous cell lines

- DF-1 cells are a continuous line of chicken embryo fibroblasts derived from 10 day old East Lansing eggs (Himly et al., 1998). Cells were maintained in Dulbecco's modified essential medium (DMEM, Sigma) supplemented with 10% FBS unless otherwise stated.
- Vero cells are a kidney epithelial cell line derived from the African green monkey. These cells were maintained in EMEM (Sigma) supplemented with 10% FBS.
- Baby hamster kidney (BHK-21) cells are a cell line originally derived from 1 day old Syrian golden hamster kidneys and were maintained in BHK-21 cell maintenance medium or 1xGMEM (Table 2.6) during infection.

2.2.3 Embryonated eggs

VALO embryonated hens' eggs (SPF) were delivered from VALO BioMedia GmbH and infected with IBV at 10 days old. SPF RIR eggs were provided by the Poultry Production Unit (PPU) at the Pirbright Institute, Compton Laboratory (2014-2015) and by the National Avian Research Facility (NARF) in Edinburgh (2015-2018).

2.3 Viruses

Stocks of IBV were grown in embryonated hens' eggs.

2.3.1 IBV Strains:

- **M41-CK**: pathogenic laboratory-adapted strain serially passaged in chick kidney cells (unknown number), replicates in CK cells, TOCs and embryonated eggs but not in continuous cell lines.
- **M41-K:** Recombinant molecular clone of M41-CK, pathogenic, replicates in CK cells, TOCs and embryonated eggs but not in continuous cell lines.
- **M41-R:** Recombinant molecular clone of M41-CK, non-pathogenic due to four point mutations in nsp10, 14, 15 and 16. Replicates in primary CK cells, TOCs and embryonated eggs but not in continuous cell lines.
- **Beau-R:** Recombinant molecular clone of Beau-CK, non-pathogenic lab strain, replicates in CK cells, continuous avian cells (DF-1) and continuous mammalian cells (Vero) due to an extended host tropism (Casais et al., 2001, Bickerton et al., 2018)
- **QX L1148A:** Pathogenic field strain originating from a Chinese isolate, infects oviducts *in vivo* causing fluid retention and penguin like stance in infected chickens. Obtained as a gift from Prof. Richard Jones, University of Liverpool (Worthington et al., 2008). Does not replicate in cell culture, only in tracheal organ cultures and embryonated eggs.
- **4/91:** Pathogenic field strain originating in the UK, also known as 793B. Obtained as a gift from Intervet, UK. Does not replicate in cell culture, only in tracheal organ cultures and embryonated eggs.

2.3.2 Fowlpox virus (FPV)

- Stocks of FPV expressing the T7 RNA polymerase (FPV-T7) were propagated in chicken embryo fibroblast (CEF) cells.

2.3.3 Vaccinia viruses

- **rVV M41K-delS:** a recombinant VV containing the entire M41-K genome cDNA with the S gene deleted.
- **rVV M41K-delS1:** a recombinant VV containing the entire M41-K genome cDNA with the gene encoding the S1 subunit deleted.

2.4 Infection of embryonated hens' eggs with IBV

Prior to infection with IBV, 10 day old embryonated hens' eggs were candled using a lamp to check general embryo health. The air sac was marked using pencil and a small hole was drilled into the shell using a Bosch Dremel Engraver drill approximately 1cm above the air sac. Each egg was inoculated with 100 - 300µl of IBV using a 1ml syringe and a 25G needle. Post-inoculation the inoculation site was cleaned with 70% ethanol (in H_2O) and the hole was sealed with nail varnish. Infected eggs were incubated at 37˚C for 24-48hrs depending on the predicted lethality of the virus. Embryos were monitored regularly by candling during this time to assess any decline in health. Eggs were chilled at 4˚C for at least 4 hours to cull the embryo before allantoic fluid was harvested. Allantoic fluid from the infected eggs was clarified by centrifugation at 500 x g for 5 minutes before storage at -80˚C.

2.5 Ultracentrifuge purification of IBV

IBV was purified by ultracentrifugation into a sucrose gradient (30-60%). At least 400ml of IBV-infected allantoic fluid was clarified by centrifugation at 1,200 x g for 15 minutes. The supernatant was layered onto a 30% sucrose cushion and centrifuged at 130,000 x g for 2 hours. Supernatant was discarded and the pellet covered in 100µl phosphate buffered saline (PBS, supplied by Central Services Unit at The Pirbright Institute, recipe in Table 2.9). The pellet was left at 4˚C overnight. A 30-60% sucrose gradient was prepared using a gradient

maker and the pellet was added to the surface of the gradient before centrifugation at 130,000 x g for 2 hours. After centrifugation, the top layers of sucrose were removed by pipetting and the band of virus was pipetted into another tube. The band was added to 30ml PBS, layered onto a 30% sucrose cushion and centrifuged at 130,000 x g for 2 hours. PBS and sucrose were discarded and the pellet was re-suspended in 100µl PBS containing 0.01% sodium azide (NaN_3).

Table 2.9: 1X Phosphate buffered saline (PBS) solution, provided by Central Services Unit at The Pirbright Institute

Ingredient	***Final Concentration***
Sodium chloride	137mM
Disodium phosphate	4.3mM
Monopotassium phosphate	1.47mM
Potassium chloride	2.7mM
H_2O	(Dissolved in 8L)

2.6 Glycosylation inhibitors and deglycosylation enzymes

Kifunensine (Kif) (α-mannosidase I inhibitor, Sigma) stock solutions were prepared in PBS at 2mM and diluted in 1xBES for use during infection. Initial stocks were donated as a gift from Dr Simon Spiro. Kif was used at 20µM, diluted in 1XBES and added at the time of infection.

Swainsonine (SW) (α-mannosidase II inhibitor, Sigma) stock solutions were prepared in methanol (MeOH) at 1mg/ml and diluted to appropriate concentrations in 1xBES for use during infection.

Endoglycosidase H (Endo H) and Peptide-N-Glycosidase F (PNGase F, New England Biolabs) digests were prepared as per the manufacturer's instructions using purified M41-CK or Beau-R and incubated at 37˚C for 1 hour. Digests were analysed by SDS-PAGE followed by western

blot (WB) using a monoclonal antibody against the S2 subunit of the S protein (26.1, Priomab). Digestion was confirmed by observation of a band shift compared to undigested samples.

2.7 CellTiter-Glo cell viability assay (Promega)

2.7.1 Inhibitor treatments

Cells were seeded in clear-bottomed 96 well plates with opaque sides and used at 80-90% confluency. Cells were washed once in PBS and appropriate media containing a range concentrations of Kif or SW was added to each well. Cells were incubated at 37°C. CellTiter-Glo (CTG) reagents were added to cells as per the manufacturer's instructions and data was generated using a GloMax plate reader.

2.7.2 Temperature sensitivity

Cells were seeded as described above. Confluent monolayers of cells were washed once in PBS and incubated at 37°C or 41°C. CTG reagents were added and data was generated as described above.

2.8 RNA extraction and Reverse Transcription (RT)

RNA from supernatant or allantoic fluid was extracted using QIAGEN RNeasy mini kits (based on column chromatography) following the RNA clean-up protocol according to the manufacturer's instructions. RNA was eluted from columns in 35µl RNAse free water and stored at -20˚C.

RNA from infected tissues was extracted according to the RNA clean-up protocol in the QIAGEN RNeasy mini-kit, following homogenisation in a TissueLyser II using a metal bead. Tissues were added to 500µl PBS and homogenised for 2-4 minutes until completely homogenous. Homogenised solutions were centrifuged for 3 minutes at 10,000 x g in a

benchtop refrigerated micro-centrifuge and 170µl of the supernatant was used for RNA extraction. The remainder was stored at -80°C and the pellets were discarded.

cDNA was generated by reverse transcription (RT) using SuperScript III or IV (SSIII, SSIV, Invitrogen), according to manufacturer's instructions. The thermocycler programs for use with SSIII and SSIV are detailed in Tables 2.10 and 2.11.

Table 2.10: SuperScript III thermocycler program

Temperature	***Time***
25°C	10 minutes
50°C	60 minutes
70°C	15 minutes
18°C	Hold

Table 2.11: SuperScript IV thermocycler program

Temperature	***Time***
23°C	10 minutes
55°C	10 minutes
80°C	10 minutes
18°C	Hold

2.9 Polymerase chain reaction (PCR)

PCR was performed using *Taq* DNA polymerase (Invitrogen, product number 10342020) according to manufacturer's instructions. The recipe for a standard PCR is detailed in Table 2.12 and the thermocycler program in Table 2.13. Primers are detailed in Table 2.14.

Table 2.12: Standard PCR recipe

Reagent	*Volume*	*Final concentration*
10X PCR Rxn Buffer	5µl	1X
$MgCl_2$	2µl	2mM
dNTPs	1µl	0.2mM
(+) primer	1µl	0.2 pmol
(-) primer	1µl	0.2 pmol
***Taq* DNA polymerase**	0.5µl	2.5U
Template DNA	5µl	---
Nuclease free H_2O	34.5µl	---

Table 2.13: Standard PCR Cycle

Temperature	*Time*	*Number of cycles*
95°C	3 mins	1
95°C	45 seconds	25
Annealing temp	30 seconds	
72°C	Varied	
72°C	5 mins	1
18°C	Hold	1

Table 2.14 Oligonucleotides (custom synthesised by Sigma-Aldrich):

Name	*Sequence*	*Target region*
BG56 (5′ - 3′)	CAACAGCGCCCAAAGAAG	3' UTR
BG93/100 (3′ - 5′)	GCTCTAACTCTATACTAGCCT	3' UTR
BG42 (5′ - 3′)	AATAATGGCAATGATGAC	S1
BG46 (5′ - 3′)	CATCAAAATCACTAATGG	S2
BG136 (3′ - 5′)	AACTGCCACAAACATACTGC	S1
BG142 (3′ - 5′)	AGGGATCAAATACTTCTGTG	S2
M20 (5′ - 3′)	GGAATGGGCATAATAAGG	Nsp10
M23 (3′ - 5′)	CGGGTACGGGGTAGCAGTG	Nsp10
4/91 2+ (5′ - 3′)	TGCCTTTAGGCCTGGTCAAG	4/91 S
4/91 7- (3′ - 5′)	TTCAAAGTATTGCGTTAGCT	4/91 S
GPT F (5′ - 3′)	ATGAGCGAAAAATACATCGTC	GPT selection marker
GPT R (3′ - 5′)	TTAGCGACCGGAGATTGGC	GPT selection marker
Random primer	GTTTCCCAGTCACGATCNNNNNNNNNNNNNN	----

2.10 Sanger sequencing

PCR products were generated using specific primers and the products were sent to Source Bioscience (Nottingham) for Sanger sequencing, as per the service provider's requirements. 4µl of PCR product was added to 20µl of H_2O. Stock solutions (10µM) of forward and reverse primers were diluted 1:1 with H_2O and sent separately alongside the diluted PCR product. Sequencing reads were processed and analysed using Staden Sequence Analysis Package (Staden, 1996). Alignments were generated using BioEdit (Hall, 1999).

2.11 NetNGlyc Server Prediction

S gene consensus sequences generated by RT-PCR and Sanger sequencing were entered into the NetNGlyc 1.0 Server to identify potential N-linked glycosylation sites (PNGS). Predictions were made based on the server's algorithms to provide a ranking of the sites most likely to be glycosylated at the identified asparagine residues. Scores above 0.5 generally indicate true glycosylation sites.

2.12 Reverse genetics using vaccinia virus (VV)

Recombinant IBVs were generated using a well-established reverse genetics system based on vaccinia virus (VV) (Casais et al., 2001, Britton et al., 2005). The first stage is homologous recombination between a recombinant VV and a plasmid containing the *gpt* gene and viral gene sequence containing the desired modification. This is followed by six rounds of plaque purification before DNA extraction in preparation for rIBV rescue. The entire process is described in Figure 2.1.

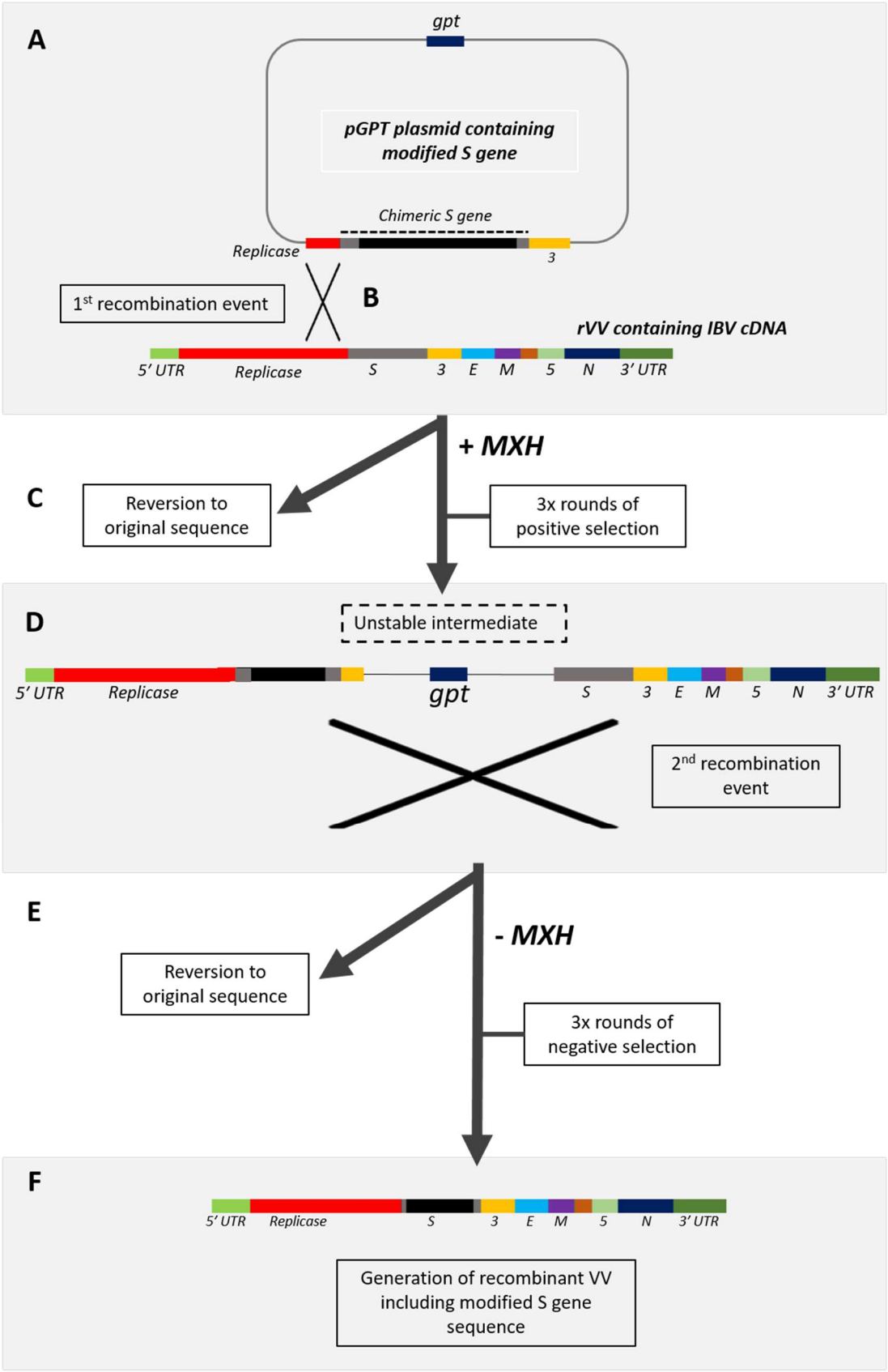
A
gpt
pGPT plasmid containing modified S gene
Chimeric S gene
Replicase
3
1st recombination event
B
rVV containing IBV cDNA
5' UTR
Replicase
S
3
E
M
5
N
3' UTR
C
+ MXH
Reversion to original sequence
3x rounds of positive selection
D
Unstable intermediate
5' UTR
Replicase
gpt
S
3
E
M
5
N
3' UTR
2nd recombination event
E
- MXH
Reversion to original sequence
3x rounds of negative selection
F
5' UTR
Replicase
S
3
E
M
5
N
3' UTR
Generation of recombinant VV including modified S gene sequence

Figure 2.1: Reverse genetics process for generation of recombinant IBVs (rIBVs). (A) Cells were infected with an rVV containing the rIBV M41-K cDNA and transfected with a vector containing the *gpt* gene and the desired sequence for insertion/mutation. **(B)** The first homologous recombination event between the IBV cDNA and the pGPT vector occurred due to the presence of identical flanking regions. **(C)** Selection for successful recombination events was achieved through three rounds of plaque purification in the presence of selection agents MPA, Xanthine and Hypoxanthine (MXH). **(D)** This resulted in the generation of an unstable intermediate rVV, containing the *gpt* gene between repeat sequences in the IBV cDNA. **(E)** The rVVs were then subjected to three rounds of plaque purification in the absence of selection agents (MXH), inducing a second recombination event and loss of the *gpt* gene but retention of the insertion/mutation, as a result of recombination between the repeat sequences. **(F)** Following the six rounds of plaque purification, ministocks were generated in Vero cells and each isolate was screened to check for the correct insertion and to verify the loss of the *gpt* gene. DNA was extracted from large stocks of rVV and used for virus rescue in CK cells, with the addition of rFPV-T7 and a plasmid expressing the IBV N gene.

2.12.1 pGPTNEB193 vectors

The first stages of the reverse genetics process used a plasmid containing the guanine phosphoribosyl transferase (*gpt*) gene, which allows purine synthesis by an alternative pathway in the presence of xanthine and hypoxanthine. The plasmid also contained either the Beaudette S2 subunit sequence or the sequence of the ectodomain of the 4/91 S protein.

pGPTNEB193 vectors were designed to include recombinant S genes to generate rIBVs M41K-BeauR(S) and M41K-4/91(S). DNA sequences were synthesised and cloned into pGPTNEB193 by GeneArt and used for homologous recombination. Two vectors were used for the generation of rIBVs M41K-BeauR(S) and M41K-4/91(S): pGPT-M41-BeauR-S1 and pGPT-M41-4/91-S, respectively.

2.12.2 Homologous recombination:

The first recombination event occurs between the pGPT plasmid and repeat sequences in the rVV (Figure 2.1A and B). Recombinant VV containing M41-K cDNA with a deletion or modification in the S gene (rVV M41K-del-S or rVV M41K-delS1-BeauR-S2) was sonicated for 2 minutes (70% amplitude) and diluted in 500µl of EMEM to an approximate multiplicity of infection (MOI) of 0.2. Semi-confluent (50-60%) monolayers of Vero cells were infected with rVV M41K-del-S in duplicate and incubated for 2 hours at 37°C (5% CO_2). After washing twice in OPTIMEM (Invitrogen), cells were transfected with 10µg of the relevant pGPT vector using Lipofectin (Life Technologies) as per the manufacturer's instructions. Transfected cells were incubated at 37°C for 1 hour after which transfection solution was replaced with 1xEMEM (5ml). Cells were incubated at 37°C overnight. Selection agents (75µM mycophenolic acid (MPA), 165µM Xanthine, 184µM Hypoxanthine; MXH) were added to each well and cells were incubated at 37°C for a further 48 hours. After incubation, cells were scraped into the supernatant and harvested before storage at -20°C in a screw-cap vial.

2.12.3 Transient dominant selection (TDS) by plaque purification

Confluent monolayers of Vero cells were infected with 500µl of sonicated rVV containing the desired rIBV cDNA diluted in 1xEMEM (10^{-1}, 10^{-2} and 10^{-3}). Cells were incubated for 1-2 hours at 37˚C. Virus inoculum was removed and replaced with 3 ml per well of an overlay solution of 1xEMEM containing 1% agar and selection agents MXH (Table 2.15). Overlay was left to set before cells were incubated at 37˚C for 72 hours. Cells were stained with 2ml per well of 1xEMEM/1% agar overlay containing 0.01% Neutral Red and incubated for a further 24 hours at 37˚C until plaques were visible in the monolayer. Three plaques per virus isolate were picked using a cut pipette tip and added to 400µl of 1xEMEM. Each plaque was sonicated and used to repeat the plaque purification process three times in the presence of MXH (Figure 2.1C) and then 3 times in the absence of MXH (Figure 2.1E).

Table 2.15: Overlay medium containing MXH selection agents

Ingredient	***Final concentration***	***Supplier and catalogue number***
2xEMEM	1X	See Table 2.8
2% Agar (in H_2O)	1% w/v	Sigma-Aldrich, A9539
Mycophenolic acid (MPA)	75µM	Sigma-Aldrich, M3536
Xanthine Sodium Salt (X)	165µM	Sigma-Aldrich, X3627
Hypoxanthine (H)	184µM	Sigma-Aldrich, H9636

2.12.4 Generation of rVV ministocks in Vero cells

Confluent monolayers of Vero cells were infected with the final plaques from the TDS process. Plaques were sonicated for 2 minutes and 150µl of supernatant was added to the cells with 350µl 1xBES. Infected cells were incubated at 37˚C for 2 hours before 2.5ml of 1xBES was added to each well. Cells were incubated at 37˚C for 72 hours or until cytopathic

effect (cpe) was observed. Cells were scraped into supernatant and centrifuged at 5000 x g for 5 minutes. Supernatant was discarded and cell pellets were re-suspended in 700µl 1xBES. DNA was extracted from 200µl of each ministock following the DNA extraction from blood and tissue samples protocol in the QIAGEN DNA Extraction Kit according to the manufacturer's instructions. DNA was eluted in 200µl nuclease-free H_2O. PCR was carried out using primers covering the *gpt* gene to ascertain which ministocks had lost the selection marker. A second PCR was carried out using primers covering the S gene (Table 2.13) to verify that the insertion was correct (Figure 2.1E). Any ministocks with the correct insert which were negative for *gpt* presence were selected for generation of large stocks in BHK-21 cells.

2.12.5 Generation of large stocks in BHK-21 cells

rVV ministocks were diluted 1:200 in 1xGMEM and 2ml was used to infect BHK-21 cells seeded in T150 tissue culture flasks. Cells were washed once in PBS. Cells were incubated at 37˚C for 2 hours before addition of 18ml of 1xGMEM to each flask. Flasks were incubated at 37˚C until cells had completely detached from the surface of the flask (approximately 72 hours). Supernatant and cells were pooled for each rVV and centrifuged at 500 x g for 15 minutes. Supernatant was discarded and pellets re-suspended in 2ml Tris-EDTA (TE) buffer (Table 2.16) per flask and stored at -20˚C.

Table 2.16: Tris-EDTA (TE) buffer, pH 9

Ingredient	***Final concentration***
Tris-HCl (pH 9)	10mM
EDTA (pH 9)	1mM

2.12.6 Partial purification of rVV by ultracentrifugation

Cells were freeze-thawed (dry ice/37˚C) three times and sonicated for 2 minutes to ensure adequate cell lysis. Cell lysates were centrifuged at 500 x g for 10 minutes (4˚C) to remove

the nuclei. TE buffer (pH 9) was added to the supernatant to make up a total volume of 13ml. This was layered onto 16ml of a 30% sucrose solution (in TE buffer, pH 9) and centrifuged at 36,000 x g for 1 hour at 4˚C. Supernatant and sucrose were discarded and the pellet re-suspended in 5ml TE buffer (pH 9). Partially purified rVVs were stored at -20˚C.

2.12.7 Large-scale DNA extraction by phenol-chloroform

Partially purified rVVs were thawed and an equal volume (5ml) of Proteinase K buffer (Table 2.17) was added to each isolate along with 200µl of Proteinase K solution (Sigma, 20mg/ml). Solutions were incubated at 50˚C for 2.5 hours before DNA extraction by phenol-chloroform (Thermo Fisher). An equal volume of phenol-chloroform (10ml) was added to each sample and mixed thoroughly before centrifugation at 1,200 x g for 15 minutes. The upper aqueous phase was carefully transferred to a clean tube and the extraction was repeated once more to purify the DNA. A chloroform extraction was then performed where an equal volume of chloroform (Sigma-Aldrich/Merck) was added to the upper aqueous phase of the previous purification, mixed well and centrifuged for 15 minutes at 1,200 x g. Again, the upper aqueous phase of the solution was transferred to a fresh tube and 2.5 volumes of absolute ethanol (kept at -20˚C) and 0.1 volumes of 3M sodium acetate were added to precipitate the DNA. The solution was mixed by inversion and centrifuged at 2,300 x g for 45 minutes. Following centrifugation 10ml of 70% ethanol (in H_2O, kept at -20˚C) was added to the pellet and incubated on ice for 5 minutes in order to dissolve any salts before centrifugation at 2,300 x g for 45 minutes. The ethanol was carefully poured off and pellets were left to air-dry for 10 minutes. Excess ethanol present on the inside of the tube was removed using paper towel and pellets were dissolved in 100µl H_2O (nuclease-free). DNA was stored at 4˚C overnight then quantified using a Nanodrop 1000.

Table 2.17: 2X Proteinase K buffer

Ingredient	*Final concentration*
Tris-HCl (pH 7.5)	200mM
EDTA	10mM
SDS	0.4% w/v
NaCl	400mM

2.12.8 Pulsed field gel electrophoresis (PFGE) of rVV DNA

Approximately 1µg of rVV DNA was digested with *Sal*I (Invitrogen) according to the manufacturer's instructions. The quality of the DNA was assessed by pulsed-field gel electrophoresis (PFGE). A 1% agarose (Bio-Rad, molecular grade) gel was prepared using 0.5X TBE buffer (Thermo Fisher, 10X stock). Gel solutions were heated for 2 minutes in a microwave and set in 12.7 x 14cm frames on a level surface. Buffer (0.5X TBE) was added to the CHEF-DR-II gel tank with the cooling unit switched on and left to cool to 4˚C. Loading dye was added to the digested DNA and the sample was heated to 65˚C for 10 minutes. Each sample was loaded onto the gel using cut tips to avoid shearing the DNA. The gel was run under the following conditions: initial pulse time = 0.1S, final pulse time = 1S, duration = 6-16 hours, voltage (V) = 6.0 V/cm.

Following electrophoresis the gel was removed from the tank, placed in a 0.1µg/ml solution of ethidium bromide and incubated at room temperature on an orbital shaker for 30 minutes. The gel was washed in 400ml of H_2O (Sigma) and incubated for a further 30 minutes. After washing, the gel was visualised using a Bio-Rad Gel Doc EZ, according to the manufacturer's instructions.

2.12.9 Rescue of rIBVs in CK cells

Semi-confluent monolayers of CK cells seeded onto 6 well tissue culture plates were infected with a recombinant fowlpox virus expressing the bacteriophage T7 RNA polymerase (rFPV-T7) (Britton et al., 1996) at an MOI of 10 (500µl per well). Cells were incubated at 37˚C for 1 hour then washed twice with OPTIMEM (Life Technologies). Cells were transfected with 10µg of rVV DNA and 5µg of a plasmid expressing the IBV M41 N protein (pCi-Neo-M41-N). The N protein is expressed in complement as it required for the synthesis of new virions (Siu et al., 2008). The plasmid and rVV DNA were diluted in 1.5ml of OPTIMEM (per well) and then added to 30µl of Lipofectin in 1.5ml of OPTIMEM. Transfection solutions were added to the cells and then incubated overnight at 37°C.

Following incubation, transfection media was removed, and 5ml of 1x BES added. The cells were then incubated at 37°C until extensive rFPV cpe was observed; this usually occurred at 72 hours post-infection. Supernatant from each well was harvested and rFPV removed by filtering through a 0.22µm filter. Filtered supernatant was stored at -80°C. To determine whether rIBV was successfully rescued, rIBV M41K-BeauR(S) samples were serially passaged three times to increase viral titre. Confluent monolayers of CK cells were inoculated with 1ml of supernatant and incubated for 1 hour at 37°C followed by addition of 2ml of 1xBES. Cells were incubated for 48 hours at 37°C, until visible cpe was observed. The supernatant was removed and passaged a further two times. After the third passage, RNA was extracted from the viral samples and screened to confirm rescue of rIBV and to identify the presence of the desired mutation.

IBV 4/91 does not replicate in cell culture and so for rIBV M41K-4/91(S) isolates, rescue supernatant was discarded and 500µl 1xBES was added to each well and plates were freeze-thawed (-80˚/room temperature) in an attempt to lyse the cells and release the rIBV. After freeze-thaw, cells were scraped into the media and passed through a needle and syringe multiple times then filtered through a 0.22µm filter unit to remove the rFPV. The filtered cell

lysate was used to infect 10 day-old embryonated RIR eggs for passaging. Allantoic fluid was screened after each passage and stocks were generated at egg passage 2 (EP2).

2.13 Immunofluorescence (IF) staining for confocal microscopy

Cells were seeded onto glass coverslips in 24 well tissue culture plates, infected with IBV and incubated for 24 hours at either 37˚C or 41˚C after which they were washed once with PBS and fixed in a solution of 4% paraformaldehyde (PFA) in PBS for 20 minutes on an orbital shaker. Cells were washed again in PBS and permeabilised using 0.1% Triton X-100 in PBS for 10 minutes. Blocking solution consisted of 0.5% BSA in PBS and was also used to dilute primary and secondary antibodies. Cells were incubated in blocking solution for 1 hour then incubated in primary antibody for 1 hour. Primary antibody dilutions are listed in Table 2.17. Between primary and secondary antibody incubations, cells were washed 3 times in PBS for 5 minutes per wash. Cells were incubated in secondary antibody solutions (Invitrogen AlexaFluor 488/568, diluted 1/500 in blocking solution) for 1 hour under foil and washed a further 3 times before counterstaining with DAPI, diluted 1/10,000 in type II endotoxin free water, for 5 minutes. Cells were washed once in water before coverslips were mounted onto glass microscope slides using VectaShield mounting medium (Vector Labs) and sealed with nail varnish before imaging using a Leica confocal microscope.

Table 2.18 Primary antibodies

Antibody	***Target***	***Application***	***Dilution***	***Source***
A13	S1	IF	1/200	Mockett et al, 1984
Anti-S2 (26.1)	S2	IF/WB	1/500	Priomab
Anti-dsRNA (J2)	dsRNA	IF	1/1000	Scicons
Anti-β-actin	β-actin	IF/WB	1/1000	Cell Signalling Technologies
Anti-α-tubulin	α-tubulin	IF/WB	1/1000	Abcam
Chicken anti-IBV (polyclonal)	IBV	IF	1/500	Abcam

2.14 SDS-PAGE and western blot

2.14.1 Western blot using cell lysate:

Following infection with IBV as described previously, cells were washed once in cold PBS and 350µl of cold RIPA lysis buffer (Table 2.19) containing 1X protease inhibitor cocktail (PIC, Thermo Fisher) was added to each well. Cells were incubated on ice for 20 minutes before being scraped into the buffer using a cell scraper. Buffer and cells were centrifuged at 10,000 x g for 3 minutes to pellet cell debris. Cell lysate was mixed with Laemlli Sample Buffer (containing β-mercaptoethanol) at a ratio of 1:3 and heated to 80˚C for 10 minutes. 15µl of each sample was loaded onto a 4-20% Mini-PROTEAN TGX Precast protein gel (Bio-Rad) and run for 1 hour at 150V in running buffer (Table 2.20). Protein was transferred onto a nitrocellulose membrane using a Bio-Rad Trans Blot machine, according to the manufacturer's instructions. Membranes were incubated in blocking solution (5% milk powder (Marvel) in PBS containing 0.1% Tween-20 (PBS-T)) for 1 hour at room temperature or overnight at 4˚C. Primary antibodies were diluted in blocking solution and applied to membranes for 1 hour at room temperature. Primary antibody dilutions are listed in Table 2.18. Membranes were subjected to 3 x 5 minute washes in 0.1% PBS-T on an orbital shaker at room temperature. LI-COR secondary antibodies for western blot were diluted 1/15,000 in blocking solution and applied to membranes for 1 hour at room temperature. Membranes were washed in PBS-T three times followed by one wash in H_2O before visualisation on a LI-COR Odyssey Scanner following the protocol for western blot imaging according to the manufacturer's instructions.

Table 2.19 RIPA lysis buffer

Ingredient	*Final concentration*
Sodium chloride (NaCl)	5M
Trisaminomethane hydrochloric acid (Tris-HCl)	1M
Igepal	5% v/v
Sodium deoxycholate	5% w/v
Sodium orthanovate	1M
Sodium fluoride	1M
PIC (Thermo Fisher, 78430, 100X stock)	1X

Table 2.20 SDS-PAGE Running buffer

Ingredient	*Final concentration*
Tris-HCl buffer (pH 7.4)	247mM
SDS	34mM
Glycine	1.92M

2.14.2 Western blot using ultracentrifuge-purified IBV

For purified samples, 3µl of purified virus was mixed with 2µl of Laemlli Sample Buffer containing β-mercaptoethanol and heated to 80˚C for 10 minutes. Heated samples were loaded onto protein gels and processed for western blot as described above. It should be noted that the protein concentration in the purified virus samples was undetermined prior to western blot analysis.

2.15 Mass spectrometry (MS) methods: N-glycosylation mapping

Methods provided and performed by Stuart Armstrong (University of Liverpool)

2.15.1 Protein digestion

The purified IBV sample was diluted with 50mM ammonium bicarbonate (NH_4HCO_3). Proteins were reduced by the addition of dithiothreitol (Sigma) (3mM final) and heated at 60°C for 10 minutes. The samples were returned to room temperature, and iodoacetamide (Sigma) (9mM final) added for 30 minutes in the dark to alkylate the proteins. The sample was split and proteins were digested with either trypsin or chymotrypsin (Sigma) and left to incubate at 37°C overnight. The resulting peptide samples were then dried using a centrifugal vacuum concentrator (Eppendorf). Deglycosylation and $H_2{}^{18}O$ labelling was performed as described by Zhang *et al* (2016). Peptides were re-suspended in 50mM ammonium bicarbonate buffer prepared in $H_2{}^{18}O$ (97% ^{18}O, Sigma Aldrich). The peptide samples were split and PNGase F (Sigma) added to only one of the samples and incubated at 37°C for 2 hours. Samples were then acidified with trifluoroacetic acid (1% (v/v) final). Peptides were concentrated and desalted using C18 Stage tips (ThermoFisher Scientific) and then samples dried using a centrifugal vacuum concentrator (Eppendorf). Peptides were re-suspended in 0.1% (v/v) trifluoroacetic acid and 5% (v/v) acetonitrile (Zhang et al., 2016).

2.15.2 NanoLC MS ESI MS/MS analysis

Peptides were analysed by on-line nanoflow LC using the Ultimate 3000 nano system (Dionex/Thermo Fisher Scientific). Samples were loaded onto a trap column (ThermoScientific, PepMap100, C18, 300µm × 5mm) then resolved on an analytical column (Easy-Spray PepMap® RSLC 50cm × 75µm inner diameter, C18, 2µm, 100Å) fused to a silica nano-electrospray emitter (Dionex). The column was operated at a constant temperature of

30°C and the LC system coupled to a Q-Exactive HF mass spectrometer (Thermo Fisher Scientific). Chromatography was performed with a buffer system consisting of 0.1% formic acid (buffer A) and 80% acetonitrile in 0.1% formic acid (buffer B). The peptides were separated by a linear gradient of 3.8 – 50% buffer B over 90 minutes at a flow rate of 300nl/min. The Q-Exactive HF was operated in data-dependent mode with survey scans acquired at a resolution of 60,000 and scan range 350-2000m/z. Up to the top 10 most abundant isotope patterns with charge states +2 to +5 from the survey scan were selected with an isolation window of 2.0Th and fragmented by higher energy collisional dissociation with normalized collision energies of 30. The maximum ion injection times for the survey scan and the MS/MS scans were 100 and 45ms respectively, and the ion target value was set to 3E6 for survey scans and 1E5 for the MS/MS scans. MS/MS events were acquired at a resolution of 30,000. Repetitive sequencing of peptides was minimized through dynamic exclusion of the sequenced peptides for 20s.

2.15.3 Bioinformatic analysis

Spectral data were analysed using the PEAKS studio 8.5 software (Bioinformatics Solutions Inc., Waterloo, ON, Canada). Tandem MS data were searched against the predicted protein sets of IBV (Uniprot, June 2015) and *Gallus gallus* (NCBI Refseq Feb 2016) (46255 sequences combined). Search parameters were as follows; precursor mass tolerance set to 10ppm and fragment mass tolerance set to 0.05Da. Two missed tryptic cleavages were permitted. Carbamidomethylation (cysteine) was set as a fixed modification and oxidation (methionine), HexNAcetylation (asparagine, + 203.08Da), deamidation of asparagine (+0.9840Da), and deglycosylated asparagine ^{18}O labelling (+2.9890Da) were set as a variable modifications. The false discovery rate was set at 1%.

2.16 Mass spectrometry (MS) methods: Glycan analysis

2.16.1 Protein digestion

The purified IBV sample was diluted with 50mM ammonium bicarbonate (Sigma-Aldrich) and 0.1% (w/v) Rapigest (Waters, Elstree, UK). Samples were then incubated at 80°C for 10 minutes and reduced with 3mM dithiothreitol (DTT) at 60°C for 10 minutes then alkylated with 9mM iodoacetimde at room temperature for 30 minutes in the dark. The sample was split and proteins were digested with either trypsin or chymotrypsin (Sigma) and left to incubate at 37°C overnight. Samples were then acidified with trifluoroacetic acid (1% (v/v) final) and precipitated Rapigest removed. Peptides were concentrated and desalted using C18 Stage tips (ThermoFisher Scientific) and then samples dried using a centrifugal vacuum concentrator (Eppendorf). Peptides were re-suspended in 0.1% (v/v) trifluoroacetic acid and 5% (v/v) acetonitrile.

2.16.2 LC MS/MS

LC-MS/MS analysis was performed on an Orbitrap Fusion Tribrid mass spectrometer (ThermoScientific), attached to an Ultimate 3000 nano system (Dionex). Peptides were loaded onto the trapping column (ThermoScientific, PepMap100, C18, 300µm × 5mm), and then resolved on an analytical column (Easy-Spray C18 75µm × 500mm 2µm bead diameter column) using a 30-min gradient from 96.2% A (0.1% FA) and 3.8% B (80% MeCN 19.9% H_2O 0.1% FA) to 50% B at a flow rate of 300nL min−1. The mass spectrometer was operated in data dependent mode to automatically switch between MS and MS/MS acquisition using HCD and EThcD. MS1 scan was acquired from 450–1800 m/z (60 000 resolution, 4e5 AGC, 50ms injection time) followed by EThcD MS/MS acquisition of the precursors with the highest charge states in an order of intensity and detection in the Orbitrap. HCD (30 000 resolution, 3e5 AGC, 60ms injection time, collision energy (%) = 28). ETD scan range 120-2000m/z (30 000 resolution, 1e5 AGC, 120ms injection time). The Fusion was run in product dependent acquisition mode (HCDpdETD), which generates a pair of HCD and ETD spectra.

Acquisition was triggered when fingerprint ions (m/z 204.0867(HexNac)), 138.0545(HexNac fragment), and 366.1396(HexNacHex) were detected within top 20 product ions.

2.16.3 Data analysis

The EThcD data was searched against the IBV spike glycoprotein (UniProt, P12651) using Byonic (v2.13.1, Protein Metrics, Inc.). The search parameters were as follows: Trypsin (RK) and Chymotrypsin (FLWY) cleavage sites. Initial precursor and fragment mass tolerances were set at 10 and 20 ppm, respectively, and up to two missed cleavages were allowed for enzyme digestion. Cysteine carbamidomethylation was set as a fixed modification, and methionine oxidation, asparagine deamination were set as 'rare1' modifications. EThcD was chosen as the fragmentation type. Glycan modifications were searched against a 'narrow' Byonic 'N-glycan 50 common biantennery' library and were set as 'rare1' modifications. Two common modifications and 1 rare modification were allowed to be included per peptide. All other settings were set at the default values. For glycopeptides, a Byonic score of >300 and a PEP2D score of <0.005 was considered a good score, which reflects the absolute quality of the peptide-spectrum match (Bern et al., 2012).

2.17 Assessment of replication kinetics in primary and continuous cells

Confluent monolayers of cells seeded in 6 well plates were washed once in PBS and infected with IBV at an MOI of 0.1 or 0.01 unless otherwise stated. Infected cells were incubated at 37˚C or 41˚C for 1 hour. Following incubation, cells were washed twice with PBS and 3ml of 1xBES was added to each well. Cells were incubated at 37˚C or 41˚C and supernatant was harvested at 1, 24, 48, 72 and 96 hours post-infection and stored at -80˚C.

2.18 IBV titration by plaque assay

Virus titration by plaque assay was performed in 12 well plates of CK cells at 90-100% confluency. Viruses were diluted 10 fold in 1xBES and each dilution plated in triplicate. Infected cells were incubated for 1 hour at 37˚C after which virus was removed from cells and 1ml of overlay (1XBES containing 1% agar) was added per well. Infected cells were incubated at 37˚C for 72 hours before fixation with 10% formaldehyde (in PBS) and staining with 0.1% crystal violet (in H_2O). An average number of plaques was calculated for each sample and used to determine the plaque forming units per ml (pfu/ml) for each sample.

2.19 Virus neutralisation assay by plaque reduction

Samples of IBV-infected CK cell supernatant were diluted to 2000pfu/ml in PBS. Monoclonal antibody A13 was diluted 1/10 in PBS then serially diluted two-fold with the pre-diluted virus samples. The final amount of virus in each solution was 10^3pfu/ml. Antibody-virus solutions were incubated for 30 minutes on an orbital shaker to ensure thorough mixing. Each dilution was used for plaque assay in CK cells (Section 2.18) and average pfu/ml values were calculated from three biological repeats.

2.20 Infection of Vero cells in the presence of trypsin

Confluent monolayers of Vero cells seeded in 6 well tissue culture plates were washed once in PBS. IBV was diluted in 1XBES medium containing tosyl phenylalanyl chloromethyl ketone (TPCK) treated trypsin (Sigma) at various concentrations. Each well was inoculated with 500µl of diluted virus and cells were incubated at 37°C for 1 hour. Cells were washed twice in PBS and 3ml of 1XBES (+TPCK-trypsin) was added to each well. Cells were incubated for 24 hours

at 37°C. Following incubation, IBV-induced cpe was assessed under a light microscope and supernatant from each well was harvested and stored at -80°C.

2.21 Infection of *ex vivo* tracheal organ cultures (TOCs)

Trachea from 19 day-old SPF RIR embryos were extracted and divided into sections using an automated microtome. Sections were separated by hand and individually placed into glass test tubes containing 1ml of TOC growth medium (Table 2.4). TOCs were incubated at 37˚C for 24 hours (no CO_2) rotating at approximately 8 revolutions per hour (rph). TOCs were assessed 24 hours prior to infection; those exhibiting poor ciliary activity were discarded. Healthy TOCs were incubated for a further 24 hours at 37˚C (8rph). On the day of infection, TOCs were washed once in PBS.

For ciliostasis assessments, 10^4pfu of IBV were added to each tube in 100µl of TOC growth medium. Ten replicates were infected for each virus. TOCs were incubated upright (no rotation) at 37˚C for 1 hour before addition of 900µl of TOC growth medium to each tube. TOCs were incubated at 37˚C (8rph) for a total of 96 hours. Ciliary activity in each TOC was assessed under a light microscope at the time of infection and then every 24 hours. Each TOC was assigned a score of 0-4 based on the proportion of visibly beating ciliated cells. A score of 1 indicates 25% of cilia visibly beating, a score of 4 indicates 100% visible beating. These scores were converted to percentages to provide an average ciliary activity score.

For assessment of replication kinetics, TOCs were prepared in the same way. TOCs were infected with $1x10^4$pfu of IBV in a total volume of 500µl and incubated upright for 1 hour. After this incubation TOCs were washed twice in PBS and 1ml of fresh TOC growth medium was added to each tube. TOCs were incubated at 37˚C (8rph). Supernatant from triplicate TOCs was harvested at 0, 24, 48, 72 and 96 hours post-infection.

2.22 Assessment of ciliostatic dose (CD_{50}): titration in TOCs

Embryonic TOCs were prepared as described above. For non-cell culture adapted strains of IBV, titration was achieved by calculation of the ciliostatic dose (CD_{50}) for each sample. TOCs were washed once in PBS. Two-fold serial dilutions of virus samples were prepared in TOC medium. TOCs were washed once in PBS and infected with 500µl of each virus dilution in triplicate. Infected TOCs were incubated at 37°C (no CO_2, 8rph) for 6 days. Each TOC was examined under a light microscope to assess ciliary activity and designated living or dead. Those exhibiting less than 25% ciliary activity or complete ciliostasis were deemed dead. CD_{50} values were calculated based on the Reed-Muench method (Reed and Muench, 1938).

2.23 *In vivo* methods:

All *in vivo* methods were performed according to Home Office and ASPA regulations by trained individual licence holders in the Experimental Animal House at Compton or the Biological Services Unit at Pirbright.

2.23.1 Infection of SPF RIR chickens with IBV

8 day-old SPF RIR chicks were infected with IBV via the ocular-nasal route using a P200 pipette to administer 100µl of diluted virus to the eyes and nares of each bird.

2.23.2 Assessment of IBV-induced clinical signs

Chickens were housed in colony cages in groups of 12-15 with various enrichments including pecking blocks, perches, mirrors and edible enrichment. From day 3 post-infection (rIBV M41K-BeauR(S)) and day 2 post-infection (rIBV M41K-4/91(S)), clinical signs were assessed for all groups. The total number of snicks observed in a 2 minute period was recorded by three individuals and an average was calculated for each group. Following this, each bird was assessed for respiratory and other signs of IBV infection including wheezing, rales, watery

eyes, nasal discharge and general lethargy. Any observed signs were recorded and monitored for the remainder of the experiment.

2.23.3 *Post-mortem* harvesting of tissues

Chickens were culled by an approved Schedule 1 method carried out by a trained member of Animal Services (Pirbright) and death was confirmed by cessation of heartbeat. Clean scissors, forceps and scalpels were used for each bird to collect tissue samples from the eyelid, beak, trachea, lung, kidney, gut, spleen and bursa. Sections of tissue were divided and stored in PBS and RNA Later (Thermo Fisher). Samples in RNA Later were stored at 4˚C overnight then transferred to -80˚C for storage before analysis.

2.23.4 Assessment of IBV-induced ciliostasis

Trachea were harvested from infected chickens as described above and cleaned to remove fat and debris using forceps and scalpels. Samples were sectioned into 10 rings of approximately 1mm thickness. Three sections were taken from the upper and lower parts of the trachea and four were taken from the middle. Sections were placed on a glass microscope slide and examined under a light microscope to assess the activity of the ciliated cells. Each section was assigned a score from 0-4 based on the proportion of visibly beating cells as described in Section 2.21. Scores were converted to percentages (4=100% visibly beating, 1 = 25% beating).

Chapter 3: Characterising the glycosylation profile in the IBV S protein

3.1 Introduction

N-linked glycosylation is an important modification of viral protein ectodomains that takes place in the ER and Golgi. Different classes of glycan are formed on the surface of a protein following attachment to the asparagine residue in the amino acid sequence Asn-X-Ser/Thr and subsequent trimming and processing by various cellular enzymes including mannosidases and glucosidases (Vigerust and Shepherd, 2007). Specific classes of glycan can be inhibited or removed either enzymatically or by use of enzyme inhibitors such as Kif and SW, both of which inhibit the formation of complex glycans through targeting mannosidase I and II, respectively (Elbein et al., 1990, Elbein et al., 1981).

The S protein of IBV exhibits a high level of glycosylation, similar to other viral envelope proteins including HIV gp120 and influenza HA. Glycosylation has been shown to contribute towards correct protein folding and, in turn, function. In influenza, glycosylation of the HA protein has been shown to modulate the immune response, influence receptor binding and affect virulence and antigenicity (Tate et al., 2014).

This aim of the work described in this chapter was to examine the glycan shield of the IBV S protein in more detail, identifying glycan structures on the protein surface and investigating the possible roles of specific classes of glycan in viral infectivity and immune evasion. The S proteins of four different strains of IBV, varying vastly in pathogenicity and tropism, were analysed to gain insight into the glycan profile of each strain. Two strains were analysed in more detail to define the role of specific glycans in viral infectivity and their interaction with antibodies.

3.2 Results

3.2.1 Prediction and confirmation of N-linked glycosylation sites

To assess the levels of variation in IBV S glycoprotein glycosylation, a range of IBV strains were used for the initial analyses of S gene sequences. Two laboratory-adapted strains with different levels of pathogenicity and two currently circulating pathogenic field strains were included in the analysis. The sequences of the Beau-R, M41-CK, QX and 4/91 S protein sequences were generated using strain specific primers during RT-PCR followed by Sanger sequencing and aligned using BioEdit (Hall, 1999). The alignment of the four sequences is included in Appendix A6. The S proteins shared between 82-96% amino acid homology. Table 3.1 details the sequence comparison of the four IBV strains and highlights the differences between them. The S genes of M41-CK and Beau-R shared the greatest amount of sequence homology with 96.2% sequence identity between the amino acid sequences of each strain. Less homology was exhibited between the laboratory strains and the field strains, as M41-CK and Beau-R exhibit approximately 82% homology with 4/91 or QX. These four strains were used for analysis of their N-linked glycosylation profiles as their sequences and tropisms are varied.

Table 3.1: Spike (S) gene amino acid sequence homology of IBV M41-CK, Beau-R, QX and 4/91.

	M41-CK	**Beau-R**	**QX**
Beau-R	96.2%	---	---
QX	82.3%	82.1%	---
4/91	82.4%	82.3%	84.0%

BioEdit was used to generate identity matrices showing the percentage sequence identity between the S gene sequences of the four strains.

As a result of the cellular mechanisms and pathways by which they are produced, N-Linked glycans are present on glycosylated proteins in different forms. Simple or high mannose glycans contain a high proportion of mannose molecules compared to complex glycans which are subject to trimming by cellular enzymes including mannosidases. The amino acid sequence of a protein can be used to predict the location of N-linked glycosylation sites using the identification of the amino acid motif Asn-X-Ser/Thr. The presence of this sequence alone does not imply attachment of a glycan to this site; the identity of the central amino acid (X) influences the likelihood of glycan attachment. For example if a proline follows the Asn residue, the site is unlikely to be glycosylated. Other factors are known to influence glycosylation in this manner, including the surrounding sequence of amino acids and the folding and final conformation of the protein, as this may result in masking or distortion of the glycosylation site (Gavel and Heijne, 1990). Using the online server NetNGlyc 1.0, locations in the IBV S protein sequence with potential for glycosylation were identified. These sites consist of a specific amino acid sequence comprising Asn-X-Ser/Thr (N-X-S/T), where X can indicate any amino acid except Pro. The total number of sites present in each strain varies, with the most being present in the field strains QX (34 sites) and 4/91 (32 sites), compared to the two lab strains M41-CK and Beau-R which contain 29 and 28 potential sites across the S gene, respectively. This data is summarised in Table 3.2. Of the total sites in the S protein sequence of each strain, there is a higher proportion of N-X-T motifs compared to N-X-S. This is a common trait in N-linked glycosylation (Rao and Wollenweber, 2010).

Table 3.2: Number of PNGS in each of the selected strains M41-CK, Beau-R, QX and 4/91.

Strain	*Total number of sites*	*% N-X-S*	*% N-X-T*
M41-CK	29	38	62
Beau-R	28	39	61
4/91	32	44	56
QX	34	41	59

To assess the conservation of the potential N-linked glycosylation (PNG) sites in the IBV genome, global analysis of all available published sequences of each subunit within the S gene (S1 and S2) was carried out and percentage conservation for each site was calculated. Sequences were obtained from UniProt Protein Database and analysed using Excel based on the amino acid positions in the M41-CK sequence. The results from this analysis are shown in Figure 3.1. Data are displayed for the S1 and S2 sequences separately. For S1 (Figure 3.1A), 21 sites were included in the data analysis. Of these sites, 14 were conserved in 90% or more of the 834 analysed sequences. The least frequent site was identified at position 281, present in only 9.6% of sequences. The sites identified in the S2 region of the protein were more conserved across all strains, with 11 of the total 14 sites exhibiting close to 100% conservation across all analysed sequences (Figure 3.1B). It was expected that the sites in the S2 sequences would be more conserved than those in the S1 segment, as S1 sequences are known to be more genetically diverse than S2 sequences (Gelb et al., 2005, Manswr et al., 2018). As the S1 subunit is responsible for attachment and is the main antigenic target during IBV infection, it can be postulated that the reason for the great sequence diversity is linked to avoidance of host immune responses (Bande et al., 2016, Kant et al., 1992).

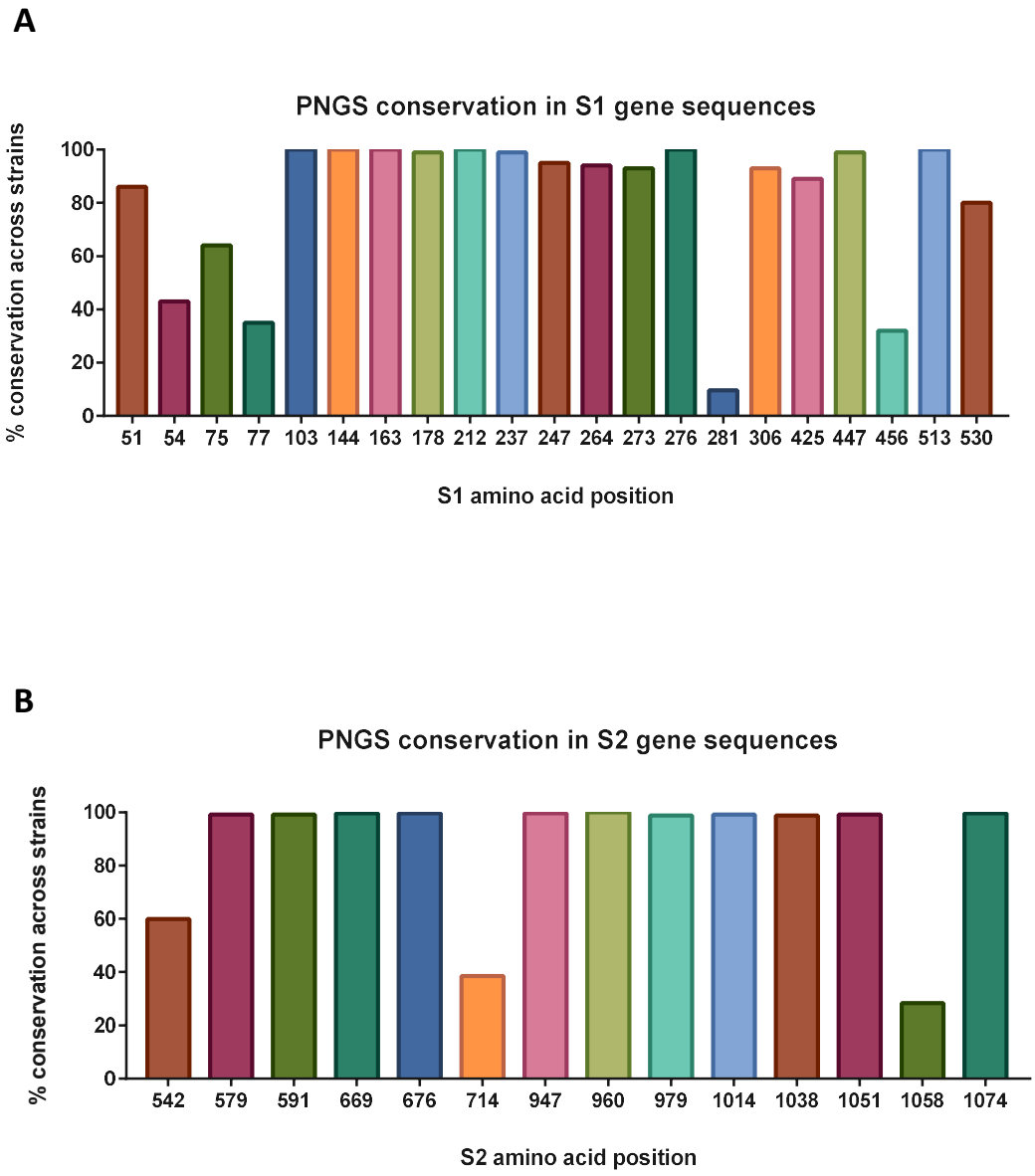

Figure 3.1: Global analysis of PNGS conservation across all available IBV strains in the S gene sequence. Using 834 protein sequences available from GenBank, the predicted N-linked glycosylation sites in the S1 segment of the IBV S gene were highlighted and assessed for conservation between strains **(A)**. The same analyses were performed on 250 sequences for the S2 segment **(B)**. The amino acid positions are based on the sequence of M41-CK, starting from the S gene start codon, including the signal sequence (amino acids 1-18 (Promkuntod et al., 2014)).

A global analysis of the glycosylation sites was performed using all the available sequences from GenBank. Separately, the data from the online server predictions in each S gene sequence was used to generate tables of data that show the positions of the sites in each of the strains selected for deeper analysis. An alignment of these four gene sequences is displayed in Appendix A6. From the data shown in Figure 3.1 it was possible to identify sites that were present in the S gene sequences of the four IBV strains used for further analysis in this chapter (Beau-R, M41-CK, QX and 4/91). This analysis was also completed by identifying any suitable asparagine residues in Asn-X-Ser/Thr motif that are present in the sequences detailed in Appendix A6. This data is summarised in Table 3.3. The numbers in the table are in reference to the amino acid positions in each strain sequence, so where the numbers differ by only one or two positions, the glycosylation site is likely to be in the same place on the S protein. Where appropriate these have been grouped together for each strain. Notable regions of the S protein structure are labelled above each table including hypervariable regions (HVRs), the putative RBD (sourced from Promkuntod *et al.* 2014) and cleavage sites. The S2' cleavage site is only present in the Beau-R S protein (Bickerton et al., 2018). Data is displayed for S1 (top) and S2 (bottom). Again, there seems to be more variation in the predicted sites among the four strains within the S1 subunit, compared to those located in the S2 subunit which are more conserved between all strains. There are also similarities between the field strains and the laboratory-adapted strains too, as there are no unique sites in the S2 subunit across the predictions for each virus. The sites present at amino acid positions 544 and 1060 (4/91) are not present in the laboratory-adapted strains and conversely the site at position 714 in M41-CK and Beau-R is not present in QX or 4/91. The differences in the patterns of glycosylation could be linked to the fact that the laboratory strains have been adapted to replicate in cell culture whereas the field strains can only be propagated in organ cultures, embryonated eggs or chickens.

Table 3.3: Amino acid positions of PNGS in IBV strains Beau-R, M41-CK, QX and 4/91. Numbering in each strain is based on the amino acid sequence of each protein, including the signal sequence. Hypervariable region (HVR) and cleavage sites (CS) are labelled. The S2' CS is only present in the Beau-R sequence.

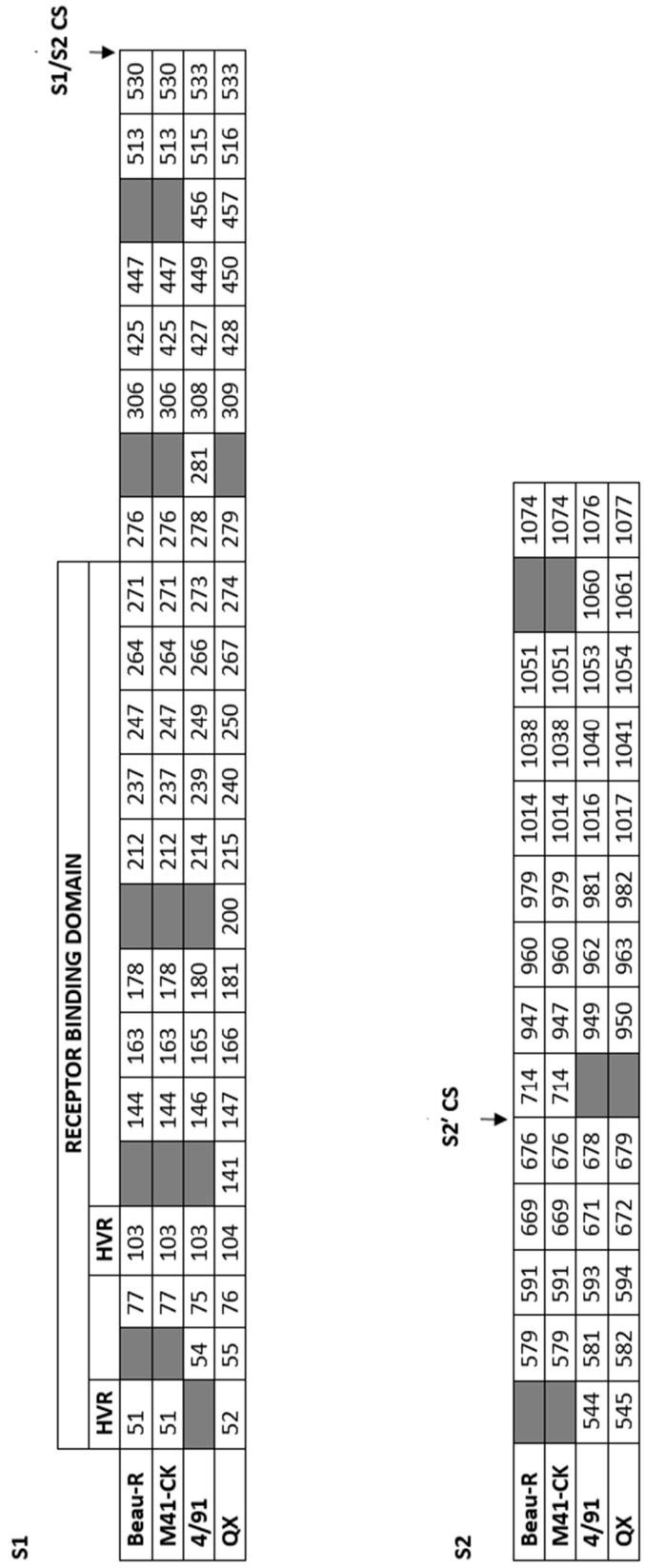

To further investigate the spatial locations of the potential sites, the S gene sequence was used to generate a model of the predicted 3D structure of the protein. Figure 3.2 shows the predicted structure of the protein, based on a model produced using the homology modelling Phyre2 server and PyMol for analysis and annotation. The models are based on the recently published IBV M41 S protein structure determined by cryo-electron microscopy (EM) (Shang et al., 2018) and demonstrate the spatial arrangement of the predicted glycosylation sites. M41-CK has been used to represent all strains as the differences in the spatial arrangement of the predicted sites are negligible. The models demonstrate that most of the predicted sites lie within the S1 subunit of the protein, quite evenly spread between the S1-NTD and S1-CTD. This is unsurprising as this subunit is responsible for attachment and N-linked glycans have been implicated in facilitating virus entry and receptor or co-receptor binding in related coronaviruses (Han et al., 2007).

There are several glycosylation sites within the putative receptor binding motif in IBV M41-CK S1, which has previously been mapped to amino acid residues 19-272 (Promkuntod et al., 2014). Ten of the predicted sites detailed in Figure 3.2B lie within this putative receptor binding domain (RBD). There is evidence of surface oligosaccharides facilitating attachment and binding in other coronaviruses (Jeffers et al., 2004, Jeffers et al., 2006) so it is likely that, if glycosylated, these sites have some function in interactions with the cellular receptors or attachment factors with which the S protein interacts. The recent structural study by Shang *at al.* identified glycosylation at 20 sites in the S protein ectodomain, corroborating the predictions of those sites detailed in Figure 3.2B (Shang et al., 2018). All of the sites identified by Shang and colleagues were present in the 29 predictions (in M41-CK) described here.

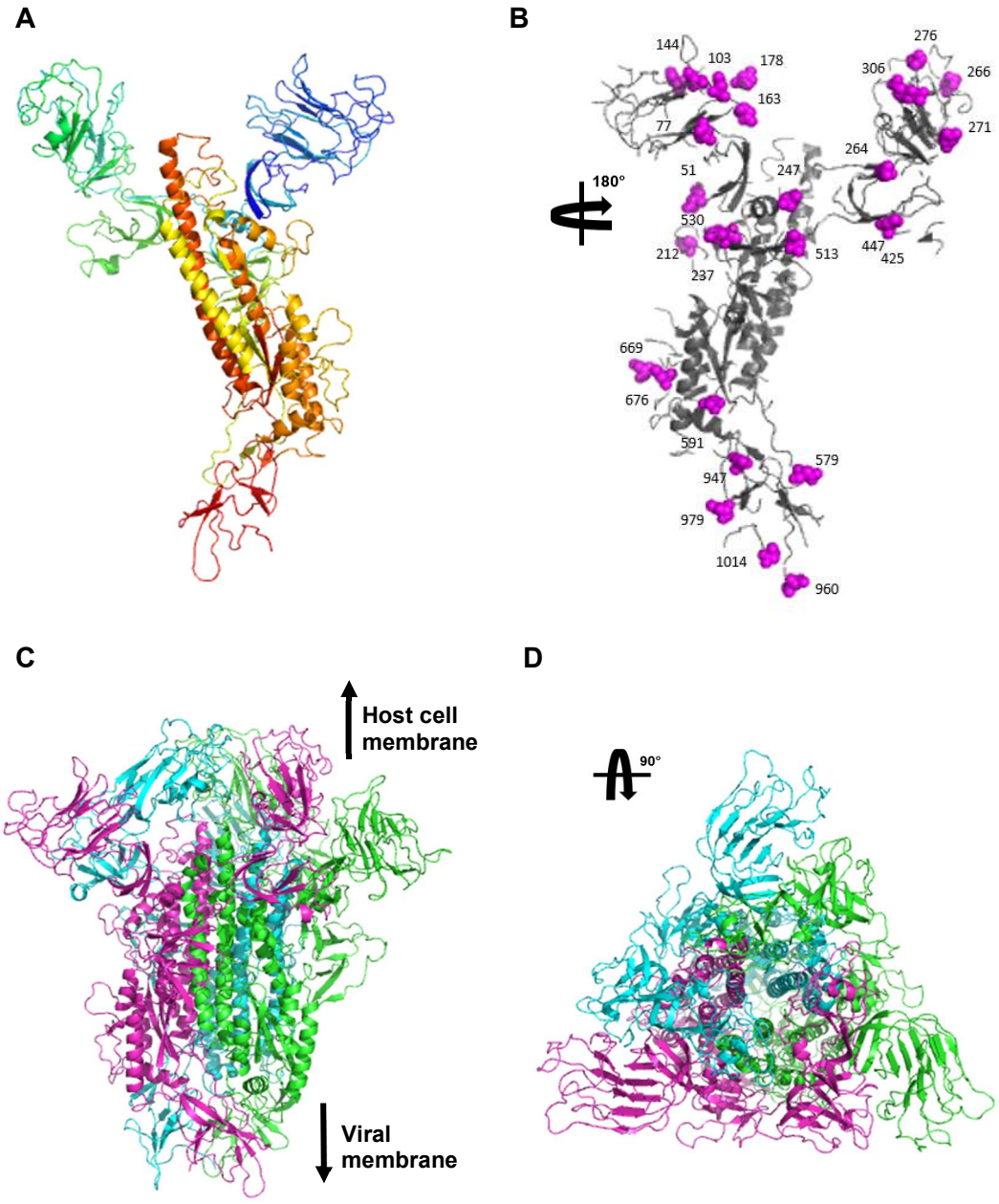

Figure 3.2: IBV S modelling based on published M41-CK structure with labelled PNGS locations. Ribbon diagram of the putative S protein structure of IBV M41-CK. **(A)** Monomeric unit of the S protein coloured by rainbow from N (blue) to C terminus (red). S1 indicated in green/blue and S2 in red/yellow/orange. **(B)** Monomeric unit of the S protein with labelled Asn residues present in PNG sites (pink), generated using PyMol. **(C)** Trimeric formation of IBV M41-CK S from a side view and **(D)** from a top view, generated using SWISS Model. Each colour represents a monomeric unit.

In order to confirm the presence of glycans at the sites identified in Figure 3.1, mass spectrometry was performed on samples of IBV M41-CK purified by ultracentrifugation and chymotrypsin or trypsin digested. Samples of M41-CK containing allantoic fluid were purified at The Pirbright Institute by ultracentrifugation. Mass spectrometry sample preparation was performed by Dr Stuart Armstrong at the University of Liverpool. Figure 3.3 shows the combined results of two experiments performed to first confirm the presence of glycans at predicted sites in the amino acid sequence using NanoLC ESI MS/MS (Methods Section 2.15) then characterise the structure of the glycans present. Firstly, glycan sites were mapped by chymotrypsin or trypsin digestion followed by PNGase F treatment in presence of deuterium oxide, or heavy water (D_2O). Any peptide modifications were highlighted using PEAKS software (BSI) and glycopeptides (chymotrypsin and trypsin digests) were analysed on a Thermo Orbitrap fusion instrument with EThcD mode (Methods Section 2.16). Data were analysed by using Byonic software (Protein Metrics) to generate cartoons representing the glycan composition.

Glycosylation was confirmed at 18 of the possible 29 asparagine sites predicted by the NetNGlyc algorithms in the M41-CK protein sequence. The sample preparation did not allow for complete coverage of the S protein sequence so it is possible that more of the predicted sites are true glycosylation sites. Of the 18 detected glycans, 10 lie within the S1 subunit and 8 in S2. The second set of MS experiments revealed the range of glycan structures present at 6 of the 18 total sites. These are detailed at amino acid positions 144, 212, 425, 513, 947 and 1014 in the S protein sequence. It is important to note the heterogeneity of the glycans at each site as this indicates that each individual S protein in the sample has a potentially different glycan profile. The majority of the glycans characterised here are high mannose glycans and are quite similar in their composition. Mass spectra for each structure are included in Appendix A1.

As described previously, the recent study by Shang *et al*. identified 20 sites at which the M41 S protein was glycosylated. Of the sites described in Figure 3.3, nine are shared between the two data sets. Interestingly, the study by Shang *et al.* did not identify glycosylation at positions 425, 530, 960, 979, 1014, 1051 and 1074, all of which were confirmed as glycosylated by the MS methods described here. Another recent study involving the IBV S protein performed similar MS techniques to identify glycosylation sites within the Beaudette S protein. This study used a Vero-adapted strain of the virus and identified glycosylation at amino acid positions 212, 237, 247, 276, 513, 591, 1051 and 1074, all of which match with confirmed sites in Figure 3.3, except 237 and 276 (Zheng et al., 2018). There were differences in the strains and methods used in each study, offering some explanation for the differences in the results. Across all three studies, there were no differences in the predicted sites but those identified as true glycosylation sites differed slightly.

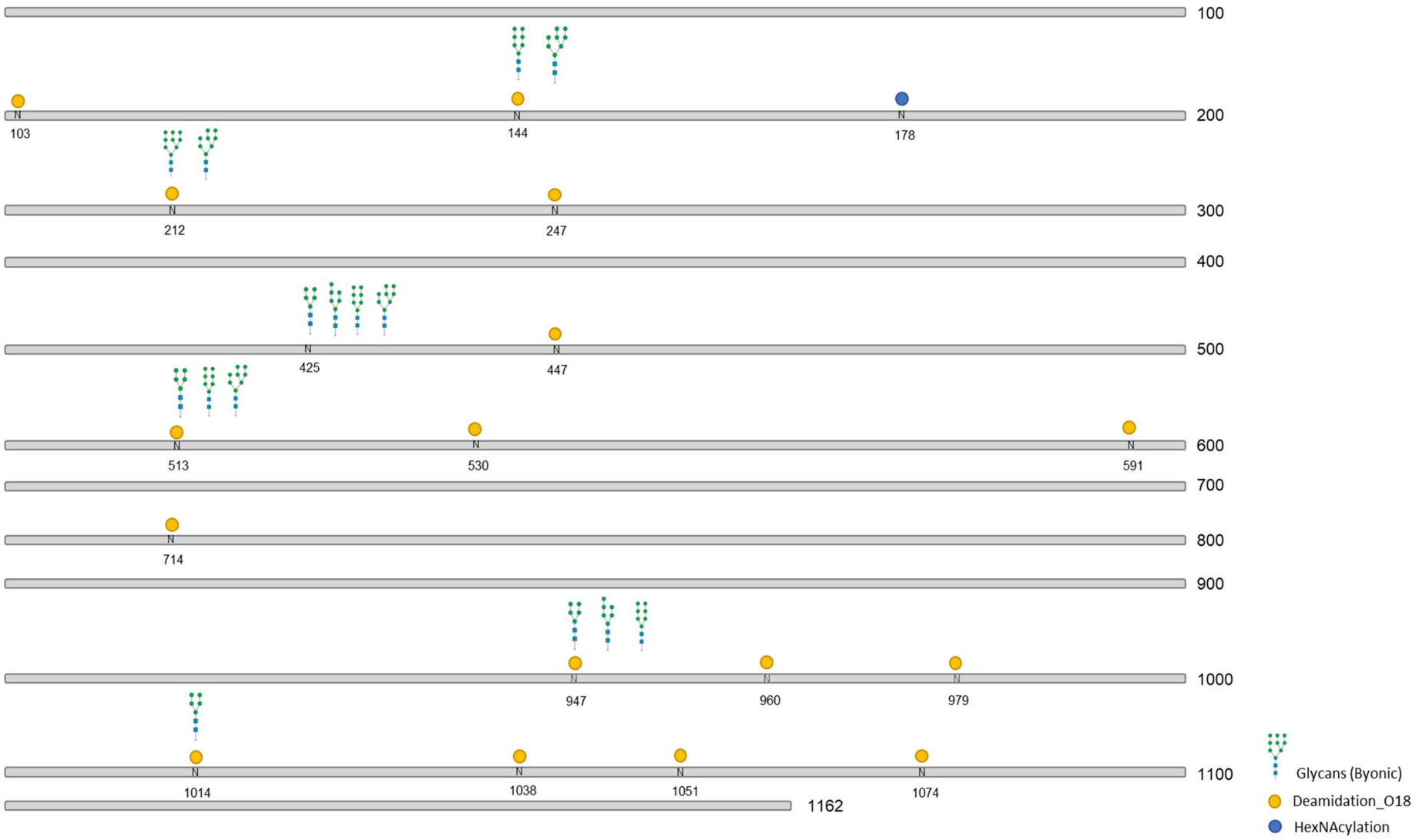
100
200
300
400
500
600
700
800
900
1000
1100
1162
N
103
144
178
212
247
425
447
513
530
591
714
947
960
979
1014
1038
1051
1074
Glycans (Byonic)
Deamidation_O18
HexNAcylation

Figure 3.3: Confirmation of N-linked glycosylation and characterisation of glycan structures in the IBV M41-CK S protein. Purified samples of IBV M41-CK were subjected to trypsin and chymotrypsin treatment to separate the peptides followed by NanoLC ESI MS/MS mass spectrometry in the presence of heavy water (D_2O) to determine the presence of glycans at each site. Sites where the presence of a glycan was detected are indicated by coloured dots. Sites where the glycan structure has been predicted using LC MS with EThcD mode are indicated by cartoons (generated using Byonic software). Mannose molecules are indicated by green circles and N-acetylglucosamine (GlcNAc) molecules are represented by blue squares. Figure produced by Dr Stuart Armstrong (University of Liverpool).

3.2.2 Assessment of the effects of S protein glycosylation inhibition in IBV

Assessment of the types of glycans present in the IBV S protein profile was carried out using inhibitors and enzymatic treatments affecting the various classes of glycan. Kif was used to identify the presence of complex glycans on the surface of the protein. Endo H and PNGase F were used to cleave simple or high mannose glycans from closer to the glycan core, to achieve near complete or complete deglycosylation, respectively. Figure 3.4 describes the general structure of an N-linked glycan and indicates the action of the aforementioned inhibitors and enzymes.

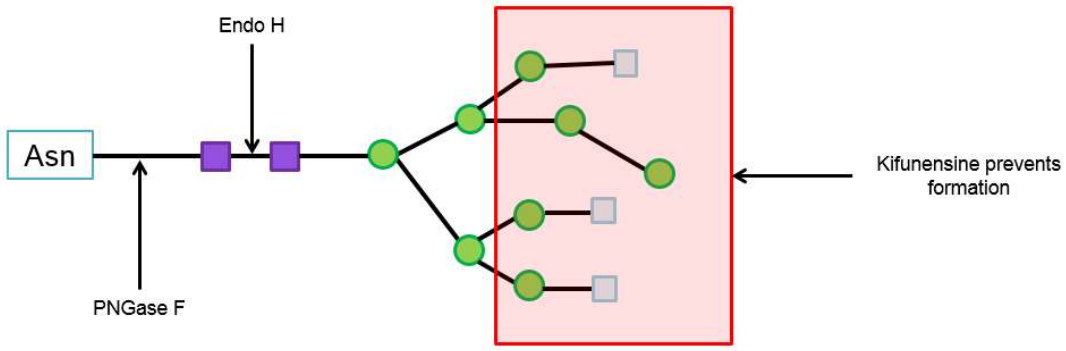

Figure 3.4: N-linked glycan structure and inhibitor action. Schematic representation of possible glycan structures. GlcNac molecules are indicated by purple squares and mannose molecules are indicated by circles. PNGase F cleaves all glycans at the GlcNac core resulting in full deglycosylation of the treated protein. Endo H acts further downstream of the GlcNac core to remove high mannose and some hybrid glycans, resulting in near complete deglycosylation. Kif is an inhibitor which acts on the cellular ER enzyme α-mannosidase I to prevent the trimming and processing of the core glycans to result in complex glycans, inhibiting the formation of this class of oligosaccharide only, leaving simple and hybrid oligosaccharides intact.

In order to demonstrate the different actions of these inhibitors and therefore elucidate the range of glycans present on the surface of IBV S, samples of purified virus were treated with deglycosylating enzymes (Endo H and PNGase F) to remove high mannose and some hybrid glycans from the surface of the protein. Alongside these treatments, CK cells were infected with either M41-CK or Beau-R and treated with the α-mannosidase I inhibitor Kif, with the aim of producing viruses that expressed S without complex glycosylation. These treated samples were compared to purified wild-type M41-CK and Beau-R. Figure 3.5 shows a western blot using the monoclonal S2 antibody 26.1 to demonstrate the change in molecular weight when different classes of glycan are removed from the surface of the S protein. For both M41-CK and Beau-R, the samples were run in the order untreated purified IBV (UT), Kif-treated cell lysate (Kif), Endo H treated purified IBV, PNGase F treated IBV. Molecular weights were compared to a Bio-Rad protein standard (M) to assess any changes following each treatment.

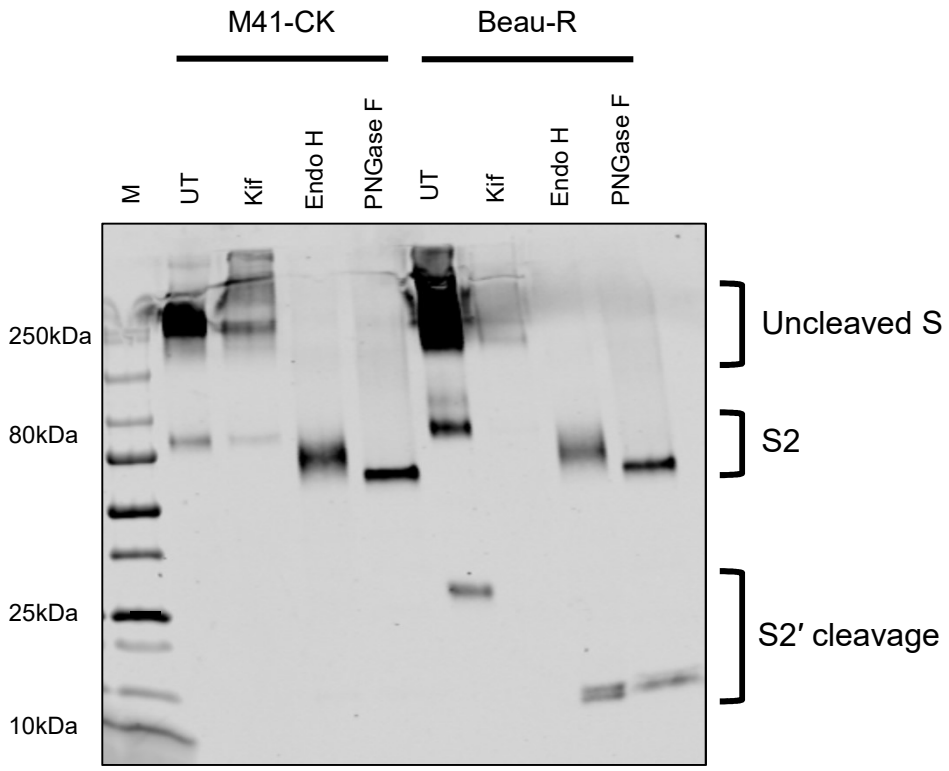

Figure 3.5: IBV S displays different classes of glycan. Ultracentrifuge-purified samples of IBV propagated in embryonated eggs were treated with deglycosylating enzymes that affect different types of glycan and protein size was compared to untreated (UT) virus samples. Endo H targets high mannose and some hybrid glycans while PNGase F targets all glycans. For inhibition of complex glycan formation, cells were treated with the mannosidase I inhibitor Kif at 20µM at the time of infection with IBV (MOI = 1). Protein lysates were harvested at 24hpi and used for western blot. S protein was detected using a monoclonal antibody against the S2 subunit (26.1, PrioMab). Changes in protein sizes indicate loss of glycan mass. Band sizes were compared to Bio-Rad Precision Plus All Blue Protein Standards.

In the untreated (UT), wild-type samples of purified M41-CK (left) or Beau-R (right), the S2 antibody 26.1 produced a distinct band at approximately 80kDa, which indicates the S2 subunit of the S protein. There was also a large smear of approximately 250kDa at the top of each of these lanes. This is thought to indicate uncleaved, glycosylated S protein. The additional smaller band of approximately 30kDa in the Beau-R samples is thought to indicate cleavage at the secondary cleavage site in the S2 subunit, known as the S2' site. This site is thought to contribute to the extended host range of Beau-R, allowing the virus to infect Vero cells as well as primary avian cells (Bickerton et al., 2018). The Kif treated samples, to the right of the UT lanes, highlight an interesting difference between the two viral strains used for this experiment. In the M41-CK Kif samples, the staining was fainter compared to the untreated samples. While this could indicate a reduction in glycosylation levels in this sample, it could also indicate a smaller amount of protein in the sample. As this sample is derived from cell lysate rather than purified virus it is feasible that less protein was present and therefore a fainter band was produced by the S2 antibody. A loading control was not used for this experiment so exact conclusions concerning the levels of protein in each sample are difficult to draw. In the Kif-treated Beau-R sample, the effect of this inhibitor is more obvious, as there was no recognition of the S2 subunit or the putative S2’ cleavage product at all. The faint smear at the top of the lane indicates that S protein is still present, however the recognition of S2 has been lost following treatment with Kif. This presented an interesting line of investigation regarding the involvement of complex glycosylation and the S2 epitope recognised by 26.1, as the treatment with Kif had clearly interfered with the process of recognition by this monoclonal antibody.

Different effects were observed in the enzymatically deglycosylated samples, located in the Endo H and PNGase F lanes in Figure 3.5. There were notable changes in the bands observed in the lanes for the samples treated with each enzyme. For both treatments, a band was recognised in both the M41-CK and Beau-R samples, indicated at approximately 70-75kDa.

The bands in the Endo H treated samples are slightly larger than the those in the PNGase F samples for both viruses, owing to the fact that PNGase F removes all glycans at the GlcNAc core, whereas complex glycans are resistant to Endo H treatment and would still have been present on the protein following treatment. In the Beau-R samples, the S2' cleavage product was also still recognised following partial and complete deglycosylation.

The 70-75kDa band in these samples could be indicative of several things. It is possible that this is the uncleaved S with partial glycosylation, and that the treatment has resulted in a notable shift in band size of the whole protein from approximately 250kDa to 75kDa. While glycans themselves do not exhibit a particularly heavy molecular weight, glycosylated proteins appear heavier than they are as a result of the bulky, branched nature of their attached glycans, so removing them could feasibly result in the dramatic size change observed here. It has been reported that glycan mass constitutes approximately half the molecular weight of HIV gp120, a similar glycoprotein to IBV S (Lasky et al., 1986, Leonard et al., 1990). This could explain the dramatic band shift observed in these samples. However, the absence of the S2 band between the uncleaved and S2' bands cannot be explained in this context, unless S2 recognition has been lost entirely in all the Beau-R samples.

Another explanation of the shift in band sizes is that the band at 70-75kDa is, in fact, the S2 band, where the treatment with Endo H or PNGase F has resulted in a shift of only 5-10kDa. With this hypothesis it is also important to note the absence of the uncleaved S band at 250kDa. One possibility for this loss is that the enzyme treatment has somehow increased cleavage of the S protein into its respective subunits, resulting in more distinct S2 susceptible to recognition by the antibody. This may explain the brighter band intensity in the M41-CK samples following enzymatic treatment.

Overall, these results clearly demonstrate a range of glycan structures present on the surface of the IBV S protein in both M41-CK and Beau-R samples. While there are some unanswered

questions regarding the changes in band recognition in some of the samples, it can be assumed that treatment with the α-mannosidase inhibitor Kif has affected the binding capacity of the monoclonal antibody 26.1 to the S2 subunit of the protein, indicating a potential role for complex glycosylation in this process.

During glycan processing, several different enzymes act on the oligosaccharides to create different classes of glycan. The α-mannosidases I and II are involved in the generation of complex glycans and are located in the ER and Golgi, respectively (Aebi et al., 2010, Stanley, 2011). To confirm that the loss of S2 recognition in Beau-R was specific to Kif treatment and inhibition of α-mannosidase I, another mannosidase inhibitor, SW was used to disrupt the processing of hybrid glycans in both M41-CK and Beau-R. SW specifically acts on α-mannosidase II to inhibit glycan trimming and processing in the Golgi.

Western blot was used to assess whether the S protein could still be detected by mAb following SW treatment in IBV-infected cells. CK cells were infected with either Beau-R or M41-CK and treated with SW. Cell lysates were processed and analysed by western blot using the S2 monoclonal antibody 26.1. Figure 3.6 shows that there was no change in mAb recognition of the S2 subunit by the 26.1 antibody following SW treatment, demonstrating that the effect seen in Figure 3.5 can be attributed to the inhibition of complex glycan formation by Kif. The additional S2' band at 30kDa was not seen in this experiment. This is thought to be due to the nature of the samples, as those used for deglycosylation in Figure 3.5 are purified IBV and are, as such, much more concentrated than the cell lysates analysed during cellular inhibitor treatments. There is also a more general reduction in the band intensity in the Beau-R samples compared to the M41-CK samples in this experiment, indicating that either there are less cells in the Beaudette samples due to more extensive IBV-induced cpe, or that the S2 antibody is less reactive with the Beau-R protein compared to M41. This is an important consideration when interpreting these results given the lack of

loading control, however the levels of protein recognition between the treated and untreated samples shows that in this experiment SW had no effect on S2 binding by 26.1.

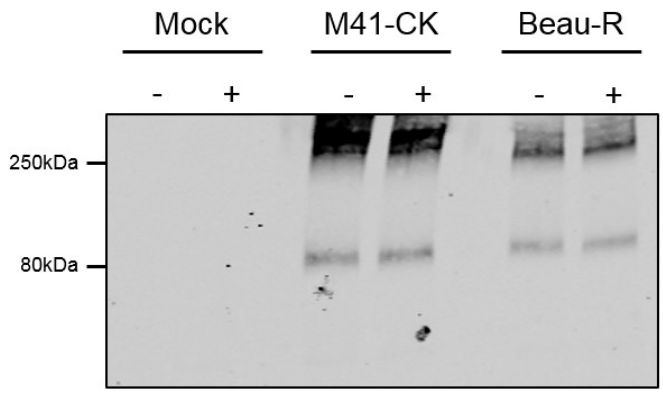

Figure 3.6: SW has no effect on mAb recognition of S2 in M41-CK or Beau-R infected CK cells. CK cells were mock-infected or infected with M41-CK or Beau-R at an MOI of 1. SW was added to cells at the time of infection. Cells were lysed using RIPA lysis buffer after 24 hours incubation at 37°C and proteins were separated by SDS-PAGE followed by western blot. S2 was detected using the mAb 26.1 followed by incubation with LI-COR IRDye 700CW secondary antibody diluted in blocking solution. Membranes were visualised using the LI-COR Odyssey.

To assess whether the effects observed by western blot were reflected in conformational protein as opposed to linear, infections in CK cells in the presence of Kif were carried out to investigate whether a similar reduction in antibody recognition would be observed in M41-CK infected/Kif-treated cells compared to Beau-R infected/Kif-treated cells. The results from these infections and IF staining are shown in Figure 3.7. As expected, there is no difference in the α-tubulin staining between the mock untreated and Kif-treated cells, indicating that the cell viability has not been affected by the inhibitor treatment. There was a marked reduction in the signal observed for S2 staining in the Beau-R infected/Kif-treated samples; however S2 was still clearly detected by the mAb 26.1 following M41-CK infection with Kif treatment. Interestingly this again suggests that complex glycans are involved in allowing the mAb to recognise the specific epitope required for binding in Beau-R but not M41-CK. There could be a slightly different conformation or sequence in M41-CK where the complex glycans are not required for recognition. There could also be differences in the class of glycan attached to the sites present in this epitope in M41-CK; complex glycans may not even be present here and so the protein may remain unaffected by Kif treatment.

It is also imperative to note the quality of the staining in the Beau-R infected, Kif-treated cells in the bottom right panel of Figure 3.7. The tubulin staining appears to be fainter than in these cells than in the other samples, indicating that the treatment has affected the overall health of the cells. In contrast, data from cell viability assays suggests that there is no effect on CK cell viability following treatment with Kif (Appendix A2), so this could be an anomalous result.

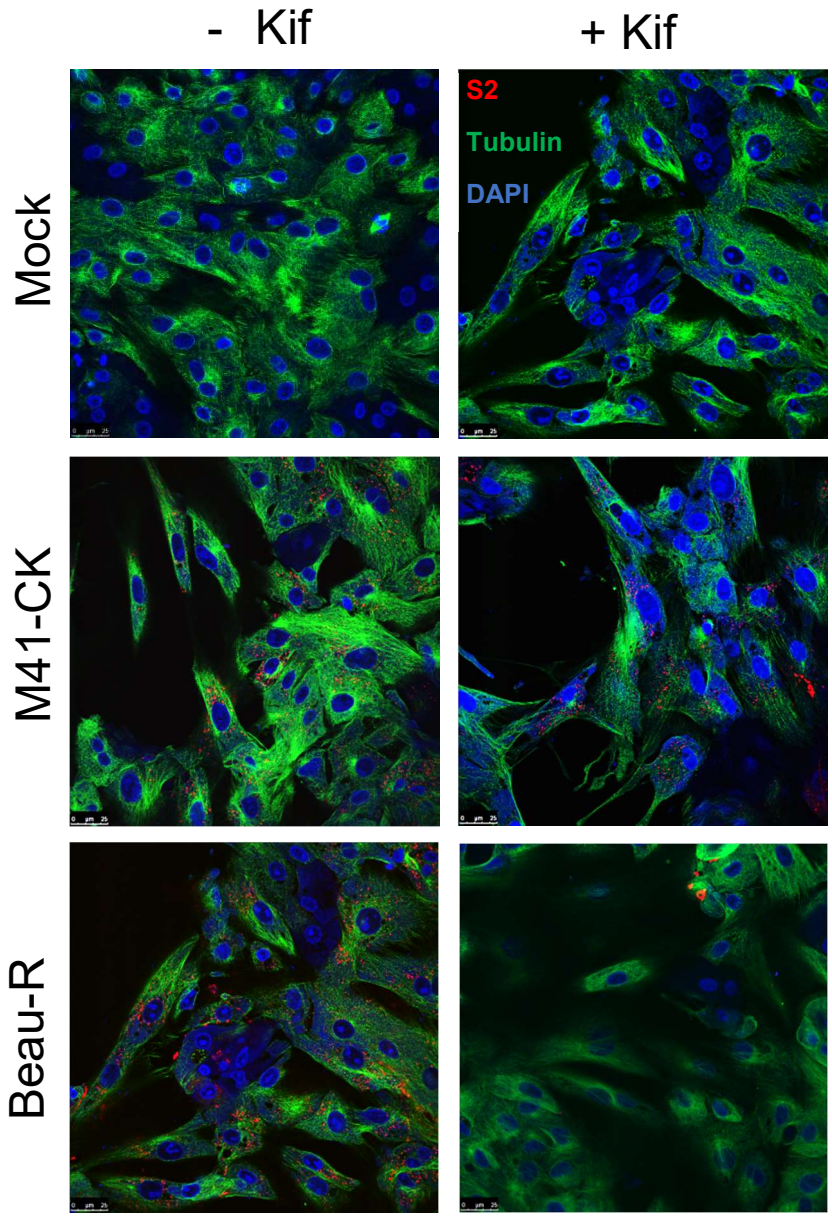

Figure 3.7: Kif treatment reduced monoclonal antibody binding of S2 during Beau-R but not M41-CK infection in CK cells. CK cells on coverslips were infected with M41-CK or Beau-R at an MOI of 1. Kif (20µM) was added to the media (1xBES) at the time of infection. Cells were incubated for 24 hours at 37°C before fixation in 4% paraformaldehyde in PBS. Cells were permeabilised using 0.1% Triton in PBS and blocked in 0.5% BSA in PBS. A monoclonal antibody against S2 (26.1) was used to detect the S protein. Cells were also stained for α-tubulin. Cells were stained with secondary antibodies AlexaFluor 568 IgG2a (S2, red) and 488 IgG1 (α-tubulin, green) and nuclei were counterstained with DAPI (blue).

The pattern of glycosylation present on a given protein can differ depending on the cell type in which it is produced (Goh and Ng, 2018). Beau-R exhibits an extended host tropism compared to M41, in that it is able to infect and successfully replicate in continuous cell lines as well as primary CK cells, due to the additional cleavage site present in the S2 subunit as recently described (Bickerton et al., 2018). To assess whether the antibody recognition loss seen in CK cells was reflected in other cell types, chicken fibroblast (DF-1) cells were seeded onto coverslips, infected with Beau-R and treated with Kif before staining for IF. M41-CK is unable to infect DF-1 cells and so was excluded from the experiments.

Figure 3.8 shows the images taken from these experiments. As expected, no S2 was detected in either of the mock samples. The α-tubulin staining is also unchanged following treatment with Kif. In the Beau-R infected samples, there was a loss of S2 recognition by the monoclonal antibody 26.1 following Kif treatment for 24 hours, compared to the untreated samples. Again, the signal for the S2 antibody was severely depleted in the treated cells compared to the infected control, confirming the results observed by western blot and indicating that removal of complex glycans from the protein has removed or distorted the epitope recognised by the antibody.

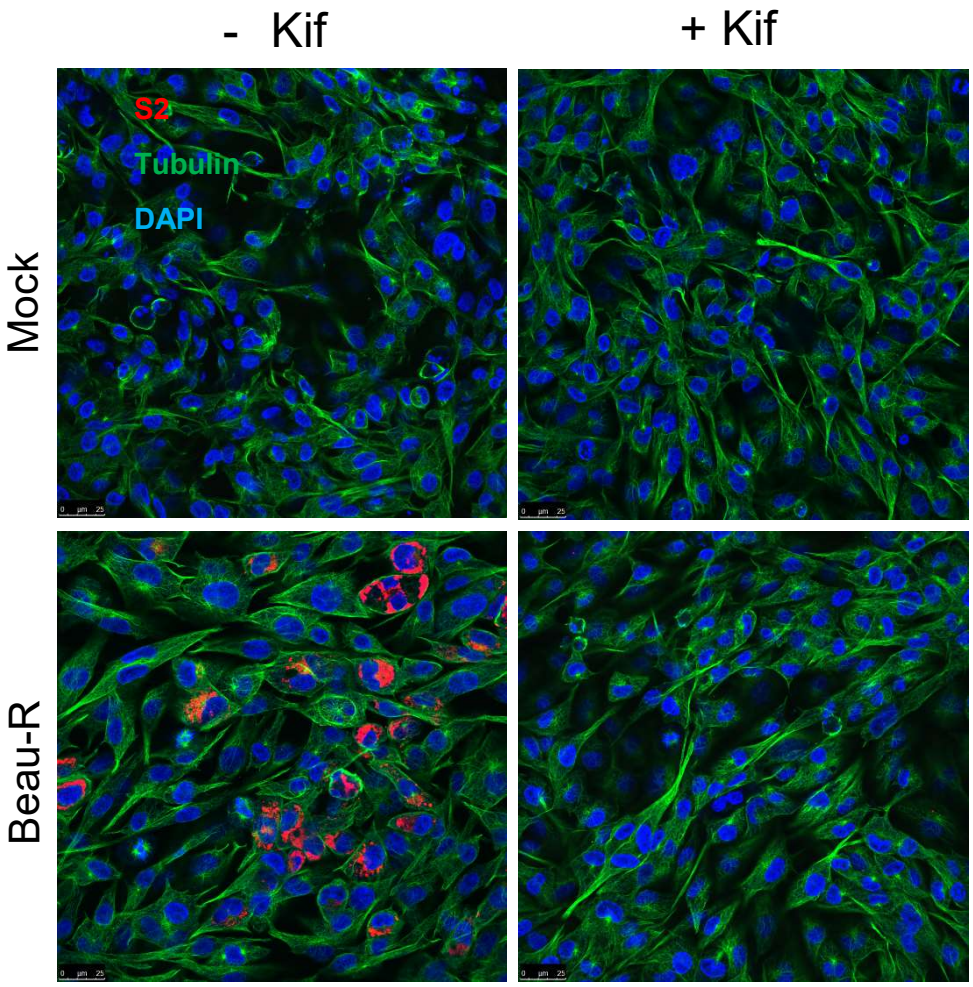

Figure 3.8: Kif treatments cause monoclonal antibody recognition loss for Beau-R S2 in DF-1 cells. DF-1 cells seeded onto coverslips were infected with Beau-R (MOI = 1) or mock infected with 1xBES. At the time of infection, Kif was added to the supernatant (20µM). Cells were incubated for 24 hours at 37°C before fixation in 4% paraformaldehyde in PBS. Cells were permeabilised using 0.1% Triton in PBS and blocked in 0.5% BSA in PBS. A monoclonal antibody against S2 (26.1) was used to detect the S protein. Cells were also stained for α-tubulin. Cells were stained with secondary antibodies AlexaFluor 488 IgG2a (S2) and 568 IgG1 (α-tubulin) and nuclei were counterstained with DAPI (blue).

The effects seen in Figures 3.5-8 indicate a potential role for complex glycans in protein folding and antibody recognition, however a role for these glycans in infection and replication has not been defined. To address whether inhibiting the formation of these glycans had any effect on viral infectivity and to confirm that the Kif treated samples were, in fact, infected, supernatant from IBV-infected/Kif-treated CK cells was used for plaque assay in CK cells. The average viral titres for M41-CK and Beau-R following treatment with Kif are shown in Figure 3.9. For both M41-CK and Beau-R, no significant change in viral titre was observed following treatment with Kif. There is a reduction in Beau-R titre following treatment but it is not statistically significant (p = 0.1499). Taken together these results suggest that complex glycans are non-essential for IBV infection but may have some function in contributing to the proper conformation of the protein and arrangement of its epitopes.

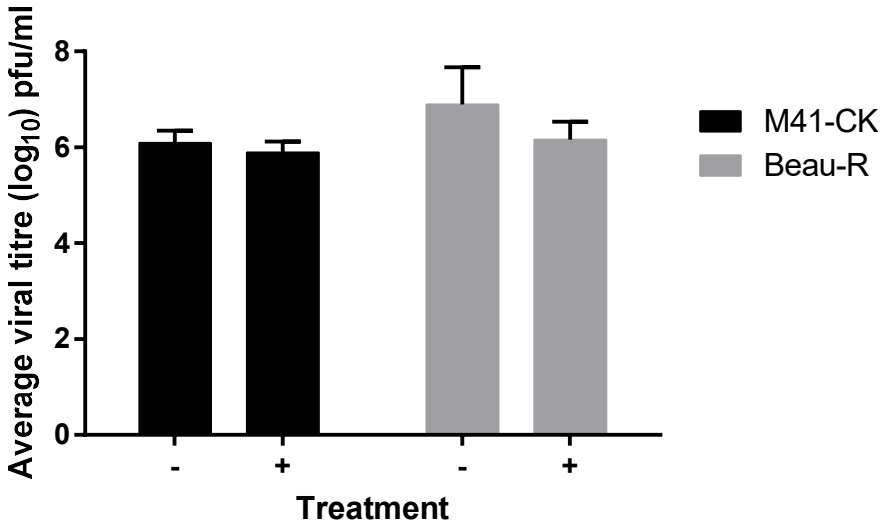

Figure 3.9: Treatment with Kif does not affect viral titre in CK cells. Cells were infected with either M41-CK (black) or Beau-R (grey) at an MOI of 1 for 24 hours either in the presence (+) or absence (-) of Kif (20μM). Supernatant was harvested and used for titration by plaque assay in CK cells. Infections were repeated 3 times and mean values for each treatment are displayed with standard deviation (SD). Statistical analysis of untreated and treated values for each virus were completed using unpaired t-test.

Further investigations were carried out to provide a more comprehensive understanding of the role of complex glycans in antibody recognition of the S protein using another monoclonal antibody, known as A13, directed against the S1 subunit. Again, recognition of the S protein was assessed by infection of CK cells with IBV in the presence of Kif, followed by IF to assess any changes in S protein detection following the inhibition of complex glycan formation. Figure 3.10 shows the confocal images from these infections using the A13 antibody and a polyclonal antibody recognising a range of IBV proteins (chIBV). This antibody was used as a control to confirm infection in the cells.

No staining was observed in the mock cells, bar the nuclei (DAPI), as expected. There was no change in S1 recognition by A13 following Kif treatment in either M41-K or Beau-R infected cells, indicating that the removal of complex glycans has not impacted the structure or formation of the epitope recognised by this antibody and that the effects observed with 26.1 are antibody specific. The chIBV staining was diffuse throughout the cytoplasm of the infected cells in both the treated and untreated samples.

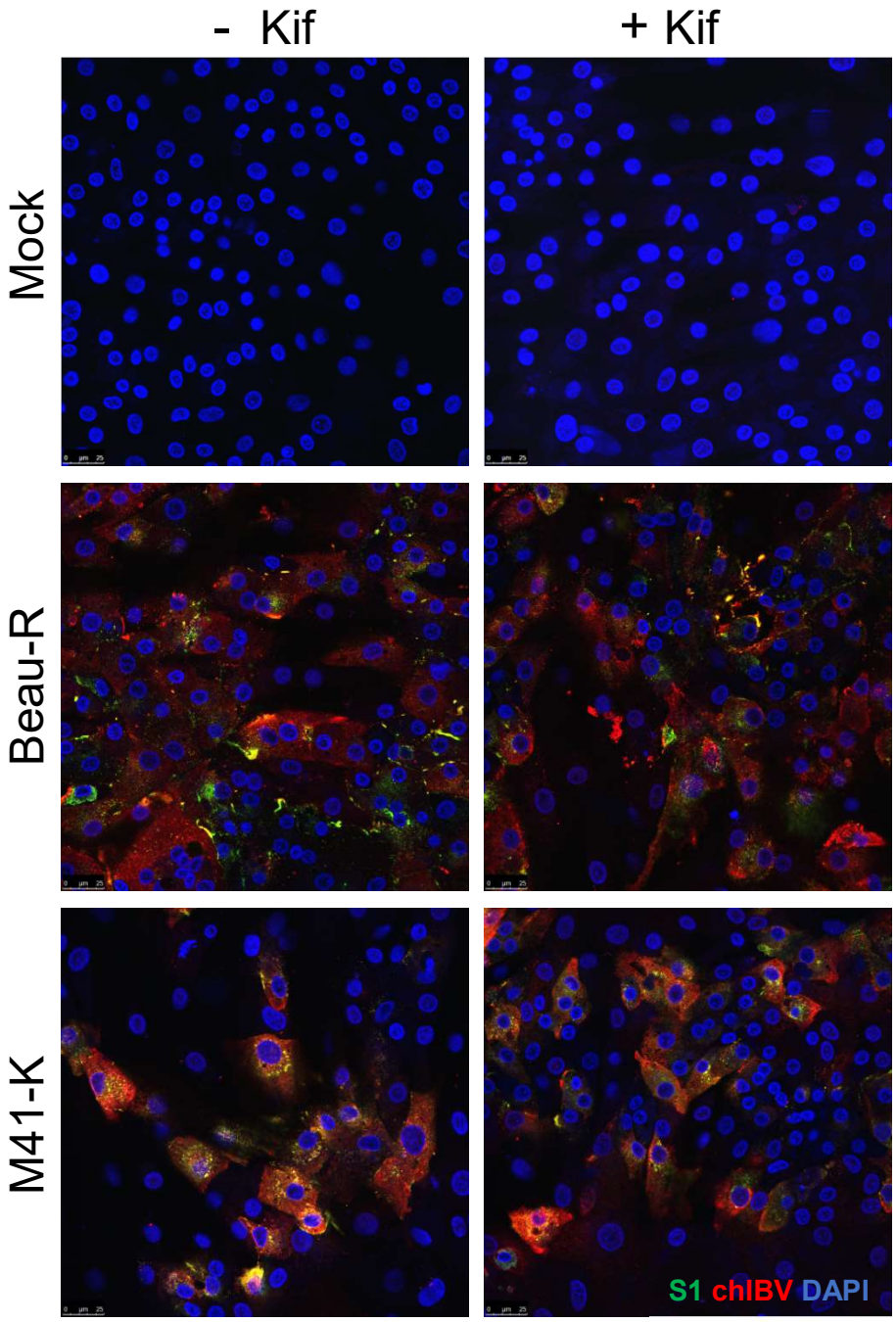

Figure 3.10: Recognition of S1 by monoclonal antibody A13 is not affected by Kif treatment.

CK cells were seeded onto glass coverslips and infected with Beau-R or M41-K at an MOI of 1 and incubated for 24 hours either in the presence (+) or absence (-) of Kif (20 µM). Cells were fixed in 4% PFA and stained using a monoclonal antibody against S1 (A13) and a polyclonal antibody against IBV (chIBV). Cells were stained with AlexaFluor Goat anti-Mouse IgG 488 (S1, green) and AlexaFluor Donkey anti-chicken IgG 568 (IBV, red). Nuclei were counterstained using DAPI (blue).

The involvement of surface glycans in evasion of the immune response and neutralising epitope shielding is well known (reviewed by Vigerust and Shepherd, 2007). As antibody binding to Beau-R S2 was clearly reduced following Kif treatment, effects on virus neutralisation were assessed using an antibody against the IBV S1 subunit (A13) by plaque reduction assay. Beau-R and M41-K were used to infect CK cells and those treated with Kif were compared to untreated infected samples of CK cell supernatant in their susceptibility to neutralisation by monoclonal antibody. Figure 3.11 shows the average viral titre of untreated and Kif-treated samples, in the presence of decreasing concentrations of A13. This allows identification of the concentration at which the antibody becomes neutralising to the virus.

The data clearly show that A13 did not neutralise Beau-R even at the highest concentration of antibody. This result was expected as published data has shown Beaudette strains to be resistant to A13 neutralisation (Mockett et al., 1984). M41-K was susceptible to neutralisation by A13. The dilution at which neutralisation occurred was between 1/64 and 1/128 for the UT samples. Kif treatment resulted in some slight variations in the data for M41-K neutralisation, with the suggestion of a trend towards a minor reduction in its susceptibility to A13 neutralisation, however the differences were very small and not statistically significant. Kif treatment had no effect on Beau-R, which remained resistant to neutralisation in the presence of the inhibitor. The inhibiting action of Kif in these samples was confirmed by western blot on the cell lysates from these samples to show loss of Beaudette S2 recognition by 26.1 (Figure 3.12).

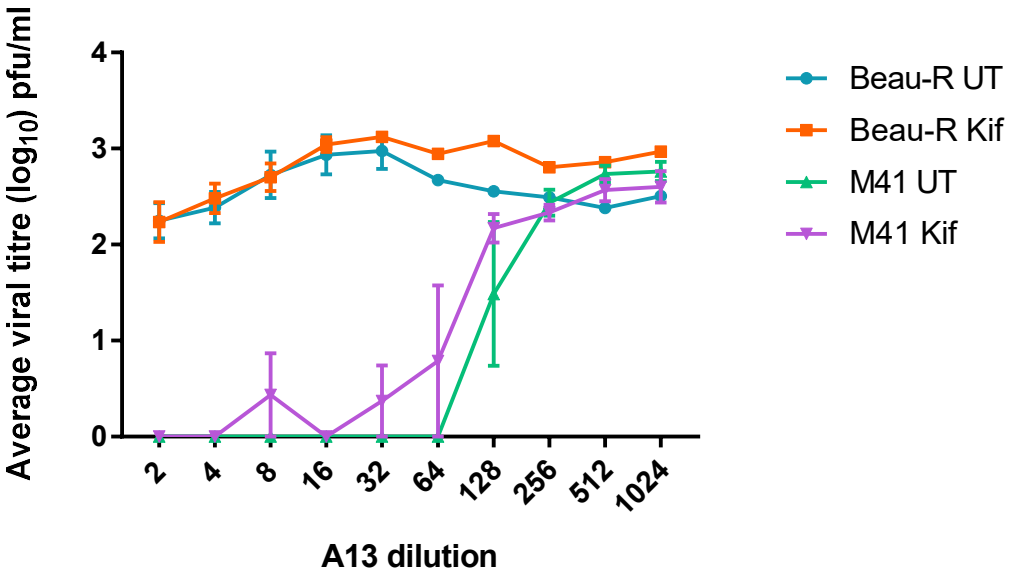

Figure 3.11: Kif treatment does not affect A13-mediated virus neutralisation in M41-K or Beau-R infections. Infected CK cell supernatant (untreated (UT) and Kif-treated) was diluted to 2000pfu/ml and incubated with decreasing concentrations of the S1 monoclonal antibody A13. Virus-antibody solutions at each dilution were used for plaque assay in CK cells. The average viral titres (log_{10}) of three biological repeats are shown in pfu/ml and are displayed with SEM. Each set of data was analysed by unpaired t-test.

Confirmation of the effects of Kif in the experiments detailed in Figure 3.11 was achieved through analysis of cell lysates by western blot. The S1 antibody A13 is incompatible for use in western blot and so anti-S2 (26.1) was used to verify the inhibitor action in these samples through loss of S2 subunit recognition. Figure 3.12 shows the western blot confirming this effect in the cell lysates from the original infections used for Figure 3.11. The cell supernatant was used for the plaque reduction assay and the cell lysates were harvested and used for western blot with 26.1. The 80kDa band indicating S2 recognition was present in both the untreated and the Kif-treated M41 samples, again demonstrating that Kif treatment had no effect on the recognition of the M41 S2 subunit by 26.1. In the Beau-R samples, the S2 band was visible only in the untreated sample and recognition was lost in the Kif-treated sample. The bands indicating the presence of β-actin in the Beau-R samples appeared slightly fainter than those seen in the M41-infected samples. This may be due to the nature of the strains, as Beau-R is known to cause more extensive cpe in infected cells compared to M41 strains, meaning a proportion of the cells may have been lost during washing steps as they may have become detached during infection.

This result consolidates previous results, further demonstrating that inhibition of complex glycan formation by Kif treatment affects recognition of the S2 subunit by 26.1 by some mechanism. It also confirms that the effect is only seen in Beau-R infected cells and that the inhibition has no effect on M41 S2 recognition.

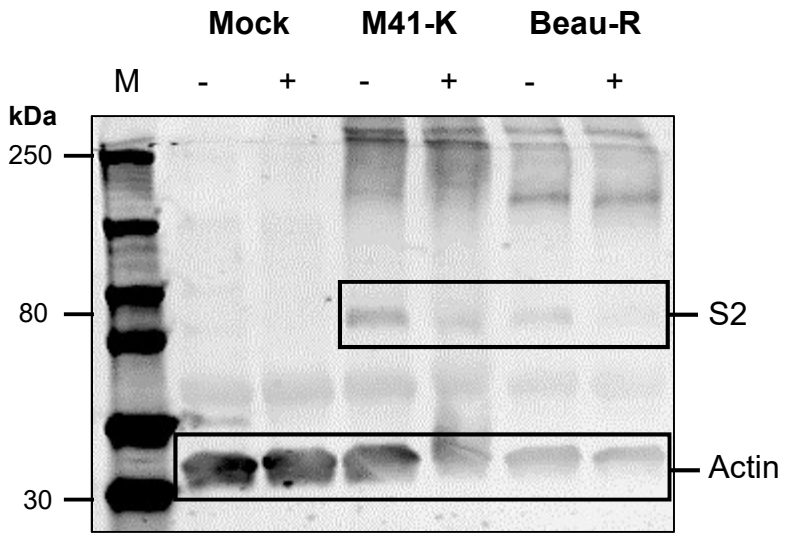

Figure 3.12: S2 subunit binding by 26.1 is reduced following Kif treatment. CK cells were infected with IBV or mock-infected in the presence (+) and absence (-) of Kif and incubated for 24 hours at 37°C. Cell lysates were harvested using RIPA lysis buffer and used for SDS-PAGE followed by western blot using a monoclonal S2 antibody (26.1) and anti-β-actin (Sigma). The S2 subunit is indicated at approximately 80kDa. Band sizes were compared to Bio-Rad Dual Colour Standards.

Using the PNGS predictions detailed in Figures 3.1 and 3.2, attempts were made to generate a mutant virus with a modified S protein removing 9 of the PNGS highlighted by the NetNGlyc algorithms. These nine sites were chosen for modification based on the scores assigned to each site indicating the likelihood of glycan attachment and thus utilisation by the virus. The plasmid detailed in Figure 3.13 was synthesised by GeneArt and used in attempts to generate the virus through vaccinia virus-based reverse genetics. The plasmid was designed to include N to A mutations in each of the nine sites (Figure 3.13B), hence removing the glycosylation sequences from the gene. The plasmid was used for homologous recombination followed by plaque purification to isolate a virus containing the correct mutations. The reverse genetics process is described in detail in Methods Section 2.12. After numerous attempts at virus rescue using recombinant vaccinia virus (rVV) DNA containing full length IBV cDNA with the modified S gene in both CK and Vero cells, it can be concluded that rescue of this virus (M41-delPNGS) is not possible. This suggests an essential role for the combination of these specific glycan sites most likely in protein folding and virus assembly. While a positive control was not specifically included for the rescue attempts, other recombinant viruses were rescued successfully at the same time, indicating that the rescue system was not the issue in recovering M41-delPNGS.

It is likely that the virus could not be rescued in CK cells due to incorrect protein folding. While each glycan is unlikely to be crucial for virus replication individually, the collective mutations may have affected protein folding pathways in the ER and Golgi during protein synthesis to a degree where the virus cannot incorporate correctly folded S proteins and thus becomes non-viable.

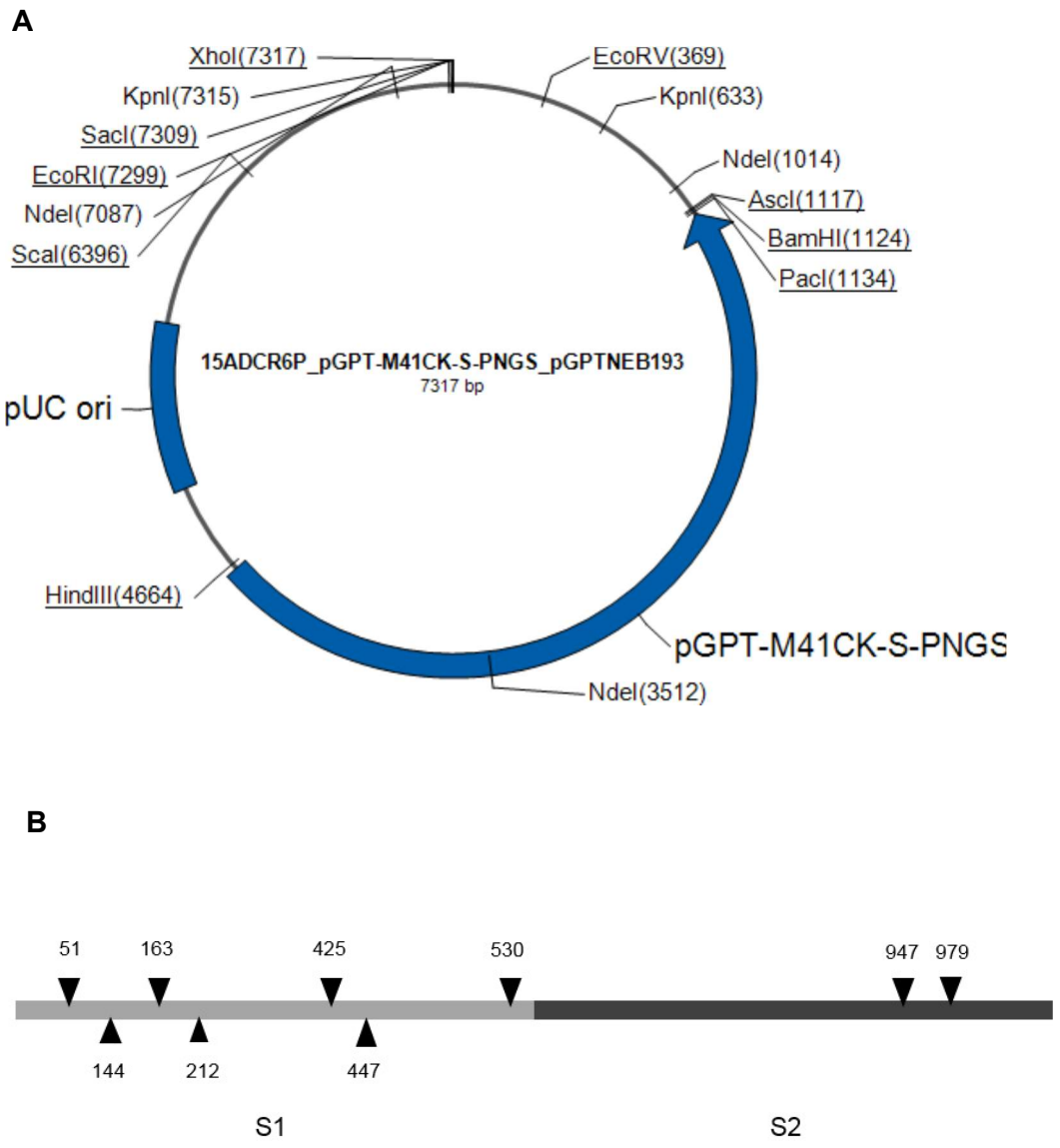

Figure 3.13: Rescue of rIBV M41-delPNGS with 9 mutations in PNGS is not possible. (A) The plasmid (generated by GeneArt) detailed was used to generate a recombinant vaccinia virus (rVV) containing full length IBV cDNA with a modified S protein containing 9 mutations in each glycosylation site. **(B)** Schematic representation of the modified M41CK-S-PNGS S gene. Mutations were introduced at 7 PNGS in the S1 subunit and 2 in the S2 subunit. Asn positions are indicated by black arrows.

3.3 Discussion

The N-linked glycosylation profile of IBV, until recently, has remained relatively understudied compared to other coronaviruses, where its importance has been proposed in processes such as virus entry and immune evasion (Han et al., 2007, Walls et al., 2016b). Four strains of IBV were chosen for analysis based on their differences in virulence and pathogenicity. Three pathogenic strains (M41-CK, QX and 4/91) and one non-pathogenic strain (Beau-R) were selected for sequence analysis to characterise the levels of glycosylation present in each strain. M41-CK and Beau-R were selected for more in-depth analysis based on their feasibility of propagation in cell culture and the differences in their *in vitro* tropisms.

To begin the assessment of N-linked glycosylation in the IBV S protein, the sequences of four strains of IBV were analysed to identify any PNGS with the amino acid sequence N-X-S/T. The results from this analysis show a high level of potential glycosylation in each strain with similar numbers of suitable Asn sites present in each sequence (Table 3.2). The results highlight a difference between the lab-adapted strains and the field strains in that the field strains QX and 4/91 contain more PNGS than M41 or Beau-R. There is some variation in the numbers of potential sites present in the S proteins of other coronaviruses; for example the S glycoproteins of the betacoronaviruses SARS and MERS contain far fewer potential sites than any of the IBV strains selected for analysis, with 22 and 25 potential sites, respectively (Yuan et al., 2017). However across all coronaviruses the S protein exhibits a generally high level of glycosylation. In some viruses the presence of such a high density of glycans on the surface of the protein has been implicated in epitope masking and immune evasion (Walls et al., 2016b).

The S1 subunit of the IBV S glycoprotein was shown to contain the majority of the N-X-S/T sequences. To assess the global conservation between a wider range of IBV strains, the S gene sequences were analysed and percentage conservation for all available gene sequences

was calculated (Figure 3.1). The majority of the sites identified in the S1 subunit are highly conserved among IBV strains, being present in between 80 and 100% of the 834 analysed sequences. The high level of conservation among all strains indicates a definite role for glycosylation in coronaviruses, otherwise the sites would have been lost through evolution. The sheer number of potential sites present in these viruses shows that they must play an important part in the success of these viruses.

Recently published structures of IBV S proteins, elucidated by cryo-EM, have allowed more accurate modelling of the strains described here to assess the spatial positioning of the glycosylation sites in relation to the whole protein conformation. M41-CK was used here as a representative strain to show the positioning of each site on the 3D models generated using PyMol and SWISS Model. The recently published structure of IBV M41-CK provided a basis for the models detailed in Figure 3.2, with 100% confidence in the sequence identity (Shang et al., 2018). The models further demonstrate the higher density of glycosylation sites present in the S1 subunit of the protein. As this subunit constitutes the globular head of the protein and is responsible for attachment to host cells, this is unsurprising. In other RNA viruses with similar glycoproteins such as influenza, glycosylation has been shown to be involved in binding to receptors on host cells, facilitating virus entry (Londrigan et al., 2011).

The number of potential sites present in a given protein sequence does not indicate attachment of an oligosaccharide to this site. Many factors influence the likelihood of glycan attachment, including the amino acid sequence surrounding the asparagine, not just the N-X-S/T motif itself. Purified samples of IBV M41-CK were used for analysis by MS to further investigate which sites showed evidence of oligosaccharide attachment and which were unlikely to be utilised by the virus. The results from the MS experiments in Figure 3.3 indicate a high proportion of sites with evidence of glycan attachment; at least 18 of the 29 sites present in the sequence are utilised by the virus for glycosylation. There could be a higher

number of utilised sites as the coverage of the protein sequence achieved during the experiments was not complete. Improvements could be made in future repeats of the experiment with more concentrated samples, however this may not be ethically viable due to the number of embryonated eggs required to produce the quantities of virus used for purification. A recent study using MS techniques to analyse the S protein of a Vero-adapted strain of Beau-R showed far fewer utilised sites following their analysis of the glycosylation profile. Only 8 sites were identified as being positive for glycan attachment out of a potential 29 (Zheng et al., 2018). It is possible that the Vero adaptation process has reduced the number of utilised sites in the glycoprotein, or that the LC-MS/MS technique used is less sensitive than the EThcD techniques used in this analysis. Two separate instruments were used for analysis of the M41-CK strain described here, providing a more robust analysis. Another recent study investigating the structure of the M41 S protein ectodomain identified 20 glycosylation sites, similarly to the numbers identified in Figure 3.3 (Shang et al., 2018). Comparing the two sets of data reveals that of the 20 sites identified by Shang *et al.*, 9 are consistent with sites identified on the S protein M41-CK by MS methods in this study. More sites were identified in the S2 subunit of the protein in Figure 3.3 compared to the published results. This is not to say that either list is exhaustive. There are differences in the methods for each dataset which may have altered the results slightly. For instance, the protein studied by Shang and colleagues was expressed in insect cells whereas the protein studied here was wild-type as the material used for the experiment was derived from purified virus particles propagated in embryonated eggs. The differences in these production methods may have influenced the conformation and glycan profile of each protein, resulting in the detection of different glycosylation sites. Nonetheless the identification of 9 sites across both methods validates the results shown in Figure 3.3, indicating that these sites may be conserved even after the high number of passages in CK cells to which M41-CK has been subjected.

MS techniques were also used to begin to characterise the structures of the glycans present at these sites. Structures were elucidated at six of the sites present in the S glycoprotein, with relatively similar oligosaccharide compositions consisting of mainly simple high mannose glycans. The heterogeneity of the structures present at each site implies that the glycosylation profile varies between individual glycoproteins within a sample of virus. Other studies have used the same MS techniques to provide detailed characterisation of the glycan shield in other coronaviruses such as HCoV-229E (Walls et al., 2016b). More detailed results were obtained from these experiments, including a more diverse range of glycan classes, possibly due to sample preparation method using protein expression in human cell lines compared to the purification of infected allantoic fluid described here. It is important to note that a more diverse range of glycans was detected during the MS experiments but their detection fell below the limit of significance compared to the other structures and so were not included in the final results. Overall it appears that protein expression systems in human and insect cell lines may provide better coverage of the protein compared to the purification methods described here. However the data described are more likely to be accurate and relevant to the natural host of IBV, as the virus was propagated in embryonated eggs.

While not fully characterised using MS techniques, a diverse range of glycans has been detected on the S glycoproteins of both M41-CK and Beau-R using other techniques. PNGase F treatment demonstrates the contribution of N-linked glycosylation to the overall molecular weight of the protein, possibly suggesting that more than half the protein's weight is attributed to N-linked glycans. Endo H and Kif were used to demonstrate the presence of different classes of glycan present on the protein surface. Taken together the results show that the IBV S glycoprotein displays all three major classes of glycan: high mannose, complex and hybrid (Figure 3.5). Treatment with the α-mannosidase I inhibitor Kif (Elbein et al., 1990) highlighted an important difference between M41-CK and Beau-R; following inhibition of complex glycan formation, recognition of the S2 subunit by the mAb (26.1) was completely

lost in Beau-R but not in M41-CK. This indicates that the epitope recognised by this mAb has been either distorted or lost following removal of complex glycans from the surface of the protein. The mAb 26.1 has been shown to bind to residues 546-725 in S2 (Kusters et al., 1989). There are five PNGS in this epitope, three of which were confirmed by MS (Figure 3.3), so it is likely that interference with the attachment and processing of glycans at these sites in Beau-R is the reason for the loss in mAb recognition, most likely through epitope distortion. These sites are also present in the M41-CK sequence however they may not be affected by complex glycan removal. The differences in S recognition by 26.1 in the M41-CK samples was also of interest. With a visibly stronger S2 band intensity observed in the M41-CK-Kif samples, it appeared that the recognition of the uncleaved proportion of S was lost, indicating that potentially more cleaved S2 was present in the sample. This could be linked to the glycosylation site present just before the S1/S2 cleavage site at M41 position 530 (confirmed by MS in Figure 3.3). Perhaps the change in glycosylation status at this position altered the cleavage rates of the protein within this sample. Further investigation into the action and mechanisms involved in Kif treatment would be required to add proof to this hypothesis.

Treatment with another inhibitor (SW) was used to confirm that the effect observed here was Kif specific (Figure 3.6). SW treatment did not result in a change in mAb recognition by western blot, showing that the results observed with 26.1 were due to Kif treatment and inhibition of complex glycan formation. This raises an interesting point about the different pathways involved in protein synthesis and folding affected by these inhibitors. The greater effects observed with Kif treatment compared to SW treatment could indicate that the action of ER α-mannosidase I may be more crucial to the proper synthesis and folding of the protein. The ER modifications are more likely to affect the fundamental folding processes in protein synthesis, related to the involvement of glycosylation in the calnexin cycle and ERAD pathways. SW acts on α-mannosidase II which resides in the Golgi. This enzyme acts after

processing in the ER has been completed and the protein has been transported to the Golgi, having already achieved an adequate conformation. While modifications that occur in the Golgi are important, they may play a less crucial role in the proper folding and epitope presentation of the glycoprotein compared to those that occur in the ER.

Further investigation into Kif-induced mAb recognition loss was carried out using immunofluorescence in avian cells. Figures 3.7 and 3.8 both reiterate the loss of S2 recognition following Kif treatment, showing the effect is not cell type-specific. There was no change in viral titre following Kif treatment in CK cells, indicating that complex glycans are not required for infection (Figure 3.9). Glycosylation has also been shown to be non-essential for viral infectivity in HIV glycoprotein gp120, supporting the data described here (Rathore et al., 2017). Further investigations would be required to assess more specific effects of the inhibitor in different processes during viral replication. These experiments were also only performed after 24 hour treatments. Passaging the virus in the presence of Kif could provide more information on how the virus would compensate for the lack of complex glycans, if an effect would be seen at all. Similar effects in loss of antibody recognition following glycosylation site deletions have been observed in HIV, with the presence of glycan-dependent epitopes dictating binding to the gp120 envelope protein (Doran et al., 2014).

In related studies, Kif has mainly been used for investigations into the glycosylation of the HIV-1 surface glycoprotein gp120, in which there were notable effects on virus neutralisation with monoclonal antibodies following Kif treatment (Walker et al., 2010). The data from the plaque reduction assays (Figure 3.12) indicate that Kif treatment has not had an effect on Beau-R neutralisation by the monoclonal antibody A13, which has been shown not to interact with other Beaudette strains in past studies (Mockett et al., 1984). The data for M41-K neutralisation are slightly more variable following Kif-treatment, but the differences in neutralisation between the treated and untreated samples are not significant. It would be

beneficial to study this in more detail using a range of antibodies targeting different epitopes on the S protein, to assess which were most affected by the removal of complex glycans. Other inhibitors could also be used to disrupt the formation of other classes of glycan to elucidate their role in susceptibility to virus neutralisation.

Another important consideration regarding experiments involving Kif concerns the location of the mannosidases on which the inhibitor has an effect within the cell. As mentioned previously, mannosidases are important players in the ERAD pathways, which regulate the protein folding process in the ER. Interference with these pathways can not only lead to altered glycosylation profiles in glycoproteins but also the accumulation of incorrectly folded proteins, due to the suppression of the regulation mechanisms. In-depth analysis of these pathways is beyond the scope of the project however this may be important to remember when analysing future experiments with Kif, taking into account any off-target effects that may have arisen as a result of disruption of these critical cellular pathways.

Assessment of the role of individual glycans in viral replication would be beneficial to start to target specific sites for vaccine development, in order to render the virus more susceptible to the host immune response, for example. Attempts were made to generate a recombinant virus containing a modified S glycoprotein with mutations in the individual glycosylation sites, based on the information generated by the NetNGlyc 1.0 Server. The combination of mutations included in the modified S protein was not compatible with virus rescue, indicating that these glycosylation sites are essential for virus viability. It is unclear whether all the mutated sites are individually important to the virus or whether the effect is cumulative. Given the crucial involvement of glycosylation in protein folding pathways in the ER and Golgi, it is likely that the mutated protein was not able to achieve a native conformation and was targeted to for degradation. The protein could also have been misfolded and incorporated into virions in the wrong conformation, leading to altered or reduced function.

Mutations in N-linked glycosylation sites have been shown to impact rescue in other viruses due to interference in protein folding. It has also been suggested that mutations in the PNGS closer to the N-terminus of the protein are more likely to impact folding and hence virus rescue (Shi et al., 2005, Herbert et al., 1997, Helenius and Aebi, 2001), providing a possible explanation for the failure of M41K-delPNGS rescue. It could also be true that the mutant virus was, in fact, recovered with the modified S protein, but was then incapable of productive infection on subsequent passages and amplification. In any case, this recombinant virus could not be detected in any of the amplification attempts and so it can be concluded that this amount of mutations is incompatible with rIBV rescue.

It has been shown that IBVs with fewer mutations can be rescued and characterised *in vitro*. Recently, Zheng *et al.* demonstrated notable effects in cell-cell spread and fusion activities following N to D mutations in individual N-linked glycosylation sites in the IBV Beaudette S protein (Zheng et al., 2018). As this data is all based on a Vero-adapted strain of Beaudette, it would be highly beneficial to study the effects of PNGS mutation in a more relevant pathogenic virus such as M41, where the mutations could be studied in an *in vivo* setting as well as *in vitro*. As there is now a more robust set of data surrounding the IBV glycosylation profile, individual glycosylation sites can be selected for mutation in the M41 S glycoprotein based on information from the MS experiments described in Figure 3.3. These experiments will provide more insight into the role of specific glycans in protein function and the virus lifecycle.

Chapter 4: Generation and characterisation of rIBV M41K-BeauR(S) to assess the role of the S protein in IBV pathogenesis

4.1 Introduction:

The spike (S) protein of IBV is involved in several parts of the virus lifecycle including attachment to an unknown receptor and fusion of viral and cellular membranes. The protein is cleaved into two subunits, S1 and S2. Previous work has shown that the S1 subunit is involved in viral entry into host cells as it contains the putative receptor binding domain (RBD) whereas S2 is responsible fusion of viral and cellular membranes and has been shown to determine cell tropism (Wickramasinghe et al., 2011, Bickerton et al., 2018). However, the role of the S protein in IBV pathogenicity has remained relatively unexplored. This is largely due to a lack of reverse genetics system for modifying genes in a pathogenic virus. In previous studies, the ectodomain of the S protein from a pathogenic strain of IBV was inserted into a non-pathogenic genome but this was not sufficient to confer pathogenicity to the recombinant virus (Hodgson et al., 2004). Since this study, another reverse genetics system based on a pathogenic IBV strain has been developed to better understand IBV pathogenesis. The pathogenic molecular clone known as M41-K was generated from a pathogenic lab strain of IBV, M41-CK.

Here, the genome of M41-K has been altered using reverse genetics to replace the S protein with that of a non-pathogenic strain, Beau-R (a non-pathogenic molecular clone of the Beau-CK lab strain). The replication and pathogenicity of the resultant recombinant virus rIBV M41K-BeauR(S) have been assessed both *in vitro* and *in vivo* to further elucidate the S protein's role in the virus lifecycle and disease pathogenesis.

4.2 Results

4.2.1 Generation and rescue of rIBV M41K-BeauR(S)

The rIBV M41K-BeauR(S) was generated by reverse genetics using VV as a vector for the IBV full length cDNA. TDS was used to modify the IBV cDNA using the plasmid detailed in Figure 4.1, containing the Beaudette S1 sequence flanked by a section of the sequence of the M41 replicase gene at the 5' end and a section of the Beaudette S2 sequence at the 3' end. The recombinant S gene sequence detailed in Figure 4.1 was inserted into an rVV containing full length M41-K cDNA comprising the Beaudette S2 gene sequence and a deleted S1 sequence (rVV M41K-delS1-BeauR-S2), thus generating full length rVV M41K-BeauR(S).

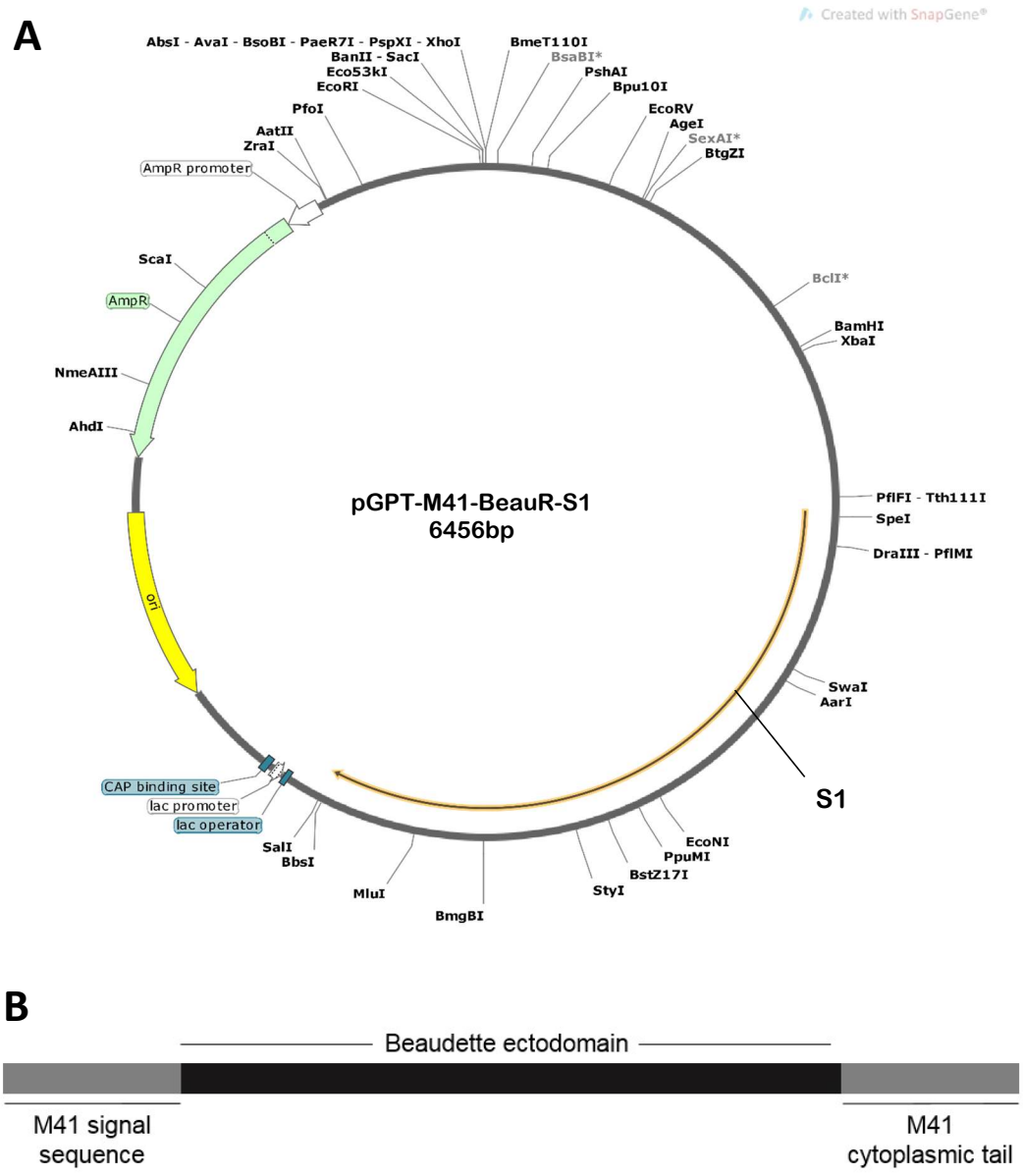

Figure 4.1: (A) Plasmid map of pGPT-M41-BeauR-S1 used to generate rIBV M41K-BeauR(S) containing the recombinant S sequence comprising the Beaudette S1 subunit with flanking regions of the M41 replicase gene at the 5' end and Beaudette S2 at the 3' end within the pGPT plasmid vector. The AmpR gene and the lac promoter sequence are highlighted along with the pUC origin of replication site (ori). The S1 gene is indicated. The plasmid map was generated from the plasmid sequence using SnapGene. **(B)** Schematic diagram detailing the structure of the chimeric S gene in the recombinant virus rVV M41K-BeauR(S), comprising the Beaudette-derived ectodomain flanked by the M41 transmembrane domain and cytoplasmic tail.

Following the completion of six rounds of plaque purification as part of the TDS process (Methods Section 2.12.3), two rVV isolates were chosen based on PCR verification of the loss of the selection gene (*gpt*) and the presence of the correct insertion – the Beaudette-derived S gene. Large stocks of these two rVV M41K-BeauR(S) isolates were propagated BHK-21 cells. DNA was extracted from the cells by phenol-chloroform extraction and the quality of the DNA used to rescue the recombinant virus was assessed using PFGE. A *Sal*I digest was performed to separate a fragment containing the rIBV DNA from the rVV DNA.

Figure 4.2 shows the PFGE image analysing the rVV DNA extracted from infected BHK-21 cells. The band at approximately 33.5kb indicates the full length IBV cDNA in both isolates (1 and 2). The presence of this fragment demonstrates the successful generation of rVV M41K-BeauR(S) and that the DNA is of sufficient quality to attempt rIBV rescue in CK cells.

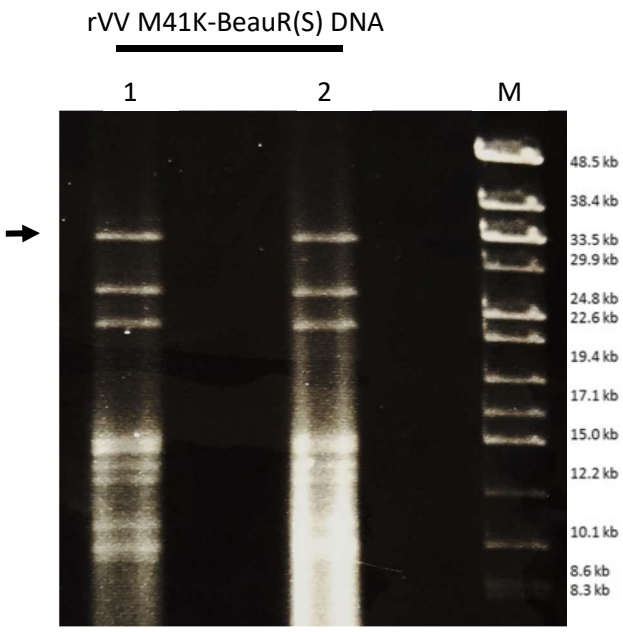

Figure 4.2: Analysis of full length rIBV M41K-BeauR(S) cDNA within vaccinia virus (VV) vector DNA. VV DNA was extracted from BHK-21 cells infected with stocks of two isolates (1 and 2) of recombinant VV containing IBV M41K-BeauR(S) cDNA. The DNA was digested using *Sal*I (Invitrogen) to produce a fragment of approximately 33.5kb. 1µg of DNA from each isolate was analysed by PFGE. The *Sal*I fragment containing full length IBV cDNA is indicated by a band at approximately 33.5kb. Band sizes were compared to a BioRad 8-48kb DNA Standard (M).

After several attempts, rIBV M41K-BeauR(S) was successfully rescued in CK cells using FPV-T7 with the addition of a plasmid containing the IBV M41 nucleocapsid (N) gene, to package the genomic RNA. Following rescue, the virus was passaged in CK cells and embryonated eggs to amplify the amount of virus present. Figure 4.3 shows an agarose gel of the positive PCR from the first egg passage (EP) indicating IBV presence and a successful virus rescue. A band of approximately 500bp was present in each of the three M41K-BeauR(S) lanes (1, 2 and 3). This showed that IBV was present in all of the rescue isolates. A previously analysed sample of cDNA, known to be positive for IBV QX, was used as a positive control for the PCR. The size of the band in this lane (+) was slightly larger than the band for the M41K-BeauR(S) isolates, due to the longer PCR product generated by this set of primers in QX samples.

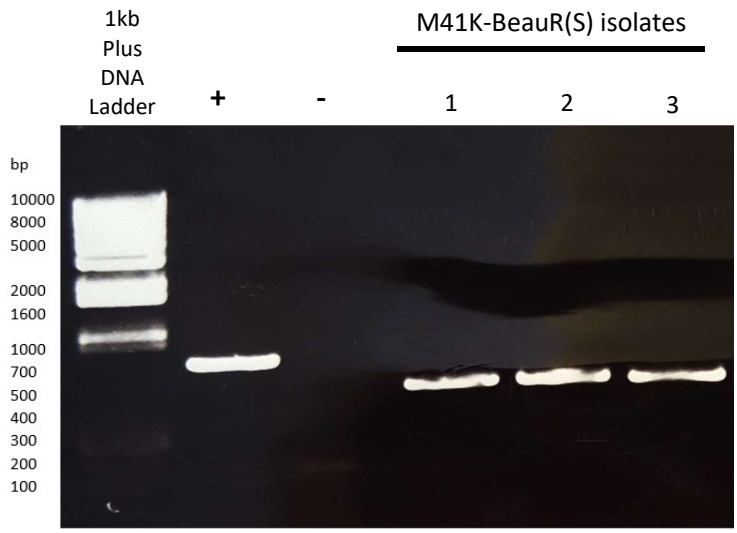

Figure 4.3: Confirmation of rIBV M41K-BeauR(S) rescue. RNA was extracted from allantoic fluid from the first passage of M41K-BeauR(S) in three replicate embryonated hens' eggs (EP1) and used for RT-PCR (Invitrogen SuperScript IV, Invitrogen *Taq* DNA Polymerase) with primers covering the 3' UTR of the IBV genome (BG56 and BG93/100). A DNA band of approximately 500bp indicates presence of IBV in the samples. + = IBV QX cDNA, - = H_2O.

In order to verify the identity of the rescued virus, cDNA generated from infected allantoic fluid was analysed by RT-PCR and Sanger sequencing using primers covering the overlap between the M41-K backbone and the Beaudette-derived S gene. Figure 4.4 shows an example of the sequence analysis, confirming the presence of the Beau-R sequence within the M41-K genome. The recombinant S protein comprises the Beaudette ectodomain with the cytoplasmic tail and transmembrane domain of M41-K. Inclusion of the M41 sections of the gene sequence preserves the interactions of S with other viral proteins.

The rescued virus was confirmed to be positive for the correct recombinant S gene. As shown in Figure 4.4A, the viral genome sequence of M41K-BeauR(S) is homologous to M41-K until position 483 (within the recombinant S gene sequence), at which point the gene is then homologous to the Beau-R S sequence, thus conserving the signal sequence of the M41 S gene. The S sequence of the recombinant virus matches the Beau-R sequence until position 3357, at which point it becomes homologous to M41-K, thus conserving the CT and TM domains at the end of the recombinant S gene.

This shows that the entire process of generation and virus recovery for rIBV M41K-BeauR(S) was successful and that the intended recombinant sequence was not altered as a result of rescue passaging.

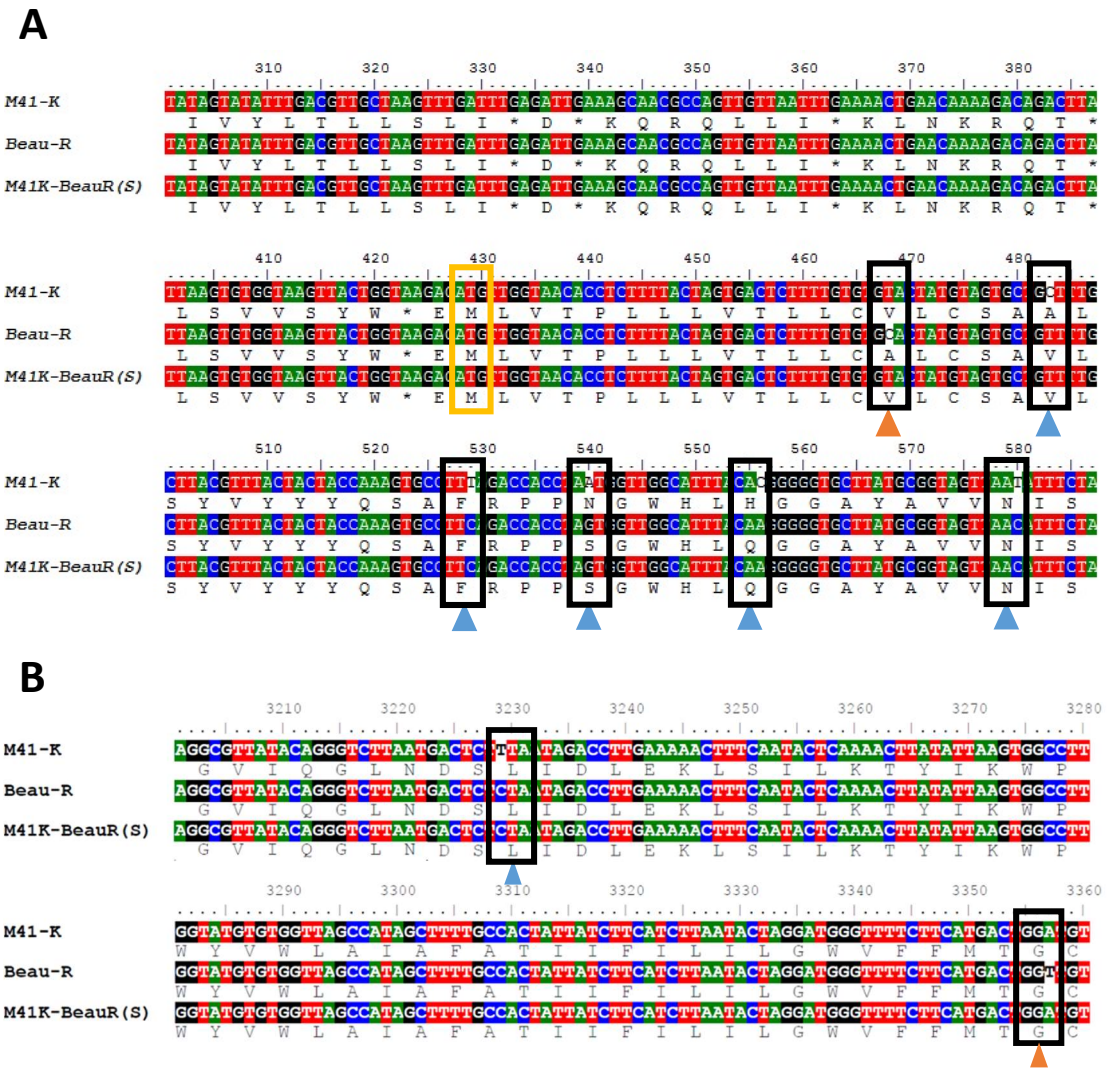

Figure 4.4: Example sequence alignment of M41K-BeauR(S), M41-K and Beau-R stocks. Stocks of M41K-BeauR(S) were propagated in embryonated hens' eggs and the allantoic fluid containing the virus was used for RT-PCR followed by Sanger sequencing using primers covering the S gene sequence and the flanking regions. Differences between the consensus sequences are highlighted. The S gene start codon is highlighted in yellow at position 428. Arrows indicate M41K-BeauR(S) sequence homology to the M41-K genome (orange) or the Beau-R genome (blue). Numbers indicate the nucleotide position within the recombinant S gene including flanking regions of the M41 signal sequence **(A)** or the cytoplasmic tail at the 3' end of the gene **(B)**.

4.2.2 In vitro *characterisation of rIBV M41K-BeauR(S)*

From the three successfully rescued isolates of M41K-BeauR(S), two were randomly selected for the propagation of virus stocks in embryonated eggs. These stocks were used to characterise the virus *in vitro*. Figure 4.5 shows the replication kinetics of M41K-BeauR(S) in primary CK cells (Fig. 4.5A) and cpe caused by the virus in CK cells after 48 hours (Fig. 4.5B). M41K-BeauR(S) follows the same replication pattern as Beau-R and causes similar levels of cpe in the infected cells, indicating that it has adopted the characteristics of the S protein donor strain. All viruses used for this experiment reached peak titre at 24 hpi. There was no statistically significant difference between any of the peak viral titres.

The similarities in the cpe induced by Beau-R and M41K-BeauR(S) shown in Figure 4.5B indicate that the virus infection and spread through the cell monolayer occurred in a similar manner. This was expected as both viruses contain the same S ectodomain. Again, this demonstrates that M41K-BeauR(S) adopted the *in vitro* tropism of the S donor strain, Beau-R.

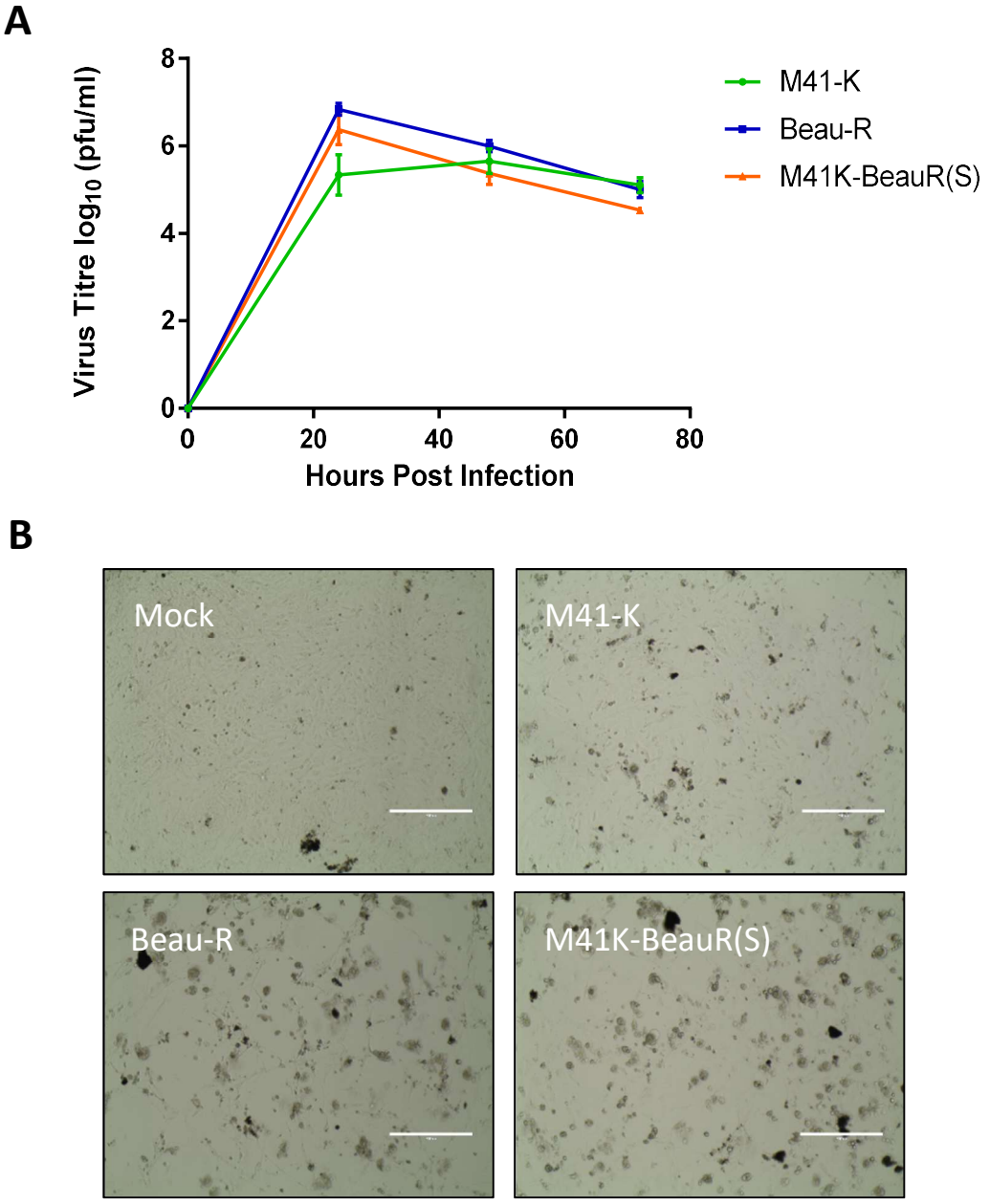

Figure 4.5: rIBV M41K-BeauR(S) replicates in primary chick kidney (CK) cells. (A) Cells were infected with M41-K, Beau-R or M41K-BeauR(S) at an MOI of 0.1 and incubated at 37˚C for 96 hours. Supernatant was harvested at 1, 24, 48, 72 and 96 hours post-infection and titrated by plaque assay on CK cells. Average viral titre at each time point is displayed with standard SEM in pfu/ml. Data were analysed by One-Way ANOVA to compare replication of the three viruses **(B)** IBV-induced cytopathic effect (cpe) in CK cells at 48 hpi infected at an MOI of 0.1 with M41-K, Beau-R or M41K-BeauR(S) compared to mock infected cells.

Due to the presence of the Beaudette S protein ectodomain, it was hypothesised that M41K-BeauR(S) would be capable of replicating in both avian and mammalian continuous cell lines, exhibiting an extended host tropism compared to M41-K which can only infect primary CK cells. To test this hypothesis, continuous cell lines were infected with M41K-BeauR(S) and the viral replication kinetics were assessed. Figure 4.6 shows the replication kinetics of M41K-BeauR(S), Beau-R and M41-K in Vero cells (Fig. 4.6A) and DF-1 cells (Fig. 4.6B).

In Vero cells the recombinant virus was unable to reach the same titre as Beau-R but did exhibit similar replication kinetics over 96 hours. Given that the stock of M41K-BeauR(S) used to infect the Vero cells was propagated in embryonated eggs and was not adapted to Vero cells, it is unsurprising that there was some difference between the titres. Differences between the titres of Beau-R and M41K-BeauR(S) at both 72 and 96 hpi were statistically significant. M41-K is unable to replicate in Vero cells due to its restricted tropism. Both M41K-BeauR(S) and Beau-R replicated to significantly higher titres from 24 hpi onwards.

DF-1 cells are a chicken fibroblast cell line which also support Beaudette replication (Himly et al., 1998). Replication of M41K-BeauR(S) in these cells is significantly lower than Beau-R at 24 and 48 hpi, but the virus is able to replicate to significantly higher titres than M41-K, further demonstrating that the recombinant virus M41K-BeauR(S) has adopted the extended host tropism of the Beaudette strain. This characteristic is conferred by the Beaudette S gene, demonstrating that the ectodomain of the Beau-R S protein is sufficient to alter viral tropism.

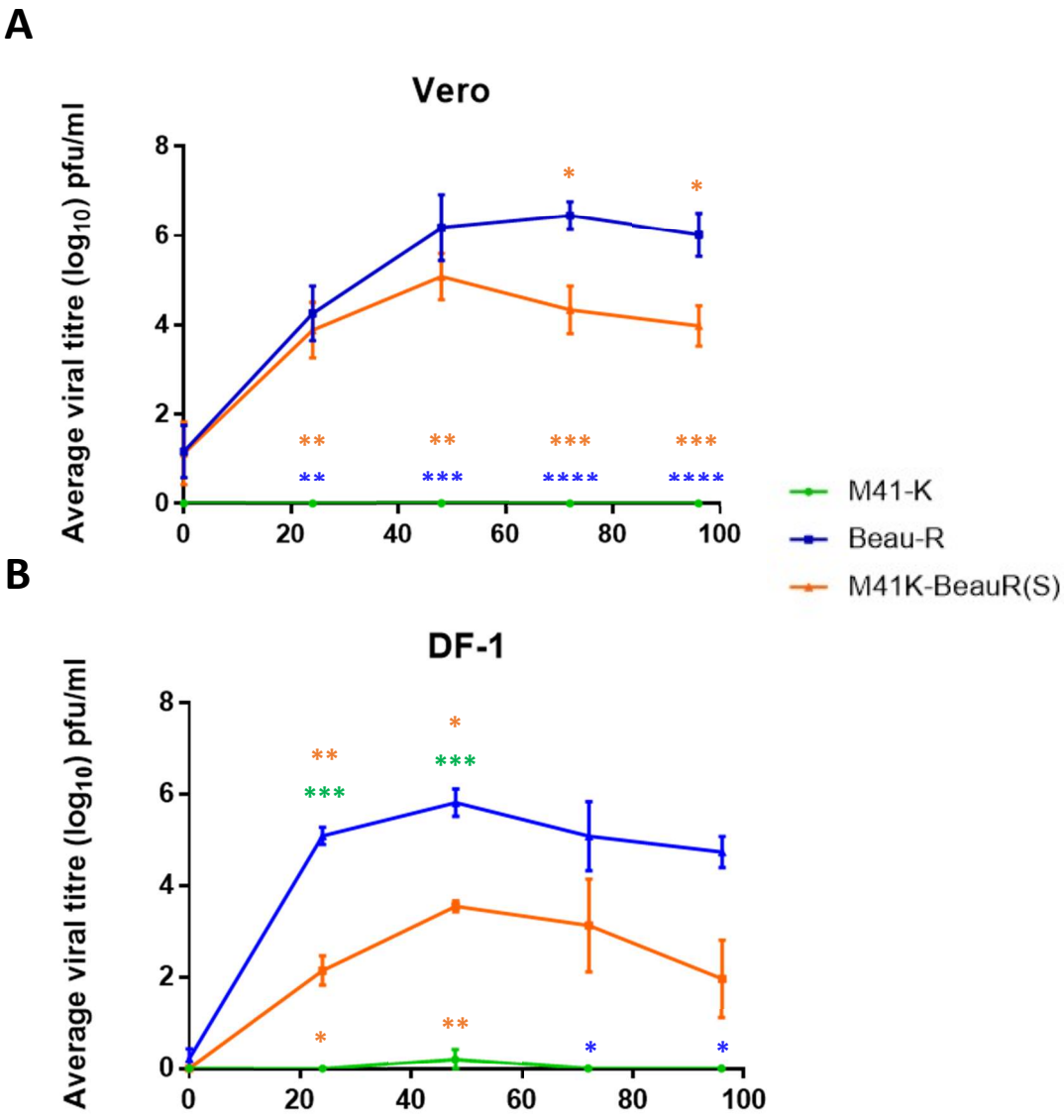

Figure 4.6: Demonstration of extended host tropism: *in vitro* replication characteristics of rIBV M41K-BeauR(S) in continuous cell lines. Confluent monolayers of Vero cells **(A)** and DF-1 cells **(B)** were infected with M41-K (green), Beau-R (blue) or M41K-BeauR(S) (orange) at an MOI of 0.1 and incubated at 37°C for 96 hours. Supernatant was harvested at 24 hour intervals and titrated by plaque assay in CK cells in triplicate. Log10 values of average viral titres are shown in pfu/ml with SEM. Infections were performed in triplicate and average values were analysed by One-Way ANOVA for each time point. Comparisons between each virus are indicated by coloured asterisks above the relevant line, matched to the colour of each group in the key (* indicates $p < 0.02$, ** $p < 0.01$, *** $p < 0.001$, **** $p < 0.0001$).

Distribution of the recombinant S protein in infected primary CK cells was assessed using indirect immunofluorescence with a monoclonal antibody against the S2 subunit of the protein. Figure 4.7 shows the distribution of the protein in CK cells infected with M41K-BeauR(S) compared to the parent viruses M41-K and Beau-R. Cells were also stained for α-tubulin as a cellular control. There was no S2 staining visible in the mock infected cells, as expected. In the Beau-R infected cells, staining of the S protein was diffuse throughout the cytoplasm. There appeared to be less Beau-R infected cells compared to the M41-K samples, however this may have been due to image frame variance rather than true infection rate. In the M41-K infected samples, staining was again diffuse throughout the cytoplasm, similar to what was observed in the M41K-BeauR(S) infected cells, in which there was also a visibly higher proportion of infected cells.

Taken together these results show that the S protein is diffuse throughout the cytoplasm of all infected cells independent of the virus strain. M41K-BeauR(S) was able to infect and replicate in CK cells to similar levels as both the parent viruses M41-K and Beau-R. It also demonstrates that the recombinant nature of the S protein in M41K-BeauR(S) had no effect on the binding ability of the monoclonal S2 antibody 26.1.

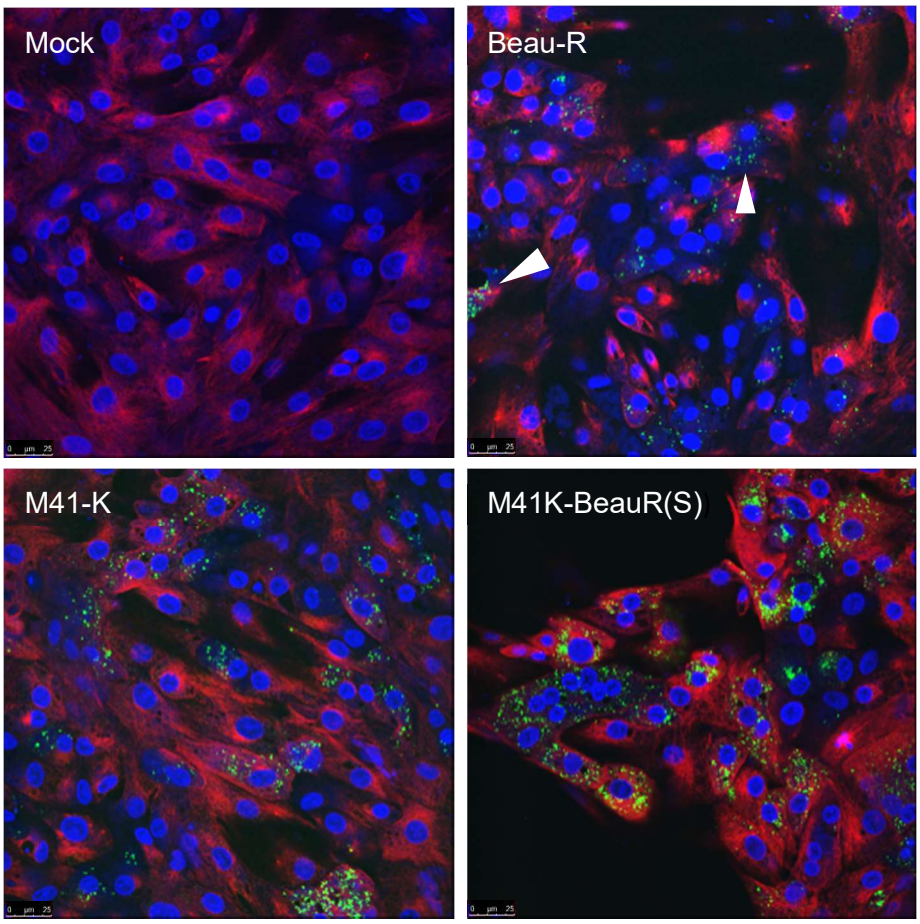

Figure 4.7: rIBV M41K-BeauR(S) exhibits the same S protein distribution as M41-K and Beau-R in infected CK cells. CK cells were infected with Beau-R, M41-K or M41K-BeauR(S) at an MOI of 1 and distribution of the S protein was compared to mock infected cells using a monoclonal antibody against the S2 subunit (26.1). Nuclei were stained with DAPI (blue). Alpha-tubulin is stained in red (AlexaFluor 568 Goat anti-mouse IgG1) and S2 is stained in green (AlexaFluor 488 Goat-anti-mouse IgG2a).

As the primary site of IBV replication *in vivo* is the epithelial cells of the trachea, M41K-BeauR(S) replication was also characterised in *ex vivo* tracheal organ cultures (TOCs). Figure 4.8 shows the replication kinetics of the recombinant virus and the two parent viruses in tracheal organ cultures. All three viruses reached peak titres at 24 hpi, with very little variance between the values. After this point, virus titres began to decrease steadily in M41K-BeauR(S) infected TOCs. Both M41-K and Beau-R exhibited a small increase in titre from 48 to 72 hpi. There was a small difference in titre at 72hpi between the two parent viruses and the recombinant M41K-BeauR(S) which is of statistical significance.

This demonstrates that M41K-BeauR(S) followed the same pattern of replication in *ex vivo* cultures as well as in primary cells and reached the same peak titres as the parent viruses M41-K and Beau-R. It also shows that the insertion of the Beaudette sequence into the M41-K genome has not affected the ability of the recombinant virus to replicate in tracheal epithelial cells.

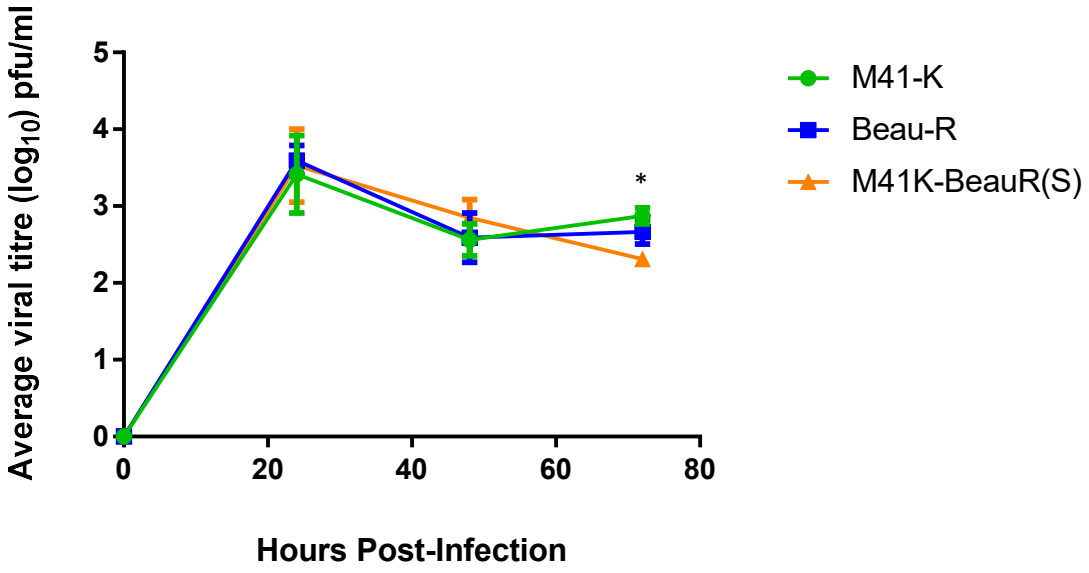

Figure 4.8: Viral replication kinetics of M41K-BeauR(S) in *ex vivo* tracheal organ cultures (TOCs) compared to M41-K and Beau-R. TOCs were infected with 1x10^{4}pfu/ml of either M41-K (green), Beau-R (blue) or M41K-BeauR(S) (orange) and incubated at 37˚C rotating at 8rph for 96 hours. Supernatant was harvested from each TOC at 24 hour intervals and titrated by plaque assay in chick kidney (CK) cells. Infections were replicated 3 times and average viral titres are displayed with standard error of the mean (SEM). Values at each time point were analysed by One-Way ANOVA (* indicates $p < 0.01$). At 72hpi the difference between M41-K and Beau-R titres is not significant but the difference between the parent viruses and M41K-BeauR(S) is significant.

During *in vivo* infections, pathogenic strains of IBV infect and destroy the ciliated epithelial cells of the trachea in infected birds. This destruction leads to ciliostasis and cessation of ciliary activity, resulting in secondary bacterial infections and increased mortality. In industrial studies for vaccine development, IBVs are usually predicted to be pathogenic if they cause extensive (more than 50%) reductions in ciliary activity during infection *in vivo*. Beau-R is an exception to this general rule, as it causes ciliostasis *ex vivo* but is non-pathogenic *in vivo*.

As an indicator of pathogenicity, the ability of M41K-BeauR(S) to cause ciliostasis was assessed *ex vivo*. TOCs were infected with M41K-BeauR(S), M41-K or Beau-R and ciliary activity was recorded over 96 hours. Figure 4.9 shows the effects on ciliary activity over the course of the experiment. While ciliary activity on the mock infected cultures remains close to 100% throughout the experiment, it is almost completely ablated in those infected with M41K-BeauR(S) by 48 hours post-infection. The majority of ciliary activity is diminished in all infected groups by 72 hours post-infection. From 48 hours post-infection, values for ciliary activity in M41-K and M41K-BeauR(S) infected TOCs were significantly different to the mock and from 72 hours post-infection, this was true for all infected groups. The statistical analysis displayed in this figure indicates that each group was compared to the mock. From 48 hours post-infection, ciliary activity values for each of the infected groups is significantly different from the mock-infected group.

These results further demonstrate that the recombinant virus M41K-BeauR(S) can infect and maintain replication in tracheal epithelial cells and is also capable of causing ciliostasis in these cells at 37°C.

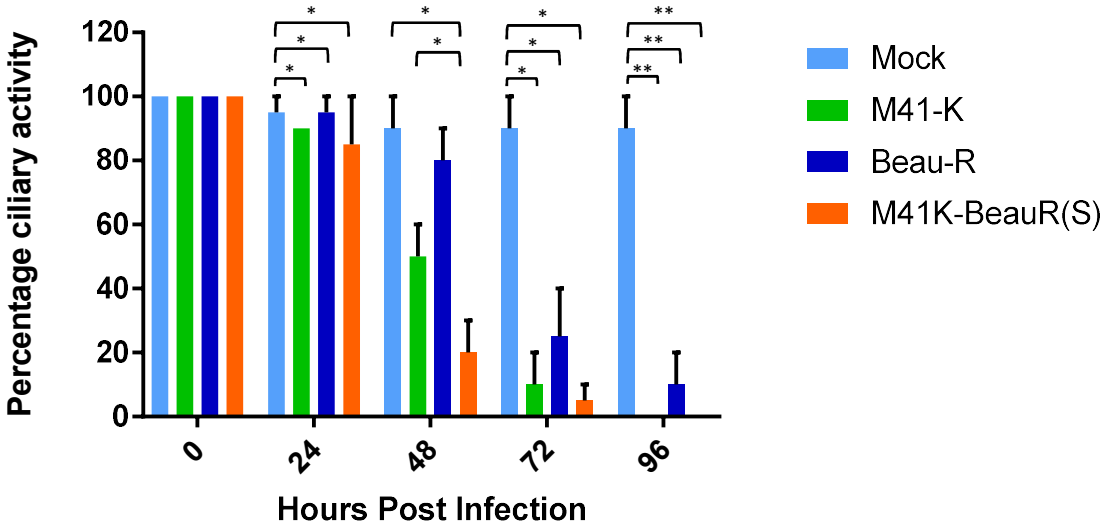

Figure 4.9: rIBV M41K-BeauR(S) induced ciliostasis is comparable to M41-K *ex vivo.* TOCs were infected with 1x10^5 pfu of each virus in replicates of 10. Ciliary activity of each TOC was assessed under a light microscope at 24 hour intervals. TOCs were given a score from 1-4 (0=ciliostasis, 1=25% beating, 2=50% beating, 3=75% beating, 4=100% beating). The average values are displayed as percentages with standard deviation (SD). Data were analysed by One-Way ANOVA followed by Tukey's multiple comparison test, allowing comparison between viruses at each time point. Significance is indicated (* indicates $p < 0.04$, ** indicates $p < 0.005$).

4.2.3 In vivo *analysis of rIBV M41K-BeauR(S) pathogenesis*

The results displayed in Figures 4.5 – 4.9 show that the recombinant virus M41K-BeauR(S) is able to replicate efficiently in both primary and continuous cells, indicating that the inserted S gene did not impair viral replication or infectivity. They also clearly demonstrate that the virus has adopted the *in vitro* tropism of Beau-R. The effect of the S gene modification on replication *in vivo*, however, remained to be assessed.

Pathogenicity of M41K-BeauR(S) was investigated and compared to the pathogenic parent viruses M41-K (molecular clone) and M41-CK (population). Groups of 12 SPF RIR chickens were infected with IBV or mock-infected with PBS at 8 days of age via the ocular-nasal route, according to the protocol outlined in Methods Section 2.23.1. Clinical signs, including snicking and rales, were assessed daily from day 3 pi and recorded for each bird. *Post-mortem* (PM) tissue samples were taken from three randomly selected birds in each group on days 4 and 6 pi. Ciliary activity in the trachea of these birds was also assessed on days 4 and 6 pi. On day 7 pi, the remaining six birds in each group were culled and tissues were harvested. Details of the experimental plan are shown in Figure 4.10.

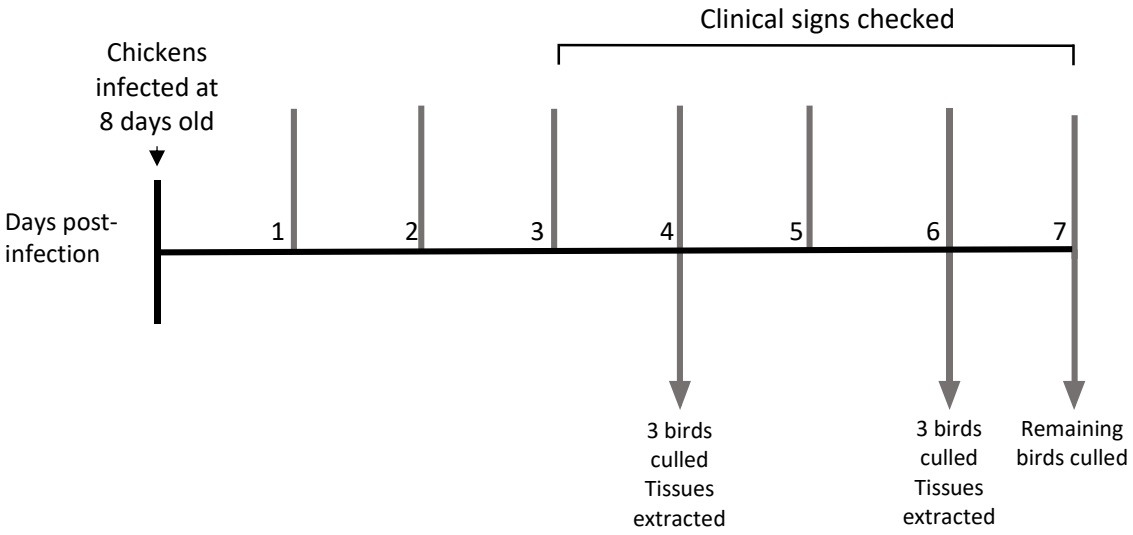

Figure 4.10: Experimental plan for M41K-BeauR(S) pathogenicity assessment. Groups of 12 SPF RIR chicks were infected at 8 days old with $1x10^4$ pfu of either M41-K, M41K-BeauR(S) or M41-CK by the ocular-nasal route. A mock group was inoculated with PBS by the same method. Clinical signs were recorded from day 3 to 7 pi. Three birds from each group were selected at random on days 4 and 6pi and tissues were extracted for PM analysis. All remaining birds were culled on day 7pi.

As described, any IBV-induced clinical signs in the infected birds were assessed every day from day 3 to day 7 pi. The breathing of each bird was assessed to identify any infected animals exhibiting rales. The number of snicks in each group on each day was also calculated. Clinical signs from the infected birds are shown in Figure 4.11.

The percentage of birds exhibiting rales in each group is shown in Figure 4.11A. The mock infected birds displayed no rales on any of the observation days pi. Similar observations were made in the M41K-BeauR(S) infected group. Conversely, the percentage of birds exhibiting rales in the M41-K and M41-CK infected groups increased over the course of the experiment to peaks of approximately 90% and 70%, respectively. Again, the number of snicks in the M41-K and M41-CK infected groups increased over the course of the experiment, with the peak values occurring on days 6 and 7, respectively. Very few snicks were recorded in the M41K-BeauR(S) infected group on any of the observation days. Even fewer still were observed in the mock infected group (Fig.4.11B).

Overall, few respiratory signs were observed in the M41K-BeauR(S) infected group compared to the M41 infected birds (Fig. 4.11A and Fig. 4.11B). This indicates that the recombinant virus is non-pathogenic as it was unable to cause clinical disease in infected chickens.

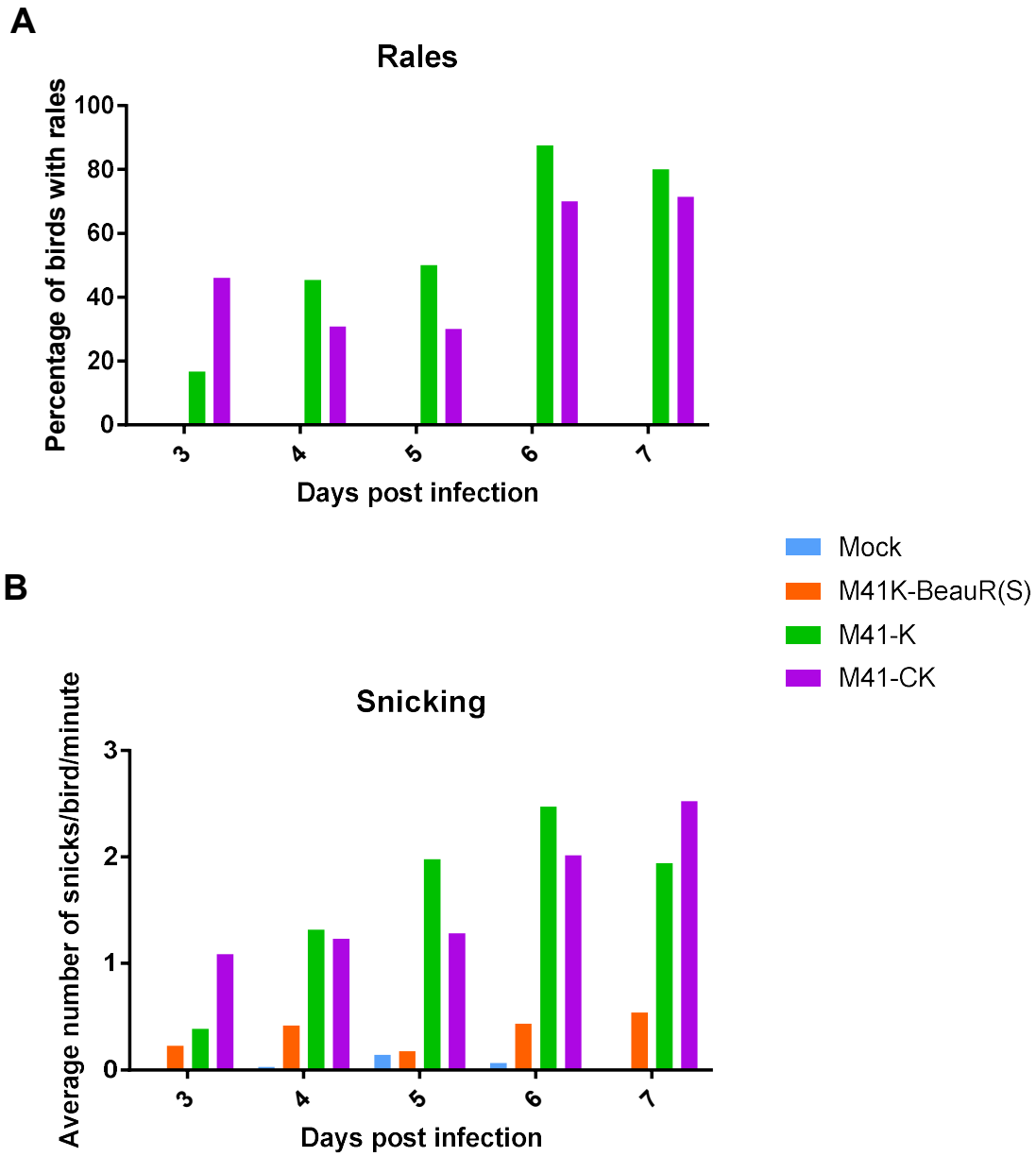

Figure 4.11: rIBV M41K-BeauR(S) causes mild clinical signs *in vivo*. (A) From day 3 pi, the breathing of each bird was assessed daily and those exhibiting rales were noted. The number of birds exhibiting rales is shown expressed as a percentage of the total number of birds in each group. **(B)** The average number of snicks per bird per minute was recorded daily for each group.

Tracheal ciliary activity in the infected birds was measured under a light microscope on days 4 and 6 pi, according to the protocol outlined in Methods Section 2.23.4. A percentage ciliary activity was calculated for the birds in each group in order to assess the ciliary damage induced by infection with IBV (Figure 4.12). Ciliary activity in the mock infected group remained close to 100% in all birds on both days pi. Similar results were seen in the M41K-BeauR(S) infected birds, where, again, there appeared to be no effect on ciliary activity on either day pi. In the M41-K and M41-CK infected groups, ciliary activity was ablated by day 4 pi. By day 6 pi the ciliary activity had recovered slightly but was still significantly reduced compared to the both the M41K-BeauR(S) and mock infected groups. This indicated that infection with the recombinant virus M41K-BeauR(S) had no effect on the ciliary activity in the trachea. There were no statistically significant differences between the values for ciliary activity in the M41-K and M41-CK control groups.

The chickens infected with M41K-BeauR(S) showed very few respiratory signs of infection and ciliary activity in the trachea was largely unaffected by infection. Taken together the results from Figures 4.11 and 4.12 indicate that rIBV M41K-BeauR(S) is attenuated in chickens and unable to cause ciliostasis *in vivo*. Clinical signs and ciliary activity observed in the M41K-BeauR(S) infected birds were similar to those observed previously in experiments assessing Beau-R pathogenicity. Previous studies demonstrated that Beau-R did not cause clinical signs and so, in line with the principles of the 3Rs, it was not chosen as a control for this experiment (Hodgson et al., 2004).

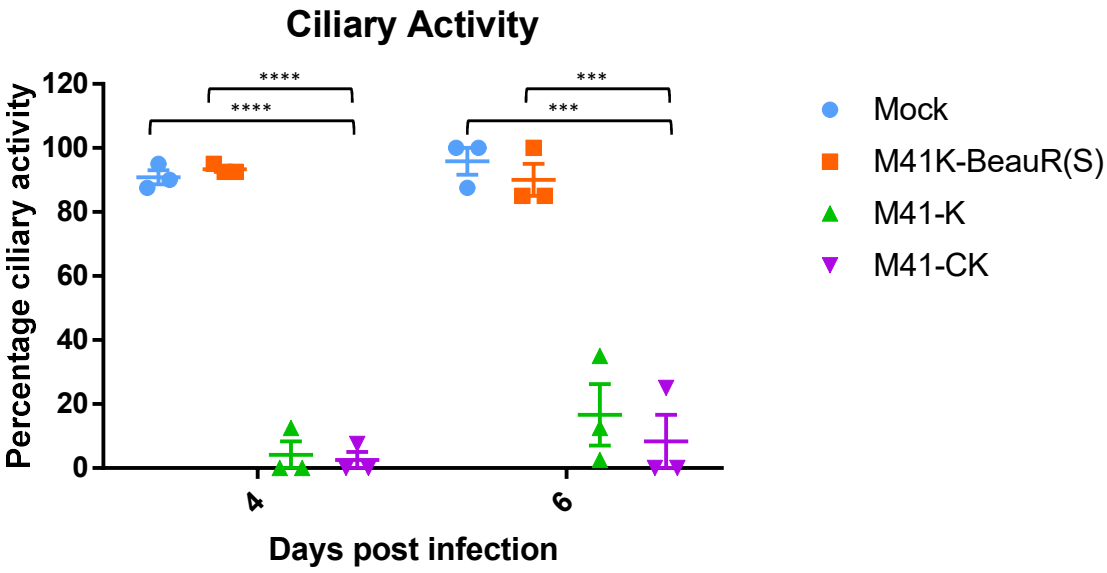

Figure 4.12: rIBV M41K-BeauR(S) does not affect ciliary activity *in vivo*. Trachea from the three birds culled on days 4 and 6 was divided into 10 x 1mm sections (3 from the dorsal section, 4 from the medial section and 3 from the terminal section) and ciliary activity was assessed under a light microscope. Ciliary activity for each group on each day pi is expressed as a percentage with SEM. Average values of percentage ciliary activity for each day were analysed by One-Way ANOVA followed by Tukey's multiple comparison test to compare mean values in each group (*** indicates $p < 0.0004$, **** indicates $p < 0.0001$). Significance between the mock, and M41-K and M41-CK groups is indicated as well as significance between M41-K and M41-CK compared to M41K-BeauR(S). Differences between the mock group and M41K-BeauR(S) were not significant, nor were the differences between M41-K and M41-CK.

Assessment of virus dissemination from the sites of infection was performed by RNA extraction from a panel of homogenised tissues extracted on days 4 and 6 pi followed by RT-PCR using primers covering the 3' UTR of the IBV genome (BG56 and BG93/100). Isolation of viable virus from the trachea was achieved by infection of embryonated eggs with tracheal homogenate followed by screening of the infected allantoic fluid by RT-PCR. The results from these experiments are summarised in Table 4.1. The PCR results from each of the three individual birds on days 4 and 6 are detailed alongside clinical signs for each bird and any observations noted during the PM examinations.

The pattern of dissemination for the two pathogenic control viruses is very similar, with the viruses reaching the trachea by day 4 and remaining present to day 6 pi. Both M41-K and M41-CK appear to have been cleared from the beak and eyelid by day 6 pi. M41K-BeauR(S) is present in the beak and eyelid on day 4 pi but only in the eyelid on day 6 pi. Virus can be detected in the trachea of 1 of the 3 birds on day 4 and day 6 pi by standard RT-PCR and in two of the three virus isolation samples on day 6 pi. This difference can be attributed to the increased sensitivity of the virus isolation technique, as any virus present in the sample is likely to have been amplified during the infection in the embryonated egg. IBV was not detected in any of the remaining tissues for any of the groups.

Table 4.1: Assessment of *in vivo* virus dissemination by RT-PCR.

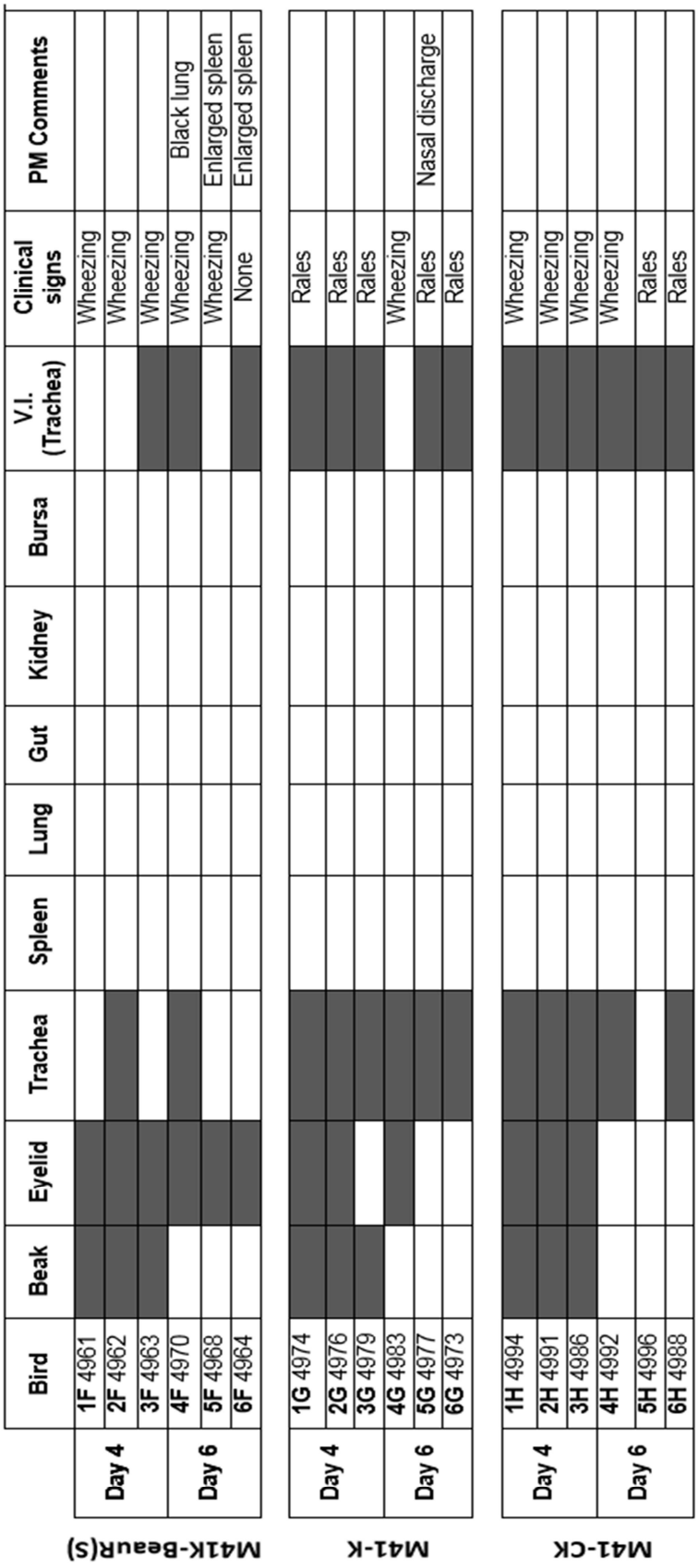

	Bird	Beak	Eyelid	Trachea	Spleen	Lung	Gut	Kidney	Bursa	V.I. (Trachea)	Clinical signs	PM Comments
M41K-BeauR(S)												
Day 4	1F 4961	■	■								Wheezing	
	2F 4962	■	■	■							Wheezing	
	3F 4963	■	■							■	Wheezing	
Day 6	4F 4970		■	■						■	Wheezing	Black lung
	5F 4968		■								Wheezing	Enlarged spleen
	6F 4964		■							■	None	Enlarged spleen
M41-K												
Day 4	1G 4974	■	■	■						■	Rales	
	2G 4976	■	■	■						■	Rales	
	3G 4979	■		■						■	Rales	
Day 6	4G 4983		■	■							Wheezing	
	5G 4977			■						■	Rales	Nasal discharge
	6G 4973			■						■	Rales	
M41-CK												
Day 4	1H 4994	■	■	■						■	Wheezing	
	2H 4991	■	■	■						■	Wheezing	
	3H 4986	■	■	■						■	Wheezing	
Day 6	4H 4992			■						■	Wheezing	
	5H 4996									■	Rales	
	6H 4988			■						■	Rales	

Samples positive for detection of IBV genome are indicated by shaded boxes. Homogenate from the trachea was also used for virus isolation (V.I.) in embryonated eggs. M41K-BeauR(S) group = F, M41-K group = G, M41-CK group = H.

Results from the PCR screening shown in Table 4.1 indicated that there was a lot of variation in the presence of each strain in the eyelid and trachea. To quantify the amount of virus present in these tissues of each bird, samples of trachea and eyelid were taken on days 4 and 6 pi from 3 birds selected at random from each group. *Ex vivo* TOCs were infected with homogenised trachea or eyelid samples from each day. Viral load in each sample was calculated by ciliostatic dose (CD_{50}) using the Reed-Muench method (1938).

Figure 4.13 shows the quantities of virus present in each sample on each day post-infection for eyelid (Fig. 4.13A) and trachea (Fig. 4.13B). On day 4 pi, average viral load in the M41K-BeauR(S) infected group was significantly lower than in the group infected with M41-CK in the trachea ($p < 0.05$). By day 6 viral load in the M41 infected groups was more similar to the M41K-BeauR(S) group, which remained relatively low on both days. There was some variation between individual birds in the M41K-BeauR(S) infected group, with almost no detectable virus in the trachea on either day pi.

In the eyelid samples at day 4pi, viral load is significantly lower in the M41K-BeauR(S) and M41-K infected birds compared to the M41-CK infected birds ($p < 0.01$). Each group contains data from 3 individual birds apart from M41-CK day 4pi which contains data from 2 birds. The viral load in the third sample was greater than the dilutions measured and can be assumed to be greater than 3 $\log_{10}CD_{50}$/ml. On day 6, there are no significant differences between the viral loads in the eyelid in any of the infected groups.

The data displayed here indicate that M41K-BeauR(S) is able to disseminate from the sites of infection to the trachea in the infected birds but is present at significantly lower levels than the pathogenic parent viruses (M41-K and M41-CK).

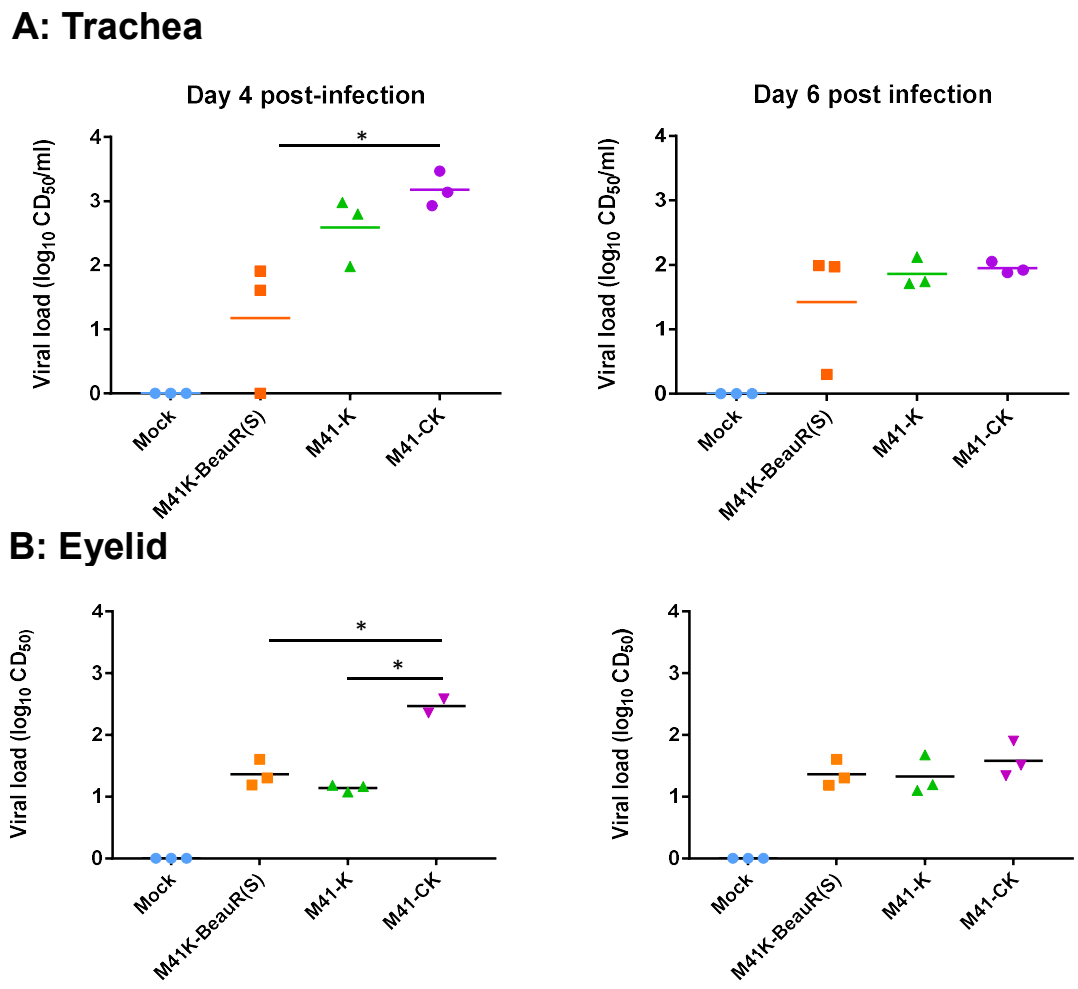

Figure 4.13: Quantification of viral load in extracted tissues measured by ciliostatic dose (CD_{50}). (A) Homogenate from sections of trachea from three birds culled on day 4 (left panels) and day 6 (right panels) pi was titrated in *ex vivo* tracheal organ cultures (TOCs). Homogenate was serially diluted in TOC growth medium and 500µl of each dilution was used to infect TOCs in replicates of 5. TOCs were incubated for 6 days at 37°C (8rph) after which each TOC was assessed under a light microscope for ciliary activity. Those exhibiting ciliostasis were recorded as positive for IBV presence. Ciliostatic dose (CD) was then calculated using the Reed-Muench method (1938). Log_{10} CD_{50} values are displayed for each bird. Data were analysed by One-Way ANOVA using multiple comparisons (* indicates $p < 0.05$). **(B)** Viral load in samples of eyelid homogenate was measured by the same method as in the trachea (* indicates $p < 0.01$).

4.3 Discussion:

A recombinant IBV has been generated using a VV based reverse genetics system where the S gene from a non-pathogenic IBV was inserted into the genome of a pathogenic strain. The resulting virus is known as M41K-BeauR(S) and was successfully rescued and characterised both *in vitro* and *in vivo* to compare replication and pathogenicity with the parental viruses M41-K and Beau-R.

The recombinant virus M41K-BeauR(S) has adopted the *in vitro* replication characteristics of the S donor strain Beau-R. The virus replicates to similar titres as both parent viruses in CK cells (Figure 4.5A) but exhibits the extended host tropism of Beau-R, where it is able to infect and replicate in mammalian (Vero) cells (Figure 4.5 and Figure 4.6A). At present, there are several hypotheses concerning the extended host tropism of Beau-R. Certain studies have attributed it to an additional cleavage site present in the S2 segment of the S protein which allows cleavage by cellular proteases, allowing entry into Vero cells (Belouzard et al., 2012, Yamada and Liu, 2009, Bickerton et al., 2018). Other groups have identified the presence of a heparan sulphate (HS) binding site as a selective binding factor for IBV in Vero cells (Madu et al., 2007). The replacement of the S gene in M41K-BeauR(S) allows the virus to be propagated in continuous cell lines, conferring a huge advantage for vaccine development. Having already been approved for vaccine production, Vero cells provide a good system for producing vaccines on an industrial scale. As the current vaccine production process involves the use of hundreds of embryonated hens' eggs per batch, a platform to produce rationally attenuated viruses in cell culture would be extremely beneficial to the vaccine industry, both financially and ethically. With further investigation this virus could be used for a vaccine-challenge experiment to assess the level of protection conferred by M41K-BeauR(S).

S genes in other coronaviruses have been shown to alter viral tropism, in line with the results described here. One example is MHV, the tropism of which is dependent on the S gene.

Studies have shown that replacing the S gene in MHV alters the ability of the virus to infect and replicate in hepatocytes (Navas et al., 2001). Other parts of the MHV genome have also been implicated in tropism, however, suggesting that the S gene is not the sole determinant (Zhang et al., 2015).

The results from the pathogenicity experiment show that M41K-BeauR(S) did not cause any IBV related respiratory clinical signs in the infected chickens (Figure 4.11A and B), indicating that the Beaudette-derived S gene has attenuated the virus. Previous work described the insertion of the M41 S gene into the Beaudette genome, to determine whether this would generate a pathogenic virus (BeauR-M41(S)) (Casais et al., 2003). While the resultant virus did adopt the tropism of M41 *in vitro*, it was completely attenuated *in vivo* (Hodgson et al., 2004). The results from that study showed that the ectodomain from a pathogenic virus was not sufficient to alter the pathogenicity of Beau-R. In contrast, the experiments described here demonstrate that modifying the ectodomain of the M41 S protein can attenuate this pathogenic virus. Taken together this shows that the Beaudette genome is too attenuated to support changes in its genome which should alter pathogenicity and that the M41 based reverse genetics system is a useful tool for studying IBV pathogenesis.

Through *ex vivo* and *in vivo* comparisons, it is clear that M41K-BeauR(S) is unable to induce ciliostasis in the natural host (Figures 4.9 and 4.11C, respectively). As the exact process of ciliostasis in the host is unknown, we cannot conclude that the S gene is responsible for ciliostasis in pathogenic IBV infections. It is likely that the virus itself does not cause ciliostasis directly but rather the host immune response to the infection. It has been shown that IBV infection induces the innate immune response, increasing expression of TLRs and downstream signalling molecules. Macrophage numbers in the trachea of infected birds are also increased during infection (Kameka et al., 2014). Induction of pro-inflammatory cytokines has also been demonstrated in the trachea of IBV infected birds. It is suggested

that the excessive immune response induced by infection with certain strains of IBV leads to inflammation in the infected tissues causing the pathology associated with the disease (Jang et al., 2013). Investigating the immune response to infection in the bird could elucidate the reasons why there is a lack of ciliostasis in the M41K-BeauR(S) infected birds. The lower viral load in the tissues (Figure 4.12) may have resulted in an altered immune response to the infection, thus altering the pathogenesis and development of disease. Assessing the populations of immune cells attracted to the sites of infection and what effect this has on the tissues would be beneficial in the elucidation of the involvement of the host response to IBV infection.

It is also possible that the gene replacement in M41K-BeauR(S) has disrupted the interactions of the other viral proteins which may be responsible for influx of immune cells. For other coronaviruses, interactions between the S and M proteins have been studied. One study looked at the interaction of chimeric M proteins with the other structural proteins of MHV. They noted a reduction in the number of S proteins incorporated into the virions, indicating a disrupted interaction with the S protein (Kuo et al., 2016). This could be the case for the recombinant virus described here; the chimeric nature of the recombinant S protein may have disturbed interactions with M and hence disrupted viral replication in the bird. An interesting line of future investigation would be to generate a recombinant virus including Beaudette M and S genes in an M41 genome to assess what effect this would have on replication and dissemination *in vivo*.

While M41K-BeauR(S) is completely non-pathogenic, it has retained the ability to disseminate from the sites of infection, demonstrated by the fact that the virus was detected in the trachea from day 4pi (Figure 4.12A). Beau-R cannot disseminate through the bird during infection as shown in previous pathogenicity studies where it could not be detected in the trachea by PCR (Armesto et al., 2009). Having assessed the viral load in the extracted

tissues from the infected birds, it is clear that the recombinant virus was present in the trachea but in much lower levels compared to the pathogenic control viruses (Figure 4.12A). Lower levels of the virus in the trachea may also be responsible for the lack of ciliostasis in these tissues. The virus is also present in lower levels in the eyelid (Figure 4.12B), indicating that M41K-BeauR(S) replication is not as efficient as M41-K *in vivo*. The reason for this disparity is likely to be multifactorial however one hypothesis for the differences in virus levels is that M41K-BeauR(S) may be sensitive to the higher body temperature of a bird compared to the *in vitro* incubation temperature of 37°C (discussed in detail in Chapter 6).

Overall, M41K-BeauR(S) has adopted both *in vitro* and *in vivo* characteristics of Beau-R, with the exception of the recombinant virus's ability to disseminate from the sites of inoculation to the trachea. This implies that the S protein is a factor in IBV pathogenicity. The differences between *in vitro* and *in vivo* results highlight an interesting area of investigation, demonstrating that the results from *in vitro* studies are not always reflected in the natural host.

Chapter 5: Generation and characterisation of M41K-4/91(S) to assess the effect of IBV genome modification on pathogenesis

5.1 Introduction

Previous studies have generated viruses where S genes from pathogenic viruses have been inserted into the genome of Beau-R (Hodgson et al., 2004, Armesto et al., 2011). These viruses did not adopt a pathogenic phenotype despite the insertion of a pathogenic S protein, most likely due to the extreme attenuation of Beau-R. With the development of a reverse genetics system based on the pathogenic M41 strain, it is possible to modify and replace genes within the context of a pathogenic virus, therefore examining the involvement of specific genes in IBV pathogenesis. M41K-BeauR(S) (described in Chapter 4) was generated to elucidate the influence of the S gene on IBV pathogenicity. This virus demonstrates that the S gene is a factor in IBV pathogenicity and that a recombinant virus will adopt the tropism of the S donor strain.

To demonstrate that the observed alterations on pathogenicity can be solely attributed to the insertion of the Beaudette-derived S protein ectodomain, another recombinant IBV was generated in which the genome of M41-K was modified to include the S protein of a pathogenic field strain of IBV 4/91 (also known as 793B). The resultant virus is known as M41K-4/91(S) and has been characterised both *ex vivo* and *in vivo* to assess the effects of inserting the S ectodomain from a pathogenic virus into the genome of another, heterogeneous pathogenic virus.

5.2 Results:

5.2.1 Generation and rescue of rIBV M41K-4/91(S)

The recombinant IBV (rIBV) M41K-4/91(S) was generated by reverse genetics using VV-based reverse genetics. The reverse genetics system is described in more detail in Chapter 4 and Methods Section 2.12. The ectodomain of 4/91 S was inserted into the M41-K genome using the plasmid detailed in Figure 5.1A. The plasmid includes a selection marker and a recombinant S gene sequence comprising the ectodomain of 4/91 S with the signal sequence, transmembrane domain and cytoplasmic tail of M41-K to maintain interactions between the S protein and other viral proteins such as the M protein (Figure 5.1B).

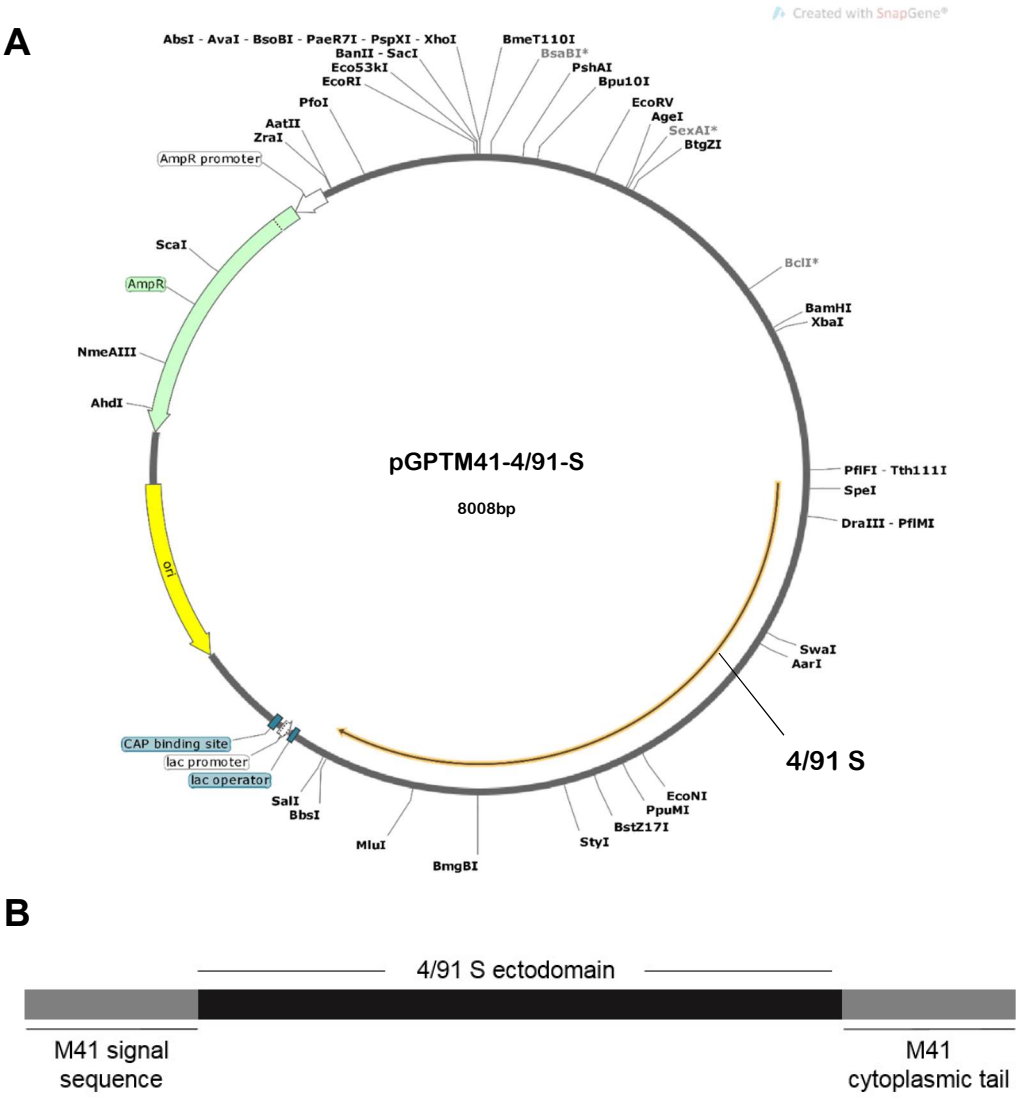

Figure 5.1: (A) Plasmid map of pGPT-M41-4/91(S) used to generate rIBV M41K-4/91(S) containing the recombinant S sequence comprising the 4/91 ectodomain with flanking regions of the M41 signal sequence at the 5' end and cytoplasmic tail at the 3' end within the pGPT plasmid vector. The ampicillin resistance gene (AmpR) and the lac promoter sequence are highlighted along with the pUC origin of replication site (ori). The recombinant 4/91 gene is indicated. The plasmid map was generated from the plasmid sequence using SnapGene. **(B)** Schematic diagram detailing the structure of the chimeric S gene in the recombinant virus rVV M41K-4/91(S), comprising the 4/91-derived ectodomain flanked by the M41 signal sequence and cytoplasmic tail.

Following the successful generation of recombinant vaccinia virus DNA containing M41K-4/91(S) cDNA by reverse genetics, attempts to recover the virus were made in CK cells. As previously described, the virus rescue system involved infection of CK cells with FPV-T7 and transfection with rVV DNA and a plasmid containing the IBV N protein (Methods Section 2.12.9).

After numerous attempts, the recombinant virus M41K-4/91(S) was successfully generated in primary CK cells. As recombinant IBVs have previously adopted the cell tropism of the strain from which their S gene was derived, M41K-4/91(S) should be refractory for replication in CK cells (Armesto et al., 2011). Therefore alternative techniques for harvesting and completing the virus rescue were employed. Several lysis methods were used to extract potential viable virus from the cells. The cells used for virus rescue were subjected to freeze-thawing followed by homogenisation through a needle to allow the virus to escape the cells. This material was immediately used for passage in embryonated eggs in order to amplify any potential infectious virus. Allantoic fluid was screened by RT-PCR to check for virus presence using primers covering the 3' UTR of the IBV genome. IBV was detected in the first passage in the allantoic fluid of embryonated eggs (Fig. 5.2) and this fluid was used to generate stocks of the recombinant virus to use for further experiments.

This demonstrates that it is possible to recover a recombinant IBV containing an S gene that exhibits only 82.4% amino acid sequence homology to the backbone strain M41.

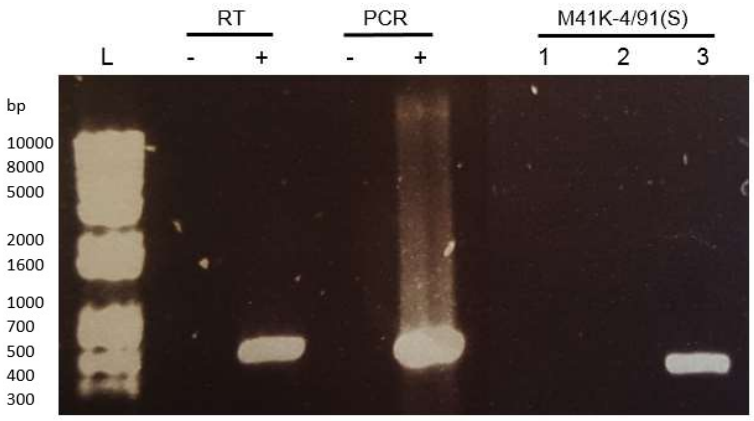

Figure 5.2: rIBV M41K-4/91(S) was successfully rescued in CK cells. Three replicate wells of CK cells (1, 2 and 3) were infected with FPV-T7 and transfected with VV DNA containing IBV M41K-4/91(S) cDNA along with a plasmid expressing the N protein of M41. After 96 hours incubation, cells were subjected to freeze-thaw (-80/37°C) followed by lysis using a needle and syringe. The resulting cell lysate was used to infect embryonated eggs and RNA from the allantoic fluid of each egg was extracted and used for screening by RT-PCR using primers BG56 and BG93/100. Band sizes were compared to Invitrogen 1kb Plus DNA Ladder (L). H_2O was used as a negative control for both the RT and PCR (-). Known Beaudette-positive RNA and DNA samples were used as positive (+) controls for the RT reaction and PCR, respectively. A band of approximately 500bp is indicative of IBV presence. The PCR product generated by this primer set is slightly shorter in M41 compared to Beau-R, hence the PCR product for the M41K-4/91(S) sample is smaller (approximately 400bp) than those observed in the + samples.

Stocks of M41K-4/91(S) were propagated in embryonated eggs for use in all subsequent experiments. The sequence identity was confirmed by Sanger sequencing across the entire S gene to verify that the recombinant gene contained the M41 signal sequence and cytoplasmic tail and the ectodomain sequence of 4/91. An example of the DNA sequence alignment for the three viruses is displayed in Figure 5.3. The sequence of the recombinant S gene in M41K-4/91(S) was homologous to the M41 S gene sequence up to position 55 in the nucleotide sequence after which it matched the sequence encoding the 4/91 S ectodomain until position 3363. At this point the sequence was again homologous to M41.

This confirmed that the recombinant virus contained the correct S gene sequence and that no point mutations had occurred in the S gene throughout the virus generation and rescue process.

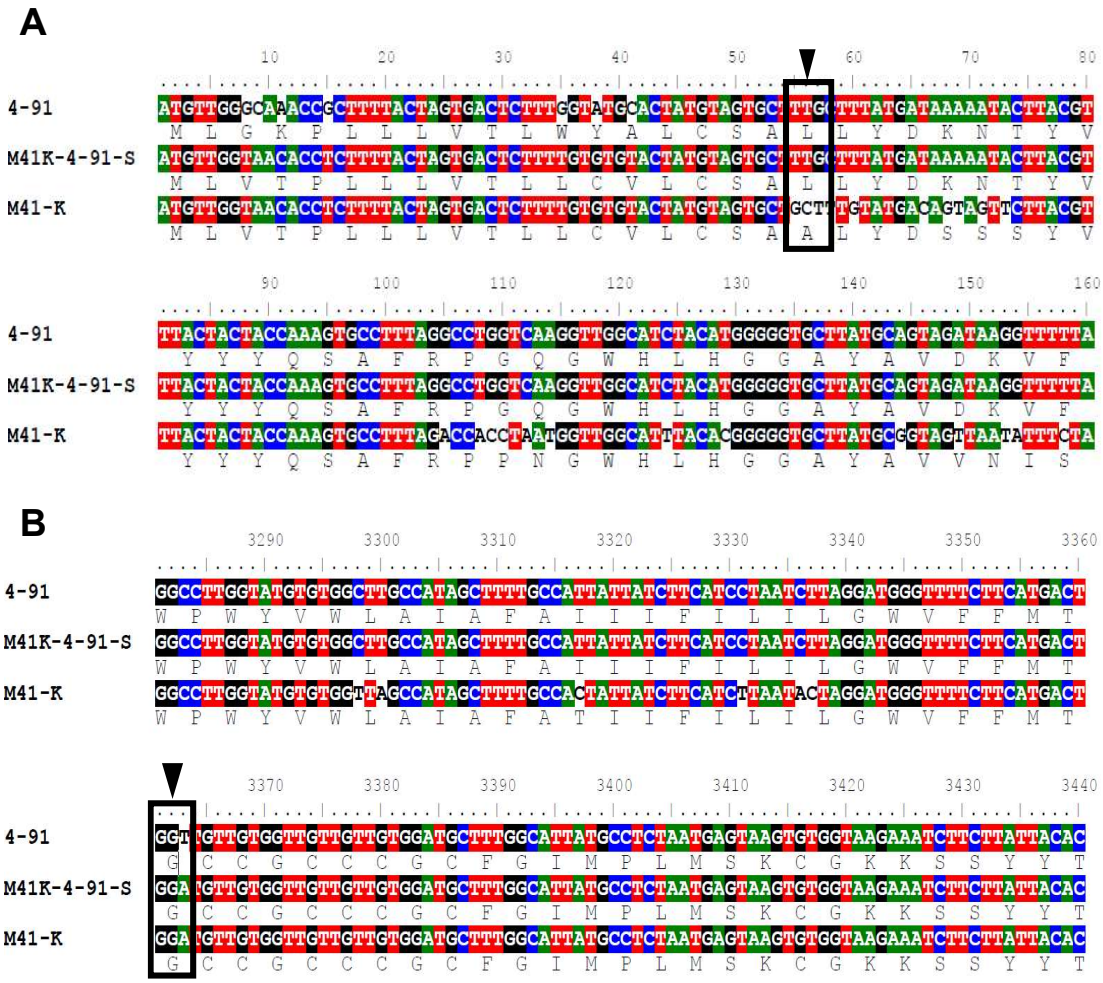

Figure 5.3: Example of alignment of IBV M41K-4/91(S), M41-K and 4/91 amino acid sequences. Stocks of 4/91, M41K-4/91(S) and M41-K were propagated in embryonated eggs before RNA extraction from allantoic fluid followed by RT-PCR and Sanger sequencing to obtain sequences for the S gene in each virus. Nucleotide sequences were aligned using BioEdit. Nucleotide positions are indicated from the first base of the S gene. **(A)** The M41K-4/91(S) sequence matches M41 until position 55 (indicated by the black box and arrow), after which it matches the 4/91 ectodomain sequence. **(B)** From position 3363, the M41K-4/91(S) sequence matches the CT and TM domain sequence of M41.

5.2.2 In vitro *and* ex vivo *characterisation of rIBV M41K-4/91(S)*

As previously discussed, the S protein is a determinant of *in vitro* tropism for IBV and as such it was expected that rIBV M41K-4/91(S) would lose the capacity to replicate in cell culture with the insertion of the 4/91-derived S protein. To test this hypothesis, CK cells were infected with M41-K, 4/91 or M41K-4/91(S) and incubated at 37°C for 48 hours. Signs of IBV-induced cpe were assessed under a light microscope. Figure 5.6 shows the microscope images from these infections.

Extensive cpe was observed in the M41-K infected cells, with numerous clearings in the monolayer and patches of rounded cells throughout. As expected, no signs of IBV-induced cpe were seen in the 4/91 infected cells, which remained healthy and comparable to the mock infected cells. The M41K-4/91(S) infected cells did not exhibit any signs of infection and were also comparable to the mock infected cells. This indicates that M41K-4/91(S) is unable to infect and successfully replicate in CK cells, having adopted the tropism of 4/91, the strain from which the recombinant S gene was derived.

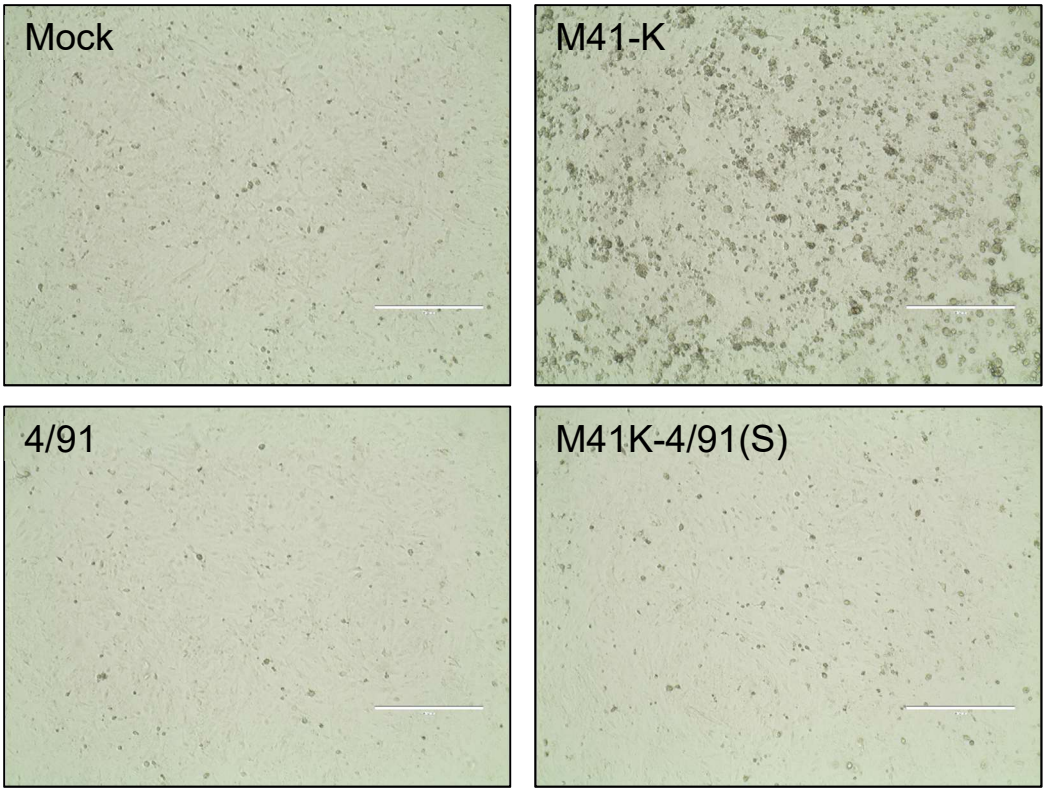

Figure 5.4: rIBV M41K-4/91(S) does not cause cpe in CK cells. CK cells were infected with M41-K, 4/91 or M41K-4/91(S) and incubated at 37°C for 48 hours. Cells were assessed for any signs of IBV-induced cpe, including rounded cells and clearings in the monolayer, compared to mock-infected cells. Images were taken on an EVOS Light Microscope, 10X objective.

The S protein has been shown previously to be a determinant of cell tropism (Casais et al., 2003). As indicated in Figure 5.4, the recombinant virus M41K-4/91(S) is unable to replicate in cell culture, exhibiting a similar tropism to the previously generated rIBV BeauR-4/91(S) (Armesto et al., 2011) and so replication kinetics were assessed in *ex vivo* TOCs alongside the two parent viruses M41-K and 4/91. TOCs were infected with each of the three viruses and samples of supernatant were harvested at 24 hour intervals from the time of infection. The samples of supernatant from each time point were titrated in TOCs in order to calculate the ciliostatic dose (CD_{50}) values for each virus. The results from these experiments are shown in Figure 5.5.

All three of the viruses were able to replicate in these cultures. M41-K and 4/91 followed fairly similar patterns of replication over the course of the experiment, with the peak titres occurring at 48 hpi in both cases. M41K-4/91(S) replicated as well, if not slightly better than either of the parent viruses, with the peak titre occurring at 72 hpi. There was no significant difference between the replication kinetics of any of the viruses, but M41K-4/91(S) appeared to replicate to higher titres than M41-K and 4/91 at 24, 48 and 72 hpi. Overall, the data described here demonstrate that the presence of a heterologous S protein has not impaired virus replication in *ex vivo* TOCs.

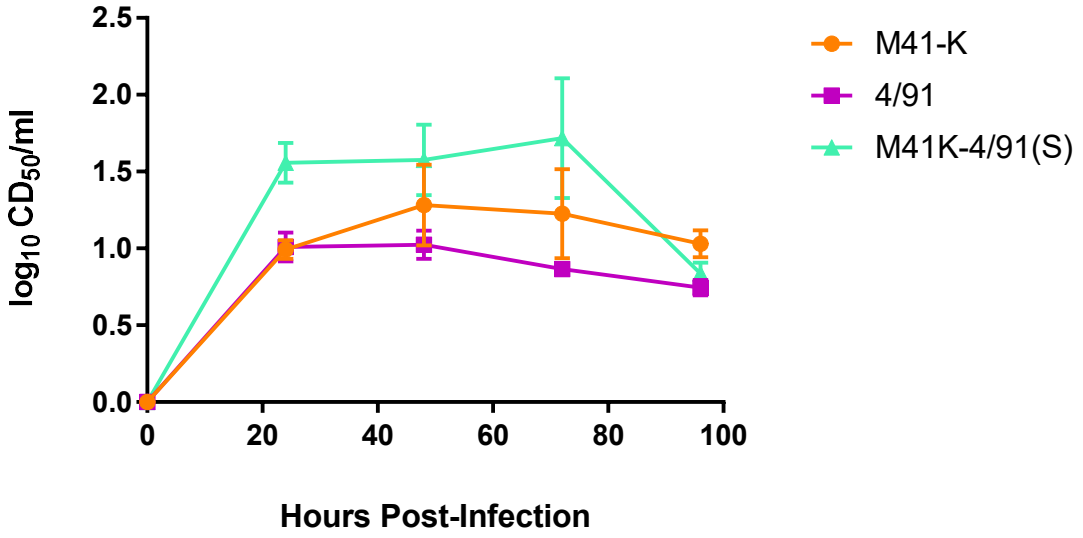

Figure 5.5: rIBV M41K-4/91(S) replicates well in *ex vivo* TOCs. TOCs from 19 day old RIR embryos were infected in triplicate with either M41K-4/91(S), M41-K or 4/91 and incubated at 37°C (rotating). The titre of each virus was determined by titration in TOCs prior to the assessment of replication kinetics. TOCs were infected with the equivalent of $1x10^4$ pfu in 500µl. Supernatant was harvested at 24 hour intervals and used for titration in embryonic TOCs. Serial dilutions of supernatant from each time point was used to infect TOCs. After 6 days incubation at 37°C, TOCs were assessed to identify the dilution at which 50% of the TOCs were exhibiting ciliostasis. Average data are displayed with SEM at each time point. Data were analysed by One-Way ANOVA followed by Tukey's multiple comparison test. There was no statistically significant difference between the replication kinetics of any of the viruses.

Induction of ciliostasis is used as a marker of pathogenicity in IBV infection *in vivo*, with a virus being considered pathogenic if infection reduces ciliary activity by more than 50%. To compare the progression of ciliostasis in TOCs infected with M41K-4/91(S), 4/91 and M41-K, changes in ciliary activity were measured over 96 hours. The results are shown in Figure 5.6.

M41-K, 4/91 and M41K-4/91(S) all induce dramatic reductions in ciliary activity by 48 hours pi with a gradual decline to 96 hours pi. The lowest levels of ciliary activity are observed in the 4/91-infected TOCs. There is a slight reduction in the ciliary activity in the mock-infected TOCs but the average remains above 80% throughout the experiment. The values for ciliary activity observed in the infected TOCs at all time points from 48 hpi onwards are significantly reduced compared to the mock-infected TOCs (**** indicates $p < 0.0001$). There is no significant difference between the values for ciliary activity in any of the infected groups. In general, all three viruses induce similar reductions in ciliostasis but M41K-4/91(S) appears to act more slowly than the two parental viruses M41-K and 4/91.

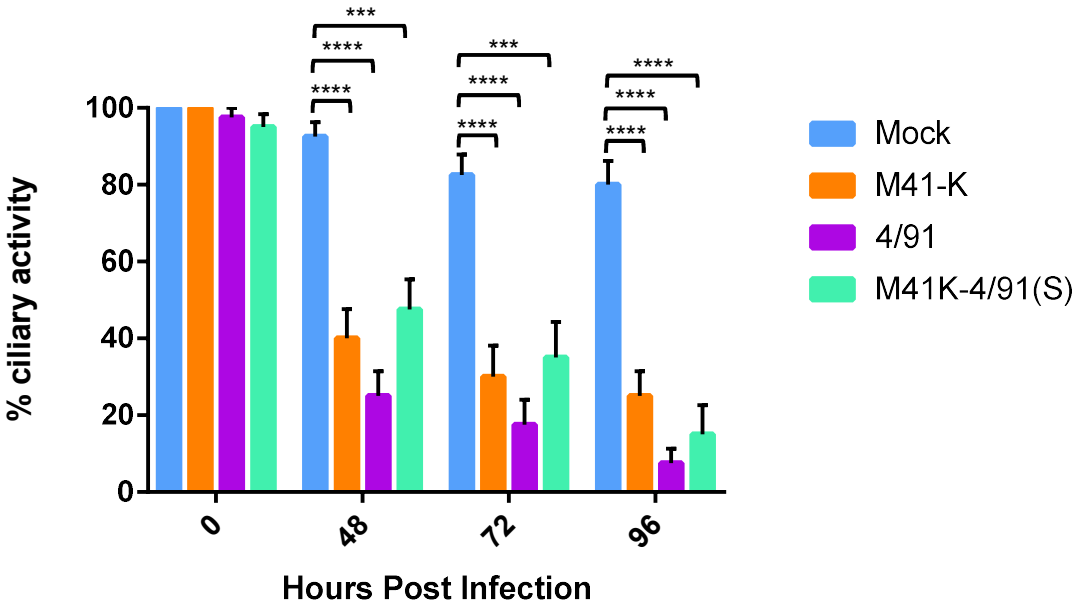

Figure 5.6: M41K-4/91(S) induces ciliostasis in *ex vivo* TOCs. Embryonic TOCs were infected with M41K-4/91(S), M41-K and 4/91 in replicates of ten, or mock infected with TOC maintenance medium. TOCs were incubated at 37°C and ciliary activity was assessed under a light microscope at the time of infection and then every day from 48 hpi. Each TOC was given a percentage score of ciliary activity and the averages for each virus are displayed with SEM. Data were analysed by One-Way ANOVA followed by Tukey's multiple comparison test to compare the average values at each time point (*** $p < 0.002$, **** $p < 0.0001$).

5.2.3 In vivo *analysis of rIBV M41K-4/91(S) pathogenesis*

The results from the *in vitro* and *ex vivo* experiments outlined in Figures 4-6 demonstrate that the recombinant virus M41K-4/91(S) is able to replicate efficiently in TOCs and cause significant reductions in ciliary activity. It is also clear that the virus has adopted the restricted tropism of 4/91, in that it cannot cause cpe in primary CK cells.

To investigate the effects of the insertion of the recombinant S gene *in* vivo, pathogenicity of the rIBV M41K-4/91(S) was assessed in SPF RIR chickens and compared to the parent viruses M41-K and 4/91. Groups of 15 chickens (12 in the mock-infected group) were infected at 8 days old via the ocular-nasal route with IBV or PBS. Clinical signs were assessed from day 2 to day 7 pi. Five birds from the IBV-infected groups or 4 birds from the mock-infected group were culled on days 4 and 6 pi. Tissues were harvested PM from each of these birds for analysis. Details of the experimental plan are included in Figure 5.7.

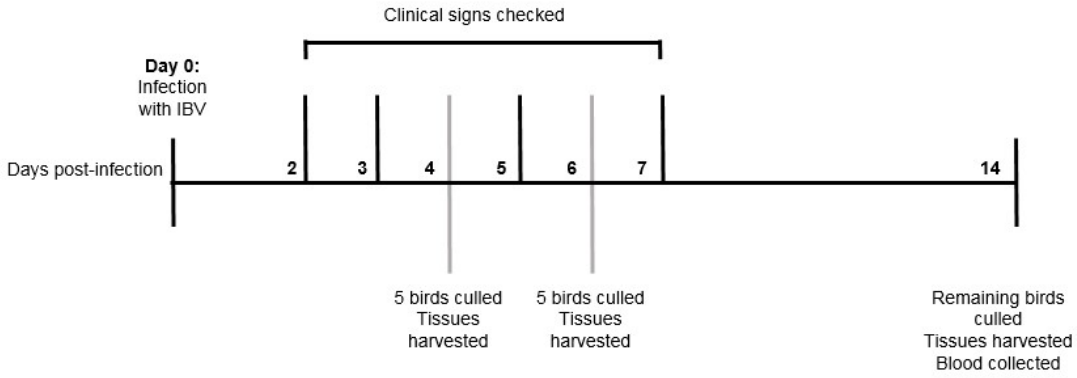

Figure 5.7: Experimental plan for *in vivo* pathogenicity assessment. RIR chicks were infected at 8 days old by the ocular-nasal route with either M41-K, 4/91 or M41K-4/91(S) or mock infected (PBS). IBV-induced clinical signs were observed from day 2 to day 7 pi. Five birds from each group were culled on days 4 and 6 and tissues were harvested for *post-mortem* analysis. On day 14pi, clinical signs were checked, the remaining birds in each group were culled and blood and tissues were harvested for analysis.

Clinical signs were observed from day 2pi. Figure 5.8 shows the collated data for the observations made on each day post inoculation for birds exhibiting snicking and rales. The peak clinical signs for the recombinant virus M41K-4/91(S) occur much earlier than the two pathogenic control groups (M41-K and 4/91). Until day 5, there was a similar level of snicking observed across all three IBV-infected groups. From day 5 onwards there are considerably more snicks in the two control groups compared to the M41K-4/91(S) group, with the peak occurring on day 4 followed by a steady decrease to day 14 (Fig. 5.8A). A similar pattern is seen for the number of birds exhibiting rales, with the peak in the M41K-4/91(S) group occurring at day 5, with no rales observed on subsequent days. The rales patterns observed in the control groups are quite different. For the M41-K infected group, there is a steady increase with a plateau of 60% exhibiting rales on day 5. For the 4/91 infected birds however, there is a more dramatic increase from day 2 to day 3, after which it increases steadily to day 5pi and then decreases again with no birds exhibiting rales on day 14pi (Fig. 5.8B). As 4/91 is a field strain and is not laboratory adapted in the same way as M41, the enhanced clinical signs in this group were expected.

While the patterns differ somewhat between all the infected groups, it is still clear that the recombinant virus M41K-4/91(S) is inducing classical symptoms of IBV infection, showing that the modification of the S gene has not altered the virus' ability to cause disease. Interestingly, it appears that M41K-4/91(S) may be cleared earlier than M41-K and 4/91, indicated by the earlier decrease in observed clinical signs in this group.

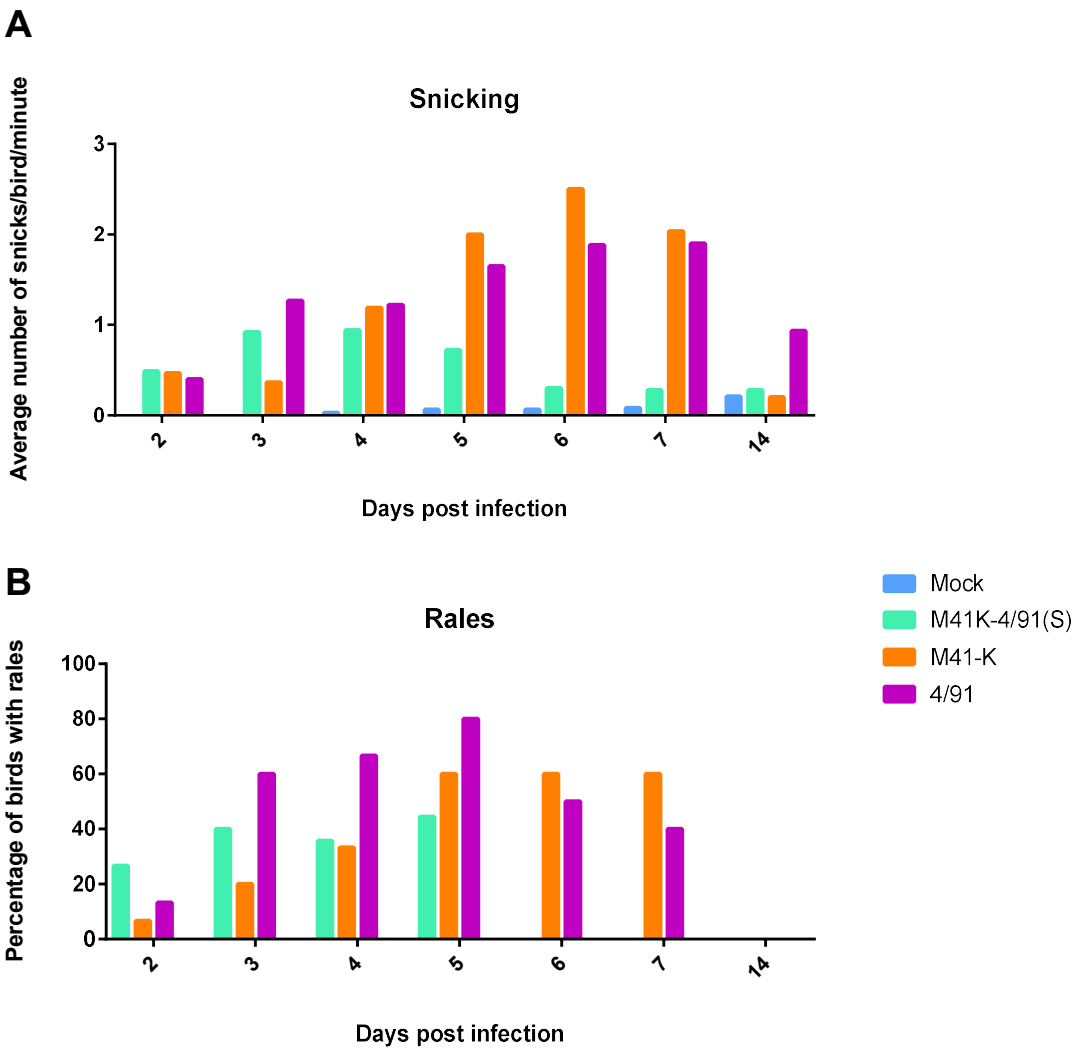

Figure 5.8: rIBV M41K-4/91(S) induces respiratory clinical signs. From day 2 pi, the number of snicks in each group was recorded and the average number per bird per minute was calculated for each day **(A)**. The breathing of each bird was assessed daily from day 2 pi and those exhibiting rales were noted. The percentage of birds exhibiting rales was calculated for each group **(B)**.

Another assessment of pathogenicity measured during the infections is the effect of IBV on tracheal ciliary activity. This is an important consideration for the poultry industry as loss of ciliary activity can result in fatal secondary bacterial infections. In this experiment, ciliary activity in the trachea of the birds culled on days 4 and 6pi was measured under a light microscope and a percentage score was calculated for each group. These scores are displayed in Figure 5.9. The observed effects on ciliary activity are similar across the infected groups, with all three viruses causing a significant reduction in ciliary activity on both days 4 and 6 pi compared to the mock infected birds. On day 4 pi there is some variation between the average percentage ciliary activities in each of the groups. The most dramatic decrease is seen in the 4/91 infected group, where complete ciliostasis has been induced by day 4pi with no recovery observed on day 6 pi. As mentioned, this is unsurprising due to the nature of this field strain. There is no statistical difference between the reductions in ciliary activity in each of the IBV-infected groups on either day pi, despite the considerable variation in the values of the M41-K infected birds on day 4 pi and the M41K-4/91(S) infected birds on day 6 pi.

The ciliary activity in the M41K-4/91(S) group however was comparable to the two control groups, with the values falling somewhere between that of M41-K and 4/91. M41K-4/91(S) caused near complete ciliostasis by day 4 pi with only a slight recovery on day 6 pi. Interestingly, the virus appears to have induced comparable damage in the trachea to the two control viruses, without having caused the extensive clinical signs observed in the control groups. Ciliary damage induced by M41K-4/91(S) occurs slightly earlier than the damage observed in the M41-K infected trachea, with a slower decline in ciliary activity from day 4 to day 6 pi.

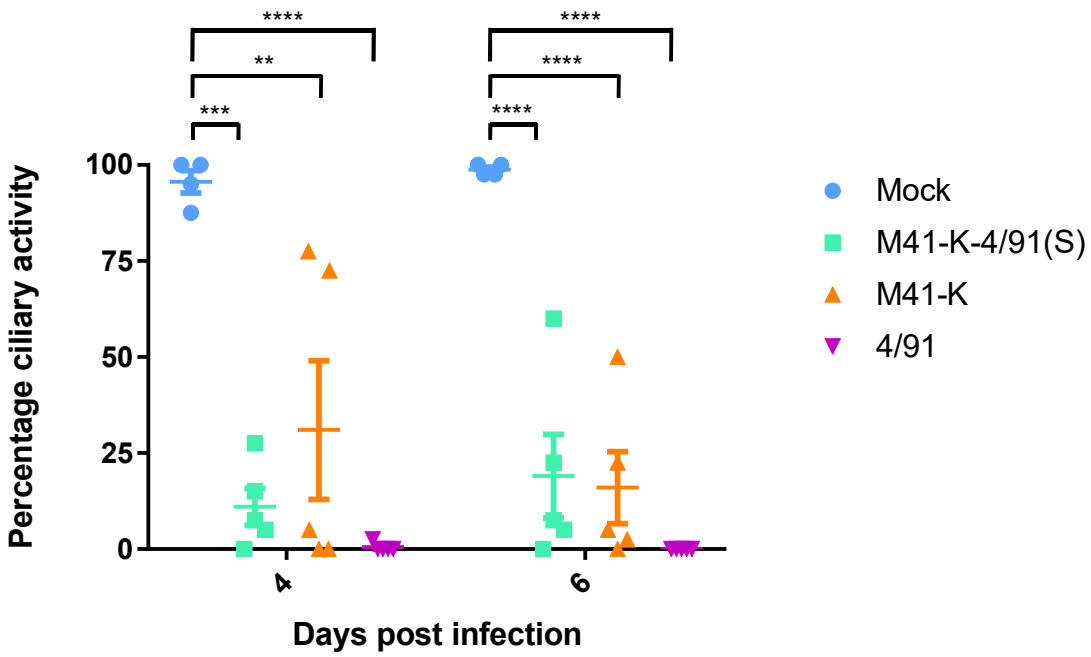

Figure 5.9: rIBV M41K-4/91(S) causes significant reductions in ciliary activity in infected chickens. Trachea were extracted from 5 birds in each group on days 4 and 6pi. Trachea were sectioned, examined under a light microscope and the average percentage ciliary activity was calculated for each group. Average values are displayed with SEM. Data were analysed by One-Way ANOVA followed by Dunnett's multiple comparison test to compare mean values in each group to the mock (** indicates $p = 0.0013$, *** indicates $p = 0.001$, **** indicates $p < 0.001$).

There are marked differences between IBV strains in their ability to disseminate from the sites of infection and their replication in different tissues. For example Beau-R is unable to disseminate from the eyes/nares to the trachea and is unable to cause disease in the infected chicken (Hodgson et al., 2004). To identify any differences in the dissemination patterns of M41K-4/91(S), M41-K and 4/91, RNA was extracted from *post-mortem* trachea samples and used for RT-PCR to detect IBV present in the sample. The results from the virus detection are summarised in Table 5.1. As expected, none of the trachea samples from the mock infected group were positive for IBV presence. IBV was detected in all day 4 pi trachea samples from the M41K-4/91(S) infected birds and the 4/91 infected birds. Four out of five birds in the M41-K infected group were positive for IBV.

Table 5.1: Assessment of virus dissemination *in vivo*

Tissue	Group			
	Mock	M41K-4/91(S)	M41-K	4/91
Trachea	0/5	5/5	4/5	5/5

Taken together the results show that the recombinant virus M41K-4/91(S) was capable of inducing clinical symptoms of IBV infection as well as causing dramatic reductions in ciliary activity. In terms of reaching the trachea, the dissemination pattern of the M41K-4/91(S) was the same as the parent viruses M41-K and 4/91, indicating that the ability of the virus to spread from the sites of infection to the primary replication sites was not altered as a result of the S protein modification.

5.3 Discussion

The recombinant IBV M41K-4/91(S) has been generated using VV-based reverse genetics and has been characterised both *ex vivo* and *in vivo* to analyse the effects of gene replacement on replication and pathogenesis in IBV. The virus has been successfully rescued in CK cells and amplified in TOCs before characterisation of both replication in *ex vivo* TOCs and *in vivo* pathogenesis.

The successful rescue of M41K-4/91(S) further demonstrates the possibility of generating recombinant IBVs containing S glycoproteins of significant sequence divergence compared to the viral backbone, as shown with other recombinant viruses such as M41K-BeauR(S), BeauR-M41(S) and BeauR-4/91(S) (Armesto et al., 2011, Hodgson et al., 2004). While the M41 and Beau-R S genes exhibit 96% amino acid sequence homology, M41 and 4/91 similarity is closer to 82%. This shows that both the M41-K and Beau-R genomes can support the insertion of divergent S genes *in vitro.*

The *in vitro* assessment of M41K-4/91(S) shows that the virus replicates well in embryonic TOCs (Figure 5.5) and has adopted the tropism of the S donor strain 4/91, in that it has lost the ability to replicate in cell culture, indicated by its inability to cause cpe (Figure 5.4). As previously discussed, the S gene has been shown to play an important role in determining the cellular tropism of IBV (Casais et al., 2003). M41K-4/91(S) is therefore expected to replicate in *ex vivo* cultures and embryonated eggs but not in cell culture, mirroring the tropism of 4/91. This does however limit the *in vitro* characterisation of M41K-4/91(S) to assessment of replication kinetics and induction of ciliostasis due to the nature of the 4/91-derived S protein. The analysis of M41K-4/91(S) replication is therefore confined to studies in embryonated eggs and TOCs. Assessment of M41K-4/91(S) replication in TOCs revealed that the insertion of the 4/91 S protein did not impact the replication capacity of the virus as it remained able to replicate successfully in these cultures. There were some slight

differences between the replication patterns of the three viruses in TOCs. M41K-4/91(S) was able to replicate in TOCs to similar titres as M41-K and 4/91 and followed the same pattern of replication as the S donor strain 4/91. M41-K exhibited a slightly different pattern of replication, but the differences are not significant. While the protocols involved in *ex vivo* characterisation are extremely labour intensive and expensive compared to cell culture techniques, this type of characterisation does provide a more relevant insight into replication in the host.

The increased titres of M41K-4/91(S) compared to the other viruses may be linked to the progression of ciliostasis in these cells. In *ex vivo* cultures, M41K-4/91(S) induced ciliostasis occurs at a slower rate than that induced by 4/91 (Figure 5.6). This means that more cells are susceptible to virus infection for a longer period of time, extending the period in which infectious virus can be produced.

Adoption of the S donor strain cell tropism has been demonstrated previously with the generation of BeauR-4/91(S), where the recombinant virus lost the ability to grow in cell culture and exhibited a restricted tropism profile compared to Beau-R (Armesto et al., 2011). The extended host tropism of Beau-R could be applied to M41K-4/91(S) with the insertion of the S2' cleavage site, which may allow the virus to infect *in vitro* cell cultures (Bickerton et al., 2018). Insertion of this small modification could provide a platform for propagating M41K-4/91(S) in cell culture to allow more in depth characterisation and a possible system for rational vaccine development against pathogenic field strains.

As previously discussed, there have been investigations into the role of the S gene in IBV pathogenicity where S genes from pathogenic viruses have been inserted into the genome of Beau-R (BeauR-M41(S) and BeauR-4/91(S)), to assess whether the resultant viruses would adopt a pathogenic phenotype. However these viruses remained attenuated despite the S gene modifications and so it was concluded that the S gene was not a pathogenicity

determinant for IBV. At the time, these findings were contrary to research with other, related coronaviruses, in which the S gene had been shown to dramatically alter the virulence and *in vivo* tropism of MHV and TGEV (Phillips et al., 1999, Navas et al., 2001, Sanchez et al., 1999). In contrast, the generation of M41K-BeauR(S) showed that a recombinant IBV can be attenuated following the insertion of the Beaudette S ectodomain, suggesting that the S gene is a pathogenicity factor in IBV infection. Taking the results from previous studies into account, the S gene cannot be termed a pathogenicity determinant as its replacement in a non-pathogenic virus (Beau-R) did not result in an altered pathogenicity. The contradiction in these studies raised an interesting question regarding the effects of gene replacement in IBV and whether it was this process that caused the attenuation in M41K-BeauR(S) rather than the presence of the S gene. The generation of M41K-4/91(S) described here has demonstrated that the process of gene modification does not interfere with pathogenicity and that the S gene does contribute to the virulence of a recombinant IBV. This is evident in the clinical signs and ciliostasis induced by the virus, which are comparable to those induced by the pathogenic parent viruses M41-K and 4/91 (Figures 5.8 and 5.9).

There are some differences in the patterns of clinical signs induced by each virus. For example, the peak in clinical signs induced by M41K-4/91(S) occurs earlier in the course of infection than 4/91 or M41-K (Figure 5.8). This is followed by a dramatic decrease in respiratory symptoms, possibly indicating that the virus is cleared by the birds more quickly than the control viruses. This could be due to the recombinant nature of the virus; although M41K-4/91(S) has remained pathogenic following the S gene modification, the chimeric nature of the virus may have rendered it more susceptible to the host immune response and thus less able to sustain infection for as long as either M41-K or 4/91. Without further investigation into the immune responses induced following M41K-4/91(S) infection it is difficult to draw conclusions on the reasons for the early-onset clinical signs observed here. Future investigations following these experiments will include assessment of neutralising

antibody induction following infection with M41K-4/91(S) using the serum collected on day 14pi. Antibody responses to 4/91 (793B) and M41 have been measured in other IBV pathogenicity studies but detectable levels of neutralising antibody were not found until day 21pi for either virus (Benyeda et al., 2009). It would be interesting to compare the responses following M41K-4/91(S) infection to identify any differences in the host response to infection with a pathogenic recombinant IBV.

Without further modifications there would not be scope to use M41K-4/91(S) as a vaccine due to the extensive clinical signs and ciliary damage induced by the virus. However this work demonstrates that a heterologous S gene from a different serotype can be inserted into the genome of a pathogenic IBV without affecting the pathogenicity of the resultant virus and further reiterates that the M41-based reverse genetics system can be used to effectively study IBV pathogenicity, demonstrating that the M41 genome can support insertion of large, heterologous gene sequences.

Chapter 6: Investigation into cellular factors influencing IBV tropism

6.1 Introduction

There are multiple factors that influence viral tropism which originate from both the virus and the host cell. In order for a cell to be infected it must express the correct receptors with which the surface proteins of the virus can interact. It must also provide the correct environment for the virus to attach and enter successfully, allowing its proteins to be properly processed. The local temperature and protease composition are both well studied conditions that can contribute to the intracellular environment required to allow virus interaction/replication within host cells.

IBV strains exhibit a wide range of tropisms both in cell culture and in the infected host. Some strains are capable of infecting a wider range of host cells *in vitro*, thought to be due to the presence of extra receptors on the host cell and/or different sequences in the viral attachment protein, spike (S). The S protein of the virus is thought to be solely responsible for *in vitro* tropism. It has been shown for other coronaviruses that the S protein determines hepatotropism *in vivo* (Navas et al., 2001). Mutations in the coronavirus S protein have been implicated in the acquisition of additional tissue tropisms, as demonstrated with feline coronaviruses (Rottier et al., 2005). The Beaudette S2 subunit is responsible for the extended host tropism observed with this strain of IBV *in vitro* (Bickerton et al., 2018), although this strain is incapable of maintaining replication *in vivo* (Hodgson et al., 2004).

The work described in this chapter aimed to examine the environmental requirements of the S protein necessary for IBV infection and maintenance of replication in a range of cell types, including protease requirements for proper cleavage events and the effects of temperature variation on viral replication.

6.2 Results

6.2.1 Protease requirements

It is well established that Beaudette strains of IBV exhibit an extended host tropism compared to M41 strains. This feature is thought to be due to the presence of a secondary cleavage site, located downstream of the S1/S2 furin site, in the S2 subunit which may be subject to further cleavage by cellular proteases (Bickerton et al., 2018). To demonstrate the presence of the S2' site in IBV Beau-R, purified IBV was used for analysis by SDS-PAGE, under reducing conditions, followed by western blot using the 26.1 monoclonal antibody against the S2 protein (PrioMab). The presence of the S2' cleavage product is indicated in Figure 6.1 by the presence of a band of approximately 30kDa. The 80kDa bands detected in both the M41-CK and Beau-R sample indicate the presence of S2. The large smear of approximately 250kDa+ is thought to be present as a result of S glycoprotein glycosylation.

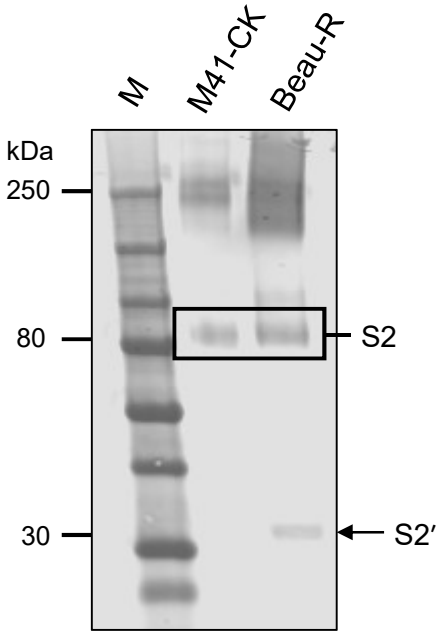

Figure 6.1: Demonstration of secondary cleavage site (S2') in Beau-R. Samples of purified M41-CK and Beau-R were analysed by SDS-PAGE followed by western blot using the 26.1 monoclonal antibody against the S2 subunit of the S protein. The indicated band at approximately 30kDa is thought to be a degradation product of the S2' cleavage site, only present in Beaudette samples.

Previous evidence suggests that the addition of exogenous proteases can expand viral tropism in coronaviruses, allowing entry into usually non-permissive cells (Park et al., 2016). To ascertain whether this theory applied to IBV infection, M41-K and M41-CK were used to infect Vero cells in the presence of exogenous tosyl phenylalanyl chloromethyl ketone (TPCK)-treated trypsin (Sigma). At 24 hours post-infection, the supernatant was used for titration by plaque assay on CK cells to assess quantities of infectious virus produced in the presence of trypsin. Figure 6.2 shows the viral titres of each virus in the presence of increasing concentrations of trypsin. Unlike M41-K, M41-CK is able to infect Vero cells at a very low level in the absence of trypsin. This may be due to the nature of the viruses, as M41-CK is a mixed population and M41-K originated from a viral clone. Viral titres of both M41-K and M41-CK are significantly higher in the presence of exogenous trypsin at all concentrations (0.2µg/ml - 2µg/ml). For M41-K, the lowest concentration of trypsin yielded variable results and there was a significant difference in viral titre between the two viruses. However increase in viral titre is still significant for M41-K with the addition of trypsin at 0.2µg/ml. Taken together these results show that the addition of exogenous trypsin allows these M41 strains to enter non-permissive Vero cells at relatively low concentrations.

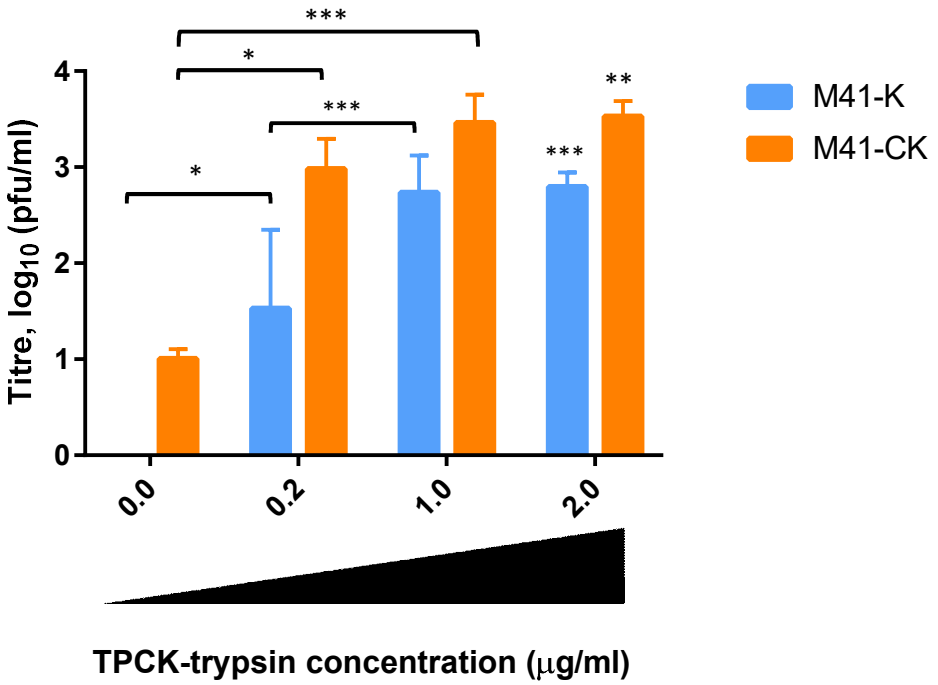

Figure 6.2: Addition of exogenous trypsin significantly increases replication of M41 strains in Vero cells. Vero cells were infected with M41-K or M41-CK at an MOI of 1, diluted in serum-free media containing varying amounts of TPCK-treated trypsin. After 1 hour incubation at 37°C, cells were washed in PBS and the media was replaced with fresh media containing TPCK-treated trypsin. Cell supernatant was harvested after 24 hours incubation at 37°C and used for titration by plaque assay on CK cells. Mean viral titres of three biological repeats are displayed for each virus at each concentration, with SEM. Data were analysed by Two-Way ANOVA followed by multiple comparison tests to compare each concentration. Significant differences are indicated (* indicates $p = 0.01$, ** indicates $p = 0.001$ and *** indicates $p < 0.001$).

Figure 6.2 demonstrates that M41 is capable of producing infectious virus in non-permissive cells in the presence of exogenous protease. The induction of cpe in infected cells is indicative of IBV infection in cell culture, with observations including cell rounding and clearings in the monolayer. To assess whether the addition of trypsin has affected the virus' ability to induce cpe, Vero cells were infected with IBV in the presence of TPCK-treated trypsin at a dose of 1µg/ml, diluted in 1XBES medium. This dose was chosen based on the results shown in Figure 6.2, where this was the lowest concentration that provided consistent results, in order to minimise cytotoxicity.

Both M41-K and M41-CK caused visibly higher levels of cpe compared to the mock-infected cells. This shows that M41-K and M41-CK are both able to cause cpe in a non-permissive cell line with the addition of exogenous trypsin. The images from these infections compared to the mock-infected cells are shown in Figure 6.3. The observation of cpe indicates that IBV is spreading from cell to cell during infection due to the presence of exogenous trypsin in the cell culture medium.

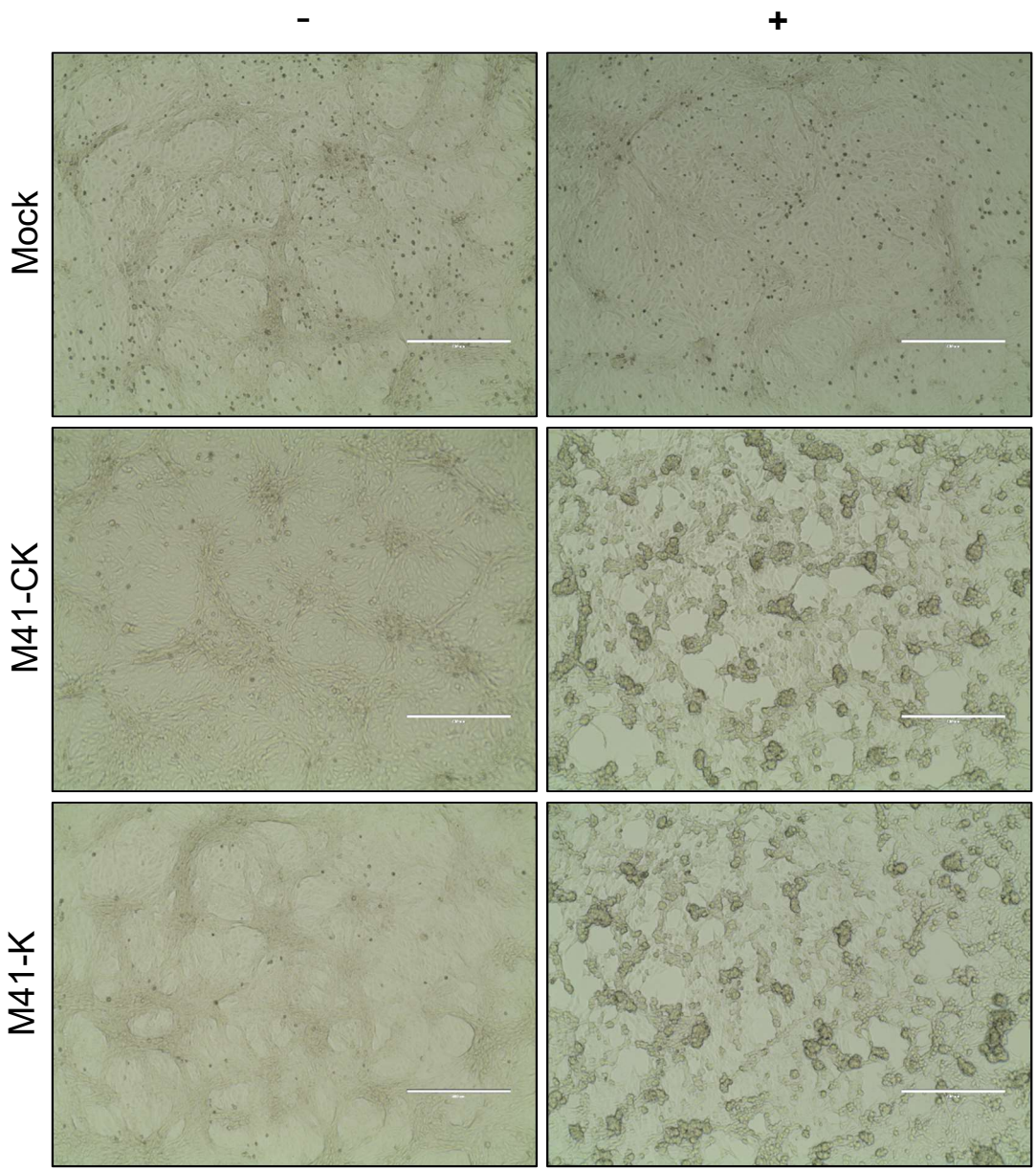

Figure 6.3: M41 causes extensive cpe in Vero cells in the presence of trypsin. Vero cells were infected with M41-K and M41-CK (MOI=1) in the presence (+) or absence (-) of TPCK-trypsin (1µg/ml). After 24 hours incubation at 37°C, signs of IBV-induced cpe, including clearings in the monolayer and rounded cells, were observed under an EVOS light microscope at 10X magnification.

To confirm IBV infection in the presence of trypsin, Vero cells were infected with M41-K or M41-CK and the presence of dsRNA was assessed by IF. The presence of dsRNA is thought to be indicative of a replicative intermediate and is found in the DMVs of coronavirus-infected cells (Knoops et al., 2008). Figure 6.4 shows confocal images of infected cells in the presence or absence of exogenous trypsin. Compared to untreated (-) cells, there is more dsRNA present in the M41 infected samples when trypsin is added, indicating an increase in the levels of infection. The distribution of dsRNA in the trypsin-treated infected cells is the same between M41-K and M41-CK.

Taken together these results show that it is possible to extend the host range of IBV using exogenous proteases such as trypsin, allowing virus entry and replication in usually non-permissive cell types.

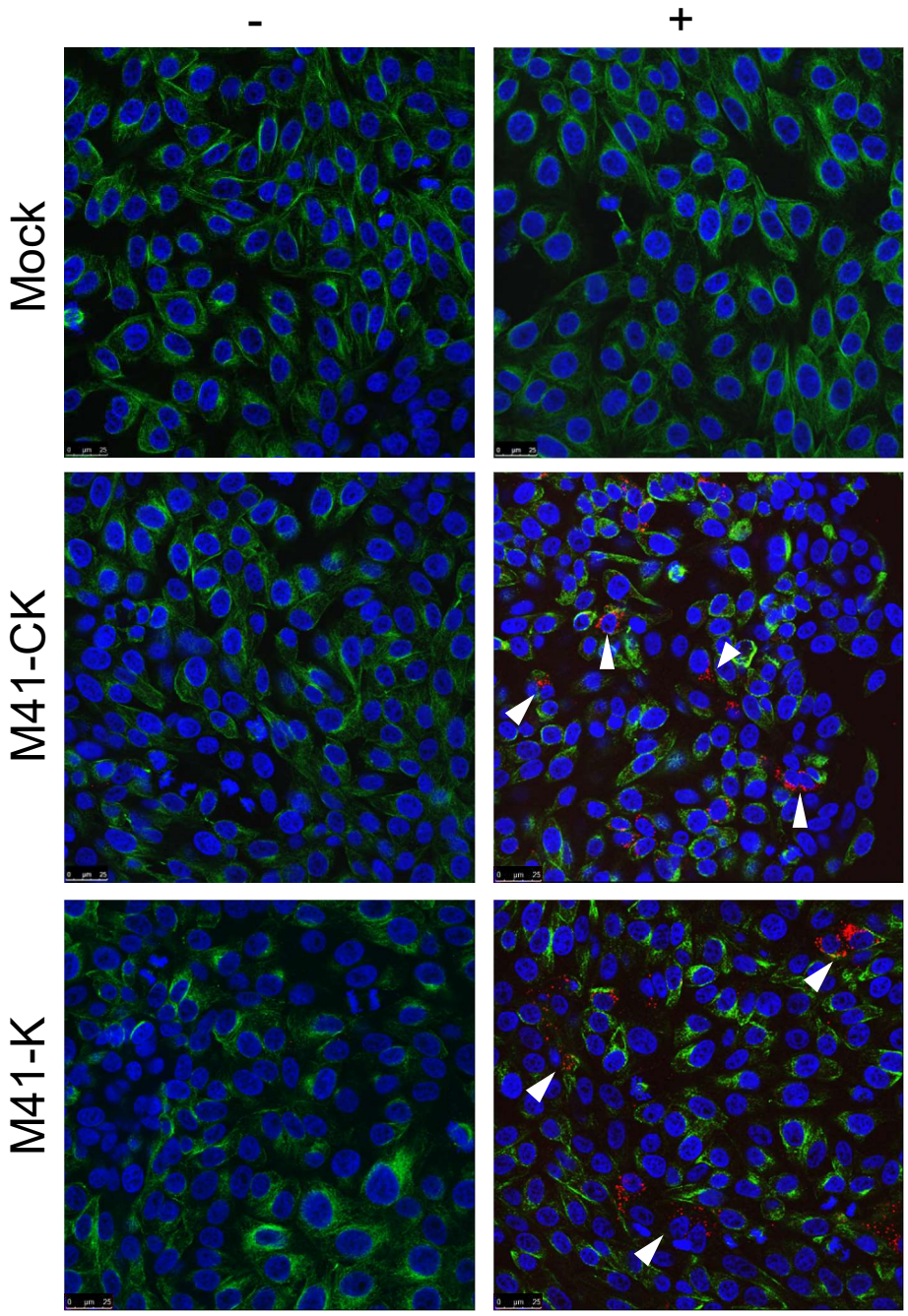

Figure 6.4: Exogenous trypsin allows infection of Vero cells by M41-K and M41-CK. Vero cells were seeded onto coverslips and infected with M41-K or M41-CK diluted in trypsin-containing media (0.00125%) and incubated for 24 hours at 37˚C. Cells were fixed in 4% PFA in PBS and permeabilised with 0.1% Triton X-100 in PBS. Cells were incubated in blocking solution (0.5% BSA in PBS) before staining with primary antibodies against dsRNA (red) and α-tubulin (green). Cells were incubated in secondary antibodies AlexaFluor Goat anti-Mouse IgG1 (α-tubulin) and IgG2a (dsRNA). Nuclei were counterstained with DAPI (blue).

The data described above clearly show that the addition of exogenous trypsin allowed M41 entry and replication in non-permissive cells over 24 hours. To assess whether this infection could be maintained, Vero cells were infected with M41-K and M41-CK in the presence of trypsin for 24 hours and the resulting supernatants were passaged a further three times on Vero cells in the presence of TPCK-trypsin. Figure 6.5 shows the viral titres from each passage with two different concentrations of trypsin (0.2µg/ml and 2µg/ml). Overall, there is a downward trend in the titres as the passage number increases for both concentrations, showing that the presence of trypsin over multiple passages does not aid M41 infection and replication in Vero cells. This indicates that trypsin is not the only factor required to maintain M41 replication in Vero cells. It should be noted that each passage was repeated only once and so further replicates should be completed before any definite conclusions are drawn.

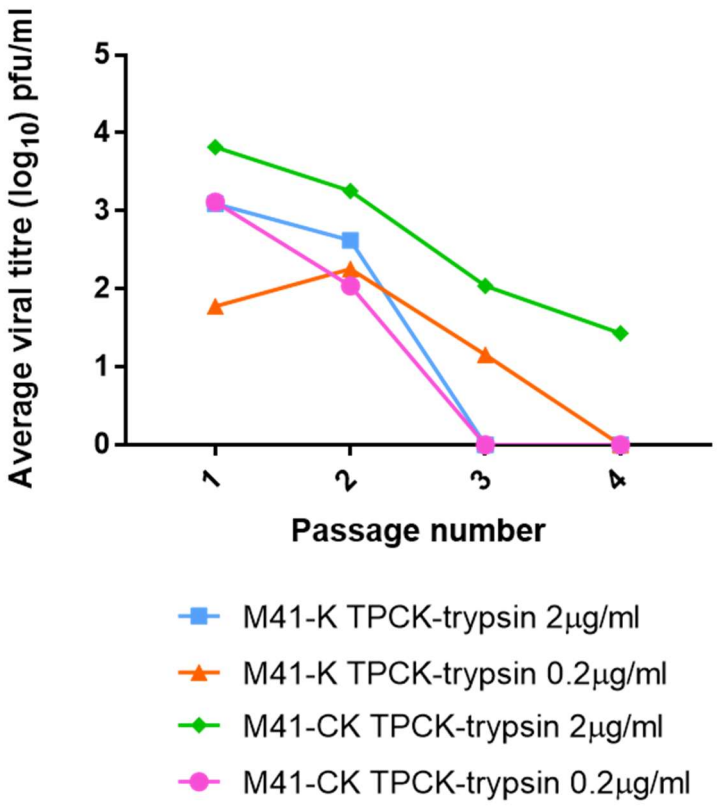

Figure 6.5: M41 replication is not maintained over passage in Vero cells in the presence of TPCK-trypsin. Vero cells were infected with M41-K and M41-CK diluted in media containing TPCK-trypsin at 2µg/ml or 0.2µg/ml for 24 hours at 37°C (Passage 1). Supernatant was harvested and infections were repeated for a further three passages with trypsin-containing media at the same concentrations. Supernatant from each passage was used for titration by plaque assay in CK cells. Viral titres (log_{10}) are displayed for each virus (*n = 1)*.

Propagation of field strains of IBV is challenging as most strains do not replicate in cell culture. To assess whether the addition of exogenous trypsin would affect field strain replication in the same way as M41 strains, Vero cells were infected with QX in the presence of TPCK-trypsin. Infected supernatant was used for plaque assay in CK cells and viral titres between treated and untreated samples were compared. Figure 6.6 shows that the addition of trypsin does allow QX to enter and replicate in Vero cells. It is important to consider that these infections were only conducted once and so further replicates would be required to confirm the result, however it is clear that there was a dramatic increase in the replicative capacity of QX in these cells following TPCK-trypsin addition.

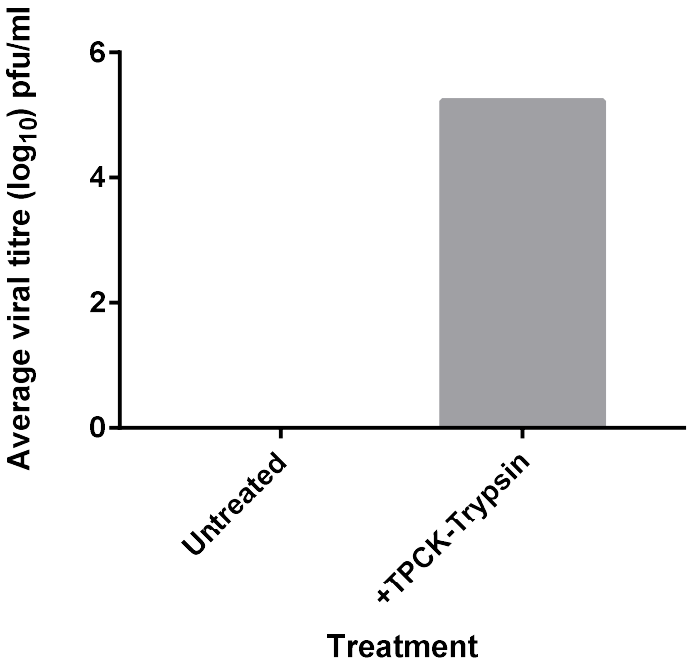

Figure 6.6: Addition of exogenous TPCK-trypsin facilitates QX infection of Vero cells. Confluent monolayers of Vero cells were washed once in PBS and infected with QX at an approximate MOI of 1, diluted in 1XBES containing TPCK-trypsin (1µg/ml). Cells were incubated for 24 hours at 37°C before supernatant was harvested and used for plaque assay in CK cells in triplicate.

6.2.2 Temperature sensitivity

There are major differences in the clinical disease caused by the different strains of IBV used in a laboratory setting. M41 is highly pathogenic and causes numerous respiratory symptoms associated with infection as well as complete destruction of the ciliated cells in the trachea. In contrast, Beau-R causes no clinical disease or ciliostasis in infected birds (Hodgson et al., 2004). In fact, during previous pathogenicity studies, Beau-R was never detected in the trachea, indicating that it cannot disseminate through the bird. *In vitro*, however, Beau-R replicates very well and can cause ciliostasis in *ex vivo* TOCs.

As part of a wider study, possible reasons for this disparity between *in vitro* and *in vivo* replication capacities of Beau-R have been investigated. One factor that was noted was the difference in incubation temperature used in the two types of study. All *in vitro* and *ex vivo* investigations were carried out at 37°C, whereas the core body temperature of a chicken is approximately 40-42°C. It was hypothesised that perhaps this was the limiting factor in the inability of Beau-R to cause clinical disease, as maybe the virus was unable to replicate and function at the higher temperature, due to being temperature sensitive.

To test this hypothesis some preliminary experiments were performed by Sarah Keep to compare replication of IBV at 41°C compared to 37°C. Figure 6.7 shows the average titres of M41-CK and Beau-R at 37°C and 41°C over a 96 hour time course. A summary of the statistical analyses is detailed in Table 6.1. At each time point post-infection, both M41-CK and Beau-R replicate to significantly higher titres at 37°C compared to Beau-R at 41°C, which remains below 10^1pfu/ml throughout the experiment. M41-CK follows the same pattern of replication at both 37 and 41°C, although titres at 37°C are significantly higher ($p < 0.0001$) from 48 hours post-infection onwards. Average titres for Beau-R at 41°C are significantly lower than M41-CK at 41°C at every time point pot-infection, showing that Beau-R replication is highly sensitive to temperature compared to M41-CK.

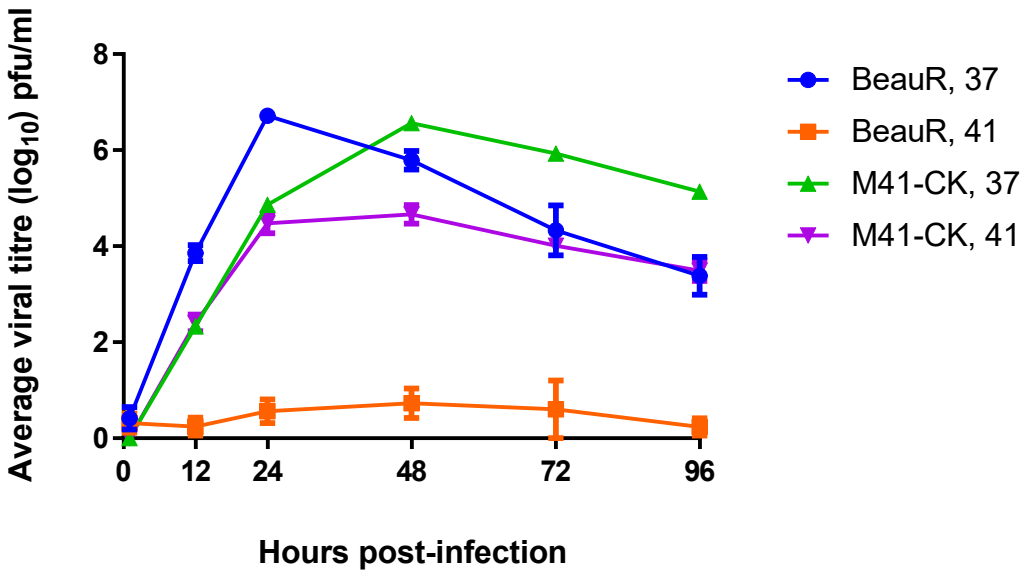

Figure 6.7: Replication of rIBV Beau-R is temperature sensitive *in vitro*. Confluent monolayers of CK cells were infected with IBV Beau-R or M41-CK at an MOI of 0.1 and incubated at either 37°C or 41°C for 96 hours. Supernatant was harvested at 1, 12, 24, 48, 72 and 96 hours post-infection and titrated by plaque assay in CK cells. The average viral titres from three biological repeats are displayed with SEM. Data were analysed by Two-Way ANOVA followed by Tukey's multiple comparisons test, summarised in Table 6.1. Experiments and statistical analyses were completed by Sarah Keep.

Table 6.1: Statistical analyses of M41 and Beau-R temperature sensitivity comparisons at 12, 24, 48, 72 and 96 hours post-infection in CK cells.

		Hours post-infection				
Comparison		***12***	***24***	***48***	***72***	***96***
BR 37	BR 41	****	****	****	****	****
BR 37	M41 37	***	****	**ns**	***	****
BR 41	M41 37	****	****	****	****	****
BR 41	M41 41	****	****	****	****	****
BR 37	M41 41	***	****	****	**ns**	**ns**
M41 37	M41 41	**ns**	**ns**	****	****	****

*A Two-Way ANOVA was used to analyse the data displayed in Figure 6.7 in order to compare each virus at each time point post-infection. *** indicates a p value of 0.0001 and **** indicates a p value of <0.0001.*

Parts of the entry and fusion process in other viruses including Sendai virus are known to be dependent on several external factors including, in some cases, temperature (Wharton et al., 2000). Following the initial investigations into temperature sensitivity shown in Figure 6.7, the involvement of the S gene in replication at 41°C was examined using a range of recombinant viruses with different S genes. As the S gene is responsible for viral attachment and fusion, characterising the replication of these recombinant viruses allows us to establish whether the processes affected by temperature sensitivity included virus entry. M41K-BeauR(S) and BeauR-M41(S) contain the ectodomain of the reciprocal S gene (either M41 or Beaudette-derived). The replication kinetics of these rIBVs at both temperatures were assessed and compared to that of the parent viruses M41-K and Beau-R.

Figure 6.8 shows the replication kinetics of the four strains of IBV at 37°C (Fig. 6.8A) and 41°C (Fig. 6.8B). At 37°C, all four viruses can establish and maintain replication over 96 hours. At 41°C, M41-K and M41K-BeauR(S) replicate to significantly higher titres than Beau-R and BeauR-M41(S). A summary of the statistical analyses for these data is displayed in Table 6.1. M41K-BeauR(S) replication has been slightly hindered by the insertion of the Beaudette-derived S gene but the virus is still capable of replication at 41°C, following a similar pattern of replication to M41-K. This shows that replacing the S gene from a virus that replicates efficiently at 41°C cannot rescue Beaudette replication at this temperature, indicating that the molecular basis of this sensitivity lies within a different viral gene.

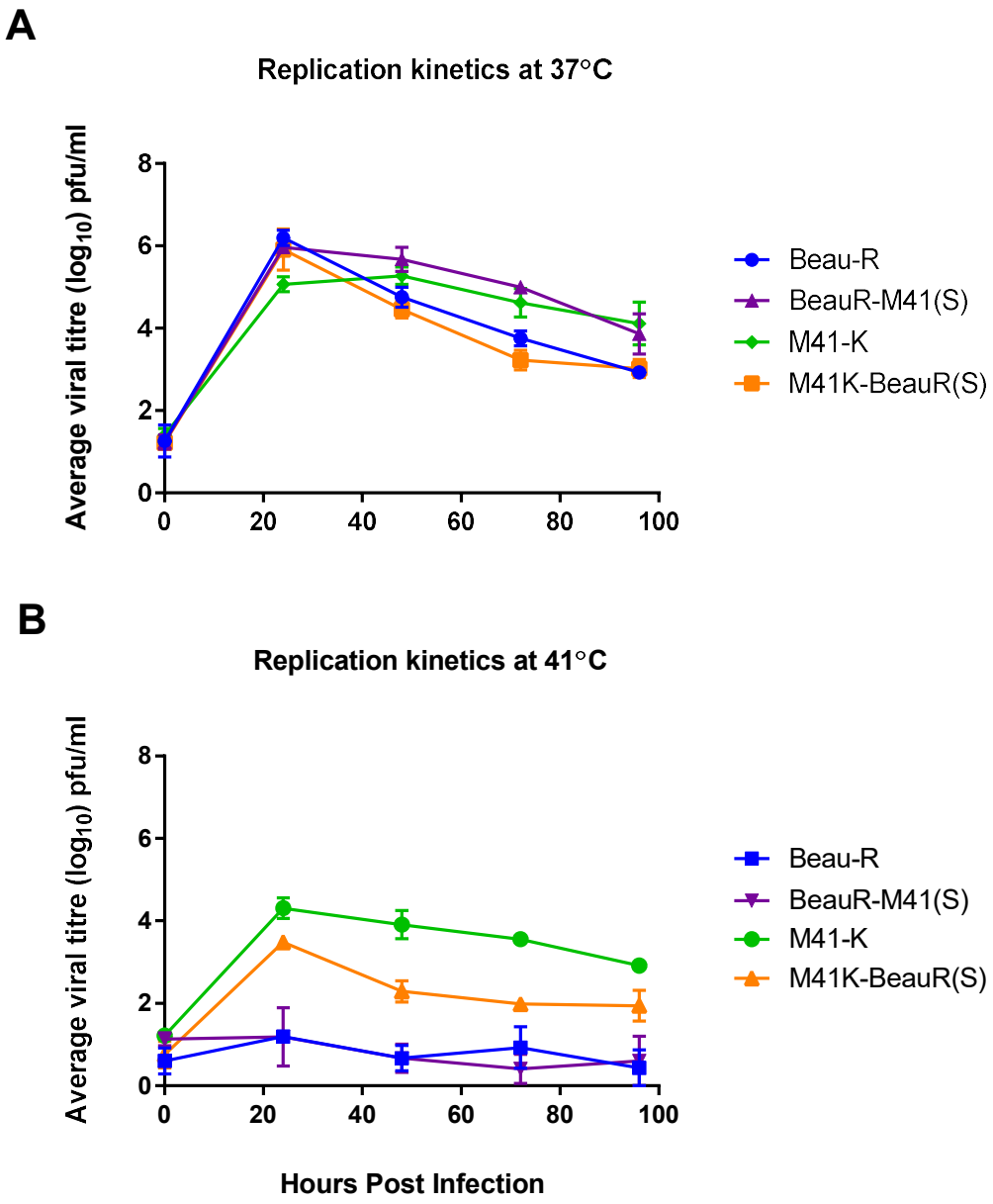

Figure 6.8: Insertion of the M41 S gene cannot rescue Beaudette replication at 41°C. Confluent monolayers of CK cells were infected with IBV at an MOI of 0.01 and incubated at 37°C **(A)** or 41°C **(B)**. Supernatant was harvested at 1, 24, 48, 72 and 96 hours post-infection and used for titration by plaque assay on CK cells. The mean viral titres of three biological repeats are displayed with SEM. Data were analysed by Two-Way ANOVA followed by Tukey's multiple comparisons test (see Table 6.1).

Table 6.1: Summary of the overall statistical differences in replication kinetics at 37°C and 41°C.

Comparison		*Significance*	*P-value*
Beau-R 37	Beau-R 41	****	<0.0001
M41-K 37	M41-K 41	*	0.0345
M41K-BeauR(S) 37	M41K-BeauR(S) 41	**	0.0023
BeauR-M41(S) 37	BeauR-M41(S) 41	****	<0.0001
M41-K 41	M41K-BeauR(S) 41	*	0.0142
Beau-R 41	BeauR-M41(S) 41	**ns**	---------
Beau-R 41	M41-K 41	****	<0.0001
M41K-BeauR(S) 41	BeauR-M41(S) 41	**	0.0018

Data were analysed by Two-Way ANOVA followed by Tukey's multiple comparisons test to compare each virus at each temperature.

To further investigate the mechanisms of replication at 41°C, the presence and distribution of dsRNA (a marker of IBV infection) in infected cells was assessed by IF using monoclonal antibodies against dsRNA (Scicons) and α-tubulin (Abcam). Figure 6.9 shows the confocal images from these infections. Again, a range of recombinant viruses was used to investigate the potential of the S gene to alter infection at different temperatures. M41-K and Beau-R are both capable of infecting CK cells at 37°C and swapping the S gene from these two viruses has no effect on their ability to replicate in these cells, as demonstrated with M41-BeauR(S) and BeauR-M41(S). At 41°C however, only M41-K and M41K-BeauR(S) are able to establish infection, as indicated by the presence of dsRNA in infected cells. There is no visible dsRNA in the cells infected with Beau-R or BeauR-M41(S) at 41°C, further implicating that the S gene does not dictate the temperature-dependent tropism of an IBV, but rather this phenotype is determined by other parts of the genome.

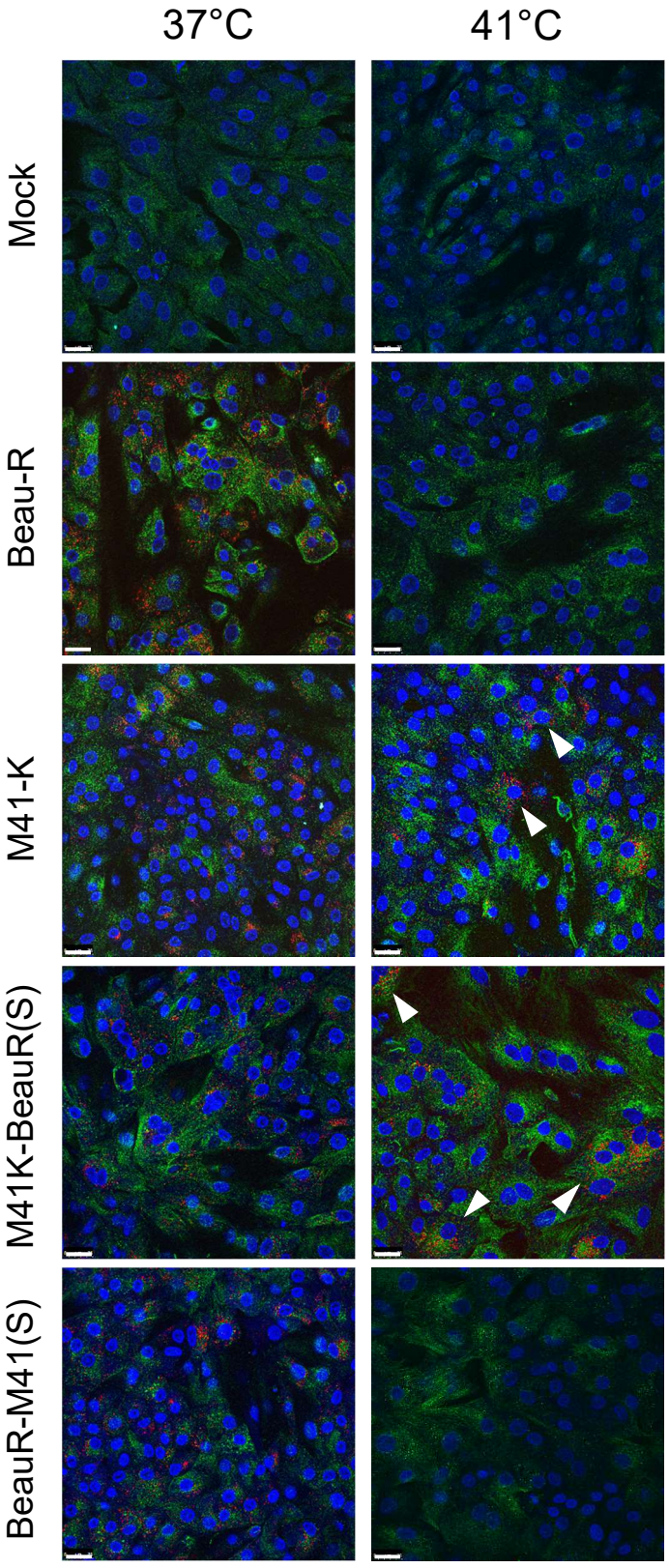
37°C
41°C
Mock
Beau-R
M41-K
M41K-BeauR(S)
BeauR-M41(S)

Figure 6.9: Detection of dsRNA in infected Vero cells is not dictated by the S gene at 41°C. CK cells on coverslips were infected with Beau-R, M41-K, M41K-BeauR(S) or BeauR-M41(S) and incubated at 37°C or 41°C for 24 hours. Cells were fixed in 4% PFA in PBS and permeabilised with 0.1% Triton X-100 in PBS before staining using primary antibodies anti-dsRNA and anti-α-tubulin. Cells were incubated in secondary antibodies AlexaFluor Goat anti-Mouse 488 IgG1 (α-tubulin, green) and AlexaFluor Goat anti-Mouse 568 IgG2a (dsRNA, red). Nuclei were counterstained with DAPI (blue). White bars = 25µm scale.

As previously mentioned, Beaudette strains of IBV exhibit an extended host tropism, dictated by specific amino acids in the S2 subunit of the S protein (Bickerton et al., 2018). In order to assess whether this tropism was affected by changes in temperature, Vero cells were infected with IBV and incubated at 41°C before assessment of dsRNA presence by IF.

Figure 6.10 shows the confocal images from the infections at 41°C compared to those at 37°C in Vero cells. As shown in Figures 6.7-6.9, M41-K is capable of replicating at 41°C in permissive CK cells. M41-K cannot replicate in Vero cells due to its restricted host tropism. The viruses used here containing M41-derived S genes (M41-K and BeauR-M41(S)) have not replicated successfully in these cells, as demonstrated by the absence of dsRNA (Fig. 6.10). Beau-R is only able to replicate in Vero cells at 37°C, not 41°C. The insertion of the S gene into the M41-K genome allowed M41K-BeauR(S) to infect and replicate in Vero cells at 41°C; its *in vitro* tropism was not affected by the increased temperature. This demonstrates that IBV requires both a permissive S gene and a competent virus backbone (i.e. M41-K) to successfully replicate in Vero cells at 41°C.

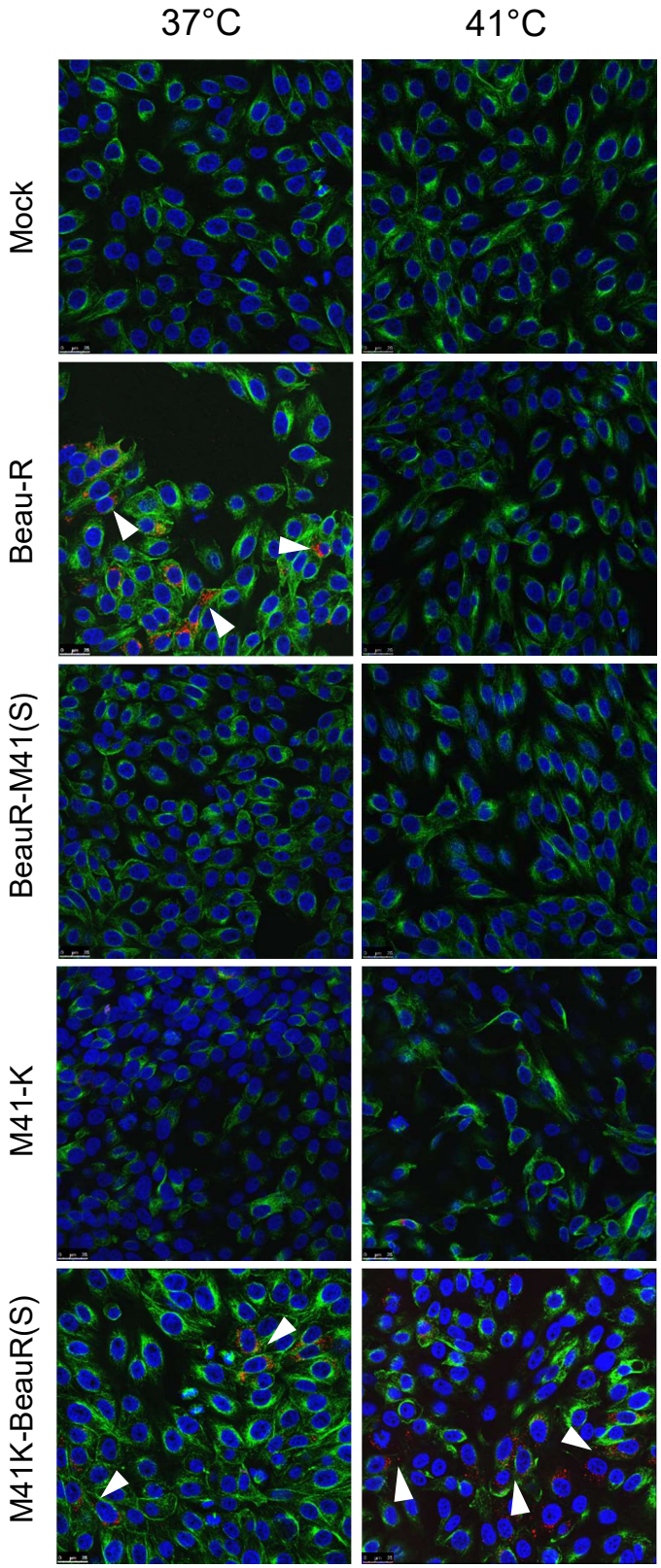
37°C
41°C
Mock
Beau-R
BeauR-M41(S)
M41-K
M41K-BeauR(S)

Figure 6.10: IBV requires more than a permissive S gene to extend host tropism at 41°C. Vero cells were infected with IBV Beau-R, BeauR-M41(S), M41-K or M41K-BeauR(S) and incubated at 37°C or 41°C for 24 hours before fixation with 4% PFA in PBS. Cells were permeabilised with 0.1% Triton X-100 in PBS and blocked in 0.5% BSA in PBS before incubation with primary antibodies against dsRNA and α-tubulin. Cells were incubated with secondary antibodies AlexaFluor Goat anti-Mouse 488 IgG1 (α-tubulin, green) and AlexaFluor Goat anti-Mouse 568 IgG2a (dsRNA, red). Nuclei were counterstained with DAPI (blue).

6.3 Discussion

Viral infection of a given cell is dependent on several factors. Some of these factors are virus-dependent and some are external environmental factors. The virus must possess the correct genetic composition and the cell must provide the correct environment for all the steps of the infection cycle to take place in a proper manner. The scope of this chapter included initial assessments of the protease requirements for IBV infection and the effects of the external environment on viral replication, with a focus on temperature.

6.3.1 Protease requirements of the IBV S protein

In some coronaviruses, proteolytic cleavage of the S protein by host cell proteases is an essential requirement for virus entry (reviewed by Millet and Whittaker, 2015). In IBV, the classical furin cleavage site present at the S1/S2 junction is required for entry into host cells. There is an extra site present in the Beaudette strains, known as the S2' site. Cleavage at this site is thought to allow these strains to enter a wider variety of cells *in vitro*, including Vero cells. The presence of the S2' site in Beau-R compared to M41-CK is demonstrated in Figure 6.1.

A large proportion of the strains of IBV are unable to be cultured *in vitro*, exhibiting a restricted tropism. These strains are often only able to replicate in whole organ cultures or in embryonated hens' eggs. Previous work with MERS-CoV showed that the tropism of a coronavirus could be extended with the addition of exogenous proteases (Millet and Whittaker, 2015, Park et al., 2016). Here, M41 was used as a tool to assess whether this was true for IBV. The addition of exogenous trypsin significantly increased the capacity of both M41-K and M41-CK to replicate in usually non-permissive Vero cells (Figure 6.2).

Trypsin is known to cleave only at exposed Arginine (R) and Lysine (K) residues in protein sequences (Olsen et al., 2004). Comparing the amino acid sequence of the Beaudette and M41 S genes highlights cleavage sites susceptible to action by trypsin. The sequence of the

Beaudette S2' site is RRKRR whereas the corresponding M41 sequence is missing the central lysine, potentially preventing the cleavage of this site in M41 by furin but still allowing its cleavage by trypsin. There are two further R residues in M41 present at positions 689 and 691 that could also theoretically be susceptible to cleavage by trypsin. To further elucidate the mechanisms behind the trypsin-mediated entry into non-permissive cells, the cleavage products of the S protein following trypsin cleavage could be examined by western blot and compared to cleavage products produced in permissive cells, such as CK cells. This would provide more information on the location of target regions for cleavage events in the coronavirus S protein.

Initial investigations into the maintenance of replication in Vero cells in the presence of trypsin show that this treatment does not increase replication over passage. In fact, the observed effect is quite the opposite. The viral titre over three passages in Vero cells decreased quite dramatically in the majority of the samples. These results are contradictory to observations in other coronaviruses such as PEDV, where passaging in the presence of trypsin resulted not only increases in viral titre, but also in the generation of trypsin-independent mutants able to replicate efficiently in cell culture (Park et al., 2011, Wicht et al., 2014).

With further investigation it would also be prudent to repeat these infections in a more relevant cell type such as avian DF-1 cells, which are also non-permissive to M41 infection. In this case Vero cells were used as a proof of principle to demonstrate that the tropism of a given IBV strain could be extended by altering the cellular environment. In addition, Vero cells are already licensed for vaccine production so propagation in this cell type is extremely relevant to the vaccine industry.

IBV is notoriously difficult to culture in a laboratory setting, with many strains only able to infect embryonated eggs or *ex vivo* organ cultures. The addition of exogenous proteases has

been shown here to allow infection of classically non-permissive cells. There is also potential for this work to be applied to more relevant, circulating field strains, such as QX and 4/91, both of which only replicate in *ex vivo* tracheal organ cultures (TOCs) and embryonated eggs. Initial investigations into the application of this technique to field strains (demonstrated with QX) showed that the addition of trypsin causes a considerable increase in the viral titres produced in CK cells (Figure 6.6). Replicates of these experiments are required to verify the result but the initial assessments are promising. Other non-cell culture adapted strains such as 4/91 should also be included in the analysis.

Generation of a platform for vaccine virus/field strain production in cell culture would dramatically reduce the numbers of embryonated eggs used in this field. The benefits would also extend to basic research as this would reduce animal costs required for studying economically important viruses, providing a potential method for *in vitro* investigations without the use of whole organs, embryos or adult birds.

6.3.2 Temperature sensitivity in IBV

Observations from previous studies with Beau-R have shown that this virus is extremely attenuated *in vivo*. The virus cannot cause clinical signs and has not been recovered from the trachea of infected birds, indicating that the virus is incapable of spreading from the sites of inoculation (eyes and nares) (Hodgson et al., 2004). To elucidate the potential mechanisms behind this attenuation, investigations were carried out into the replication of different strains of IBV at biologically relevant temperatures. The core body temperature of a chicken is between 40-42°C, therefore 41°C was chosen as a comparison to the standard *in vitro* incubation temperature of 37°C.

The initial studies carried out by Sarah Keep (Figure 6.7) revealed a stark difference in the replication capacities of Beau-R and M41-CK, with Beau-R completely unable to sustain infection and replication at 41°C. This difference corresponds to the variance in pathogenicity between the two strains, as M41-CK is highly pathogenic. Temperature sensitivity has been observed in other coronaviruses and has been linked to virus dissemination *in vivo* (Christianson et al., 1989), indicating a possible reason for the attenuation of Beau-R in chickens.

To further investigate the genetic basis of this temperature sensitivity, the replication kinetics of rIBVs with modified S genes was assessed at each temperature. The data from the assessment in CK cells (Figure 6.8) show that the S gene is not responsible for the potential of a virus to replicate at 41°C, indicating that the limiting step in this process is not virus entry, as M41K-BeauR(S) is only slightly hindered by the foreign S gene. The presence of dsRNA in these cells at 41°C consolidates this finding, as dsRNA is a marker of IBV replication (Figure 6.9). Overall the results indicate that the background genome, rather than the S protein ectodomain, is responsible for conferring sensitivity to temperature. In related coronaviruses, temperature sensitivity has been attributed to proteins encoded in the replicase gene, including nsp3 and nsp5. Studies with the *Betacoronavirus* MHV have shown that decreases in replication efficiency can be linked to the protease activities of both these proteins (Stobart et al., 2012, Stokes et al., 2010). This has also been observed in various strains of influenza, where the introduction of mutations in the polymerase genes have resulted in the generation of temperature sensitive mutants (Meyer et al., 2016). This principle has been used to investigate the use of these viruses as live-attenuated vaccines (Nogales et al., 2017). It is therefore likely that the replicase gene of Beau-R is responsible for the temperature sensitivity observed in the experiments described here. It can be hypothesised that the pathogenicity is linked to temperature sensitivity, as the replicase

gene has previously been identified as a pathogenicity determinant in IBV (Armesto et al., 2009).

Tropism has previously been shown to be dictated by the S protein of various coronaviruses, so viral tropism at higher temperatures was investigated using IF for the detection of dsRNA. The confocal images of IBV infection in Vero cells (Figure 6.10) clearly demonstrate that two factors are required to achieve the extended tropism at 41°C; the virus requires both a competent replicase gene and a permissive S gene. For this reason, the recombinant virus M41K-BeauR(S) is capable of replicating in Vero cells at 41°C, as it contains the replicase gene from M41-K and the S gene (ectodomain) from Beau-R.

There are limitations associated with using Vero cells at 41°C; as they are a primate cell line, they are adapted to growth at 37°C. Data from cell viability assays (Appendix) showed that Vero cell viability cannot be maintained for long periods of time at 41°C. These experiments must therefore be interpreted as a proof of principle and further investigations should be carried out in a more suitable cell line such as the continuous avian fibroblast cell line DF-1 cells. The replication kinetics in these cells post 24 hours should be assessed and compared to replication in CK cells at 41°C.

Other aspects to consider for future investigations include the assessment of replication at intermediate and lower temperatures. While 41°C is biologically relevant to the core body temperature of a chicken, the temperature in the upper respiratory tract is likely to be lower. Therefore investigations into viral replication at temperatures which better reflect the natural host environment may be beneficial to fully understanding the mechanisms behind IBV replication at different temperatures.

Taken together the data described here show that IBV tropism is dictated by more than the virus itself and that the cellular environment must be considered. The addition of proteases during infection can dramatically alter the tropism of IBV, potentially providing a platform

for *in vitro* propagation of field strains only capable of replication in organs or embryos. The temperature sensitivity experiments show that the S protein is not sufficient to rescue replication at higher temperatures. Further investigation into identifying the regions responsible for the temperature sensitivity observed in Beau-R infections could lead to rationally designed vaccines.

Chapter 7: Discussion

The overall aims of this thesis were to characterise the glycan profile of the IBV S gene and to further elucidate the role of the protein in viral pathogenicity and *in vitro* tropism. The aims have been achieved using a range of techniques to identify glycosylation sites on the S protein and assess the impacts of disrupting the patterns of glycosylation during protein synthesis and modification. The relationship between the IBV S gene and pathogenicity has been defined using recombinant viruses expressing heterologous S proteins. These viruses have also been used to investigate the involvement of the S protein in cellular tropism, focussing on temperature sensitivity and proteolytic activation by exogenous protease.

7.1 Characterisation of the IBV S glycosylation profile

The first objective of the work described in this thesis involved characterisation of the glycosylation profile of the IBV S protein. Previous studies have identified glycosylation sites on the surface of the S protein but only recently have there been more detailed studies into the roles of specific sites. Most recently, a thorough assessment of the role of Beaudette S glycosylation was published, detailing the generation of mutant viruses with deleted glycosylation sites and the effects of these mutations on replication and fusion (Zheng et al. 2018).

The aims of Chapter 3 were set out to characterise the glycosylation profile of a wider range of more relevant IBVs, including pathogenic strains. A large number of predicted glycosylation sites were identified on the surface of the S protein and their locations mapped onto a model of the IBV M41-CK S protein. Glycosylation was confirmed at 18 of 29 predicted sites using mass spectrometry. The structures at six of these sites were predicted using EThcD mass spectrometry, providing initial insights into the heterogeneity of oligosaccharides present in the virus population. This work builds on other recent studies of the IBV S protein,

where 20 sites were identified during structural studies by cryo-EM in M41 (Shang et al., 2018), and by mass spectrometry methods in a Vero-adapted strain of Beaudette where 8 sites were confirmed as being glycosylated (Zheng et al., 2018). The former study identified glycosylation sites on recombinant S protein expressed in insect cells, whereas Zheng and colleagues studied the S protein in viruses propagated in cell culture. There were some differences in the sites identified in each study, which can probably be attributed to the methods of protein production used in each experiment. All of the sites identified by Shang and colleagues were present in the server predictions performed using NetNGlyc 1.0, but only 9 matched those identified as true glycosylation sites in the MS experiments described in Chapter 3. As the methods of protein expression and purification differed quite a lot, it is likely that each protein presented a different glycosylation profile. Tandem MS methods were used by Zheng *et al.* to identify 8 sites on the Beaudette S protein, 6 of which were also identified in Chapter 3. More sites were identified by the methods in Chapter 3, possibly because EThcD was used as well as LC-MS/MS. However the studies involved different strains and so cannot be directly compared. The study described here possibly presents more advantages and relevance to IBV research, as the protein was derived from whole, pathogenic virus rather than produced in an insect-based cellular expression system (Shang *et al.*) or derived from a non-pathogenic Vero-adapted strain (Zheng *et al.*). Despite the differences in each study, all highlight the high number of glycosylation sites on these viral proteins and provide a good basis for further, more detailed investigation into these sites.5

N-linked glycans exist in different forms as a result of the processing pathways and cellular enzymes employed to modify proteins both during and post-translation. Different classes of glycan were identified on the S proteins of two strains of IBV, M41 and Beau-R, demonstrated by western blot following treatment with mannosidase inhibitors and deglycosylating enzymes. Some interesting results arose from these analyses, with different possible explanations for the changes observed. The loss of S2 recognition by the monoclonal

antibody in Beau-R highlights the importance of proper protein folding and the role that glycosylation plays within these processes but the other effects of the enzymatic deglycosylation treatments raised some more complicated questions about the mechanisms of each treatment. One possibility is that the deglycosylation of the protein further exposed cleavage sites and so rates of S1-S2 cleavage were increased, thus eliminating the uncleaved portion of S in the sample. Another explanation for the dramatic size change in these experiments is that glycosylation in the protein accounts for over half of the protein's apparent molecular weight when analysed by western blot. Further investigation would be required to thoroughly assess the levels of each subunit in these samples. This could be achieved through use of another antibody against the S1 subunit. Given the lack of compatible reagents for this type of experiment however, this is somewhat difficult to achieve at present. As mentioned, future experiments should also include more robust controls to account for the changes observed with each treatment.

The findings using Kif highlighted a role for complex glycans in the binding of monoclonal antibodies to their target epitopes, but only in Beau-R. Complex glycans were shown not to affect virus neutralisation by a monoclonal S1 antibody in either M41 or Beau-R. They were also shown to be dispensable for replication in CK cells. The loss of antibody recognition was confirmed by both western blot and IF, indicating that complex glycosylation is involved in monoclonal antibody recognition of both linear epitopes and conformational protein.

The importance of N-linked glycans in IBV was noted following attempts to rescue a virus with multiple mutations in predicted glycosylation sites. After numerous attempts it was concluded that this combination of mutations was incompatible with virus rescue. Given the essential role of glycosylation in protein synthesis and folding pathways it could be assumed that the mutant protein could not be folded correctly or incorporated into the virion. With the information now available from the mass spectrometry data, as well as the published

results showing the impact of individual glycosylation mutants in IBV replication (Zheng et al., 2018), future directions for this study will include the generation of recombinant viruses with fewer mutations, in an attempt to investigate the role of specific glycosylation sites in viral replication and pathogenicity.

7.2 Elucidating the role of the S protein in IBV pathogenicity

The second and third objectives of the project included generation of two recombinant IBVs with modified S proteins, in order to study how the S protein influences pathogenicity. Previous work with IBV and other coronaviruses have found conflicting results concerning the role of the S protein in pathogenicity, where replacement of the S gene did not alter the pathogenicity of an attenuated strain of IBV, with the opposite effect observed in MHV (Phillips et al., 1999, Hodgson et al., 2004). The experiments described in Chapters 4 and 5 demonstrate that the S gene is, in fact, a pathogenicity factor for IBV. The attenuation of M41-K following the insertion of the Beaudette-derived ectodomain sequence shows that the presence of this protein is sufficient to alter IBV pathogenicity in a pathogenic strain. The robustness of the reverse genetics system used to generate these viruses was further validated by the generation and characterisation of M41K-4/91(S), where the insertion of a heterologous S gene sequence did not alter the pathogenicity of the virus during infection in chickens. In addition, both these viruses adopted the tropism of the S protein donor strain, again proving that the S protein determines IBV tropism *in vitro.* The fact that M41K-4/91(S) remained pathogenic even with the insertion of a heterologous sequence approximately 18% divergent shows gives insight into the way the S protein functions as a whole and how it interacts with other viral proteins. It is clear that the recombinant virus is still able to replicate efficiently with the inserted sequence, indicating that the interaction with other viral proteins remains largely unaffected. It is important to remember that the signal sequence, transmembrane domain and cytoplasmic tail of these recombinant S proteins were preserved and homologous to the backbone strain, M41-K. As these domains are likely the

key partners in interactions with other viral proteins, theoretically there should be no change following the insertion of the modified ectodomain. In SARS, for example, it was shown that trafficking signals in the S protein cytoplasmic tail heavily influenced the outcome of infection, even following only very few mutations in this region (Youn et al., 2005). This could be studied in IBV using the same methodology of introducing targeted mutations in these domains to assess how they affect viral replication, giving clearer insight into which domains within the protein are required for maintaining the interactions between the viral proteins.

Previous research has highlighted the importance of the secondary cleavage site in the extended host tropism of Beaudette *in vitro* (Bickerton et al., 2018) which could be translated to *in vivo* findings described here. As both the M41 and 4/91 S proteins lack this cleavage site, and are highly pathogenic, it stands to reason that M41K-BeauR(S) could be entering tissues by a different mechanism than the pathogenic viruses. This could lead to an altered immune response, meaning the virus may be cleared more quickly and hence inducing fewer clinical signs. This could provide an explanation for the attenuation observed with this recombinant virus, however, further experiments would be required to investigate this hypothesis.

While the recombinant virus was without doubt pathogenic, the patterns of clinical signs induced in the infected birds over the course of the experiment differed slightly from the two parent viruses M41-K and 4/91. This indicates that the presence of the heterologous S gene sequence had some effect on the mechanisms by which the virus caused disease. Perhaps the interaction with the other viral proteins such as M has been slightly affected by the presence of the alternative sequence. As mentioned, it would be of interest to further examine the interactions of recombinant S proteins with other viral proteins, perhaps using M41K-4/91(S) as a tool to examine the effects of heterologous sequences within the protein. Studies in other coronaviruses have noted reduced incorporation of S during virion assembly

with modified M proteins (Kuo et al., 2016). It would be interesting to assess if the same effect would be seen with these recombinant S proteins.

7.3 Defining the cellular requirements of IBV tropism

The final objective of the work involved assessing the influence of the cellular environment on IBV infection and replication. Investigations into the cellular requirements of IBV infection have revealed some interesting results concerning temperature sensitivity, following initial findings that Beau-R was unable to replicate at 41°C. As the S gene has been shown to directly influence tropism in IBV, through the presence of the additional cleavage site in S2 (Bickerton et al., 2018), recombinant viruses were used to assess if this was also the defining factor in temperature sensitivity. Through assessment of replication kinetics in CK cells, it was found that the S gene did not dictate this restriction. M41K-BeauR(S) exhibits only a slight sensitivity to temperature compared to M41, providing a possible explanation for the recombinant virus' ability to disseminate to the trachea of infected birds. This is in contrast to Beau-R which exhibits complete temperature sensitivity and is unable to disseminate from the sites of infection. In other recent studies, temperature sensitivity was linked to attenuation during characterisation of a strain of Urabe mumps virus, a paramyxovirus. The temperature sensitive mutant was found to replicate to much lower titres at the non-permissive temperature, while also exhibiting a lower neurovirulence. In this study, mutations were identified in the surface glycoprotein and in the polymerase gene, which were associated to the temperature sensitive phenotype. The temperature sensitive strain showed reduced levels of transcription and protein synthesis from ORFs towards the 3' end of the genome, possibly suggesting the polymerase was less able to remain associated with the genome at the higher temperature (Schinkel et al., 2017). As Beau-R replicates very well at 37°C it could be hypothesised that the replication enzymes encoded in its genome are not adapted to replication at higher temperatures, meaning that the genome cannot be replicated efficiently *in vivo*.

Initial research into host tropism at 41°C showed that the Beaudette S gene is required to enter Vero cells but other parts of the genome are responsible for allowing the virus to efficiently replicate in these cells, as demonstrated through infections with the recombinant virus M41K-BeauR(S), where the insertion of the Beau-R S ectodomain allowed the virus to enter Vero cells and the M41 genome allowed the virus to replicate at higher temperatures, unlike any of the other viruses included in these experiments. This emphasises the fact that tropism can be defined as a multifactorial process, in that more than a permissive S gene is required to allow IBV replication in a given cell line.

The results from the temperature sensitivity experiments present a multitude of directions for future investigation. Firstly, it would be prudent to assess if the restriction in replication at 41°C is unique to Beaudette. To this end, replication of a range of IBV strains should be assessed in these experiments, including available and suitable field strains. As the S gene has been ruled out as the direct cause for temperature sensitivity, other genes in the IBV genome could be responsible for the observed phenotype. In other coronaviruses, the replicase gene has been implicated in temperature sensitivity, or more specifically certain nsps encoded within it (Stobart et al., 2012). In other RNA viruses such as influenza A, temperature sensitivity has been linked to the polymerase gene, where directed mutations can alter virulence and result in attenuation (Da Costa et al., 2015). Previously, a recombinant IBV was generated including the Beaudette replicase gene and the structural and accessory genes of M41 to investigate the role of the replicase gene in pathogenicity (Armesto et al., 2009). This virus could be used for assessment of replication kinetics at 41°C to confirm whether this gene was the cause of the temperature sensitivity observed with certain IBV strains. As other studies have linked temperature sensitivity to the viral replication machinery, effects on the synthesis of nascent IBV RNA under different conditions could be investigated using techniques such as northern blot. This could be assessed for both wild-type and recombinant strains to ascertain whether the recombinant sequences influenced

RNA synthesis at higher temperatures, providing some insight into replication in different locations within the infected bird.

The protease environment in the cell also plays a part in viral entry and host tropism, thought to be as a result of alternative proteolytic processing of the S protein. Vero cell infections with M41 in the presence of trypsin showed that the virus could utilise trypsin to enter these usually non-permissive cells. The same effect was seen with the field strain QX, providing a possible platform for propagation in cell culture. The replication pattern observed in these infections could not be maintained over multiple passage, indicating that other factors have affected how these viruses replicate under the additional S protein processing by exogenous trypsin. It could be that the S protein of these viruses has been processed incorrectly; perhaps there is an additional cleavage site present in the S protein sequence and the progeny viruses produced in the presence of the additional proteases are less able to infect cells due to overactive cleavage. The cleavage patterns of these viruses affected by the addition of trypsin should be investigated to identify regions susceptible for this activation and provide further insight into this phenomenon.

7.4 Future work

Recombinant IBVs with mutated glycosylation sites will be generated

To begin assessment of the importance of individual glycosylation sites during *in vitro* replication, fewer mutations should be introduced into the S protein of M41-K. This could be achieved through sequential repair of the plasmid used to generate the original mutant virus by site-directed mutagenesis. Following *in vitro* characterisation, pathogenicity studies could be carried out in chickens along with assessing the induction of neutralising antibodies *in vivo*, to examine whether the glycosylation sites affected pathogenesis following mutation.

The involvement of complex glycans in virus neutralisation by polyclonal antibodies will be assessed

Virus neutralisation will be assessed by plaque reduction assay as described for experiments with the monoclonal antibody against S1 (A13). Different antibodies, including polyclonal sera, will be used to further assess how complex glycans influence binding and neutralisation.

M41K-BeauR(S) will be tested as a vaccine candidate

The recombinant virus M41K-BeauR(S) was shown to be non-pathogenic, while still able to disseminate through the bird to the trachea. The virus will be used in a future vaccine-challenge experiment in chickens to assess its potential for conferring protection against IBV challenge and its capabilities in inducing neutralising antibodies.

Continuation of rIBV M41K-4/91(S) dissemination assessments

To compare the potential for virus dissemination between M41-K, 4/91 and M41K-4/91(S), the remaining tissues from day 4 and 6 post-infection will be screened by RT-PCR for detection of IBV genome. This will also provide insight into any changes in *in vivo* tissue tropism that have occurred as a result of the insertion of the heterologous S gene into the M41 genome.

The mechanism of spike cleavage by trypsin will be assessed by western blot

More experimental data is required to draw conclusions concerning the mechanisms involved in trypsin-mediated extension of host tropism. To address this, western blot techniques will be used to analyse the cleavage products under these conditions to assess the pattern of cleavage in the presence of trypsin.

Temperature sensitivity: assessment of IBV adaptation to replication at 41°C

A range of rIBVs will be passaged at 41°C to investigate the potential of IBV to adapt to replication at higher temperatures. Viruses will be sequenced following select passage numbers to identify any mutations acquired. A range of temperatures will also be tested, as the upper sections of the respiratory tract are unlikely to reach 41°C.

7.5 Limitations

There are certain limitations associated with the work described here and also with the techniques involved in future directions. The use of cellular inhibitors to assess the role of complex glycans presents issues that must be considered. The inhibitors are not specific to viral proteins and their action will also apply to other viral and cellular proteins, including receptor molecules. This should be taken into account when drawing conclusions concerning the involvement of these glycans in viral entry. There is also no accurate way of verifying the action of the inhibitor, aside from confirming the loss of S2 recognition by 26.1, as there are currently no other anti-S antibodies readily available that are compatible with western blot.

The mass spectrometry techniques described here provide some useful insights into the glycosylation profile of the IBV M41-CK S protein. Ideally, these techniques would be used to analyse the S proteins in a range of IBV strains, but there are financial and ethical constraints associated with the sample preparation. For the results described in Chapter 3, volumes

upwards of 500ml of allantoic fluid was used to generate the purified virus. While the coverage of the protein was good it was incomplete, so a huge number of eggs would be required to produce the quantities of virus needed to gain sufficient coverage of the whole protein.

The results from the *in vivo* analysis of rIBV M41K-BeauR(S) described in Chapter 4 are quite robust but there is some variation in the clinical signs between individual birds. As only 3 birds were analysed on each day, a larger sample size may have provided more information and highlighted any outliers. A balance must be achieved between adequate sample sizes and reducing the number of animals used for experiments, in line with the principles of the 3Rs. This was employed in the subsequent M41K-4/91(S) pathogenicity study described in Chapter 5, where five birds were analysed at each time point. The results from this study are much more consistent, allowing more definite conclusions to be drawn.

As described in Chapter 6, the cell type used for assessment of tropism and temperature sensitivity should be considered carefully, as Vero cells are adapted to growth at 37°C. Beaudette strains can replicate in DF-1 cells, so using this avian cell type would provide a more biologically relevant alternative to mammalian Vero cells while still accommodating the extended tropism of Beaudette. These studies are also limited by the strain of IBV, as most of the available field strains do not replicate in cell culture, only in *ex vivo* systems. These systems, such as TOCs, are optimised to 37°C and as such would not be suitable for studying replication at higher temperatures without major adjustments.

A general limitation of studying IBV is the availability of cells and tissues in which non-laboratory adapted strains will replicate. As mentioned, investigations into field strains more relevant to the vaccine industry are limited by the feasibility of propagation in cell culture. While some strains do replicate in *ex vivo* systems, the cost and labour associated with these techniques is much higher than cell culture systems. The data described in Chapter 6 provide

a possible solution to this problem, allowing field strains to replicate in cell culture following the addition of exogenous protease.

7.6 Impact

Taken together, the results described in this thesis provide more insight into the importance of the coronavirus S protein during infection both *in vitro* and *in vivo*. The glycan presence on the surface of the IBV S protein is substantial and could provide a target for more effective vaccine design, much needed in the fight to control infectious bronchitis in commercial chicken flocks. Insertion of heterologous S genes into the IBV genome presents another method for rational vaccine design and using proteases as a potential platform for propagation in cell culture would dramatically improve the vaccine production process for this economically important disease.

8 Appendix

8.1 NetNGlyc Raw data

1. Beau-R

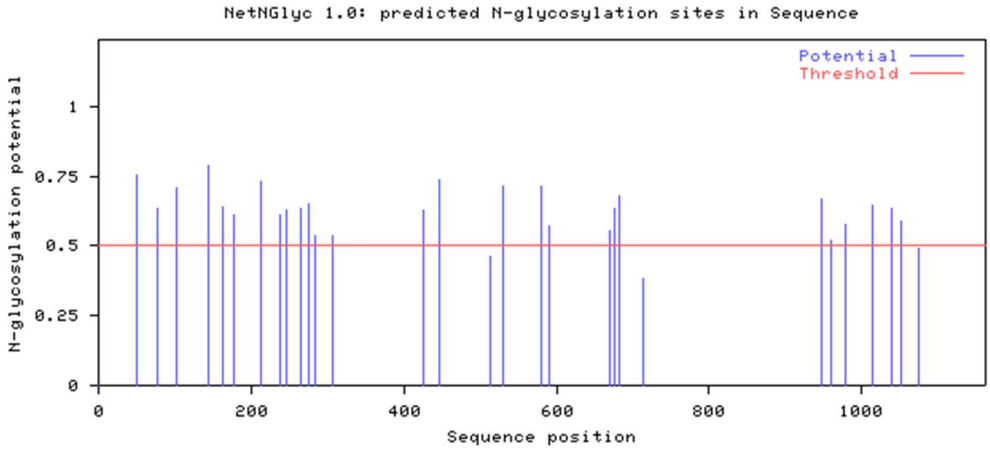

(Threshold=0.5)

SeqName	Position	Potential	Jury Agreement	N-Glyc result	
Sequence	51	NISS 0.7529	(9/9)	+++	
Sequence	77	NASS 0.6344	(7/9)	+	
Sequence	103	NFSD 0.7079	(8/9)	+	
Sequence	144	NLTV 0.7906	(9/9)	+++	
Sequence	163	NLTS 0.6421	(9/9)	++	
Sequence	178	NETI 0.6101	(6/9)	+	
Sequence	212	NGTA 0.7300	(9/9)	++	
Sequence	237	NFSD 0.6116	(8/9)	+	
Sequence	247	NSSL 0.6269	(8/9)	+	
Sequence	264	NTTC 0.6341	(8/9)	+	
Sequence	276	NETG 0.6528	(8/9)	+	
Sequence	283	NPSG 0.5364	(8/9)	+	WARNING: PRO-X1.
Sequence	306	NFSF 0.5353	(4/9)	+	
Sequence	425	NITL 0.6274	(8/9)	+	
Sequence	447	NVTD 0.7393	(9/9)	++	
Sequence	513	NETG 0.4644	(5/9)	-	
Sequence	530	NGTR 0.7149	(9/9)	++	
Sequence	579	NVTE 0.7121	(9/9)	++	
Sequence	591	NLTV 0.5724	(8/9)	+	
Sequence	669	NVST 0.5543	(5/9)	+	
Sequence	676	NISL 0.6353	(8/9)	+	
Sequence	683	NPSS 0.6803	(9/9)	++	WARNING: PRO-X1.
Sequence	714	NCTA 0.3846	(8/9)	-	
Sequence	947	NVTA 0.6688	(9/9)	++	
Sequence	960	NASQ 0.5179	(6/9)	+	
Sequence	979	NGSY 0.5788	(9/9)	++	
Sequence	1014	NKTV 0.6479	(8/9)	+	
Sequence	1038	NDTK 0.6340	(8/9)	+	
Sequence	1051	NYTV 0.5902	(7/9)	+	
Sequence	1074	NDSL 0.4929	(5/9)	-	

2. M41-CK:

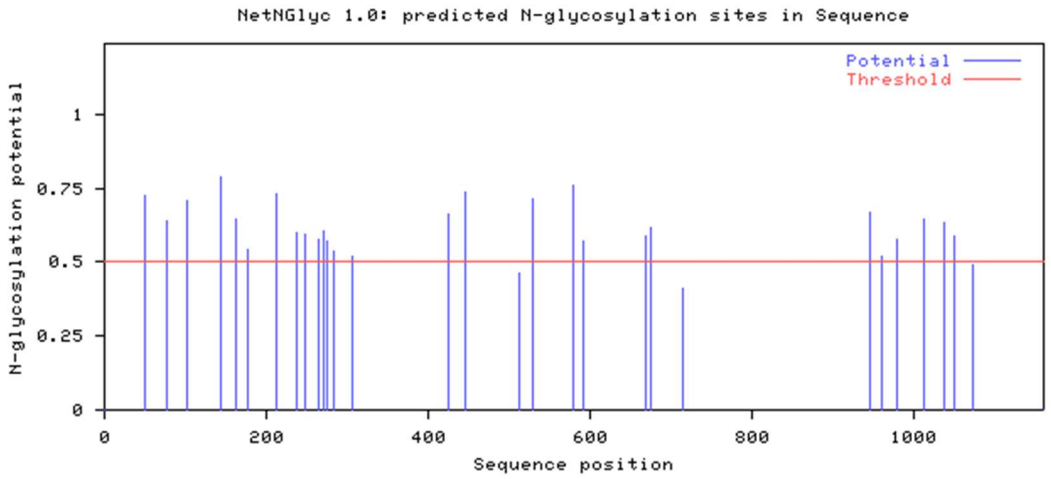

SeqName	Position	Potential	Jury Agreement	N-Glyc result	
Sequence	51 NISS	0.7274	(9/9)	++	
Sequence	77 NASS	0.6411	(7/9)	+	
Sequence	103 NFSD	0.7079	(8/9)	+	
Sequence	144 NLTV	0.7907	(9/9)	+++	
Sequence	163 NLTS	0.6463	(9/9)	++	
Sequence	178 NETT	0.5413	(4/9)	+	
Sequence	212 NGTA	0.7300	(9/9)	++	
Sequence	237 NFSD	0.6000	(7/9)	+	
Sequence	247 NSSL	0.5964	(8/9)	+	
Sequence	264 NTTF	0.5748	(7/9)	+	
Sequence	271 NFTF	0.6053	(8/9)	+	
Sequence	276 NETG	0.5708	(7/9)	+	
Sequence	283 NPSG	0.5361	(8/9)	+	WARNING: PRO-X1.
Sequence	306 NFSF	0.5200	(4/9)	+	
Sequence	425 NITL	0.6621	(9/9)	++	
Sequence	447 NVTD	0.7393	(9/9)	++	
Sequence	513 NETG	0.4646	(5/9)	-	
Sequence	530 NGTR	0.7149	(9/9)	++	
Sequence	579 NVTE	0.7628	(9/9)	+++	
Sequence	591 NLTV	0.5722	(8/9)	+	
Sequence	669 NVST	0.5898	(8/9)	+	
Sequence	676 NISL	0.6146	(8/9)	+	
Sequence	714 NCTA	0.4120	(8/9)	-	
Sequence	947 NVTA	0.6688	(9/9)	++	
Sequence	960 NASQ	0.5179	(6/9)	+	
Sequence	979 NGSY	0.5786	(9/9)	++	
Sequence	1014 NKTV	0.6477	(8/9)	+	
Sequence	1038 NDTK	0.6340	(8/9)	+	
Sequence	1051 NYTV	0.5903	(7/9)	+	
Sequence	1074 NDSL	0.4928	(5/9)	-	

3. QX-1148A:

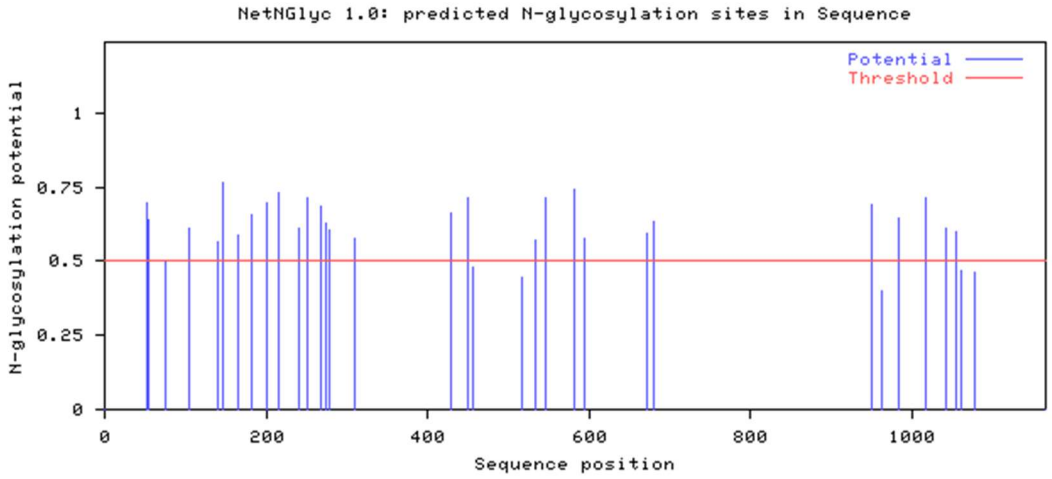

SeqName	Position	Potential	Jury Agreement	N-Glyc result
Sequence	52	NSTN 0.6977	(9/9)	++
Sequence	55	NYTN 0.6417	(9/9)	++
Sequence	76	NQSV 0.5007	(5/9)	+
Sequence	104	NFSE 0.6117	(7/9)	+
Sequence	141	NGSL 0.5683	(7/9)	+
Sequence	147	NLTV 0.7656	(9/9)	+++
Sequence	166	NFTS 0.5869	(7/9)	+
Sequence	181	NKTT 0.6548	(7/9)	+
Sequence	200	NYSI 0.6987	(9/9)	++
Sequence	215	NGTA 0.7301	(9/9)	++
Sequence	240	NFSD 0.6109	(8/9)	+
Sequence	250	NSTL 0.7169	(8/9)	+
Sequence	267	NTTL 0.6844	(9/9)	++
Sequence	274	NFTF 0.6311	(9/9)	++
Sequence	279	NVSN 0.6077	(8/9)	+
Sequence	309	NLSF 0.5778	(9/9)	++
Sequence	428	NITL 0.6603	(8/9)	+
Sequence	450	NVTD 0.7147	(9/9)	++
Sequence	457	NFSY 0.4801	(3/9)	-
Sequence	516	NETG 0.4480	(6/9)	-
Sequence	533	NSSH 0.5707	(5/9)	+
Sequence	545	NVTS 0.7170	(9/9)	++
Sequence	582	NITE 0.7402	(9/9)	++
Sequence	594	NLTV 0.5747	(8/9)	+
Sequence	672	NVST 0.5952	(5/9)	+
Sequence	679	NISL 0.6357	(8/9)	+
Sequence	950	NVTA 0.6911	(9/9)	++
Sequence	963	NASQ 0.3972	(7/9)	-
Sequence	982	NGTY 0.6466	(9/9)	++
Sequence	1017	NKTV 0.7158	(9/9)	++
Sequence	1041	NDTK 0.6106	(8/9)	+
Sequence	1054	NYTV 0.5982	(6/9)	+
Sequence	1061	NISG 0.4664	(6/9)	-
Sequence	1077	NDSL 0.4601	(7/9)	-

4. 4/91

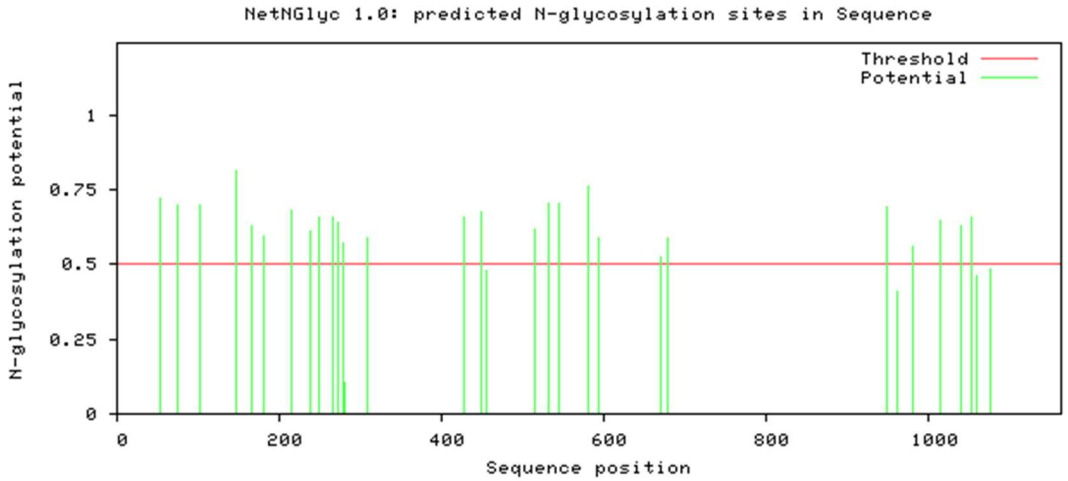

SeqName	Position	Potential	Jury Agreement	N-Glyc result
Sequence	54 NGTN	0.7207	(9/9)	++
Sequence	75 NISA	0.6990	(9/9)	++
Sequence	103 NFSD	0.6990	(8/9)	+
Sequence	146 NLTV	0.8152	(9/9)	+++
Sequence	165 NSTS	0.6301	(9/9)	++
Sequence	180 NETT	0.5936	(4/9)	+
Sequence	214 NGTA	0.6777	(9/9)	++
Sequence	239 NFSD	0.6113	(8/9)	+
Sequence	249 NSSL	0.6587	(8/9)	+
Sequence	266 NTTL	0.6573	(9/9)	++
Sequence	273 NFTF	0.6424	(9/9)	++
Sequence	278 NVSN	0.5724	(8/9)	+
Sequence	281 NASP	0.1020	(9/9)	---
Sequence	308 NLSF	0.5904	(9/9)	++
Sequence	427 NITL	0.6596	(8/9)	+
Sequence	449 NVTE	0.6762	(9/9)	++
Sequence	456 NYSY	0.4773	(5/9)	-
Sequence	515 NETD	0.6186	(6/9)	+
Sequence	532 NGTR	0.7059	(9/9)	++
Sequence	544 NVTN	0.7063	(9/9)	++
Sequence	581 NVTE	0.7607	(9/9)	+++
Sequence	593 NLTV	0.5864	(8/9)	+
Sequence	671 NVST	0.5260	(5/9)	+
Sequence	678 NISL	0.5891	(7/9)	+
Sequence	949 NVTA	0.6914	(9/9)	++
Sequence	962 NASQ	0.4101	(6/9)	-
Sequence	981 NGSY	0.5616	(8/9)	+
Sequence	1016 NKTV	0.6482	(8/9)	+
Sequence	1040 NDTK	0.6311	(8/9)	+
Sequence	1053 NYTV	0.6564	(9/9)	++
Sequence	1060 NISN	0.4617	(6/9)	-
Sequence	1076 NDSL	0.4871	(6/9)	-

Figure A1: Raw data produced from NetNGlyc server PNGS predictions. Thresholds and algorithm predictions are displayed for Beau-R, M41-CK, QX-1148A and 4/91.

8.2 Cell viability assays (CellTiter-Glo)

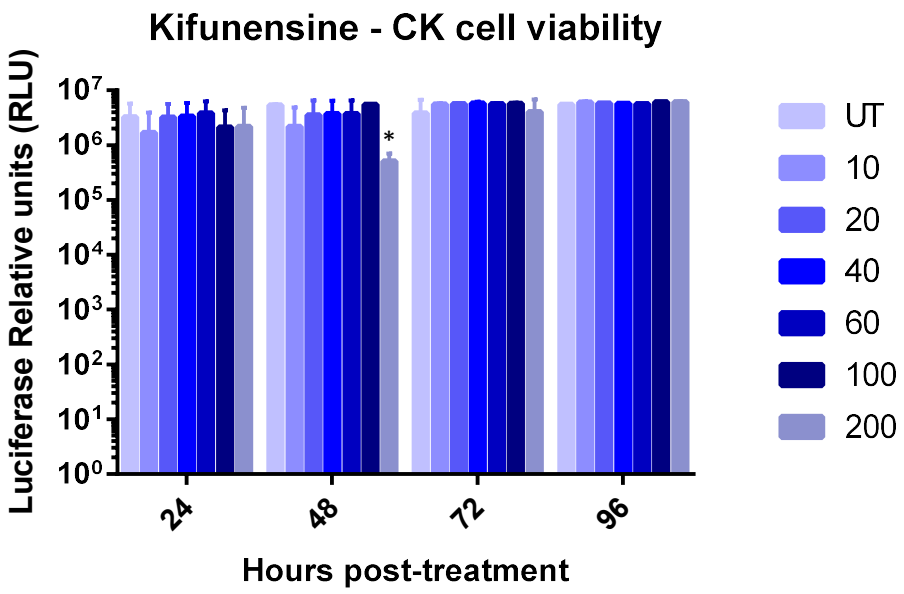

Figure A2: Kifunensine does not affect CK cell viability over 96 hours at most concentrations. Cells seeded in were treated with Kifunensine at varying concentrations (μM) and incubated at 37°C. Cell viability was measured according to the Promega CellTiter-Glo Assay protocol. Data were analysed by One-Way ANOVA followed by Tukey's multiple comparison test (* indicates $p < 0.05$).

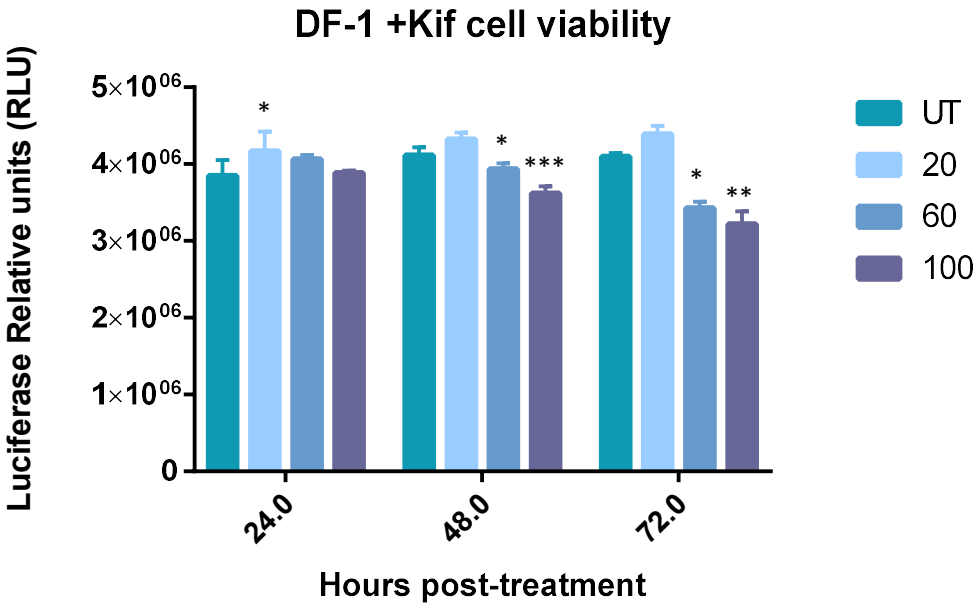

Figure A3: DF-1 cell viability is not affected following 20µM Kif treatment. Cells were seeded in 96 well plates and treated with Kif at varying concentrations (µM). Cell viability was measured using Promega CellTiter-Glo reagents. Data were analysed by One-Way ANOVA followed by Tukey's multiple comparison test (* indicates $p = 0.02$, ** indicates $p = 0.005$, *** indicates $p = 0.004$). At 24h, Cell viability was increased following treatment with 20µM Kif.

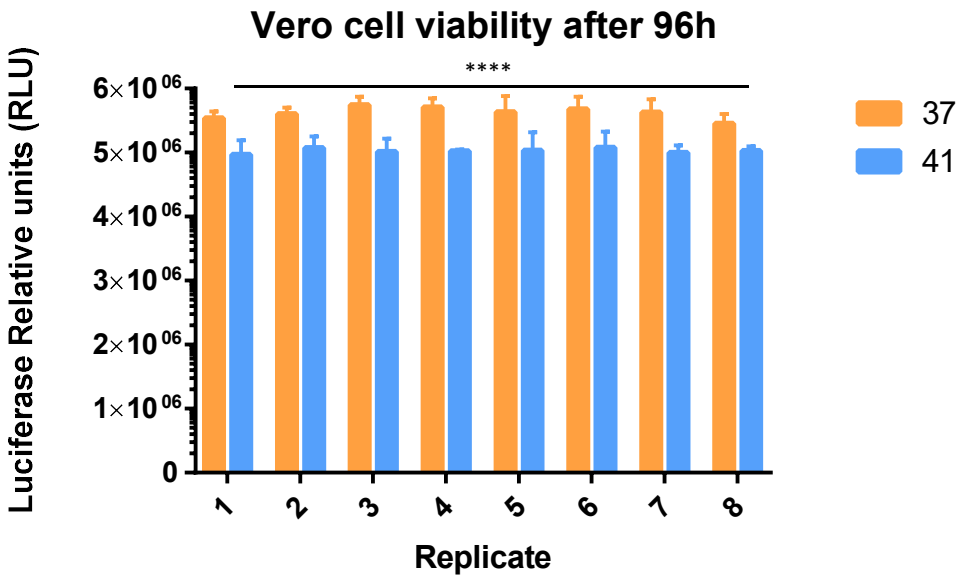

Figure A4: Vero cell viability at 41°C after 96 hours incubation. Cells were seeded in a 96 well plate and incubated at 37°C or 41°C for 96 hours. Viability was assessed using Promega CellTiter-Glo reagents according to the manufacturer's instructions. Data were analysed by unpaired t-test (**** indicates $p = 0.0002$ for all replicates).

8.3 Mass Spectra

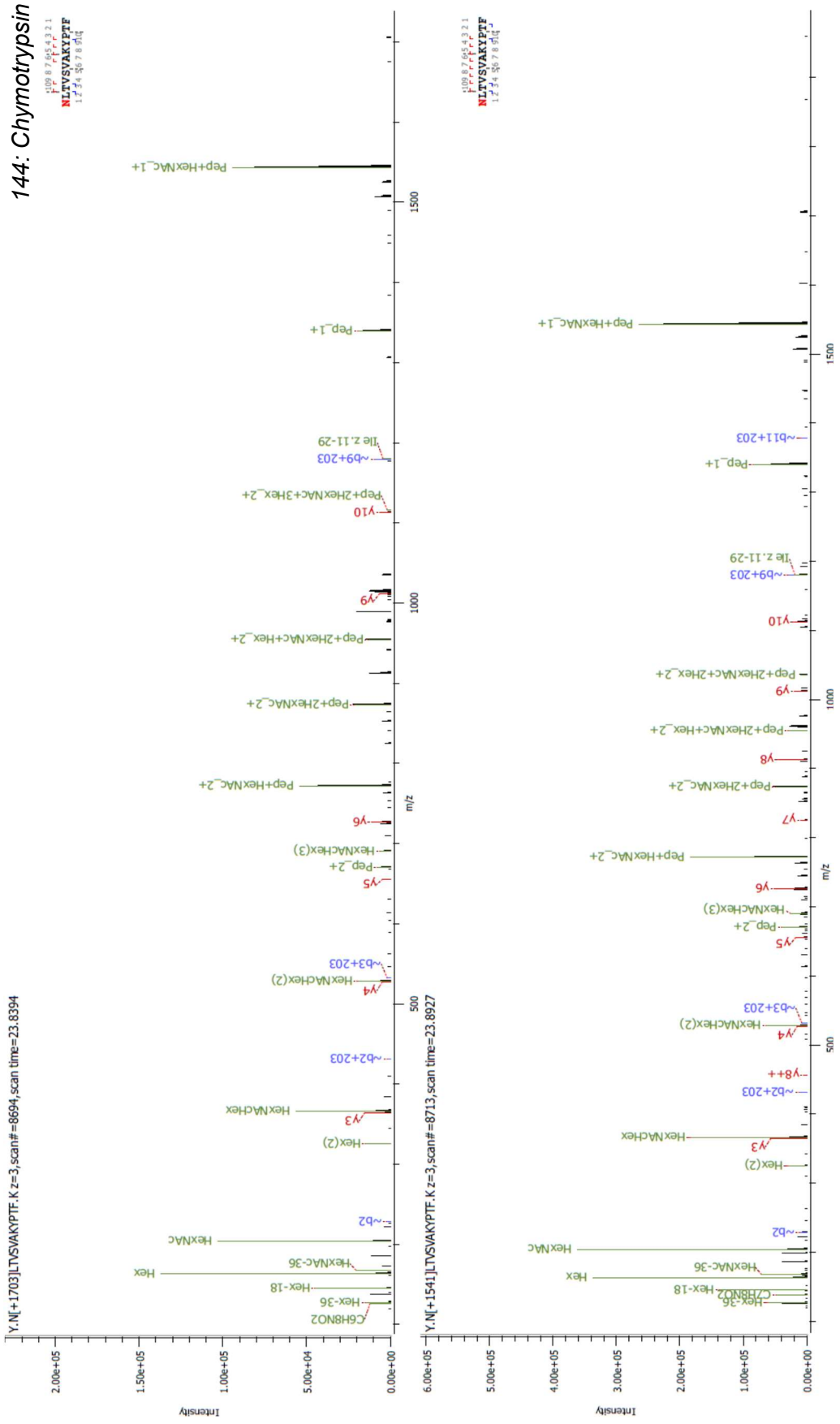

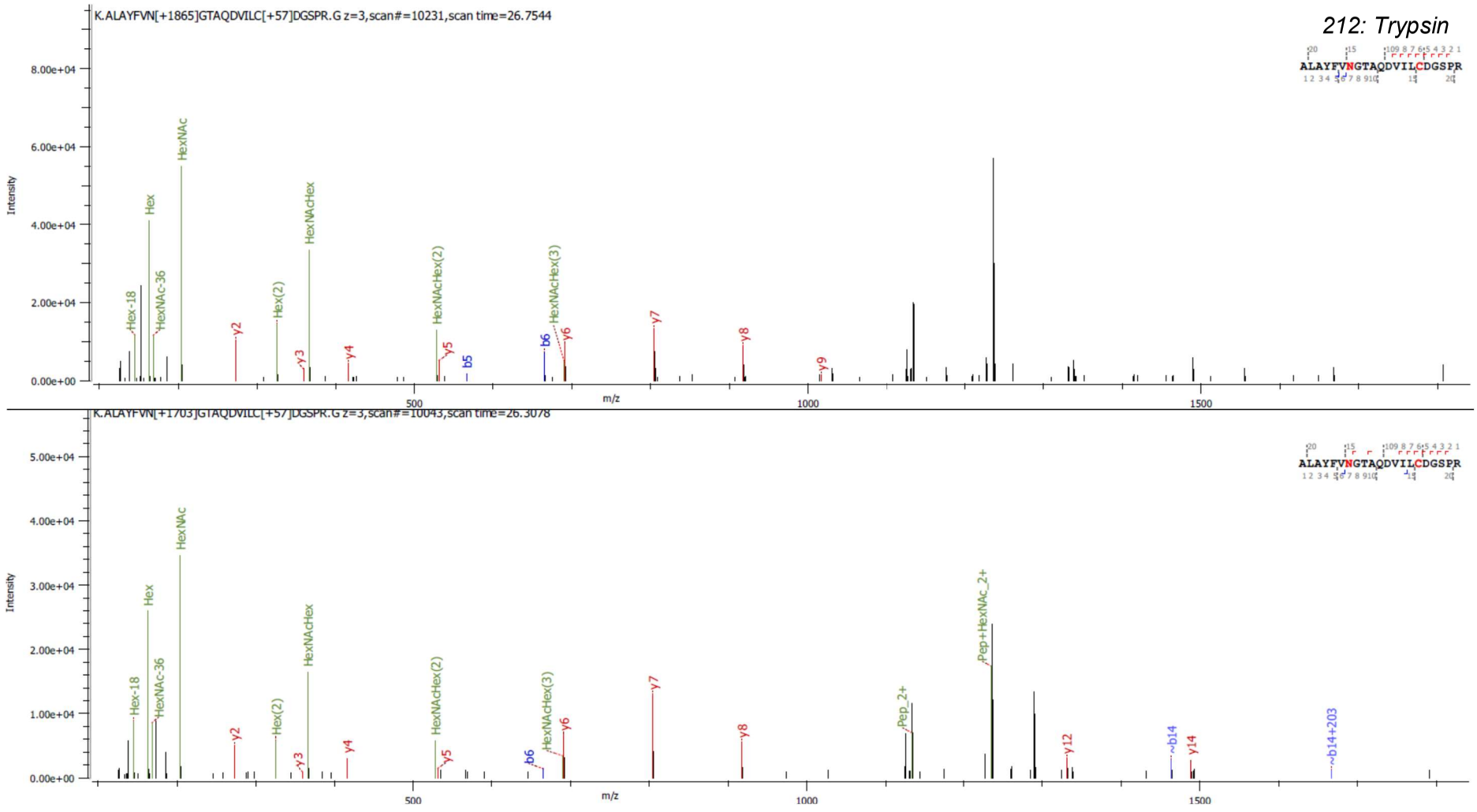
212: Trypsin
K.ALAYFVN[+1865]GTAQDVILC[+57]DGSPR.G z=3,scan#=10231,scan time=26.7544
ALAYFVNGTAQDVILCDGSPR
Intensity
m/z
Hex-18
HexNAc-36
Hex
HexNAc
y2
Hex(2)
y3
HexNAcHex
y4
HexNAcHex(2)
y5
b5
b6
HexNAcHex(3)
y6
y7
y8
y9
K.ALAYFVN[+1703]GTAQDVILC[+57]DGSPR.G z=3,scan#=10043,scan time=26.3078
Pep+HexNAc_2+
Pep_2+
y12
~b14
y14
~b14+203

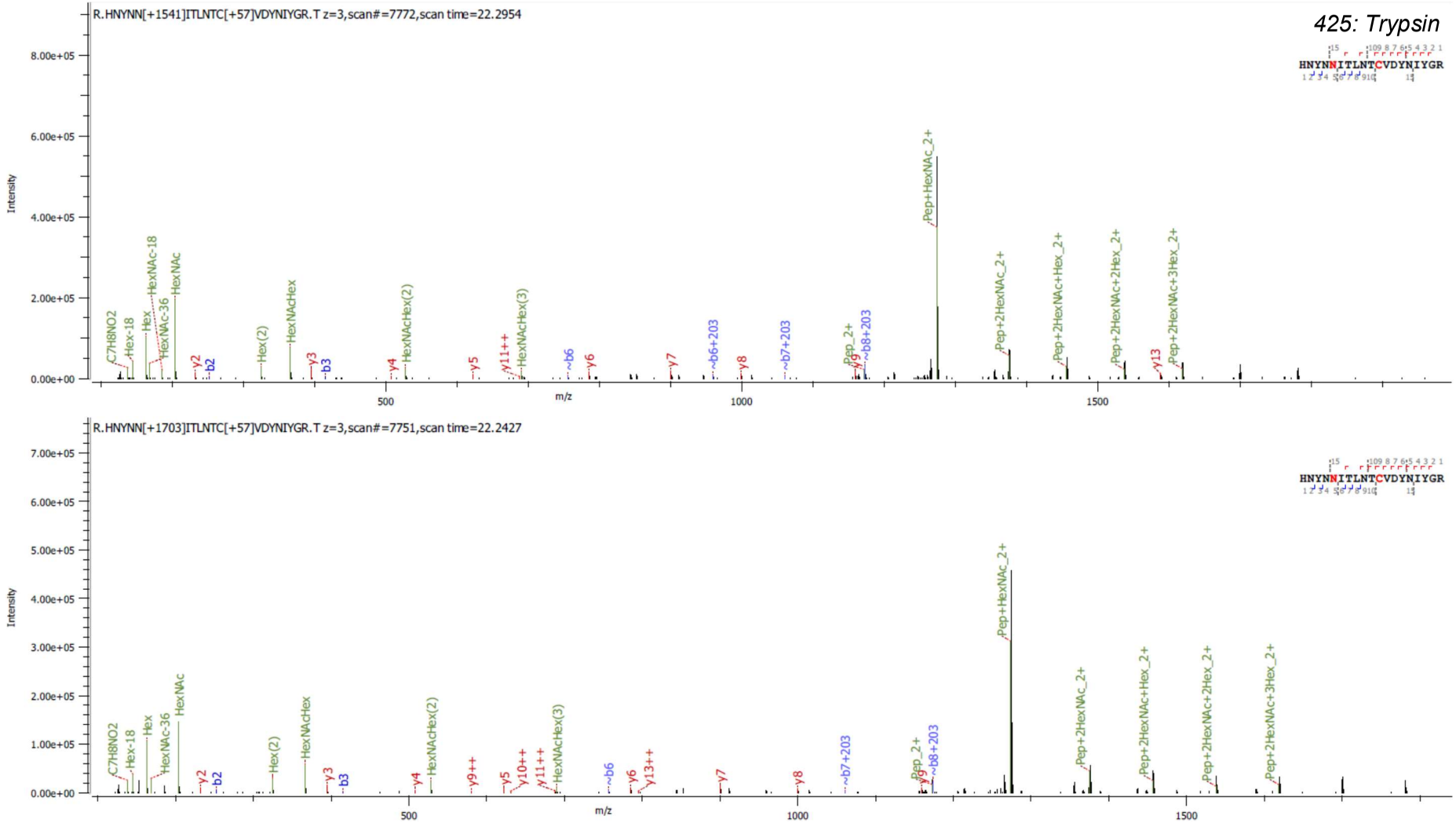
425: Trypsin
R.HNYNN[+1541]ITLNTC[+57]VDYNIYGR.T z=3,scan#=7772,scan time=22.2954
HNYNNITLNTCVDYNIYGR
Intensity
m/z
C7H8NO2
Hex-18
Hex
HexNAc-18
HexNAc-36
HexNAc
Hex(2)
HexNAcHex
HexNAcHex(2)
HexNAcHex(3)
Pep+HexNAc_2+
Pep+2HexNAc_2+
Pep+2HexNAc+Hex_2+
Pep+2HexNAc+2Hex_2+
Pep+2HexNAc+3Hex_2+
R.HNYNN[+1703]ITLNTC[+57]VDYNIYGR.T z=3,scan#=7751,scan time=22.2427
HNYNNITLNTCVDYNIYGR
Intensity
m/z
C7H8NO2
Hex-18
Hex
HexNAc-36
HexNAc
Hex(2)
HexNAcHex
HexNAcHex(2)
HexNAcHex(3)
Pep+HexNAc_2+
Pep+2HexNAc_2+
Pep+2HexNAc+Hex_2+
Pep+2HexNAc+2Hex_2+
Pep+2HexNAc+3Hex_2+

513: Trypsin

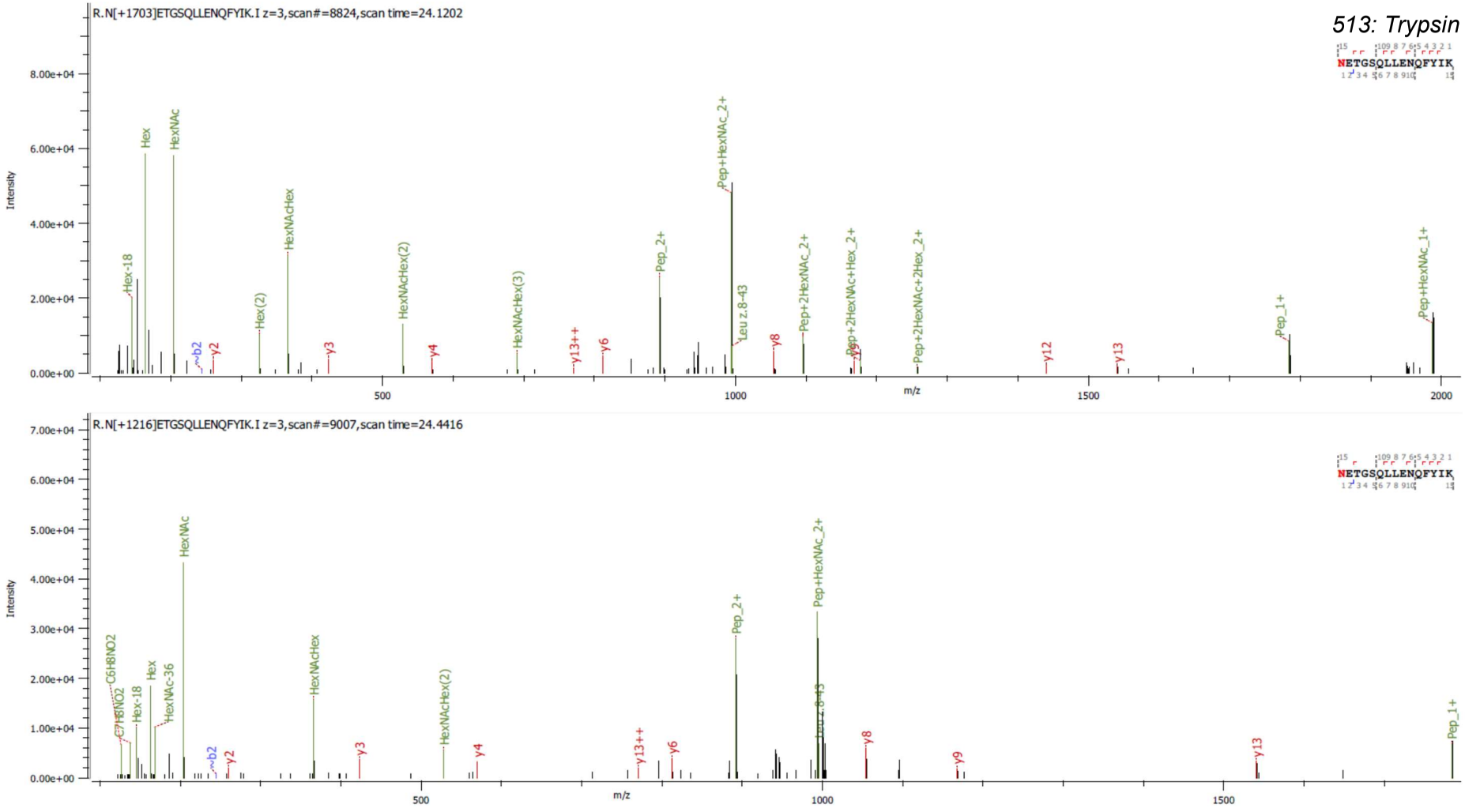
R.N[+1703]ETGSQLLENQFYIK.I z=3,scan#=8824,scan time=24.1202
NETGSQLLENQFYIK
Intensity
m/z
Hex-18
Hex
HexNAc
b2
y2
Hex(2)
HexNAcHex
y3
HexNAcHex(2)
y4
HexNAcHex(3)
y13++
y6
Pep_2+
Pep+HexNAc_2+
Leu z.8-43
y8
Pep+2HexNAc_2+
Pep+2HexNAc+Hex_2+
Pep+2HexNAc+2Hex_2+
y12
y13
Pep_1+
Pep+HexNAc_1+
R.N[+1216]ETGSQLLENQFYIK.I z=3,scan#=9007,scan time=24.4416
NETGSQLLENQFYIK
Intensity
m/z
C6H8NO2
C7H8NO2
Hex-18
Hex
HexNAc-36
HexNAc
b2
y2
HexNAcHex
y3
HexNAcHex(2)
y4
y13++
y6
Pep_2+
Pep+HexNAc_2+
Leu z.8-43
y8
y9
y13
Pep_1+

513: Trypsin

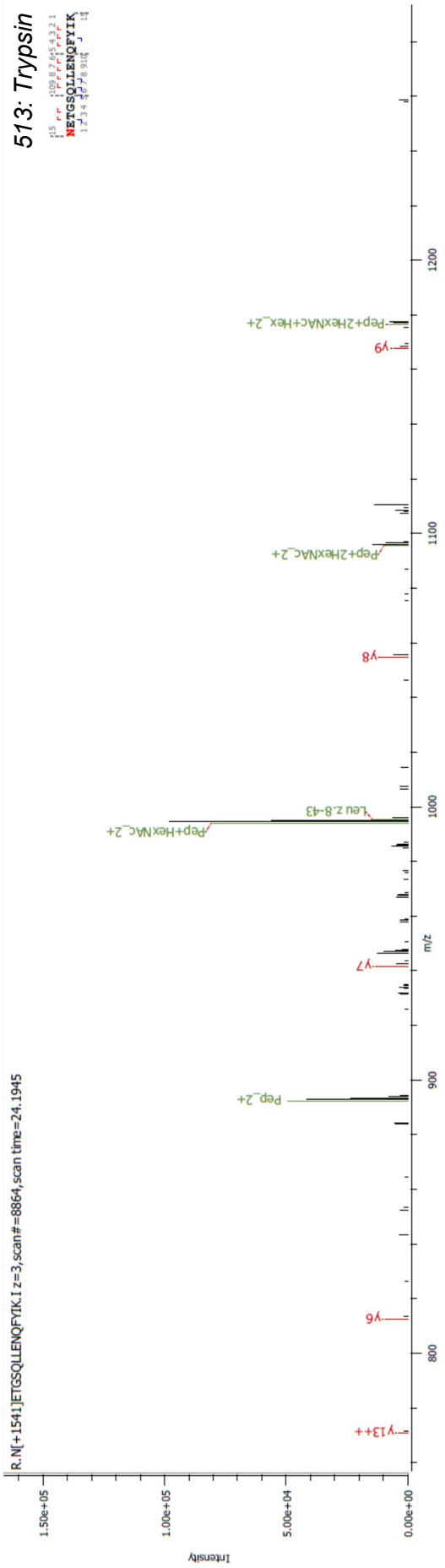
R.N[+1541]ETGSQLLENQFYIK.I z=3,scan#=8864,scan time=24.1945
NETGSQLLENQFYIK
Intensity
m/z
Pep_2+
Pep+HexNAc_2+
Leu z.8-43
Pep+2HexNAc_2+
Pep+2HexNAc+Hex_2+
y13++
y6
y7
y8
y9

947:
Chymotrypsin

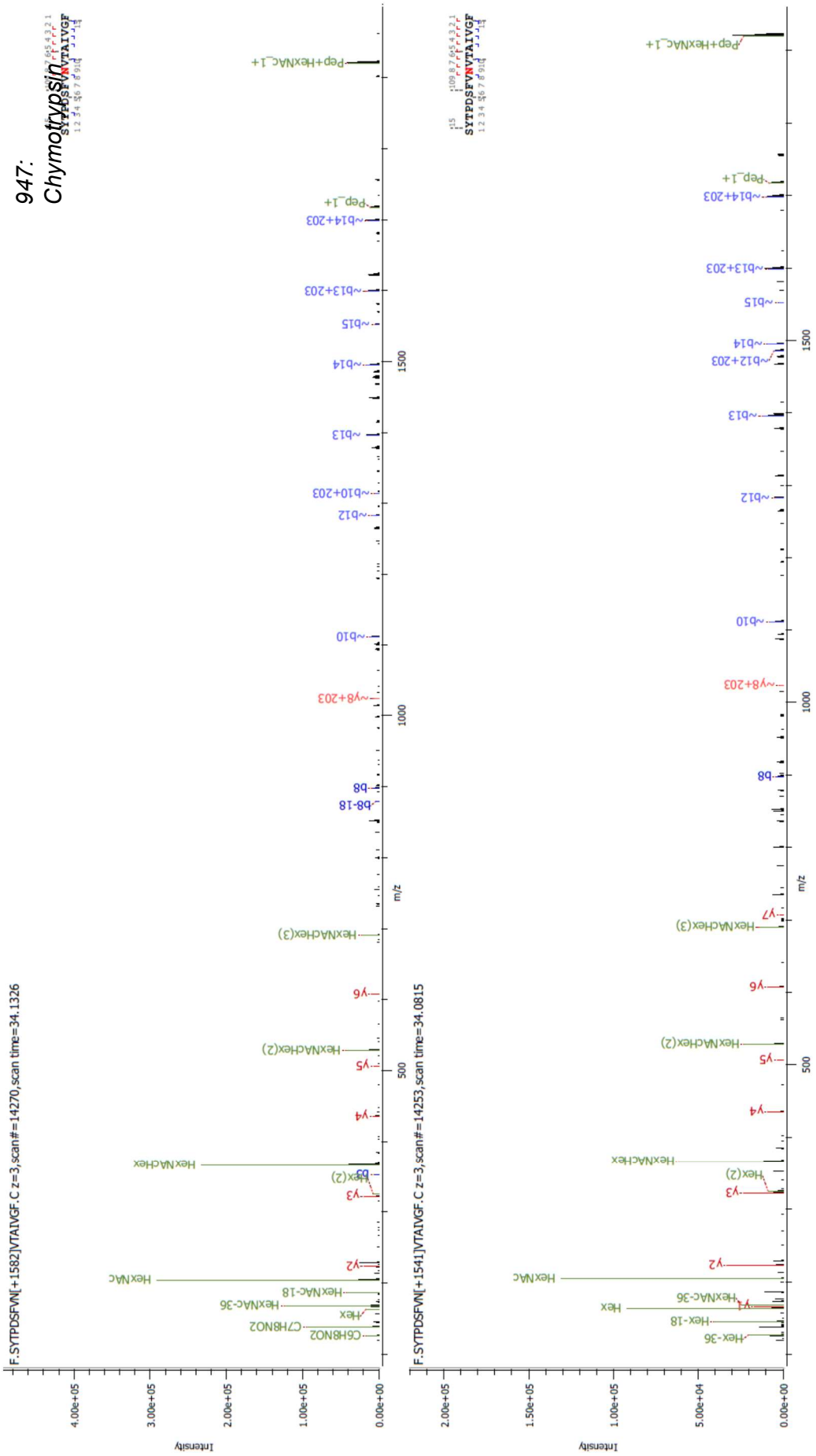

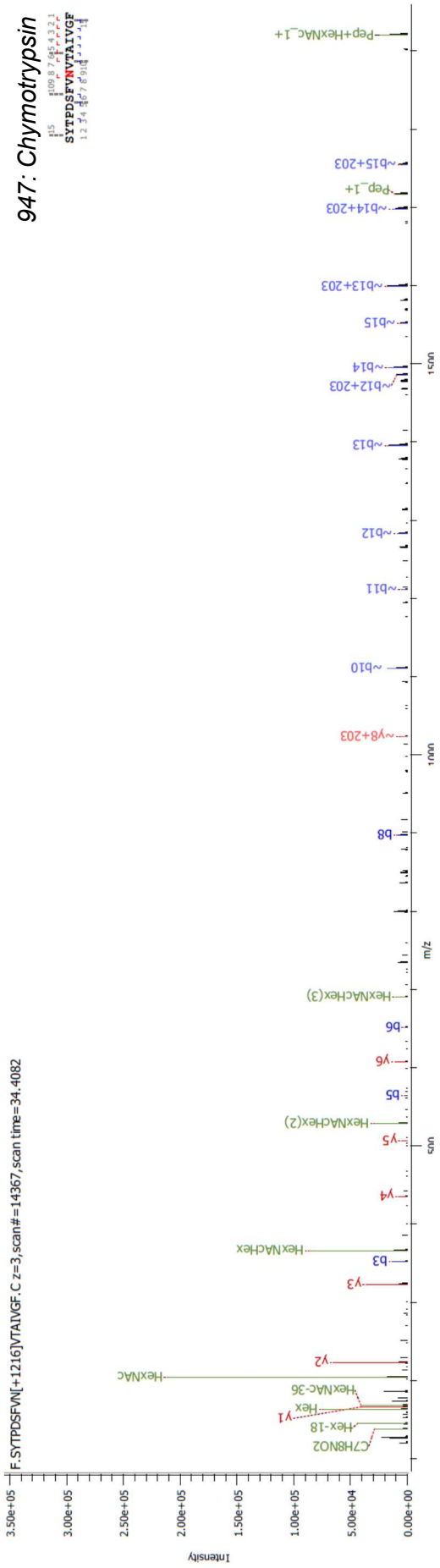
947: Chymotrypsin
SYTPDSFVNVTAIVGF
F.SYTPDSFVN[+1216]VTAIVGF.C z=3,scan#=14367,scan time=34.4082
Intensity
m/z
C7H8NO2
Hex-18
Hex
HexNAc-36
HexNAc
y1
y2
y3
b3
HexNAcHex
y4
y5
HexNAcHex(2)
b5
y6
b6
HexNAcHex(3)
b8
~y8+203
~b10
~b11
~b12
~b13
~b12+203
~b14
~b15
~b13+203
~b14+203
Pep_1+
~b15+203
Pep+HexNAc_1+

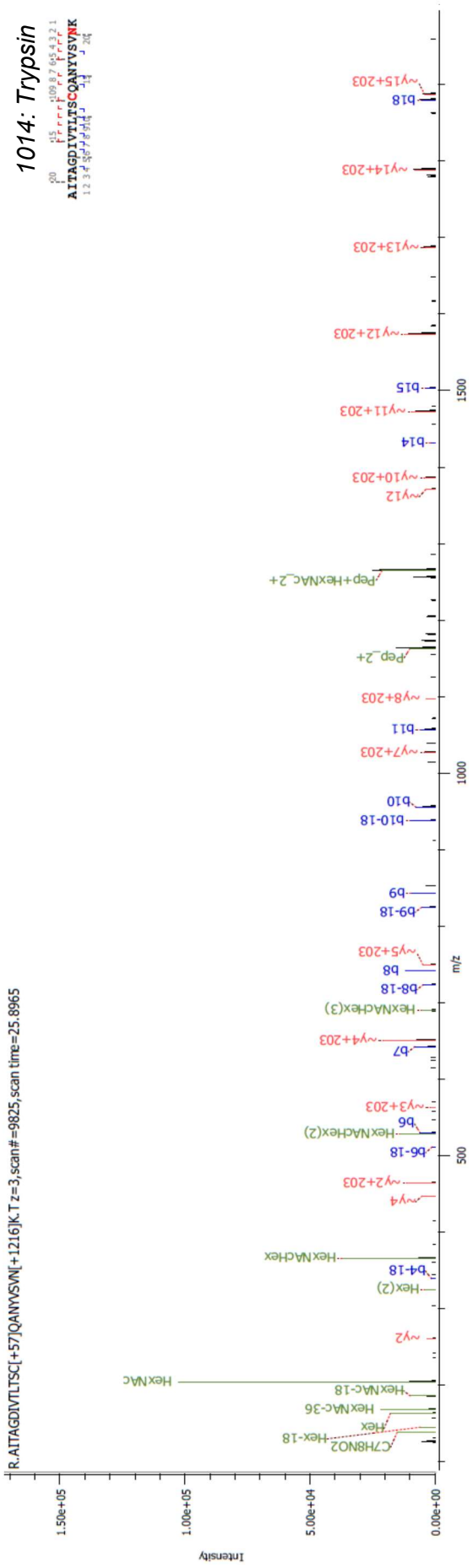
1014: Trypsin
AITAGDIVTLTSCQANYVSVNK
R.AITAGDIVTLTSC[+57]QANYVSVN[+1216]K.T z=3,scan#=9825,scan time=25.8965
Intensity
m/z
1.50e+05
1.00e+05
5.00e+04
0.00e+00
500
1000
1500
C7H8NO2
Hex-18
Hex
HexNAc-36
HexNAc-18
HexNAc
y2
Hex(2)
b4-18
HexNAcHex
y4
y2+203
b6-18
HexNAcHex(2)
b6
y3+203
b7
y4+203
HexNAcHex(3)
b8-18
b8
y5+203
b9-18
b9
b10-18
b10
y7+203
b11
y8+203
Pep_2+
Pep+HexNAc_2+
y12
y10+203
b14
y11+203
b15
y12+203
y13+203
y14+203
b18
y15+203

Figure A5: Mass spectra of glycan structures observed at amino acid positions 144, 212, 425, 513, 947 and 1014 in the IBV M41-CK S protein. Purified M41-CK samples were digested in chymotrypsin or trypsin and peptides were analysed using LC Nano MS/MS and EThcD mass spectrometers. Amino acid positions and digest conditions are indicated.

8.4 IBV S protein sequence alignment

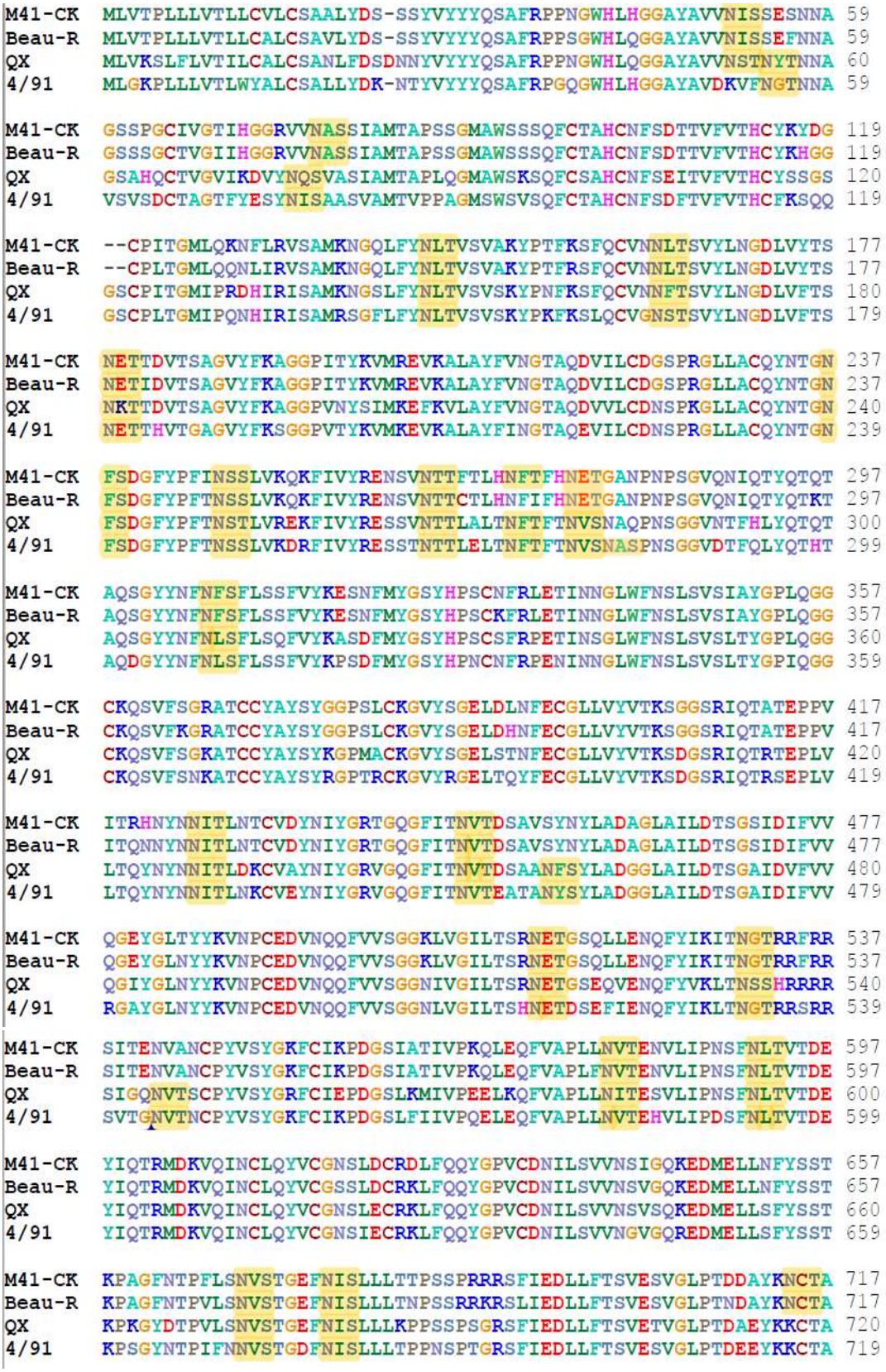

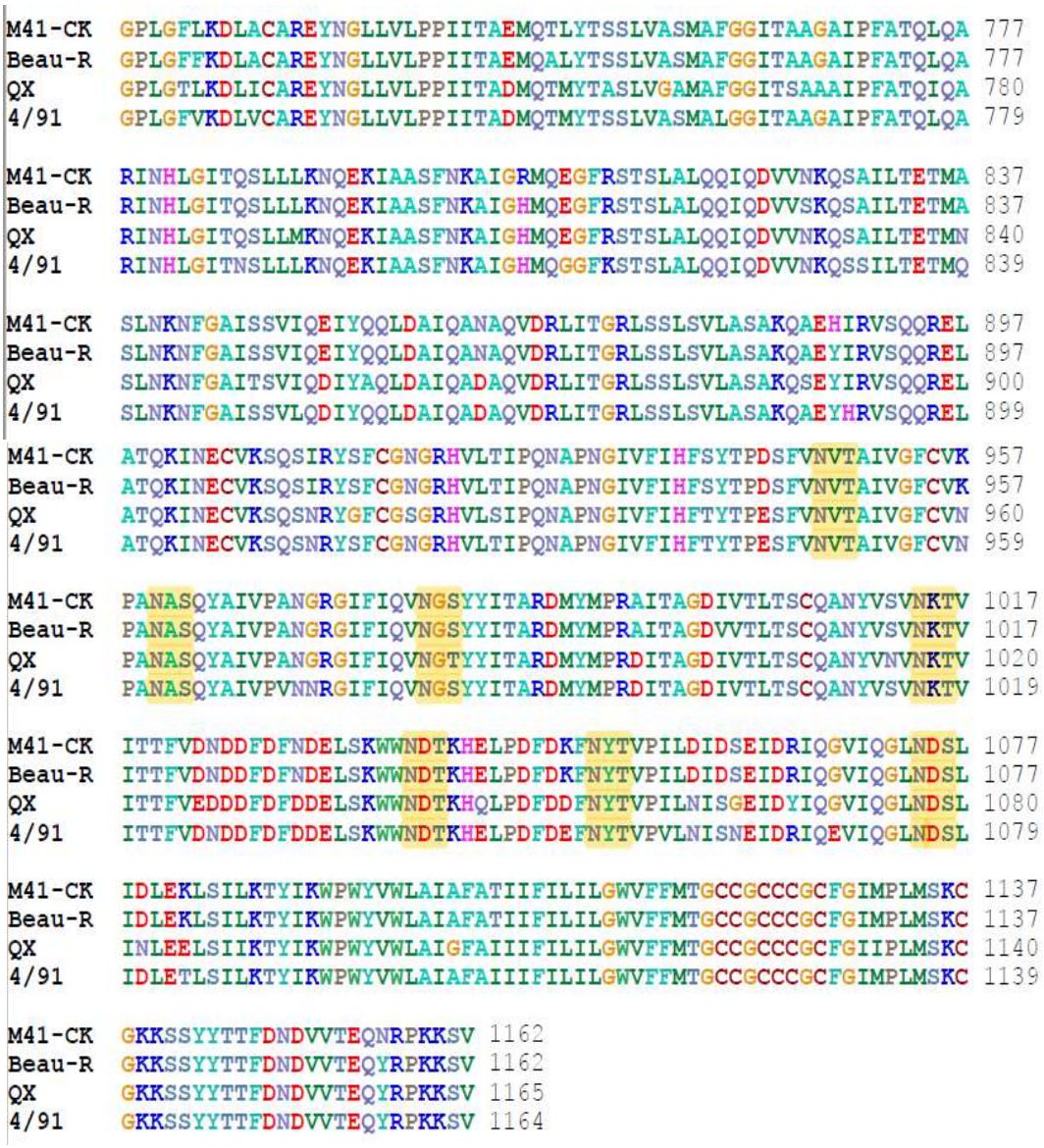

Figure A6: Amino acid alignment of M41-CK, Beau-R, QX and 4/91 S protein sequences. Sequences were generated by RT-PCR using strain-specific primers covering the S gene followed by Sanger sequencing. Sequencing reads were processed and aligned using BioEdit. Numbers indicate amino acid positions from the S gene start codon and are specific to each strain. Potential N-linked glycosylation sites (PNGS) are highlighted in yellow at the appropriate Asn (N) residue, as identified by the online server NetNGlyc 1.0.

Bibliography

ABRO, S. H., ULLMAN, K., BELÁK, S. & BAULE, C. 2012. Bioinformatics and evolutionary insight on the spike glycoprotein gene of QX-like and Massachusetts strains of infectious bronchitis virus. *Virology Journal,* 9.

AEBI, M. 2013. N-linked protein glycosylation in the ER. *Biochima Biophysica Acta,* 1833**,** 2430-7.

AEBI, M., BERNASCONI, R., CLERC, S. & MOLINARI, M. 2010. N-glycan structures: recognition and processing in the ER. *Trends in Biochemical Sciences,* 35**,** 74-82.

ALVARADO-FACUNDO, E., GAO, Y., RIBAS-APARICIO, R. M., JIMENEZ-ALBERTO, A., WEISS, C. D. & WANG, W. 2015. Influenza virus M2 protein ion channel activity helps to maintain pandemic 2009 H1N1 virus hemagglutinin fusion competence during transport to the cell surface. *Journal of Virology,* 89**,** 1975-85.

ARIYOSHI, R., KAWAI, T., HONDA, T. & TOKIYOSHI, S. 2010. Classification of IBV S1 Genotypes by Direct Reverse Transcriptase-Polymerase Chain Reaction (RT-PCR) and Relationship between Serotypes and Genotypes of Strains Isolated between 1998 and 2008 in Japan. *Journal of Veterinary Medical Science,* 72**,** 687–692.

ARMESTO, M., CAVANAGH, D. & BRITTON, P. 2009. The replicase gene of avian coronavirus infectious bronchitis virus is a determinant of pathogenicity. *PLoS One,* 4**,** e7384.

ARMESTO, M., EVANS, S., CAVANAGH, D., ABU-MEDIAN, A. B., KEEP, S. & BRITTON, P. 2011. A recombinant avian infectious bronchitis virus expressing a heterologous spike gene belonging to the 4/91 serotype. *PLoS One,* 6**,** e24352.

BAIGENT, S. J. & MCCAULEY, J. W. 2001. Glycosylation of haemagglutinin and stalk-length of neuraminidase combine to regulate the growth of avian influenza viruses in tissue culture. *Virus Research,* 79**,** 177-185.

BANDE, F., ARSHAD, S. S., HAIR BEJO, M., KADKHODAEI, S. & OMAR, A. R. 2016. Prediction and In Silico Identification of Novel B-Cells and T-Cells Epitopes in the S1-Spike Glycoprotein of M41 and CR88 (793/B) Infectious Bronchitis Virus Serotypes for Application in Peptide Vaccines. *Advanced Bioinformatics,* 2016**,** 5484972.

BANDE, F., ARSHAD, S. S., OMAR, A. R., HAIR-BEJO, M., MAHMUDA, A. & NAIR, V. 2017. Global distributions and strain diversity of avian infectious bronchitis virus: a review. *Animal Health Research Reviews,* 18**,** 70-83.

BELOUZARD, S., MILLET, J. K., LICITRA, B. N. & WHITTAKER, G. R. 2012. Mechanisms of coronavirus cell entry mediated by the viral spike protein. *Viruses,* 4**,** 1011-33.

BENTLEY, K., KEEP, S. M., ARMESTO, M. & BRITTON, P. 2013. Identification of a noncanonically transcribed subgenomic mRNA of infectious bronchitis virus and other gammacoronaviruses. *Journal of Virology,* 87**,** 2128-36.

BENYEDA, Z., MATO, T., SUVEGES, T., SZABO, E., KARDI, V., ABONYI-TOTH, Z., RUSVAI, M. & PALYA, V. 2009. Comparison of the pathogenicity of QX-like, M41 and 793/B infectious bronchitis strains from different pathological conditions. *Avian Pathology,* 38**,** 449-56.

BERN, M., KIL, Y. J. & BECKER, C. 2012. Byonic: Advanced Peptide and Protein Identification Software. *Current Protocols in Bioinformatics*.

BERNARD, S. & LAUDE, H. 1995. Site-specific alteration of transmissible gastroenteritis virus spike protein results in markedly reduced pathogenicity. *Journal of General Virology,* 76**,** 2235-2241.

BICKERTON, E., MAIER, H. J., STEVENSON-LEGGETT, P., ARMESTO, M. & BRITTON, P. 2018. The S2 subunit of infectious bronchitis virus Beaudette is a determinant of cellular tropism. *Journal of Virology*.

BIJLENGA, G., COOK, J. K., GELB, J., JR. & DE WIT, J. J. 2004. Development and use of the H strain of avian infectious bronchitis virus from the Netherlands as a vaccine: a review. *Avian Pathology,* 33**,** 550-7.

BINNS, M. M., MICHAEL E. G. BOURSNELL, CAVANAGH, D., PAPPIN, D. J. C. & BROWN, T. D. K. 1985. Cloning and Sequencing of the Gene Encoding the Spike Protein of the Coronavirus IBV. *Journal of General Virology,* 66**,** 719-726.

BONHOMME, C. J., KNOPP, K. A., BEDERKA, L. H., ANGELINI, M. M. & BUCHMEIER, M. J. 2013. LCMV glycosylation modulates viral fitness and cell tropism. *PLoS One,* 8**,** e53273.

BOSCH, B. J., VAN DER ZEE, R., DE HAAN, C. A. M. & ROTTIER, P. J. M. 2003. The Coronavirus Spike Protein Is a Class I Virus Fusion Protein: Structural and Functional Characterization of the Fusion Core Complex. *Journal of Virology,* 77**,** 8801-8811.

BOURSNELL, M. E. G., BROWN, T. D. K., FOULDS, I. J., GREEN, P. F., TOMLEY, F. M. & BINNS, M. M. 1987. Completion of the Sequence of the Genome of the Coronavirus Avian Infections Bronchitis Virus *Journal of General Virology* 68**,** 57-77.

BRAAKMAN, I. & BULLEID, N. J. 2011. Protein folding and modification in the mammalian endoplasmic reticulum. *Annual Reviews in Biochemistry,* 80**,** 71-99.

BRITTON, P., EVANS, S., DOVE, B., DAVIES, M., CASAIS, R. & CAVANAGH, D. 2005. Generation of a recombinant avian coronavirus infectious bronchitis virus using transient dominant selection. *Journal of Virological Methods,* 123**,** 203-11.

BRITTON, P., GREEN, P., KOTFIER, S., MAWDITT, K., PENZES, Z., CAVANAGH, D. & SKINNER, M. 1996. Expression of bacteriophage T7 RNA polymerase in avian and mammalian cells by a recombinant fowlpox virus. *Journal of General Virology,* 77**,** 963-967.

CASAIS, R., DAVIES, M., CAVANAGH, D. & BRITTON, P. 2005. Gene 5 of the avian coronavirus infectious bronchitis virus is not essential for replication. *Journal of Virology,* 79**,** 8065-78.

CASAIS, R., DOVE, B., CAVANAGH, D. & BRITTON, P. 2003. Recombinant Avian Infectious Bronchitis Virus Expressing a Heterologous Spike Gene Demonstrates that the Spike Protein Is a Determinant of Cell Tropism. *Journal of Virology,* 77**,** 9084-9089.

CASAIS, R., THIEL, V., SIDDELL, S. G., CAVANAGH, D. & BRITTON, P. 2001. Reverse genetics system for the avian coronavirus infectious bronchitis virus. *Journal of Virology,* 75**,** 12359-69.

CAVANAGH, D. 1983. Coronavirus IBV: Structural Characterization of the Spike Protein. *Journal of General Virology,* 64**,** 2577-2583.

CAVANAGH, D., DAVIS, P. J., COOK, J. K., LI, D., KANT, A. & KOCH, G. 1992. Location of the amino acid differences in the S1 spike glycoprotein subunit of closely related serotypes of infectious bronchitis virus. *Avian Pathology,* 21**,** 33-43.

CAVANAGH, D., DAVIS, P. J., PAPPIN, D. J., BINNS, M. M., BOURSNELL, M. E. & BROWN, T. D. K. 1986. Coronavirus IBV: partial amino terminal sequencing of spike polypeptide S2 identifies the sequence Arg-Arg-Phe-Arg-Arg at the cleavage site of the spike precursor propolypeptide of IBV strains Beaudette and M41. *Virus Research,* 4**,** 133-143.

CAVANAGH, D. & NAQI, S. 2003. Infectious bronchitis *In:* SAIF, Y. M., BARNES, H. J., GLISSON, J. R., FADLY, A. M., MCDOUGALD, L. R. & SWAYNE, D. E. (eds.) *Diseases of Poultry.* Ames, Iowa: Iowa State University Press.

CHEN, J. & LY, H. 2017. Immunosuppression by viral N proteins. *Oncotarget* 8**,** 50331-50332.

CHRISTIANSON, K., INGERSOLL, J., LANDON, R., PFEIFFER, N. & GERBER, J. 1989. Characterization of a temperature sensitive feline infectious peritonitis coronavirus. *Archives of Virology,* 109**,** 185-196.

CHU, V. C., MCELROY, L. J., CHU, V., BAUMAN, B. E. & WHITTAKER, G. R. 2006. The avian coronavirus infectious bronchitis virus undergoes direct low-pH-dependent fusion activation during entry into host cells. *Journal of Virology,* 80**,** 3180-8.

COOK, J. K., JACKWOOD, M. & JONES, R. C. 2012. The long view: 40 years of infectious bronchitis research. *Avian Pathology,* 41**,** 239-50.

CORSE, E. & MACHAMER, C. E. 2003. The cytoplasmic tails of infectious bronchitis virus E and M proteins mediate their interaction. *Virology,* 312**,** 25-34.

DA COSTA, B., SAUSSET, A., MUNIER, S., GHOUNARIS, A., NAFFAKH, N., LE GOFFIC, R. & DELMAS, B. 2015. Temperature-Sensitive Mutants in the Influenza A Virus RNA Polymerase: Alterations in the PA Linker Reduce Nuclear Targeting of the PB1-PA Dimer and Result in Viral Attenuation. *Journal of Virology,* 89**,** 6376-90.

DE WIT, J. J. 2000. Detection of infectious bronchitis virus. *Avian Pathology,* 29**,** 71-93.

DE WIT, J. J., COOK, J. K. & VAN DER HEIJDEN, H. M. 2011. Infectious bronchitis virus variants: a review of the history, current situation and control measures. *Avian Pathology,* 40**,** 223-35.

DEDIEGO, M. L., ALVAREZ, E., ALMAZAN, F., REJAS, M. T., LAMIRANDE, E., ROBERTS, A., SHIEH, W. J., ZAKI, S. R., SUBBARAO, K. & ENJUANES, L. 2007. A severe acute respiratory syndrome coronavirus that lacks the E gene is attenuated in vitro and in vivo. *Journal of Virology,* 81**,** 1701-13.

DELMAS, B. & LAUDE, H. 1990. Assembly of Coronavirus Spike Protein into Trimers and Its Role in Epitope Expression. *Journal of Virology,* 64**,** 5367-5375.

DELMAS, B. & LAUDE, H. 1991. Carbohydrate-induced conformational changes strongly modulate the antigenicity of coronavirus TGEV glycoproteins S and M. *Virus Research,* 20**,** 107-120.

DORAN, R. C., MORALES, J. F., TO, B., MORIN, T. J., THEOLIS, R., JR., O'ROURKE, S. M., YU, B., MESA, K. A. & BERMAN, P. W. 2014. Characterization of a monoclonal antibody to a novel glycan-dependent epitope in the V1/V2 domain of the HIV-1 envelope protein, gp120. *Molecular Immunology,* 62**,** 219-226.

DUBOIS-DALCQ, M. E., DOLLER, E., HASPEL, M. V. & HOLMES, K. V. 1982. Cell Tropism and Expression of Mouse Hepatitis Viruses (MHV) in Mouse Spinal Cord Cultures. *Virology,* 119**,** 317-331.

DVEKSLER, G. S., PENSIERO, M. N., CARDELLICHIO, C. B., WILLIAMS, R. K., JIANG, G.-S., HOLMES, K. V. & DIEFFENBACH, C. W. 1991. Cloning of the Mouse Hepatitis Virus (MHV) Receptor: Expression in Human and Hamster Cell Lines Confers Susceptibility to MHV. *Journal of Virology,* 65**,** 6881-6891.

ELBEIN, A. D., SOLF, R., DORLING, P. R. & VOSBECK, K. 1981. Swainsonine: An inhibitor of glycoprotein processing. *Proceedings of the National Academy of Science USA,* 78**,** 7393-7397.

ELBEIN, A. D., TROPEA, J. E., MITCHELL, M. & KAUSHAL, G. P. 1990. Kifunensine, a Potent Inhibito of the Glycoprotein Processing Mannosidase I. *Journal of Biological Chemistry,* 265**,** 15599-15605.

FANG, S. G., SHEN, H., WANG, J., TAY, F. P. & LIU, D. X. 2008. Proteolytic processing of polyproteins 1a and 1ab between non-structural proteins 10 and 11/12 of Coronavirus infectious bronchitis virus is dispensable for viral replication in cultured cells. *Virology,* 379**,** 175-80.

FEHR, A. R. & PERLMAN, S. 2015. Coronaviruses: an overview of their replication and pathogenesis. *Methods in Molecular Biology,* 1282**,** 1-23.

FERRIS, S. P., KODALI, V. K. & KAUFMAN, R. J. 2014. Glycoprotein folding and quality-control mechanisms in protein-folding diseases. *Disease Models and Mechanisms,* 7**,** 331-41.

GALLAGHER, P. 1988. Addition of carbohydrate side chains at novel sites on influenza virus hemagglutinin can modulate the folding, transport, and activity of the molecule. *Journal of Cell Biology,* 107**,** 2059-2073.

GAN, S. W., TAN, E., LIN, X., YU, D., WANG, J., TAN, G. M., VARARATTANAVECH, A., YEO, C. Y., SOON, C. H., SOONG, T. W., PERVUSHIN, K. & TORRES, J. 2012. The small hydrophobic protein of the human respiratory syncytial virus forms pentameric ion channels. *Journal of Biological Chemistry,* 287**,** 24671-89.

GAVEL, Y. & HEIJNE, G. V. 1990. Sequence differences between glycosylated and non-glycosylated Asn-X-Thr/Ser acceptor sites: implications for protein engineering. *Protein Engineering, Design and Selection,* 3**,** 433-442.

GAVRILOV, B. K., ROGERS, K., FERNANDEZ-SAINZ, I. J., HOLINKA, L. G., BORCA, M. V. & RISATTI, G. R. 2011. Effects of glycosylation on antigenicity and immunogenicity of classical swine fever virus envelope proteins. *Virology,* 420**,** 135-45.

GELB, J., JR., WEISMAN, Y., LADMAN, B. S. & MEIR, R. 2005. S1 gene characteristics and efficacy of vaccination against infectious bronchitis virus field isolates from the United States and Israel (1996 to 2000). *Avian Pathology,* 34**,** 194-203.

GLOWACKA, I., BERTRAM, S., MULLER, M. A., ALLEN, P., SOILLEUX, E., PFEFFERLE, S., STEFFEN, I., TSEGAYE, T. S., HE, Y., GNIRSS, K., NIEMEYER, D., SCHNEIDER, H., DROSTEN, C. & POHLMANN, S. 2011. Evidence that TMPRSS2 activates the severe acute respiratory syndrome coronavirus spike protein for membrane fusion and reduces viral control by the humoral immune response. *Journal of Virology,* 85**,** 4122-34.

GOH, J. B. & NG, S. K. 2018. Impact of host cell line choice on glycan profile. *Critical Reviews in Biotechnology,* 38**,** 851-867.

GONZALEZ, J. M., GOMEZ-PUERTAS, P., CAVANAGH, D., GORBALENYA, A. E. & ENJUANES, L. 2003. A comparative sequence analysis to revise the current taxonomy of the family Coronaviridae. *Archives of Virology,* 148**,** 2207-35.

GORBALENYA, A. E., ENJUANES, L., ZIEBUHR, J. & SNIJDER, E. J. 2006. Nidovirales: evolving the largest RNA virus genome. *Virus Research,* 117**,** 17-37.

GROOT, R. J. D., LUYTJES, W., HORZINE, M. C., ZEIJST, A. M. V. D., SPAAN, W. J. M. & LENSTRA, J. A. 1987. Evidence for a coiled-coil structure in the spike proteins of coronaviruses. *Journal of Molecular Biology,* 196**,** 963-966.

GUI, M., SONG, W., ZHOU, H., XU, J., CHEN, S., XIANG, Y. & WANG, X. 2017. Cryo-electron microscopy structures of the SARS-CoV spike glycoprotein reveal a prerequisite conformational state for receptor binding. *Cell Research,* 27**,** 119-129.

HALL, T. A. 1999. BioEdit: a user-friendly biological sequence alignment editor and analysis program for Windows 95/98/NT. *Nucleic Acids Symposium Series* 41**,** 95-98.

HAN, D. P., LOHANI, M. & CHO, M. W. 2007. Specific asparagine-linked glycosylation sites are critical for DC-SIGN- and L-SIGN-mediated severe acute respiratory syndrome coronavirus entry. *Journal of Virology,* 81**,** 12029-39.

HANDBERG, K. J., NIELSEN, O. L., PEDERSEN, M. W. & JORGENSEN, P. H. 1999. Detection and strain differentiation of infectious bronchitis virus in tracheal tissues from experimentally infected chickens by reverse transcription-polymerase chain reaction. Comparison with an immunohistochemical technique. *Avian Pathology,* 28**,** 327-35.

HEBERT, D. N. & MOLINARI, M. 2012. Flagging and docking: dual roles for N-glycans in protein quality control and cellular proteostasis. *Trends in Biochemical Sciences,* 37**,** 404-10.

HELENIUS, A. & AEBI, M. 2001. Intracellular Functions of N-Linked Glycans. *Science,* 291**,** 2364-2369.

HERBERT, D. N., ZHANG, J.-X., CHEN, W., FOELLMER, B. & HELENIUS, A. 1997. The Number and Location of Glycans on Influenza Hemagglutinin Determine Folding and Association with Calnexin and Calreticulin. *Journal of Cell Biology,* 139**,** 613-623.

HIMLY, M., FOSTER, D. N., BOTTOLI, I., IACOVONI, J. S. & VOGT, P. K. 1998. The DF-1 Chicken Fibroblast Cell Line: Transformation Induced by Diverse Oncogenes and Cell Death Resulting from Infection by Avian Leukosis Viruses. *Virology,* 248**,** 295-304.

HISCOX, J. A., MAWDITT, K. L., CAVANAGH, D. & BRITTON, P. 1995. Investigation of the Control of Coronavirus Subgenomic mRNA Transcription by Using T7-Generated Negative-Sense RNA Transcripts. *Journal of Virology,* 69**,** 6219–6227.

HODGSON, T., CASAIS, R., DOVE, B., BRITTON, P. & CAVANAGH, D. 2004. Recombinant infectious bronchitis coronavirus Beaudette with the spike protein gene of the pathogenic M41 strain remains attenuated but induces protective immunity. *Journal of Virology,* 78**,** 13804-11.

HU, Y., LI, W., GAO, T., CUI, Y., JIN, Y., LI, P., MA, Q., LIU, X. & CAO, C. 2017. The Severe Acute Respiratory Syndrome Coronavirus Nucleocapsid Inhibits Type I Interferon Production by Interfering with TRIM25-Mediated RIG-I Ubiquitination. *Journal of Virology,* 91.

HUBBARD, S. C. 1988. Regulation of Glycosylation. *Journal of Biological Chemistry,* 263**,** 19303-19317.

HURST, K. R., KUO, L., KOETZNER, C. A., YE, R., HSUE, B. & MASTERS, P. S. 2005. A major determinant for membrane protein interaction localizes to the carboxy-terminal domain of the mouse coronavirus nucleocapsid protein. *Journal of Virology,* 79**,** 13285-97.

JACKWOOD, M. W., HILT, D. A., CALLISON, S. A., LEE, C.-W., PLAZA, H. & WADE, E. 2001. Spike Glycoprotein Cleavage Recognition Site Analysis of Infectious Bronchitis Virus. *Avian Diseases,* 45**,** 366-372.

JANG, H., KOO, B. S., JEON, E. O., LEE, H. R., LEE, S. M. & MO, I. P. 2013. Altered pro-inflammatory cytokine mRNA levels in chickens infected with infectious bronchitis virus. *Poultry Science,* 92**,** 2290-8.

JEFFERS, S., HEMMILA, E. M. & HOLMES, K. V. 2006. Human Coronavirus 229E can Use CD209L (L-Sign) to Enter Cells. *In:* S., P. & K.V., H. (eds.) *The Nidoviruses: Advances in Experimental Medicine and Biology.* Boston, MA: Springer.

JEFFERS, S. A., TUSELL, S. M., GILLIM-ROSS, L., HEMMILA, E. M., ACHENBACH, J. E., BABCOCK, G. J., THOMAS, W. D., JR., THACKRAY, L. B., YOUNG, M. D., MASON, R. J., AMBROSINO, D. M., WENTWORTH, D. E., DEMARTINI, J. C. & HOLMES, K. V. 2004. CD209L (L-SIGN) is a receptor for severe acute respiratory syndrome coronavirus. *Proceedings of the National Academy of Science USA,* 101**,** 15748-53.

KAMEKA, A. M., HADDADI, S., KIM, D. S., CORK, S. C. & ABDUL-CAREEM, M. F. 2014. Induction of innate immune response following infectious bronchitis corona virus infection in the respiratory tract of chickens. *Virology,* 450-451**,** 114-21.

KANT, A., KOCH, G., ROOZELAAR, D. J. V., KUSTERS, J. G., POELWIJK, F. A. J. & ZEIJST, B. A. M. V. D. 1992. Location of antigenic sites defined by neutralizing monoclonal antibodies on the S1 avian infectious bronchitis virus glycopolypeptide. *Journal of General Virology,* 73**,** 591-596.

KENG, C. T., ZHANG, A., SHEN, S., LIP, K. M., FIELDING, B. C., TAN, T. H., CHOU, C. F., LOH, C. B., WANG, S., FU, J., YANG, X., LIM, S. G., HONG, W. & TAN, Y. J. 2005. Amino acids 1055 to 1192 in the S2 region of severe acute respiratory syndrome coronavirus S protein induce neutralizing antibodies: implications for the development of vaccines and antiviral agents. *Journal of Virology,* 79**,** 3289-96.

KING, A. M. Q., ADAMS, M. J., CARSTENS, E. B. & LEFKOWITZ, E. J. 2012. Order - Nidovirales *In:* KING, A. M. Q., ADAMS, M. J., CARSTENS, E. B. & LEFKOWITZ, E. J. (eds.) *Virus Taxonomy.* Elsevier.

KINT, J., DICKHOUT, A., KUTTER, J., MAIER, H. J., BRITTON, P., KOUMANS, J., PIJLMAN, G. P., FROS, J. J., WIEGERTJES, G. F. & FORLENZA, M. 2015. Infectious Bronchitis

Coronavirus Inhibits STAT1 Signaling and Requires Accessory Proteins for Resistance to Type I Interferon Activity. *Journal of Virology,* 89**,** 12047-57.

KINT, J., LANGEREIS, M. A., MAIER, H. J., BRITTON, P., VAN KUPPEVELD, F. J., KOUMANS, J., WIEGERTJES, G. F. & FORLENZA, M. 2016. Infectious Bronchitis Coronavirus Limits Interferon Production by Inducing a Host Shutoff That Requires Accessory Protein 5b. *Journal of Virology,* 90**,** 7519-7528.

KLUMPERMAN, J., LOCKER, J. K., MEIJER, A., HORZINEK, M. C., GEUZE, H. J. & ROTTIER, P. J. M. 1994. Coronavirus M Proteins Accumulate in the Golgi Complex beyond the Site of Virion Budding. *Journal of Virology,* 68**,** 6523-6534.

KNOOPS, K., KIKKERT, M., WORM, S. H., ZEVENHOVEN-DOBBE, J. C., VAN DER MEER, Y., KOSTER, A. J., MOMMAAS, A. M. & SNIJDER, E. J. 2008. SARS-coronavirus replication is supported by a reticulovesicular network of modified endoplasmic reticulum. *PLoS Biology,* 6**,** e226.

KRIJNSE-LOCKER, J. 1994. Characterization of the budding compartment of mouse hepatitis virus: evidence that transport from the RER to the Golgi complex requires only one vesicular transport step. *The Journal of Cell Biology,* 124**,** 55-70.

KUO, L., HURST-HESS, K. R., KOETZNER, C. A. & MASTERS, P. S. 2016. Analyses of Coronavirus Assembly Interactions with Interspecies Membrane and Nucleocapsid Protein Chimeras. *Journal of Virology,* 90**,** 4357-68.

KUSTERS, J. G., JAGER, E. J., LENSTRA, J. A., KOCH, G., POSTHUMUS, W. P. A., MELOEN, R. H. & ZEIJST, B. A. M. V. D. 1989. Analysis of an immunodominant region of infectious bronchitis virus. *Journal of Immunology,* 143**,** 2692-2698.

LACONI, A., VAN BEURDEN, S. J., BERENDS, A. J., KRAMER-KUHL, A., JANSEN, C. A., SPEKREIJSE, D., CHENARD, G., PHILIPP, H. C., MUNDT, E., ROTTIER, P. J. M. & HELENE VERHEIJE, M. 2018. Deletion of accessory genes 3a, 3b, 5a or 5b from avian coronavirus infectious bronchitis virus induces an attenuated phenotype both in vitro and in vivo. *Journal of General Virology*.

LANSER, J. A. & HOWARD, C. R. 1980. The polypeptides of infectious bronchitis virus (IBV-41 strain). *Journal of General Virology,* 46**,** 349-61.

LASKY, L., JE., G., FENNIE, C., BENZ, P., CAPON, D., DOWBENKO, D., NAKAMURA, G., NUNES, W., RENZ, M. & BERMAN, P. 1986. Neutralizaton of the AIDS Retrovirus by Antibodies to a Recombinant Envelope Glycoprotein. *Science,* 233**,** 209-212.

LEE, C.-W., HILT, D. A. & JACKWOOD, M. W. 2003. Typing of field isolates of infectious bronchitis virus based on the sequence of the hypervariable region in the S1 gene. *Journal of Veterinary Diagnostic Investigation,* 15**,** 344-348.

LEONARD, C., SPELLMAN, M., RIDDLE, L., HARRIS, R., THOMAS, J. & GREGORY, T. 1990. Assignment of Intrachain Disulfide Bonds and Characterization Sites of the Type 1 Recombinant Human Immunodeficiency Virus Envelope Glycoprotein (gp120) Expressed in Chinese Hamster Ovary Cells. *Journal of Biological Chemistry,* 265**,** 10373-10382.

LI, F. 2015. Receptor recognition mechanisms of coronaviruses: a decade of structural studies. *Journal of Virology,* 89**,** 1954-64.

LI, F., BERARDI, M., LI, W., FARZAN, M., DORMITZER, P. R. & HARRISON, S. C. 2006. Conformational states of the severe acute respiratory syndrome coronavirus spike protein ectodomain. *Journal of Virology,* 80**,** 6794-800.

LI, W., MOORE, M. J., VASILIEVA, N., SUI, J., WONG, S. K., BERNE, M. A., SOMASUNDARAN, M., SULLIVAN, J. L., LUZURIAGA, K., GREENOUGH, T. C., CHOE, H. & FARZAN, M. 2003. Angiotensin-converting enzyme 2 is a functional receptor for the SARS coronavirus. *Nature,* 426**,** 450-454.

LOMNICZI, B. & MORSER, J. 1981. Polypeptides of Infectious Bronchitis Virus. I. Polypeptides of the Virion. *Journal of General Virology,* 55**,** 155-164.

LONDRIGAN, S. L., TURVILLE, S. G., TATE, M. D., DENG, Y. M., BROOKS, A. G. & READING, P. C. 2011. N-linked glycosylation facilitates sialic acid-independent attachment and entry of influenza A viruses into cells expressing DC-SIGN or L-SIGN. *Journal of Virology,* 85**,** 2990-3000.

LU, L., LIU, Q., ZHU, Y., CHAN, K. H., QIN, L., LI, Y., WANG, Q., CHAN, J. F., DU, L., YU, F., MA, C., YE, S., YUEN, K. Y., ZHANG, R. & JIANG, S. 2014. Structure-based discovery of Middle East respiratory syndrome coronavirus fusion inhibitor. *Nature Communications,* 5**,** 3067.

LU, Y., LU, X. & DENISON, M. R. 1995. Identification and Characterization of a Serine-Like Proteinase of the Murine Coronavirus MHV-A59. *Journal of Virology,* 69**,** 3554–3559.

LUO, Z., MATTHEWS, A. M. & WEISS, S. R. 1999. Amino Acid Substitutions within the Leucine Zipper Domain of the Murine Coronavirus Spike Protein Cause Defects in Oligomerization and the Ability To Induce Cell-to-Cell Fusion. *Journal of Virology,* 73**,** 8152–8159.

MAATTANEN, P., GEHRING, K., BERGERON, J. J. & THOMAS, D. Y. 2010. Protein quality control in the ER: the recognition of misfolded proteins. *Seminars in Cell and Developmental Biololgy,* 21**,** 500-11.

MACKENZIE, J. 2005. Wrapping things up about virus RNA replication. *Traffic,* 6**,** 967-77.

MADU, I. G., CHU, V. C., LEE, H., REGAN, A. D., BAUMAN, B. E. & WHITTAKER, G. R. 2007. Heparan sulfate is a selective attachment factor for the avian coronavirus infectious bronchitis virus beaudette. *Avian Diseases,* 51**,** 45-51.

MAIER, H. J., HAWES, P. C., COTTAM, E. M., MANTELL, J., VERKADE, P., MONAGHAN, P., WILEMAN, T. & BRITTON, P. 2013. Infectious bronchitis virus generates spherules from zippered endoplasmic reticulum membranes. *MBio,* 4**,** e00801-13.

MAIER, H. J., NEUMAN, B. W., BICKERTON, E., KEEP, S. M., ALRASHEDI, H., HALL, R. & BRITTON, P. 2016. Extensive coronavirus-induced membrane rearrangements are not a determinant of pathogenicity. *Scientific Reports,* 6**,** 27126.

MANSWR, B., BALL, C., FORRESTER, A., CHANTREY, J. & GANAPATHY, K. 2018. Evaluation of full S1 gene sequencing of classical and variant infectious bronchitis viruses extracted from allantoic fluid and FTA cards. *Avian Pathology,* 47**,** 418-426.

MATSUYAMA, S. & TAGUCHI, F. 2009. Two-step conformational changes in a coronavirus envelope glycoprotein mediated by receptor binding and proteolysis. *Journal of Virology,* 83**,** 11133-41.

MCBRIDE, R., VAN ZYL, M. & FIELDING, B. C. 2014. The coronavirus nucleocapsid is a multifunctional protein. *Viruses,* 6**,** 2991-3018.

MEYER, L., SAUSSET, A., SEDANO, L., DA COSTA, B., LE GOFFIC, R. & DELMAS, B. 2016. Codon Deletions in the Influenza A Virus PA Gene Generate Temperature-Sensitive Viruses. *Journal of Virology,* 90**,** 3684-93.

MILLER, S. & KRIJNSE-LOCKER, J. 2008. Modification of intracellular membrane structures for virus replication. *Nature Reviews Microbiology,* 6**,** 363-74.

MILLET, J. K., GOLDSTEIN, M. E., LABITT, R. N., HSU, H. L., DANIEL, S. & WHITTAKER, G. R. 2016. A camel-derived MERS-CoV with a variant spike protein cleavage site and distinct fusion activation properties. *Emerging Microbes and Infections,* 5**,** e126.

MILLET, J. K. & WHITTAKER, G. R. 2015. Host cell proteases: Critical determinants of coronavirus tropism and pathogenesis. *Virus Research,* 202**,** 120-34.

MOCKETT, A., CVANAGH, D. & BROWN, D. K. 1984. Monoclonal Antibodies to the S1 Spike and Membrane Proteins of Avian Infectious Bronchitis Coronavirus Strain Massachusetts M41. *Journal of General Virology,* 65**,** 2281-2286.

NAVAS, S., SEO, S. H., CHUA, M. M., DAS SARMA, J., LAVI, E., HINGLEY, S. T. & WEISS, S. R. 2001. Murine coronavirus spike protein determines the ability of the virus to replicate in the liver and cause hepatitis. *Journal of Virology,* 75**,** 2452-7.

NEUMAN, B. W., KISS, G., KUNDING, A. H., BHELLA, D., BAKSH, M. F., CONNELLY, S., DROESE, B., KLAUS, J. P., MAKINO, S., SAWICKI, S. G., SIDDELL, S. G., STAMOU, D. G., WILSON, I. A., KUHN, P. & BUCHMEIER, M. J. 2011. A structural analysis of M protein in coronavirus assembly and morphology. *Journal of Structural Biology,* 174**,** 11-22.

NIETO-TORRES, J. L., VERDIA-BAGUENA, C., CASTANO-RODRIGUEZ, C., AGUILELLA, V. M. & ENJUANES, L. 2015a. Relevance of Viroporin Ion Channel Activity on Viral Replication and Pathogenesis. *Viruses,* 7**,** 3552-73.

NIETO-TORRES, J. L., VERDIA-BAGUENA, C., JIMENEZ-GUARDENO, J. M., REGLA-NAVA, J. A., CASTANO-RODRIGUEZ, C., FERNANDEZ-DELGADO, R., TORRES, J., AGUILELLA, V. M. & ENJUANES, L. 2015b. Severe acute respiratory syndrome coronavirus E protein transports calcium ions and activates the NLRP3 inflammasome. *Virology,* 485**,** 330-9.

NILSSON, T., AU, C. E. & BERGERON, J. J. 2009. Sorting out glycosylation enzymes in the Golgi apparatus. *FEBS Letters,* 583**,** 3764-9.

NOGALES, A., RODRIGUEZ, L., CHAUCHE, C., HUANG, K., REILLY, E. C., TOPHAM, D. J., MURCIA, P. R., PARRISH, C. R. & MARTINEZ-SOBRIDO, L. 2017. Temperature-Sensitive Live-Attenuated Canine Influenza Virus H3N8 Vaccine. *Journal of Virology,* 91.

OLSEN, J. V., ONG, S. E. & MANN, M. 2004. Trypsin cleaves exclusively C-terminal to arginine and lysine residues. *Molecular and Cellular Proteomics,* 3**,** 608-14.

OOSTRA, M., DE HAAN, C. A., DE GROOT, R. J. & ROTTIER, P. J. 2006. Glycosylation of the severe acute respiratory syndrome coronavirus triple-spanning membrane proteins 3a and M. *Journal of Virology,* 80**,** 2326-36.

PARK, J.-E., LI, K., BARLAN, A., FEHR, A. R., PERLMAN, S., JR, P. B. M. & GALLAGHER, T. 2016. Proteolytic processing of Middle East respiratory syndrome coronavirus spikes expands virus tropism. *Proceedings of the National Academy of Science USA,* 113**,** 12262–12267.

PARK, J. E., CRUZ, D. J. & SHIN, H. J. 2011. Receptor-bound porcine epidemic diarrhea virus spike protein cleaved by trypsin induces membrane fusion. *Archives of Virology,* 156**,** 1749-56.

PEIRIS, J. S. M., LAI, S. T., POON, L. L. M., GUAN, Y., YAM, L. Y. C., LIM, W., NICHOLLS, J., YEE, W. K. S., YAN, W. W., CHEUNG, M. T., CHENG, V. C. C., CHAN, K. H., TSANG, D. N. C., YUNG, R. W. H., NG, T. K. & YUEN, K. Y. 2003. Coronavirus as a possible cause of severe acute respiratory syndrome. *The Lancet,* 361**,** 1319-1325.

PHILLIPS, J. J., CHUA, M. M., LAVI, E. & WEISS, S. R. 1999. Pathogenesis of Chimeric MHV4/MHV-A59 Recombinant Viruses: the Murine Coronavirus Spike Protein Is a Major Determinant of Neurovirulence. *Journal of Virology,* 73**,** 7752-7760.

PING, J., LI, C., DENG, G., JIANG, Y., TIAN, G., ZHANG, S., BU, Z. & CHEN, H. 2008. Single-amino-acid mutation in the HA alters the recognition of H9N2 influenza virus by a monoclonal antibody. *Biochemical and Biophysical Research Communications,* 371**,** 168-71.

POSTHUMA, C. C., TE VELTHUIS, A. J. W. & SNIJDER, E. J. 2017. Nidovirus RNA polymerases: Complex enzymes handling exceptional RNA genomes. *Virus Research,* 234**,** 58-73.

PROMKUNTOD, N., VAN EIJNDHOVEN, R. E., DE VRIEZE, G., GRONE, A. & VERHEIJE, M. H. 2014. Mapping of the receptor-binding domain and amino acids critical for attachment in the spike protein of avian coronavirus infectious bronchitis virus. *Virology,* 448**,** 26-32.

RAJ, V. S., MOU, H., SMITS, S. L., DEKKERS, D. H., MULLER, M. A., DIJKMAN, R., MUTH, D., DEMMERS, J. A., ZAKI, A., FOUCHIER, R. A., THIEL, V., DROSTEN, C., ROTTIER, P. J., OSTERHAUS, A. D., BOSCH, B. J. & HAAGMANS, B. L. 2013. Dipeptidyl peptidase 4 is a functional receptor for the emerging human coronavirus-EMC. *Nature,* 495**,** 251-4.

RAO, R. S. P. & WOLLENWEBER, B. 2010. Do N-glycoproteins have preference for specific sequons? *Bioinformation,* 5**,** 208-212.

RATHORE, U., SAHA, P., KESAVARDHANA, S., KUMAR, A. A., DATTA, R., DEVANARAYANAN, S., DAS, R., MASCOLA, J. R. & VARADARAJAN, R. 2017. Glycosylation of the core of the HIV-1 envelope subunit protein gp120 is not required for native trimer formation or viral infectivity. *Journal of Biological Chemistry,* 292**,** 10197-10219.

READING, P. C., PICKETT, D. L., TATE, M. D., WHITNEY, P. G., JOB, E. R. & BROOKS, A. G. 2009. Loss of a single N-linked glycan from the hemagglutinin of influenza virus is associated with resistance to collectins and increased virulence in mice. *Respiratory Research,* 10**,** 117.

REED, L. J. & MUENCH, H. 1938. A simple method of estimating fifty per cent endpoints. *The American Journal of Hygiene* 27.

ROSE, D. R. 2012. Structure, mechanism and inhibition of Golgi alpha-mannosidase II. *Current Opinion in Structural Biology,* 22**,** 558-62.

ROTTIER, P. J., NAKAMURA, K., SCHELLEN, P., VOLDERS, H. & HAIJEMA, B. J. 2005. Acquisition of macrophage tropism during the pathogenesis of feline infectious peritonitis is determined by mutations in the feline coronavirus spike protein. *Journal of Virology,* 79**,** 14122-30.

RUCH, T. R. & MACHAMER, C. E. 2011. The hydrophobic domain of infectious bronchitis virus E protein alters the host secretory pathway and is important for release of infectious virus. *Journal of Virology,* 85**,** 675-85.

RUCH, T. R. & MACHAMER, C. E. 2012. The coronavirus E protein: assembly and beyond. *Viruses,* 4**,** 363-82.

RUSH, J. S. 2015. Role of Flippases in Protein Glycosylation in the Endoplasmic Reticulum. *Lipid Insights,* 8**,** 45-53.

SANCHEZ, C. M., IZETA, A., SANCHEZ-MORGADO, J. M., ALONSO, S., SOLA, I., BALASCH, M., PLANA-DURAN, J. & ENJUANES, L. 1999. Targeted Recombination Demonstrates that the Spike Gene of Transmissible Gastroenteritis Coronavirus Is a Determinant of Its Enteric Tropism and Virulence. *Journal of Virology,* 73**,** 7607-7618.

SANYAL, S. & MENON, A. K. 2009. Specific transbilayer translocation of dolichol-linked oligosaccharides by an endoplasmic reticulum flippase. *Proceedings of the National Acadamy of Sciences of the USA,* 106**,** 767–772.

SAWICKI, S. 2009. Coronavirus Genome Replication. *In:* CAMERON, C. E., GOTTE, M. & RANEY, K. (eds.) *Viral Genome Replication.* Elsevier.

SAWICKI, S. & SAWICKI, D. 2005. Coronavirus transcription: a perspective. *Current Topics in Microbiology and Immunology,* 287**,** 31-55.

SAWICKI, S. G., SAWICKI, D. L. & SIDDELL, S. G. 2007. A contemporary view of coronavirus transcription. *Journal of Virology,* 81**,** 20-9.

SCHALK, A. & HAWN, M. 1931. An apparently new respiratory disease of baby chicks. *Journal of American Veterinary Medical Association,* 78**,** 413-422.

SCHINKEL, S. C. B., RUBIN, S. & WRIGHT, K. E. 2017. Mechanisms of temperature sensitivity of attenuated Urabe mumps virus. *Virus Research,* 227**,** 104-109.

SCHWARZ, F. & AEBI, M. 2011. Mechanisms and principles of N-linked protein glycosylation. *Current Opinion in Structural Biology,* 21**,** 576-82.

SCHWEGMANN-WESSELS, C. & HERRLER, G. 2006. Sialic acids as receptor determinants for coronaviruses. *Glycoconjugate Journal,* 23**,** 51-8.

SENANAYAKE, S. D. & BRIAN, D. A. 1999. Translation from the 59 Untranslated Region (UTR) of mRNA 1 Is Repressed, but That from the 59 UTR of mRNA 7 Is Stimulated in Coronavirus-Infected Cells. *Journal of Virology,* 73**,** 8003-8009.

SHANG, J., ZHENG, Y., YANG, Y., LIU, C., GENG, Q., LUO, C., ZHANG, W. & LI, F. 2018. Cryo-EM structure of infectious bronchitis coronavirus spike protein reveals structural and functional evolution of coronavirus spike proteins. *PLoS Pathogens,* 14**,** e1007009.

SHI, X., BRAUBURGER, K. & ELLIOTT, R. M. 2005. Role of N-linked glycans on bunyamwera virus glycoproteins in intracellular trafficking, protein folding, and virus infectivity. *Journal of Virology,* 79**,** 13725-34.

SIU, Y. L., TEOH, K. T., LO, J., CHAN, C. M., KIEN, F., ESCRIOU, N., TSAO, S. W., NICHOLLS, J. M., ALTMEYER, R., PEIRIS, J. S., BRUZZONE, R. & NAL, B. 2008. The M, E, and N structural proteins of the severe acute respiratory syndrome coronavirus are required for efficient assembly, trafficking, and release of virus-like particles. *Journal of Virology,* 82**,** 11318-30.

SNIJDER, E. J. & MEULENBERG, J. J. M. 1998. The molecular biology of arteriviruses. *Journal of General Virology,* 79**,** 961-979.

SOLA, I., MORENO, J. L., ZUNIGA, S., ALONSO, S. & ENJUANES, L. 2005. Role of nucleotides immediately flanking the transcription-regulating sequence core in coronavirus subgenomic mRNA synthesis. *Journal of Virology,* 79**,** 2506-16.

STADEN, R. 1996. The Staden Sequence Analysis Package *Molecular Biotechnology,* 5**,** 233-241.

STANLEY, P. 2011. Golgi glycosylation. *Cold Spring Harbour Perspectives in Biology,* 3.

STOBART, C. C., LEE, A. S., LU, X. & DENISON, M. R. 2012. Temperature-sensitive mutants and revertants in the coronavirus nonstructural protein 5 protease (3CLpro) define residues involved in long-distance communication and regulation of protease activity. *Journal of Virology,* 86**,** 4801-10.

STOKES, H. L., BALIJI, S., HUI, C. G., SAWICKI, S. G., BAKER, S. C. & SIDDELL, S. G. 2010. A new cistron in the murine hepatitis virus replicase gene. *Journal of Virology,* 84**,** 10148-58.

SUN, X., JAYARAMAN, A., MANIPRASAD, P., RAMAN, R., HOUSER, K. V., PAPPAS, C., ZENG, H., SASISEKHARAN, R., KATZ, J. M. & TUMPEY, T. M. 2013. N-linked glycosylation of the hemagglutinin protein influences virulence and antigenicity of the 1918 pandemic and seasonal H1N1 influenza A viruses. *Journal of Virology,* 87**,** 8756-66.

TATE, M. D., JOB, E. R., DENG, Y. M., GUNALAN, V., MAURER-STROH, S. & READING, P. C. 2014. Playing hide and seek: how glycosylation of the influenza virus hemagglutinin can modulate the immune response to infection. *Viruses,* 6**,** 1294-316.

VALASTRO, V., HOLMES, E. C., BRITTON, P., FUSARO, A., JACKWOOD, M. W., CATTOLI, G. & MONNE, I. 2016. S1 gene-based phylogeny of infectious bronchitis virus: An attempt to harmonize virus classification. *Infections, Genetics and Evolution,* 39**,** 349-364.

VAN BEURDEN, S. J., BERENDS, A. J., KRAMER-KUHL, A., SPEKREIJSE, D., CHENARD, G., PHILIPP, H. C., MUNDT, E., ROTTIER, P. J. M. & VERHEIJE, M. H. 2017. A reverse genetics system for avian coronavirus infectious bronchitis virus based on targeted RNA recombination. *Virology Journal,* 14**,** 109.

VAN BEURDEN, S. J., BERENDS, A. J., KRAMER-KUHL, A., SPEKREIJSE, D., CHENARD, G., PHILIPP, H. C., MUNDT, E., ROTTIER, P. J. M. & VERHEIJE, M. H. 2018. Recombinant live attenuated avian coronavirus vaccines with deletions in the accessory genes 3ab and/or 5ab protect against infectious bronchitis in chickens. *Vaccine,* 36**,** 1085-1092.

VEENENDAAL, T., JARVELA, T., GRIEVE, A. G., VAN ES, J. H., LINSTEDT, A. D. & RABOUILLE, C. 2014. GRASP65 controls the cis Golgi integrity in vivo. *Biology Open,* 3**,** 431-43.

VENNEMA, H., GODEKE, G.-J., W.A.ROSSEN, J., F.VOORHOUT, W., C.HORZINEK, M., E.OPSTELTEN, D.-J. & J.M.ROTTIER, P. 1996. Nucleocapsid-independent assembly of coronavirus-like particles by co-expression of viral envelope protein genes. *The EMBO Journal* 15**,** 2020-2028.

VERDIA-BAGUENA, C., NIETO-TORRES, J. L., ALCARAZ, A., DEDIEGO, M. L., TORRES, J., AGUILELLA, V. M. & ENJUANES, L. 2012. Coronavirus E protein forms ion channels with functionally and structurally-involved membrane lipids. *Virology,* 432**,** 485-94.

VIGERUST, D. J. & SHEPHERD, V. L. 2007. Virus glycosylation: role in virulence and immune interactions. *Trends in Microbiology,* 15**,** 211-8.

WALKER, L. M., SIMEK, M. D., PRIDDY, F., GACH, J. S., WAGNER, D., ZWICK, M. B., PHOGAT, S. K., POIGNARD, P. & BURTON, D. R. 2010. A limited number of antibody specificities mediate broad and potent serum neutralization in selected HIV-1 infected individuals. *PLoS Pathogens,* 6**,** e1001028.

WALLS, A. C., TORTORICI, M. A., BOSCH, B. J., FRENZ, B., ROTTIER, P. J. M., DIMAIO, F., REY, F. A. & VEESLER, D. 2016a. Cryo-electron microscopy structure of a coronavirus spike glycoprotein trimer. *Nature,* 531**,** 114-117.

WALLS, A. C., TORTORICI, M. A., FRENZ, B., SNIJDER, J., LI, W., REY, F. A., DIMAIO, F., BOSCH, B. J. & VEESLER, D. 2016b. Glycan shield and epitope masking of a coronavirus spike protein observed by cryo-electron microscopy. *Nature Structural & Molecular Biology,* 23**,** 899-905.

WALLS, A. C., TORTORICI, M. A., SNIJDER, J., XIONG, X., BOSCH, B. J., REY, F. A. & VEESLER, D. 2017. Tectonic conformational changes of a coronavirus spike glycoprotein promote membrane fusion. *Proceedings of the National Academy of Science USA,* 114**,** 11157-11162.

WANG, W., NIE, J., PROCHNOW, C., TRUONG, C., JIA, Z., WANG, S., CHEN, X. S. & WANG, Y. 2013. A systematic study of the N-glycosylation sites of HIV-1 envelope protein on infectivity and antibody-mediated neutralization. *Retrovirology,* 10.

WEI, Y. Q., GUO, H. C., DONG, H., WANG, H. M., XU, J., SUN, D. H., FANG, S. G., CAI, X. P., LIU, D. X. & SUN, S. Q. 2014. Development and characterization of a recombinant infectious bronchitis virus expressing the ectodomain region of S1 gene of H120 strain. *Applied Microbiology and Biotechnology,* 98**,** 1727-35.

WEISS, S. R. & NAVAS-MARTIN, S. 2005. Coronavirus Pathogenesis and the Emerging Pathogen Severe Acute Respiratory Syndrome Coronavirus. *Microbiology and Molecular Biology Reviews,* 69**,** 635–664.

WHARTON, S. A., SKEHEL, J. J. & WILEY, D. C. 2000. Temperature dependence of fusion by sendai virus. *Virology,* 271**,** 71-8.

WICHT, O., LI, W., WILLEMS, L., MEULEMAN, T. J., WUBBOLTS, R. W., VAN KUPPEVELD, F. J., ROTTIER, P. J. & BOSCH, B. J. 2014. Proteolytic activation of the porcine epidemic diarrhea coronavirus spike fusion protein by trypsin in cell culture. *Journal of Virology,* 88**,** 7952-61.

WICKRAMASINGHE, I. N., DE VRIES, R. P., GRONE, A., DE HAAN, C. A. & VERHEIJE, M. H. 2011. Binding of avian coronavirus spike proteins to host factors reflects virus tropism and pathogenicity. *Journal of Virology,* 85**,** 8903-12.

WICKRAMASINGHE, I. N., DE VRIES, R. P., WEERTS, E. A., VAN BEURDEN, S. J., PENG, W., MCBRIDE, R., DUCATEZ, M., GUY, J., BROWN, P., ETERRADOSSI, N., GRONE, A., PAULSON, J. C. & VERHEIJE, M. H. 2015. Novel Receptor Specificity of Avian Gammacoronaviruses That Cause Enteritis. *Journal of Virology,* 89**,** 8783-92.

WILSON, L., GAGE, P. & EWART, G. 2006. Hexamethylene amiloride blocks E protein ion channels and inhibits coronavirus replication. *Virology,* 353**,** 294-306.

WINTER, C., SCHWEGMANN-WESSELS, C., CAVANAGH, D., NEUMANN, U. & HERRLER, G. 2006. Sialic acid is a receptor determinant for infection of cells by avian Infectious bronchitis virus. *Journal of General Virology,* 87**,** 1209-16.

WOLK, T. & SCHREIBER, M. 2006. N-Glycans in the gp120 V1/V2 domain of the HIV-1 strain NL4-3 are indispensable for viral infectivity and resistance against antibody neutralization. *Medical Microbiology and Immunology,* 195**,** 165-72.

WORTHINGTON, K. J., CURRIE, R. J. & JONES, R. C. 2008. A reverse transcriptase-polymerase chain reaction survey of infectious bronchitis virus genotypes in Western Europe from 2002 to 2006. *Avian Pathology,* 37**,** 247-57.

XU, C. & NG, D. T. 2015. Glycosylation-directed quality control of protein folding. *Nature Reviews Molecular Cell Biology,* 16**,** 742-52.

XU, Y., LIU, Y., LOU, Z., QIN, L., LI, X., BAI, Z., PANG, H., TIEN, P., GAO, G. F. & RAO, Z. 2004. Structural basis for coronavirus-mediated membrane fusion. Crystal structure of mouse hepatitis virus spike protein fusion core. *Journal of Biological Chemistry,* 279**,** 30514-22.

YAMADA, Y. & LIU, D. X. 2009. Proteolytic activation of the spike protein at a novel RRRR/S motif is implicated in furin-dependent entry, syncytium formation, and infectivity of coronavirus infectious bronchitis virus in cultured cells. *Journal of Virology,* 83**,** 8744-58.

YAMADA, Y., LIU, X. B., FANG, S. G., TAY, F. P. & LIU, D. X. 2009. Acquisition of cell-cell fusion activity by amino acid substitutions in spike protein determines the infectivity of a coronavirus in cultured cells. *PLoS One,* 4**,** e6130.

YANG, D. & LEIBOWITZ, J. 2015. The structure and functions of coronavirus genomic 3' and 5' ends. *Virus Research,* 206**,** 120-33.

YANG, X., ZHOU, Y., LI, J., FU, L., JI, G., ZENG, F., ZHOU, L., GAO, W. & WANG, H. 2016. Recombinant infectious bronchitis virus (IBV) H120 vaccine strain expressing the hemagglutinin-neuraminidase (HN) protein of Newcastle disease virus (NDV) protects chickens against IBV and NDV challenge. *Archives of Virology,* 161**,** 1209-16.

YANG, Y., DENG, Y., WEN, B., WANG, H., MENG, X., LAN, J., GAO, G. F. & TAN, W. 2014. The amino acids 736-761 of the MERS-CoV spike protein induce neutralizing antibodies: implications for the development of vaccines and antiviral agents. *Viral Immunology,* 27**,** 543-50.

YE, Y. & HOGUE, B. G. 2007. Role of the coronavirus E viroporin protein transmembrane domain in virus assembly. *Journal of Virology,* 81**,** 3597-607.

YOUN, S., COLLISSON, E. W. & MACHAMER, C. E. 2005. Contribution of trafficking signals in the cytoplasmic tail of the infectious bronchitis virus spike protein to virus infection. *Journal of Virology,* 79**,** 13209-17.

YUAN, Y., CAO, D., ZHANG, Y., MA, J., QI, J., WANG, Q., LU, G., WU, Y., YAN, J., SHI, Y., ZHANG, X. & GAO, G. F. 2017. Cryo-EM structures of MERS-CoV and SARS-CoV spike glycoproteins reveal the dynamic receptor binding domains. *Nature Communications,* 8**,** 15092.

YUDONG, W., YONGLIN, W., ZICHUN, Z., GENCHE, F., YIHAI, J., XIANGE, L., JIANG, D. & SHUSHUANG, W. 1998. Isolation and identification of glandular stomach type IBV (QX IBV) in chickens. *Chinese Journal of Animal Quarantine* 15.

ZAKI, A. M., VAN BOHEEMEN, S., BESTEBROER, T. M., OSTERHAUS, A. D. & FOUCHIER, R. A. 2012. Isolation of a novel coronavirus from a man with pneumonia in Saudi Arabia. *New England Journal of Medicine,* 367**,** 1814-20.

ZHANG, C., YE, Z., XUE, P., SHU, Q., ZHOU, Y., JI, Y., FU, Y., WANG, J. & YANG, F. 2016. Evaluation of Different N-Glycopeptide Enrichment Methods for N-Glycosylation Sites Mapping in Mouse Brain. *Journal of Proteome Research,* 15**,** 2960–2968.

ZHANG, R., LI, Y., COWLEY, T. J., STEINBRENNER, A. D., PHILLIPS, J. M., YOUNT, B. L., BARIC, R. S. & WEISS, S. R. 2015. The nsp1, nsp13, and M proteins contribute to the hepatotropism of murine coronavirus JHM.WU. *Journal of Virology,* 89**,** 3598-609.

ZHANG, X. & WANG, Y. 2016. Glycosylation Quality Control by the Golgi Structure. *Journal Molecular Biology,* 428**,** 3183-3193.

ZHENG, J., YAMADA, Y., FUNG, T. S., HUANG, M., CHIA, R. & LIU, D. X. 2018. Identification of N-linked glycosylation sites in the spike protein and their functional impact on the

replication and infectivity of coronavirus infectious bronchitis virus in cell culture. *Virology,* 513**,** 65-74.

ZHU, Y., YANG, D., REN, Q., YANG, Y., LIU, X., XU, X., LIU, W., CHEN, S., PENG, D. & LIU, X. 2015. Identification and characterization of a novel antigenic epitope in the hemagglutinin of the escape mutants of H9N2 avian influenza viruses. *Veterinary Microbiology,* 178**,** 144-9.

ZIEBUHR, J., SNIJDER, E. J. & GORBALENYA, A. E. 2000. Virus-encoded proteinases and proteolytic processing in the Nidovirales. *Journal of General Virology,* 81**,** 853-879.